

CENTRAL SPRINGS MODEL (CSM)

(DRAFT)

by:

Qing Sun, PhD, PE

Wei Jin, PhD, PE

Nur Ahmed, PhD

Fatih Gordu, PhD, PE

Joy Kokjohn

St. Johns River Water Management District

Hua Zhang, PhD, PG

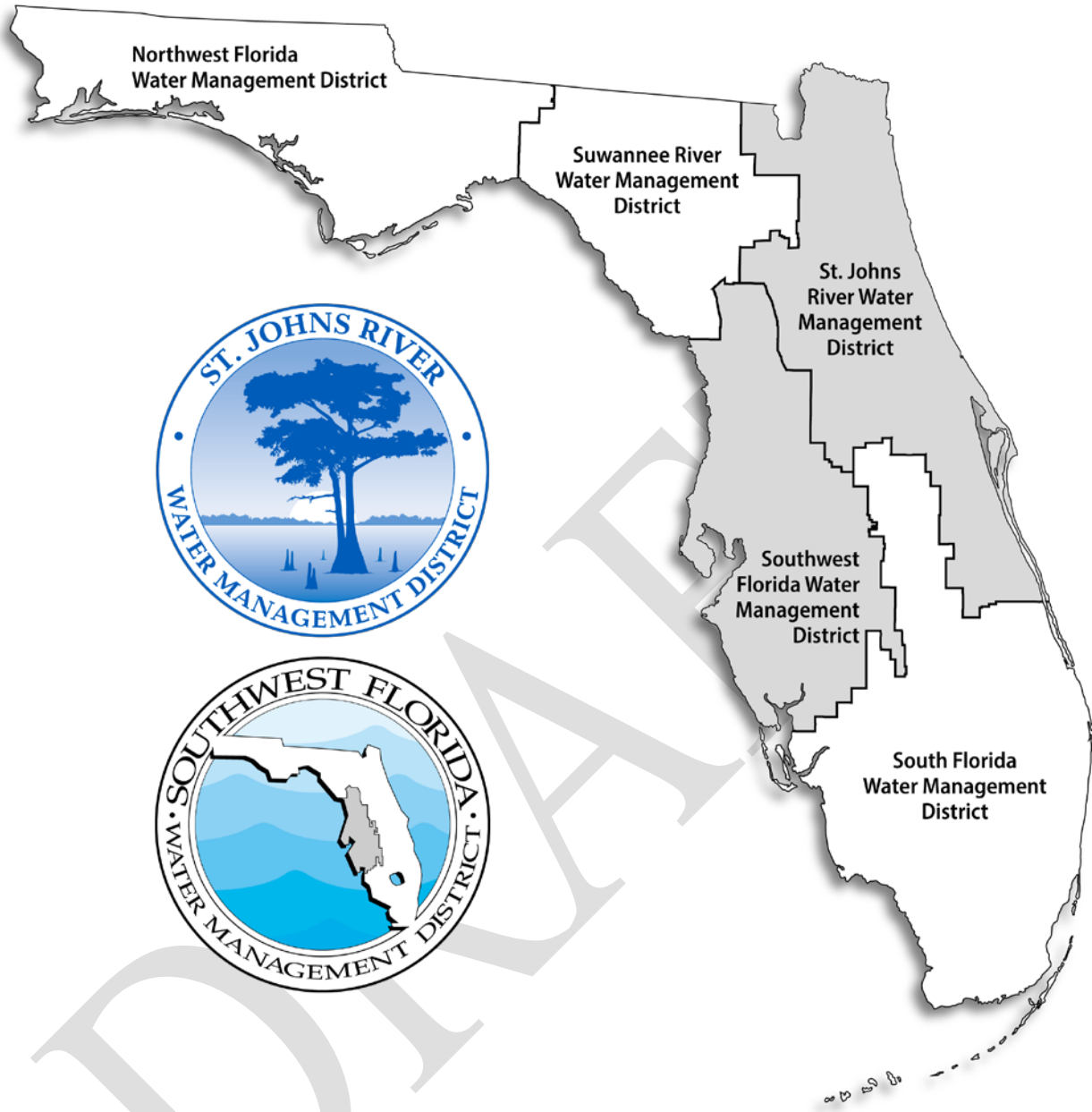
Craig Joseph, PG

Southwest Florida Water Management District



St. Johns River Water Management District
Palatka, Florida

2023



EXECUTIVE SUMMARY

The Central Springs Model (CSM) is a groundwater model developed through a collaboration between the St. Johns River Water Management District (SJRWMD) and the Southwest Florida Water Management District (SWFWMD). The model is designed to quantify the effects of current and future groundwater withdrawals on aquifer water levels, river baseflows, and spring discharges and provide data inputs for regional water supply planning, minimum flows and levels evaluations, and regulatory decisions in the Central Springs Region.

The CSM is comprised of both steady-state and transient models that cover an area from the Gulf of Mexico to the Atlantic Ocean across north-central Florida. The steady-state model represents average hydrologic conditions from 2005 to 2018, while the transient model represents 2005 annual conditions followed by 2006 to 2018 monthly conditions.

The groundwater model was developed as an application of the MODFLOW-NWT (Niswonger et al., 2011) formulation of the MODFLOW-2005 (Harbaugh, 2005) groundwater flow simulation software. MODFLOW-NWT provides enhanced rewetting capabilities in simulations of the water table of unconfined aquifers. Within the model domain, unconfined conditions occur in the Surficial Aquifer System (SAS) and in outcrops of the Intermediate Confining Unit (ICU) and the Upper Floridan Aquifer (UFA).

Individual Hydrological Simulation Program - FORTRAN (HSPF) models were generated for each primary watershed within the model domain to provide estimated recharge and maximum saturated evapotranspiration inputs to the CSM. The HSPF models are comprehensive, interconnected representations of the surface-water and near-surface groundwater flow systems and their calibrated-constrained estimates of recharge and maximum saturated evapotranspiration are components of a complete and internally consistent water budget.

The steady-state model was calibrated using an automated calibration procedure by Parameter ESTimation code (PEST). The PEST calibration process involved minimizing differences between various types of observed (or estimated) hydrological data and their model simulated equivalents through adjustment of model hydraulic parameters within defined ranges. The calibrated hydraulic parameter values along with aquifer storage parameter values were input to the transient model for model testing and refinement. The model was calibrated through a series of iterations to achieve predetermined calibration criteria for the CSM. Observation types included groundwater levels, differences in vertical groundwater levels, springflows, vertical lake leakages, and river baseflows. The CSM performed well in matching groundwater levels and springflows throughout the calibration period. Groundwater level residuals, which represent the difference between simulated and observed data, indicated a good match between the two values. Calibration results with respect to the transmissivity of the UFA and the leakance of the ICU were reasonable, with simulated potentiometric surface comparable to the observed potentiometric surface in the UFA.

The CSM was initially developed under a contractual agreement between SJRWMD and HydroGeologic, Inc. (HGL). Portions of this report were adopted or modified from draft and final reports generated by HGL for SJRWMD and SWFWMD during model conceptualization. Review of the conceptual model and interim draft steady-state and transient models by independent modeling experts allowed for the incorporation of recommendations by the reviewers in model

development and report documentation. The final draft report along with the updated steady-state and transient models are being submitted for final review by the peer reviewers with model finalization expected in January 2024.

The CSM report and model files are also being released to stakeholders for their review and comment. Recommended improvements identified by stakeholders will be incorporated into the final CSM at the discretion of SJRWMD and SWFWMD.

DRAFT

CONTENTS

Executive Summary	iii
Contents	v
List of Figures	ix
List of Tables	xiv
List of Acronyms and Abbreviations	xvi

DRAFT

1. INTRODUCTION.....	1
2. MODEL CONCEPTUALIZATION	3
INITIAL CONCEPTUAL MODEL (2015)	3
EXISTING REGIONAL MODELS OVERLAPPING WITH CSM.....	5
Northern District Model.....	5
North Florida-Southeast Georgia Model	6
East-Central Florida Transient Expanded Model	6
Volusia County Model.....	7
CENTRAL SPRINGS MODEL VERSION 1.0 (2023)	9
3. MODEL DEVELOPMENT	10
TOPOGRAPHY AND PHYSIOGRAPHY	10
LAND COVER AND WATER USE	13
Land Cover.....	13
Water Use.....	15
HYDROLOGY	18
Rainfall.....	18
Evapotranspiration	20
Rivers	22
Lakes	22
Wetlands	24
REGIONAL HYDROSTRATIGRAPHY	25
Hydrogeologic Framework	25
Surficial Aquifer System.....	26
Intermediate Confining Unit.....	26
Upper Floridan Aquifer.....	26
Middle Confining Units	27
Lower Floridan Aquifer	29
Layer Thickness	29
SPRINGS	46
Rainbow Springs and Silver Springs	47
Gulf Coastal Springs	48
Tsala-Apopka Spring Group	48
Central Springs Group	48
MODEL PARAMETERIZATION	50
MODEL BOUNDARY CONDITIONS.....	50
Constant Head Boundaries.....	50
Non-Coastal General-Head Boundaries.....	50
Non-Coastal No-Flow Boundaries.....	50
Rivers and Streams	54
Lakes	55
Wetlands, Small Lakes, and Head Streams	57
Springs	58
PUMPING AND RECHARGE WELLS.....	59
Permitted Wells.....	59

Domestic Self-Supply Wells	59
Sink Flows/Drainage Wells	59
Rapid Infiltration Basins	60
RECHARGE AND EVAPOTRANSPIRATION	64
HSPF Model Development	64
Recharge Calculation	65
Groundwater Evapotranspiration	65
4. MODEL CALIBRATION.....	71
CALIBRATION PROCEDURE	71
Steady-State Model Calibration	72
Transient Model Calibration	72
METRICS AND CRITERIA	74
Groundwater Level Residuals	78
Vertical Head Differences Across Confining Units.....	78
Spring Discharges	78
Qualitative Assessments	79
PRE-CALIBRATION SENSITIVITY ANALYSIS	81
Sensitivity Analysis Results.....	81
Sensitivity Discussion.....	81
5. STEADY-STATE CALIBRATION	88
PEST CALIBRATION	88
PEST Approach	88
Observation Data Groups.....	89
Calibration Parameter Groups.....	90
CALIBRATED PARAMETERS	91
Hydraulic Conductivity.....	91
General Head Boundary Conductance.....	109
Spring Conductance	109
River and Drain Conductance Multipliers	109
Lake and Stream Zone Multipliers	112
Recharge Multipliers.....	112
STEADY-STATE SIMULATION RESULTS	113
Groundwater Heads	113
Head Differences Across Confining Units	123
Spring Discharges	129
Water Budgets.....	133
6. TRANSIENT MODEL CALIBRATION	135
TRANSIENT MODEL PARAMETERS	135
Storage Parameters.....	135
River and Drain Conductance	142
TRANSIENT SIMULATION RESULTS	142
Groundwater Heads	142
Spring Discharges	158
River Baseflows	166

Lake Vertical Leakages.....	173
Water Budgets.....	177
Interlayer Vertical Flux.....	179
7. SUMMARY, CONCLUSION, AND LIMITATIONS.....	181
SUMMARY AND CONCLUSIONS.....	181
MODEL LIMITATIONS.....	182
8. REFERENCES.....	184
APPENDIX A– LIST OF SIMULATED SPRINGS	189
APPENDIX B – SIMULATED VERSUS OBSERVED HYDROGRAPHS OF SURFICIAL AQUIFER SYSTEM CALIBRATION TARGET WELLS	190
APPENDIX C - SIMULATED VERSUS OBSERVED HYDROGRAPHS OF UPPER FLORIDAN AQUIFER CALIBRATION TARGET WELLS.....	191
APPENDIX D - SIMULATED VERSUS OBSERVED HYDROGRAPHS OF LOWER FLORIDAN AQUIFER CALIBRATION TARGET WELLS	192
APPENDIX E - SIMULATED VERSUS OBSERVED MAY AND SEPTEMBER POTENTIOMETRIC SURFACE MAPS.....	193
APPENDIX F - SIMULATED VERSUS OBSERVED HYDROGRAPHS OF CALIBRATION TARGET SPRINGS	194
APPENDIX G – SIMULATED VERSUS ESTIMATED HYDROGRAPHS OF CUMULATIVE RIVER BASEFLOW AT GAGING STATIONS	195
APPENDIX H - SIMULATED VERSUS ESTIMATED HYDROGRAPHS OF RIVER PICKUP BASEFLOW BETWEEN GAGING STATIONS	196
APPENDIX I – SIMULATED HYDROGRAPHS OF LAKE LEAKAGE.....	197
APPENDIX J – COMPARISON OF HSPF AND MODFLOW-SIMULATED CUMULATIVE BASEFLOW OF MAJOR RIVER BASINS.....	198
APPENDIX K – COMPARISON OF HSPF AND MODFLOW-SIMULATED GROUNDWATER EVAPOTRANSPIRATION OF MAJOR RIVER BASINS.....	199

LIST OF FIGURES

Figure 1-1. Central Springs Model domain	1
Figure 2-1. Overlapping groundwater flow model boundaries with the Central Springs Model	8
Figure 3-1. Land surface elevation within the Central Springs Model domain.....	11
Figure 3-2. Physiographic provinces within the Central Springs Model domain.....	12
Figure 3-3. Land cover within the Central Springs Model domain	14
Figure 3-4. Annual average rainfall (2005 to 2018) within the Central Springs Model domain.....	19
Figure 3-5. Average actual evapotranspiration (2005 to 2017) within the Central Springs Model domain calculated using SSEBop model after bias corrections by the USGS	21
Figure 3-6. Major rivers and lakes within in the Central Springs Model domain	23
Figure 3-7. Wetlands and other water bodies within the Central Springs Model domain	24
Figure 3-8. Regional hydrogeologic framework within the Central Springs Model domain	25
Figure 3-9. Cross-section showing the transition between Middle Confining Units I and II	27
Figure 3-10. Overlapping area of Middle Confining Units I and II (HGL, 2023).....	28
Figure 3-11. Visual representation and description of the layers in the Central Springs Model	29
Figure 3-12. Thickness of layer 1 within the Central Springs Model domain.....	31
Figure 3-13. Thickness of layer 2 within the Central Springs Model domain.....	32
Figure 3-14. Thickness of layer 3 within the Central Springs Model domain.....	33
Figure 3-15. Thickness of layer 4 within the Central Springs Model domain.....	34
Figure 3-16. Thickness of layer 5 within the Central Springs Model domain.....	35
Figure 3-17. Thickness of layer 6 within the Central Springs Model domain.....	36
Figure 3-18. Thickness of layer 7 within the Central Springs Model domain.....	37
Figure 3-19. Top elevation of layer 1 within the Central Springs Model domain.....	38
Figure 3-20. Top elevation of layer 2 within the Central Springs Model domain.....	39
Figure 3-21. Top elevation of layer 3 within the Central Springs Model domain.....	40
Figure 3-22. Top elevation of layer 4 within the Central Springs Model domain.....	41
Figure 3-23. Top elevation of layer 5 within the Central Springs Model domain.....	42
Figure 3-24. Top elevation of layer 6 within the Central Springs Model domain.....	43
Figure 3-25. Top elevation of layer 7 within the Central Springs Model domain.....	44

Figure 3-26. Bottom elevation of layer 7 within the Central Springs Model domain	45
Figure 3-27. Spring and spring vent locations within the Central Springs Model domain	46
Figure 3-28. First and second magnitude spring locations within the Central Springs Model domain	47
Figure 3-29. Constant head boundary cell locations within layer 1 of the Central Springs Model domain	51
Figure 3-30. Constant head boundary cell locations within layers 2 through 7 of the Central Springs Model domain	52
Figure 3-31. General head boundary cell locations within layer 3, layer 4, and layer 6 of the Central Springs Model domain with September 2012 Upper Floridan Aquifer (UFA) potentiometric surface.....	53
Figure 3-32. River boundary cell locations within the Central Springs Model domain ...	56
Figure 3-33. Drain boundary cell locations within layer 1 of the Central Springs Model domain.....	57
Figure 3-34. Permitted well locations in the Central Springs Model domain	60
Figure 3-35. Domestic self-supply well locations within the Central Springs Model domain.....	61
Figure 3-36. Sink flow and drainage well locations within the Central Springs Model domain.....	62
Figure 3-37. Rapid infiltration basin locations within the Central Springs Model domain	63
Figure 3-38. HSPF model watersheds within the Central Springs Model domain	64
Figure 3-39. HSPF-derived monthly recharge rates within the Central Springs Model domain for January 2005	66
Figure 3-40. HSPF-derived annual recharge rates within the Central Springs Model domain for 2005	67
Figure 3-41. HSPF-derived monthly maximum saturated evapotranspiration rates within the Central Springs Model domain for January 2005	68
Figure 3-42. HSPF-derived annual maximum saturated evapotranspiration rates within the Central Springs Model domain for 2005.....	69
Figure 3-43. Estimated evapotranspiration extinction depth within the Central Springs Model domain	70
Figure 4-1. Central Springs Model calibration approach.....	71
Figure 4-2. Central Springs Model interactive web application (shinyapps.io) for the visualization of transient model outputs	73
Figure 4-3. Baseflow gage locations within the Central Springs Model domain	80
Figure 4-4. Relative sensitivity for the Surficial Aquifer System (HGL, 2023).....	85

Figure 4-5. Relative sensitivity for the Upper Floridan Aquifer	86
Figure 4-6. Relative sensitivity for the Lower Floridan Aquifer	87
Figure 5-1. Pilot point locations within the Central Springs Model domain	92
Figure 5-2. Horizontal hydraulic conductivity in layer 1 within the Central Springs Model domain.....	93
Figure 5-3. Vertical hydraulic conductivity in layer 2 within the Central Springs Model domain.....	94
Figure 5-4. Horizontal hydraulic conductivity in layer 3 within the Central Springs Model domain.....	95
Figure 5-5. Horizontal hydraulic conductivity in layer 4 within the Central Springs Model domain.....	96
Figure 5-6. Vertical hydraulic conductivity in layer 5 within the Central Springs Model domain.....	97
Figure 5-7. Horizontal hydraulic conductivity in layer 6 within the Central Springs Model domain.....	98
Figure 5-8. Horizontal hydraulic conductivity in layer 7 within the Central Springs Model domain.....	99
Figure 5-9. Vertical anisotropy ratios in layer 2 within the Central Springs Model domain	101
Figure 5-10. Vertical anisotropy ratios in layer 5 within the Central Springs Model domain.....	102
Figure 5-11. Leakance in layer 2 within the Central Springs Model domain.....	104
Figure 5-12. Leakance in layer 5 within the Central Springs Model domain.....	105
Figure 5-13. Upper Floridan Aquifer (UFA) transmissivity from PEST calibration and aquifer performance tests within the Central Springs Model domain	107
Figure 5-14. Lower Floridan Aquifer transmissivity within the Central Springs Model domain.....	108
Figure 5-15. River cell conductance within the Central Springs Model domain.....	110
Figure 5-16. Drain cell conductance within layer 1 of the Central Springs Model domain	111
Figure 5-17. Layer 1 (Surficial Aquifer System) head target scatter plot	115
Figure 5-18. Head target residuals in layer 1 within the Central Springs Model domain	116
Figure 5-19. Layer 3 (Upper Floridan Aquifer) head target scatter plot	117
Figure 5-20. Head residuals in layer 3 within the Central Springs Model domain	118
Figure 5-21. Layer 4 (Upper Floridan Aquifer) head target scatter plot	119

Figure 5-22. Head target residuals in layer 4 within the Central Springs Model domain	120
Figure 5-23. Layer 6 (Lower Floridan Aquifer) head target scatter plot	121
Figure 5-24. Head residuals in layer 6 within the Central Springs Model domain	122
Figure 5-25. Vertical head difference residuals across the Intermediate Confining Unit within the Central Springs Model domain	124
Figure 5-26. Vertical head difference residuals across the Middle Confining Unit I within the Central Springs Model domain	125
Figure 5-27. Scatter plot of vertical head difference targets across layer 2 (Intermediate Confining Unit)	126
Figure 5-28. Scatter plot of vertical head difference targets across layer 6 (Middle Confining Unit I)	127
Figure 5-29. Scatter plot of springflow targets	131
Figure 5-30. Springflow target residuals within the Central Springs Model domain	132
Figure 6-1. Specific yield of layer 1 within the Central Springs Model domain	136
Figure 6-2. Specific storage of layer 2 within the Central Springs Model domain	137
Figure 6-3. Specific storage of layer 3 within the Central Springs Model domain	138
Figure 6-4. Specific storage of layer 4 within the Central Springs Model domain	139
Figure 6-5. Specific storage of layer 5 within the Central Springs Model domain	140
Figure 6-6. Specific storage of layer 6 within the Central Springs Model domain	141
Figure 6-7. Average head residuals over the transient simulation period in layer 1 target wells	145
Figure 6-8. Average head residuals over the transient simulation period in layer 3 and layer 4 target wells	146
Figure 6-9. Average head residuals over the transient simulation period in layer 6 target wells	147
Figure 6-10. Comparison of model-simulated hydrographs to monthly observed groundwater levels at selected target wells in layer 1	148
Figure 6-11. Comparison of model-simulated hydrographs to monthly observed groundwater levels at selected target wells in layer 3 and layer 4	149
Figure 6-12. Comparison of model-simulated hydrographs to monthly observed groundwater levels at selected target wells in layer 6	150
Figure 6-13. Spatial distribution of flooded cells in September 2017	151
Figure 6-14. Spatial distribution of dry cells in May 2012	152
Figure 6-15. Comparison of simulated 2005 to 2018 average depth to water table with observed values in layer 1	153

Figure 6-16. Comparison of model-simulated heads in layer 3 and the Upper Floridan Aquifer (UFA) potentiometric surface in May 2010	154
Figure 6-17. Comparison of model-simulated heads in layer 3 and the Upper Floridan Aquifer (UFA) potentiometric surface in September 2014	155
Figure 6-18. Comparison of simulated 2005 to 2018 average vertical head difference across the Intermediate Confining Unit (ICU) with observed values at well pairs	156
Figure 6-19. Comparison of simulated 2005 to 2018 average vertical head difference across Middle Confining Unit I (MCU I) with observed values at well pairs	157
Figure 6-20. Simulated and observed hydrographs for Rainbow Springs #1	160
Figure 6-21. Simulated and observed hydrographs for Silver Springs Group.....	160
Figure 6-22. Simulated and observed hydrographs for Silver Glen Springs	161
Figure 6-23. Simulated and observed hydrographs for Alexander Springs.....	161
Figure 6-24. Simulated and observed hydrographs for Wekiwa Springs	162
Figure 6-25. Simulated and observed hydrographs for Apopka Spring	162
Figure 6-26. Simulated and observed hydrographs for Blue Spring in Orange City.....	163
Figure 6-27. Simulated and observed hydrographs for Bugg Spring	163
Figure 6-28. Simulated and observed hydrographs for Gum Spring Main.....	164
Figure 6-29. Simulated and observed hydrographs for Homosassa Spring #1	164
Figure 6-30. Simulated and observed hydrographs for Chassahowitzka Spring Main...	165
Figure 6-31. Simulated and observed hydrographs for Weeki Wachee Spring.....	165
Figure 6-32. Simulated and estimated baseflow at selected St. Johns River gages	169
Figure 6-33. Simulated and estimated baseflow at selected Ocklawaha River gages	170
Figure 6-34. Simulated and estimated baseflow at selected Withlacoochee River gages	171
Figure 6-35. Simulated and estimated baseflow at selected Hillsborough River gages .	172
Figure 6-36. Transient simulated 2005 to 2018 average lake vertical leakage.....	174
Figure 6-37. CSM simulated hydrographs of vertical leakage at lakes Weir and Panasoffkee	176
Figure 6-38. Spatial distribution of average 2005 to 2018 interlayer vertical leakage flux in the CSM transient model between the ICU and UFA	179
Figure 6-39. Spatial distribution of average 2005 to 2018 interlayer vertical leakage flux in the CSM transient model between MCU I and the LFA	180

LIST OF TABLES

Table 3-1. Summary of groundwater withdrawals in the SJRWMD portion of the Central Springs Model domain.....	16
Table 3-2. Summary of groundwater water withdrawals in the SWFWMD portion of the Central Springs Model domain	17
Table 3-3. Stratigraphy and generalized lithology of the geologic units within the Central Springs Model domain.....	25
Table 4-1. Steady-state calibration criteria (spatial statistics).....	76
Table 4-2. Transient calibration criteria (temporal statistics).....	77
Table 4-3. List of parameters and perturbation types	82
Table 4-4. Relative sensitivity for the Surficial Aquifer System.....	83
Table 4-5. Relative sensitivity for the Upper Floridan Aquifer.....	83
Table 4-6. Relative sensitivity for the Lower Floridan Aquifer	84
Table 5-1. PEST observation groups	90
Table 5-2. PEST calibration parameter groups.....	90
Table 5-3. Groundwater head residuals by layer	114
Table 5-4. Vertical head differences across the Intermediate Confining Unit	128
Table 5-5. Vertical head differences across the Middle Confining Unit I.....	128
Table 5-6. Simulated and observed discharge of first magnitude of springs.....	129
Table 5-7. Simulated and observed discharge of second magnitude of springs	130
Table 5-8. Boundary condition influx by layer within the steady-state Central Springs Model	133
Table 5-9. Boundary condition outflux by layer within the steady-state Central Springs Model	133
Table 5-10. Boundary condition net flux by layer within the steady-state Central Springs Model	134
Table 6-1. Transient model calibration statistics of target monitoring wells in the Central Springs Model domain.....	143
Table 6-2. Comparison of average 2005 to 2018 simulated and observed flux of the target springs in the transient Central Springs Model.....	159
Table 6-3. Comparison of simulated average 2005 to 2018 baseflow with river baseflow estimated from observed discharge at USGS gages in the transient Central Springs Model	167
Table 6-4. Comparison of transient model simulated lake vertical leakages to reported values	175

Table 6-5. Boundary condition influx in the CSM transient model (2005-2018) by layer	178
Table 6-6. Boundary condition outflux in the CSM transient model (2005-2018) by layer	178
Table 6-7. Boundary condition net flux in the CSM transient model (2005-2018) by layer	178

DRAFT

LIST OF ACRONYMS AND ABBREVIATIONS

AET	actual evapotranspiration
AG	agricultural
APpz	Avon Park permeable zone
APT	aquifer performance test
CD _{Lake}	lake conductance (ft ² /day)
CD _{River}	river conductance (ft ² /day)
cfs	cubic feet per second
CHD	constant head (MODFLOW package)
CII	commercial/institutional/industrial
CSM	Central Springs Model
CUP	consumptive use permit
day ⁻¹	feet per day per foot
DEM	digital elevation model
Districts	St. Johns River and Southwest Florida Water Management Districts
DRN	drain package (MODFLOW)
DSS	domestic self-supply
ECFTX	East-Central Florida Transient Expanded Groundwater Flow Model
ET	evapotranspiration
ETSatMax	maximum saturated evapotranspiration
FAS	Floridan Aquifer System
FDEP	Florida Department of Environmental Protection
ft	foot or feet
ft/day	feet per day
ft ² /day	feet squared per day
GHB	general head boundary (MODFLOW package)
HGL	HydroGeoLogic, Inc.
HSPF	Hydrological Simulation Program-FORTRAN
HUC	hydrologic unit code
ICU	Intermediate Confining Unit
in/yr	inch(es) per year
K _{river}	vertical hydraulic conductivity of river bottom (ft/day)
Kh	horizontal hydraulic conductivity
Kv	vertical hydraulic conductivity
K _{Lake}	vertical hydraulic conductivity of lake bottom (ft/day)

LFA	Lower Floridan Aquifer
LRA	landscape/recreational/aesthetic
MAE	mean absolute error
MCU	Middle Confining Unit
MD	mining and dewatering
ME	mean error
MFL	minimum flows and levels
mgd	million gallons per day
mg/L	milligrams per liter
MODFLOW	modular three-dimensional finite-difference groundwater flow model
MODFLOW-NWT	Newton formulation for MODFLOW-2005
NAVD88	North American Vertical Datum of 1988
NDM	Northern District Model
NEXRAD	Next Generation Weather Radar
NFSEG	North Florida-Southeast Georgia Regional Groundwater Flow Model
NSE	Nash–Sutcliffe efficiency coefficient
OCAPlpz	Ocala-Avon Park low permeable zone
PBIAS	percent bias
PEST	Parameter ESTimation code
PET	potential evapotranspiration
PS	public supply
R ²	coefficient of determination
RBOT	river bottom elevation
RIBs	rapid infiltration basins
RSR	ratio of root-mean-square error and standard deviation
SAS	Surficial Aquifer System
SFWMD	South Florida Water Management District
SJRWMD	St. Johns River Water Management District
SRWMD	Suwannee River Water Management District
Ss	specific storage
SSEBop	Operational Simplified Surface Energy Balance
SWFWMD	Southwest Florida Water Management District
SWOCpz	Suwannee-Ocala permeable zone
Sy	specific yield
UFA	Upper Floridan Aquifer
USGS	United States Geological Survey

WEL	well package (MODFLOW)
WUP	water use permit
ρ_s	groundwater density
ρ_f	freshwater density

DRAFT

1. INTRODUCTION

The Central Springs Model (CSM) is a regional groundwater flow model developed through a collaboration between the St. Johns River Water Management District (SJRWMD) and the Southwest Florida Water Management District (SWFWMD). The model is designed to quantify the effects of current and future groundwater withdrawals on aquifer water levels, river baseflows, and spring discharges and provide data inputs for water supply planning, evaluation of minimum flows and levels (MFL), and consumptive/water use permitting across north-central Florida. The CSM domain includes all of Marion, Volusia, Lake, Seminole, Sumter, Citrus, Hernando, and Pasco counties and parts of Alachua, Bradford, Clay, Putnam, Flagler, Brevard, Orange, Osceola, Polk, Hillsborough, Pinellas, and Levy counties (Figure 1-1).

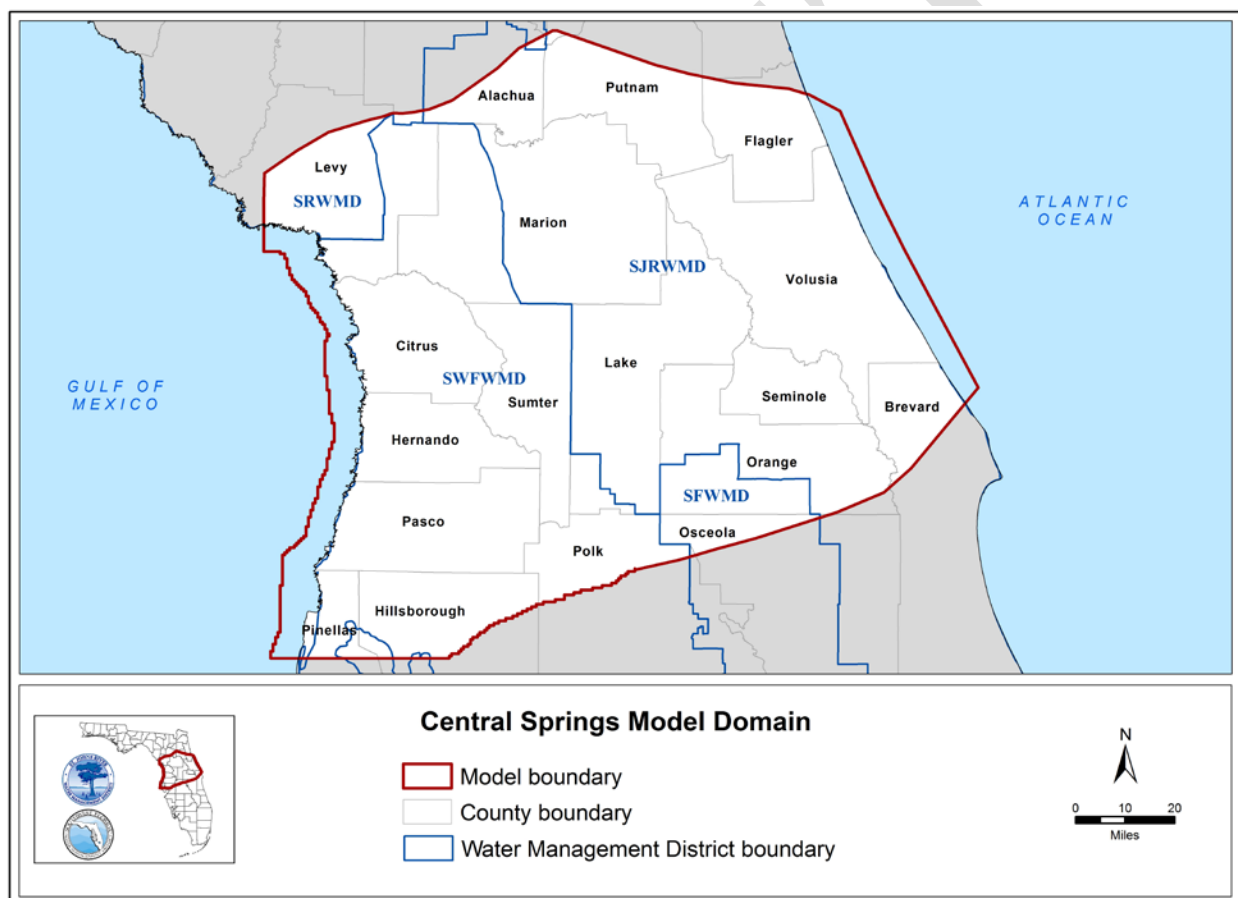


Figure 1-1. Central Springs Model domain

Note: SFWMD = South Florida Water Management District, SWFWMD = Southwest Florida Water Management District, SJRWMD = St. Johns River Water Management District, SRWMD = Suwannee River Water Management District

The initial conceptualization of the CSM was completed in 2015 by HydroGeoLogic, Inc. (HGL) through a collaborative effort between the SJRWMD, the SWFWMD, the Withlacoochee Regional Water Supply Authority, and Marion County. The conceptual model was developed based on the Northern District Model (NDM) Version 4.0 and included a model domain across north-central Florida from the Gulf of Mexico to the Atlantic Ocean. The

conceptual model used data from three existing groundwater models, including the Volusia County groundwater model, the East Central Florida model, and the North Central Florida model. The conceptual model report (HGL, 2014) was completed in December 2014, and the first external peer reviews were completed in May 2015. The project was put on hold in September 2015.

In 2020, HGL was contracted by SJRWMD to resume development of the CSM in collaboration with the SJRWMD and the SWFWMD (Districts). Two models were developed as part of this effort, including a steady-state model representing average hydrologic conditions from 2005 to 2018 and a transient model representing 2005 annual conditions followed by 2006 to 2018 monthly conditions. Draft versions of the steady-state model, transient model, and model report (HGL, 2023) were submitted by HGL to the Districts at the end of its contract in December 2022. The Districts continued to update, refine, and calibrate the draft models to generate the version of the CSM presented in this report.

2. MODEL CONCEPTUALIZATION

INITIAL CONCEPTUAL MODEL (2015)

(This section is adopted and modified from Appendix A of the HGL 2023 report)

The 2015 conceptual CSM domain covers an area from the Gulf of Mexico to the Atlantic Ocean across north-central Florida and was described in detail by HGL (2015). The conceptual model was planned to have a calibration period from the beginning of 2007 through the end of 2012 and a verification period from the beginning of 1996 to the end of 2006. Uncalibrated conceptual models were developed for steady-state and transient conditions in 1995 and 2008. These files were distributed by HGL to the Districts in 2019.

The conceptualized regional hydrogeologic framework generally follows the hydrogeologic units described by Miller (1986a), Arthur et al. (2005), and Copeland et al. (2010). These units include the Surficial Aquifer System (SAS), the Intermediate Confining Unit (ICU), the Upper Floridan Aquifer (UFA), the Middle Confining Unit (MCU) I, MCU II, and the Lower Floridan Aquifer (LFA). Units and their corresponding model layers are discussed in Chapter 3.

The UFA is conceptualized as consisting of three flow zones with unique hydraulic properties, including the Suwannee-Ocala permeable zone (SWOCpz), the Ocala-Avon Park low permeability zone (OCAPlpz), and the Avon Park permeable zone (APpz). Each flow zone comprises an individual layer in the CSM. Middle Confining Unit I and MCU II are associated with Avon Park dolostones and limestones. Middle Confining Unit II contains gypsum nodules while MCU I does not. In the eastern portion of the project area, the MCU I within the Avon Park Formation underlies and separates the UFA from the LFA. In the western portion of the project area, the MCU II within the Avon Park Formation underlies the UFA. Middle Confining Unit I may slightly overlap MCU II in the western CSM domain, though the exact location of this overlap is currently uncertain.

In the CSM, the flow system of the LFA (Oldsmar Formation) in the western portion of the project area is treated as inactive due to low observed transmissivity values and the presence of abundant gypsum nodules and brine. In this region, MCU II acts as a thick, tight, non-leaky confining unit containing abundant gypsum, with very little to no vertical hydraulic connection with the overlying UFA. Vertical boundaries and horizontal extents of the MCUs within the CSM domain have been updated using more recent data collected since development of the original 2015 conceptual model.

As defined by HGL (2015), the conceptual hydrogeologic model of the project area includes the following groundwater recharge and discharge areas:

- Riverine discharge/recharge region
- Coastal UFA discharge region
- Unconfined and semi-confined UFA recharge regions
- Ocklawaha River and St. Johns River UFA discharge region

Included in the riverine discharge/recharge region along the Withlacoochee River is the Tsala-Apopka area. East of the river, the Tsala-Apopka area is a discharge region containing Lake Panasoffkee and its contiguous springs and wetlands. West of the river, the Tsala-Apopka area is a recharge region containing Lake Tsala-Apopka. A large fraction of Withlacoochee River baseflow occurs from recharge in the Tsala-Apopka area.

Freshwater-saltwater transition zones occur in the UFA within the coastal UFA discharge region in the western part of the project area and within the St. Johns River and coastal UFA discharge regions in the eastern part of the project area.

The extent of the unconfined UFA recharge region is generally consistent with water levels from nested well pairs operated by SWFWMD and water quality studies, which indicate rapid movement of recharge into the UFA. The areal extent of this region as defined in the CSM includes and expands upon the unconfined areas defined by Ryder (1985) and Sepulveda (2002).

A simplified water-balance approach was used to estimate long-term average annual recharge to the UFA for specified watersheds within the unconfined UFA recharge region in the project area (HGL, 2015). Long-term average annual evapotranspiration (ET) rates were assumed to range between 38 inches per year (in/yr) and 42 in/yr. The smallest and largest annual recharge rates for the unconfined UFA recharge region were estimated to be 7 in/yr in the Withlacoochee watershed and 17 in/yr in Marion County, respectively.

Potentiometric surface contours in the UFA are congruent with the more permeable parts of the Suwannee Limestone and the Ocala Limestone throughout the project area. The relatively high permeability of the SWOCpz effectively controls groundwater flow to the springs in the northwestern part of the model domain. The Suwannee Limestone is absent and the Ocala Limestone is discontinuous throughout the eastern portion of the project area. Potentiometric surfaces in the UFA also suggest that the St. Johns River is a major discharge area. Poor water quality with elevated chloride concentrations exists along the river path. It is likely that the water with elevated chloride concentrations flows vertically from the LFA to the UFA in the vicinity of the St. Johns River.

Elevated sulfate concentrations generally occur in the Avon Park Formation (near or above MCU II) below an elevation of approximately -150 feet (ft) above mean sea level within portions of Citrus and Marion counties and the western portion of Sumter County. The elevated sulfate concentrations are consistent with both the presence of gypsum and relatively slow groundwater flow in the Avon Park Formation. Sulfate concentrations reported for Crystal River, Homosassa, and Chassahowitzka springs indicate relatively little springflow contribution from the Avon Park in Citrus County (Sacks, 1996).

EXISTING REGIONAL MODELS OVERLAPPING WITH CSM

(This section is adopted and modified from Appendix B of the HGL 2023 report)

As shown on Figure 2-1, there are four existing regional groundwater flow model boundaries overlapping the CSM domain. These models served as a source for relevant data and hydrologic parameter values during development of the CSM.

Northern District Model

Approximately two-thirds of the CSM extent encompasses the area covered by the NDM (HGL, 2013, 2015). The NDM and the CSM share a similar conceptual model and have the same grid size and number of model layers.

Development and enhancement of the NDM was conducted in four phases between 2007 and 2013 (HGL, 2008, 2010, 2011, and 2013). The first phase was conducted under the direction of SWFWMD in support of the Northern District Water Resource Assessment Project. During the first phase of the project, a conceptual hydrogeologic model was developed based on historical investigations, documents, and data and included the major components of the groundwater flow system, including geologic and hydrogeologic setting, groundwater sources and sinks, hydraulic properties, and groundwater-flow characteristics. Much of the conceptual framework had been established by earlier investigations of subsurface hydrogeology of the area dating back to the early 1960s.

Model development in the first phase (Version 1.0) was based on data from 1995 to 2002 and was completed in May 2008 (HGL, 2008). The second phase (Version 2.0) began in late 2008 to improve the representation of lakes, springs, rivers, and recharge inputs using additional hydrogeologic and hydrologic data and to perform additional calibration and sensitivity analyses (HGL, 2010). The third phase of model development (Version 3.0) began in early 2010 and utilized additional climatic, hydrogeologic, and hydrologic data from 2003 to 2006. Improvements were made on the representation of surface water body networks, springs, lakes, and recharge inputs. Additional calibration and sensitivity analysis were conducted and documented by HGL (2011).

The fourth phase of model development (Version 4.0) started in March 2013 (HGL, 2013). The NDM domain in the northeastern and eastern area was extended to include an area west of Lake George and the St. Johns River. The extended domain covered the entire area of Marion County. NDM Version 4.0 consists of two calibrated models; a steady-state model based on average conditions in 1995 and a transient model based on the conditions from 1996 to 2006. The NDM Version 4.0 model domain is discretized with a grid of 275 rows and 212 columns. The dimensions of each grid cell are 2,500 ft by 2,500 ft. Vertical discretization includes seven layers based on unique hydrostratigraphic characteristics. In descending order, they are as follows:

- Layer 1: SAS
- Layer 2: ICU
- Layer 3: SWOCpz
- Layer 4: OCAPlpz

- Layer 5: APpz
- Layer 6: MCU I/II
- Layer 7: LFA

NDM Version 5.0 (HGL, 2016) was developed after the 2015 CSM project. In NDM Version 5.0, the 1995 steady-state and 1996 to 2006 transient models were updated and recalibrated with additional data. A 2010 steady-state model was also developed using average pumping, hydrologic, and hydrogeologic conditions to verify the results under more recent conditions. Versions 4.0 and 5.0 were peer reviewed (Andersen and Stewart, 2016) in a cooperatively funded project by the Districts (SWFWMD, 2017).

North Florida-Southeast Georgia Model

The North Florida-Southeast Georgia Regional Groundwater Flow Model (NFSEG) Version 1.0 was developed in 2016 (Gordu et al., 2016) and later updated in 2019 to Version 1.1 (Durden et al., 2019). The active domain of the NFSEG Version 1.1 encompasses an area of approximately 60,000 square miles and includes portions of Florida, Georgia, South Carolina, the Atlantic Ocean, and the Gulf of Mexico. The southern portion of the NFSEG model overlaps with the northern portion of the CSM. In its present form, the NFSEG model is fully three-dimensional and steady state. The model consists of seven aquifer layers. In descending order, these include:

- Layer 1: SAS
- Layer 2: ICU
- Layer 3: UFA
- Layer 4: MCU I
- Layer 5: LFA
- Layer 6: Lower Semi-confining Unit
- Layer 7: Fernandina permeable zone

The active areal extent of each model layer is limited to that of freshwater flow. In layer 4 through layer 7, the extent of freshwater flow was determined primarily by intersecting the isocontour for groundwater with an estimated 10,000 milligram per liter (mg/L) total dissolved solids concentration with the estimated top elevations of the aquifers or confining units that comprise the Floridan Aquifer System (FAS).

The model domain is discretized horizontally into a finite-difference grid of 752 rows by 704 columns, with uniform cell dimensions of 2,500 ft by 2,500 ft. The model was calibrated to 2001 and 2009 steady-state conditions.

East-Central Florida Transient Expanded Model

The East-Central Florida Transient Expanded Groundwater Flow Model (ECFTX) Version 1.0 was developed in 2020 (CFWI, 2020). Initial model calibration was conducted using an average 2003 steady-state condition, which served as the initial conditions for a long-term monthly transient simulation from 2004 through 2014. The steady-state calibration procedure consisted of manually adjusting hydraulic conductivity fields to improve matches between simulated and observed heads. For transient calibration, the procedure primarily consisted of

manually adjusting hydraulic conductivity, specific storage, and drain/river cell conductance to improve matches between simulated and observed heads.

ECFTX was updated in 2022 to ECFTX Version 2.0 by conducting Parameter ESTimation code (PEST; Doherty, 2010) calibration in Seminole County and the Wekiva River springs groundwater contributing basin (Gordu et al., 2022).

Development of the ECFTX was a collaborative effort between SJRWMD, SWFWMD, and the South Florida Water Management District (SFWMD) for application in water use planning and permitting in the area of the Central Florida Water Initiative.

The ECFTX is horizontally discretized into a uniform grid with a cell size of 1,250 ft by 1,250 ft. The grid consists of 603 rows and 704 columns oriented along a north-south axis. The model is vertically discretized into 11 hydrostratigraphic layers. In descending order, they are:

- Layer 1: SAS
- Layer 2: ICU
- Layer 3: SWOCpz
- Layer 4: OCAPlpz
- Layer 5: APpz
- Layer 6: MCU I
- Layer 7: MCU I – II overlapping
- Layer 8: MCU II
- Layer 9: LFA-upper
- Layer 10: GLAUCIpu
- Layer 11: LFA-basal permeable zone

The bottom and lateral boundaries of the model were established at the estimated depths where the chloride concentration in the FAS is 5,000 mg/L.

Volusia County Model

The Volusia County model was developed for Volusia County and the adjacent area and overlaps with the northeast quadrant of the CSM domain (Williams, 2006). The model is a quasi-three-dimensional steady-state regional groundwater flow model discretized horizontally into a finite-difference grid of 100 rows by 100 columns, with uniform cell dimensions of 2,500 ft by 2,500 ft. Vertical discretization includes three aquifer layers, representing the SAS, the UFA, and the LFA, and two confining units, representing the ICU and the MCU I. Aquifer layers are simulated explicitly based upon elevation data, and confining units are simulated as non-uniform areal distributions of leakance terms.

The model was originally calibrated to predevelopment hydrologic conditions in the 1930s (Johnston et al., 1980) and to average 1995 conditions. The 1995 model was used to simulate changes in the groundwater flow system projected to occur between 1995 and 2020.

The 1995 model was recalibrated to 2002 hydrologic conditions (Williams, 2013). In 2017, the Volusia 2015 model (Sun, 2017) was developed by updating the 2002 model with climate, land use, and water use conditions from 2015. Water use, head targets, spring pool elevation,

springflow, general head boundaries (GHBs), and recharge were also updated. The 2015 model was used to evaluate potential impacts of projected water use in 2040.

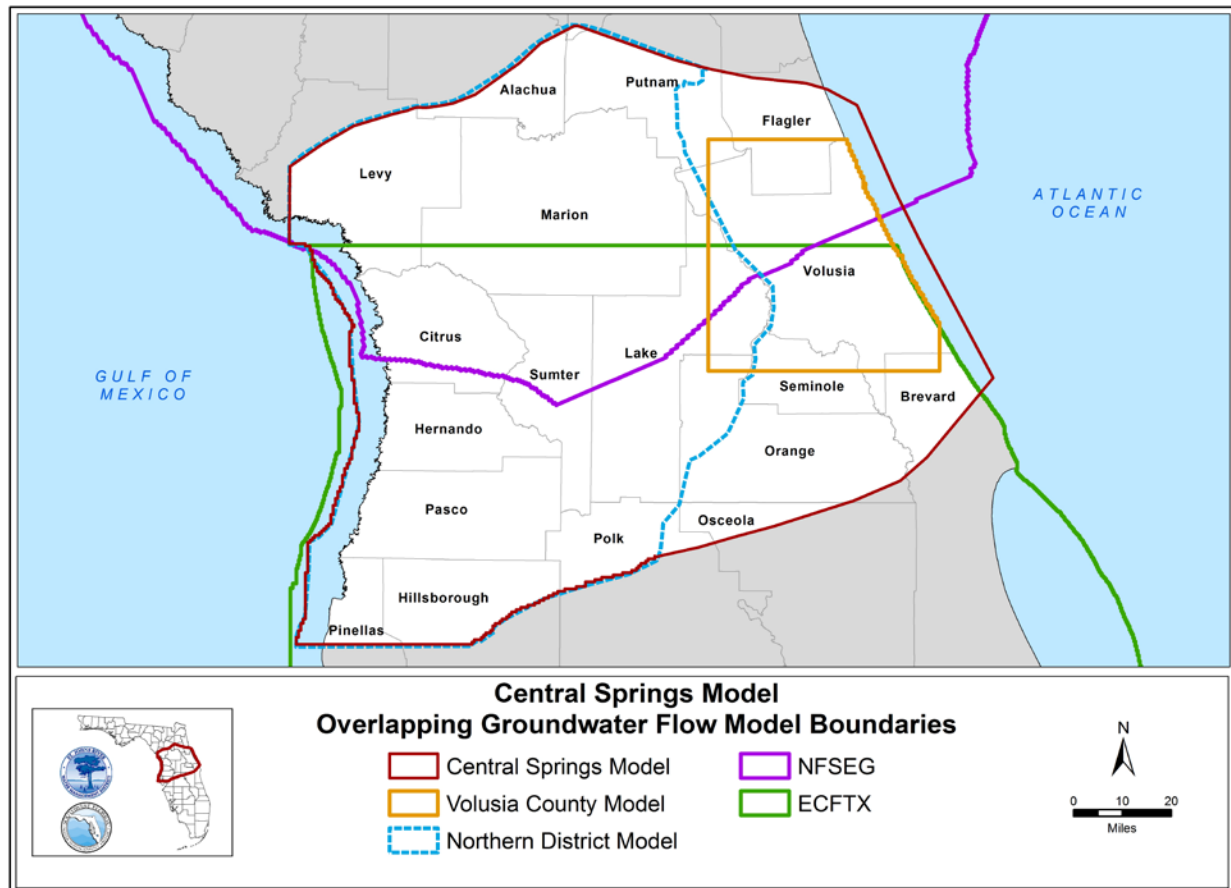


Figure 2-1. Overlapping groundwater flow model boundaries with the Central Springs Model
 Note: NFSEG = North Florida-Southeast Georgia Regional Groundwater Flow Model, ECFTX = East-Central Florida Transient Expanded Groundwater Flow Model.

CENTRAL SPRINGS MODEL VERSION 1.0 (2023)

(This section is adopted and modified from Chapter 2 and Appendix B of the HGL 2023 report)

The current version of the CSM includes a steady-state model representing average hydrologic conditions from 2005 to 2018 and a transient model representing 2005 annual conditions followed by 2006 to 2018 monthly conditions. Updates to the 2015 conceptual model included:

- Converting the model to MODFLOW-NWT
- Updating vertical layering and hydrostratigraphic elevations based on the most recent hydrogeological investigations
- Utilizing recharge and maximum saturated evapotranspiration (ET) outputs from Hydrological Simulation Program – FORTRAN (HSPF) modeling for inputs to MODFLOW
- Calibrating to average steady-state conditions from 2005 to 2018 and monthly average transient conditions from 2006 to 2018 with initial conditions set to 2005 average annual conditions
- Updating boundary condition representation of rivers, drains, and lakes
- Updating general head boundaries (GHBs) and constant head (CHD) boundaries
- Updating ET extinction depths
- Utilizing a current, revised well package
- Utilizing a United States Geological Survey (USGS) 10-meter digital elevation model (DEM) referenced to the North American Vertical Datum of 1988 (NAVD88)

The CSM is horizontally discretized into a uniform grid with a cell size of 2,500 ft by 2,500 ft and consists of 275 rows and 332 columns. The model is vertically discretized into seven hydrostratigraphic layers. The horizontal model grid remains unchanged from the 2015 conceptual model; however, the vertical discretization was revised based on newer hydrostratigraphic information as presented in Chapter 3 of this report.

The long-term steady-state model is based on average conditions from 2005 to 2018. The transient model is based on monthly stress periods from 2006 to 2018 with steady-state conditions from 2005 used as initial conditions. Each stress period contains six timesteps. The first timestep is approximately 3 days. Based on the multiplier for the length of successive time steps of 1.2, the sixth timestep is approximately 7.5 days.

3. MODEL DEVELOPMENT

TOPOGRAPHY AND PHYSIOGRAPHY

(This section is adopted and modified from Chapter 2 of the HGL 2015 report)

The topography of the project area is shown on Figure 3-1. The elevation data in the figure is from a DEM prepared by the USGS. The DEM has a horizontal resolution of 10 meters. Land-surface elevation generally varies from near mean sea level to approximately 150 ft NAVD88, although some local ridges as high as 300 ft NAVD88 exist.

The physiographic provinces in the project area, derived from the geographic information system (GIS) coverage provided by SWFWMD (Brooks, 1981), are shown on Figure 3-2. The provinces can be loosely classified into two groups based upon land-surface elevations. One group is characterized by relatively low topographic elevation (less than 50 ft NAVD88) and includes the Coastal Swamp, Gulf Coastal Lowlands, Western Valley, Tsala-Apopka Plain, parts of the Central Valley, Eastern Valley, and Atlantic Coastal Ridge.

The other group is characterized by relatively high topographic elevation (greater than 50 ft NAVD88) and includes the Brooksville Ridge, Fairfield Hills, Sumter Upland, Cotton Plant Ridge, Lake Upland, Lake Wales Ridge, Northern Highlands, Mount Dora Ridge, and Marion Upland. The dominant physiographic regions in the project area include the Coastal Swamp, Eastern Valley, Central Valley, Lake Upland, Northern Highlands, Mount Dora Ridge, Crescent City Ridge, Deland Ridge, Marion Upland, Brooksville Ridge, and Lake Wales Ridge.

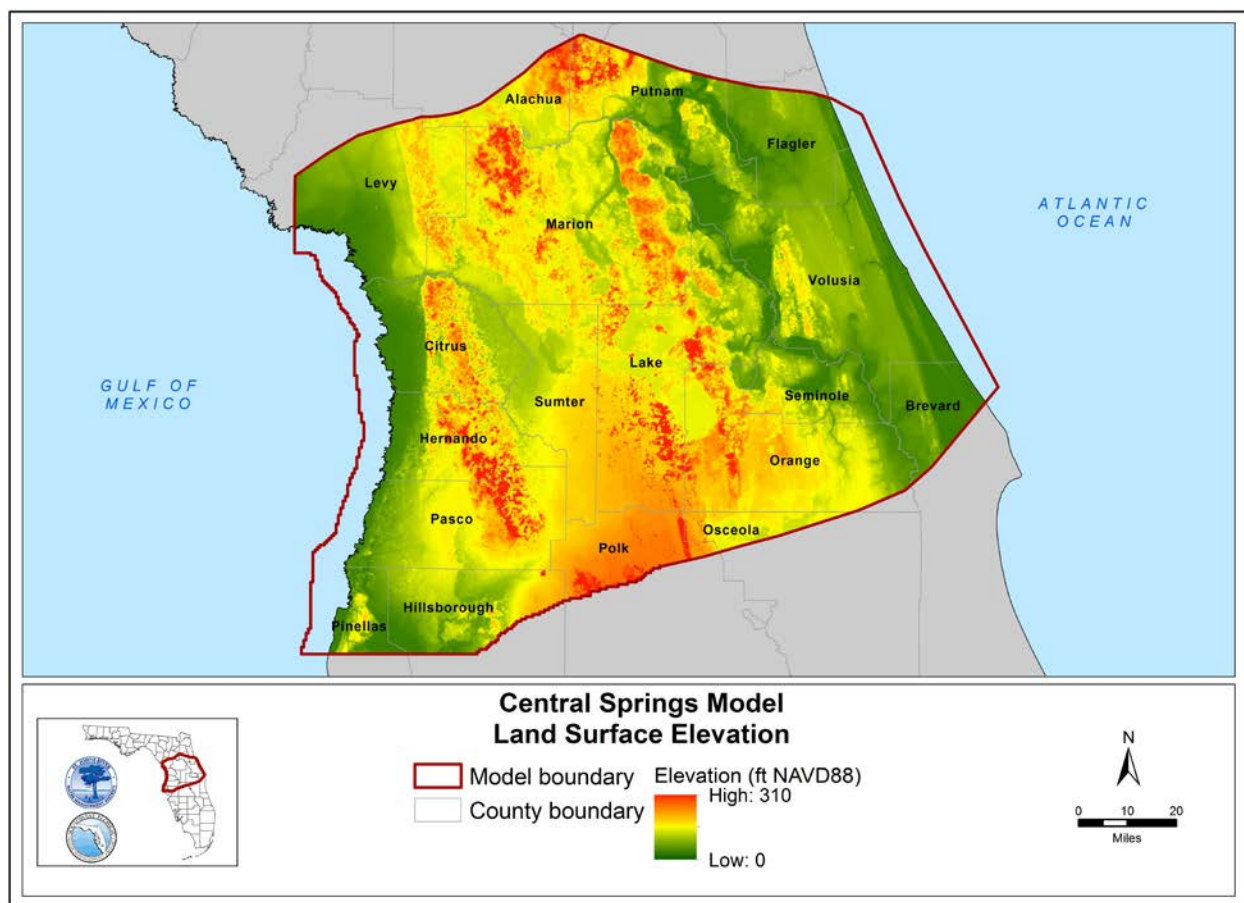


Figure 3-1. Land surface elevation within the Central Springs Model domain (based on USGS 10-meter Digital Elevation Model, ft NAVD88)

Note: ft NAVD88 = feet relative to the North American Vertical Datum of 1988

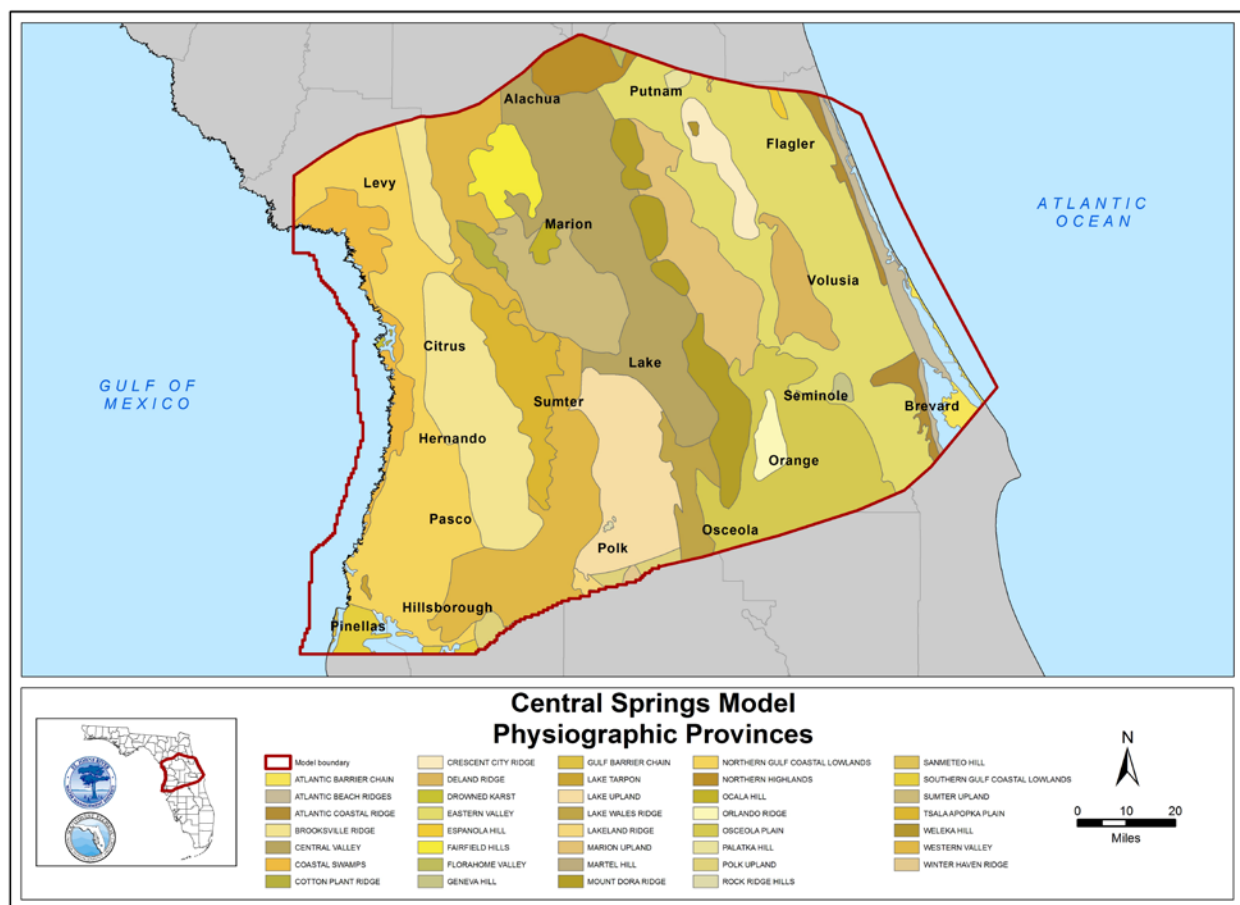


Figure 3-2. Physiographic provinces within the Central Springs Model domain (Brooks, 1981)

LAND COVER AND WATER USE

Land Cover

Land cover data from the National Land Cover Database (NLCD) for 2001 was used in the HSPF models to develop estimates of runoff, maximum ET and recharge rates, and landscape and agricultural irrigation return flows. Land cover presents a distribution of pervious and impervious surfaces that are used in separating runoff and infiltration from total rainfall and irrigation. The distribution¹ of land cover types across the project area, shown on Figure 3-3, includes:

- Wetland (Woody Wetlands and Emergent Herbaceous Wetlands) - 32.3%
- Development or urban (Developed High, Medium, and Low Intensity, and Open Space) - 18.1%
- Forest (Deciduous, Evergreen, and Mixed Forest) - 16.5%
- Agriculture (Hay/Pasture and Cultivated Crops) - 12.5%
- Water - 11.3%
- Scrub/Herbaceous (Shrub/Scrub and Herbaceous) - 7.7%
- Unclassified - 1.2%
- Barren - 0.3%

¹ Percentages do not total 100 due to rounding of individual values.

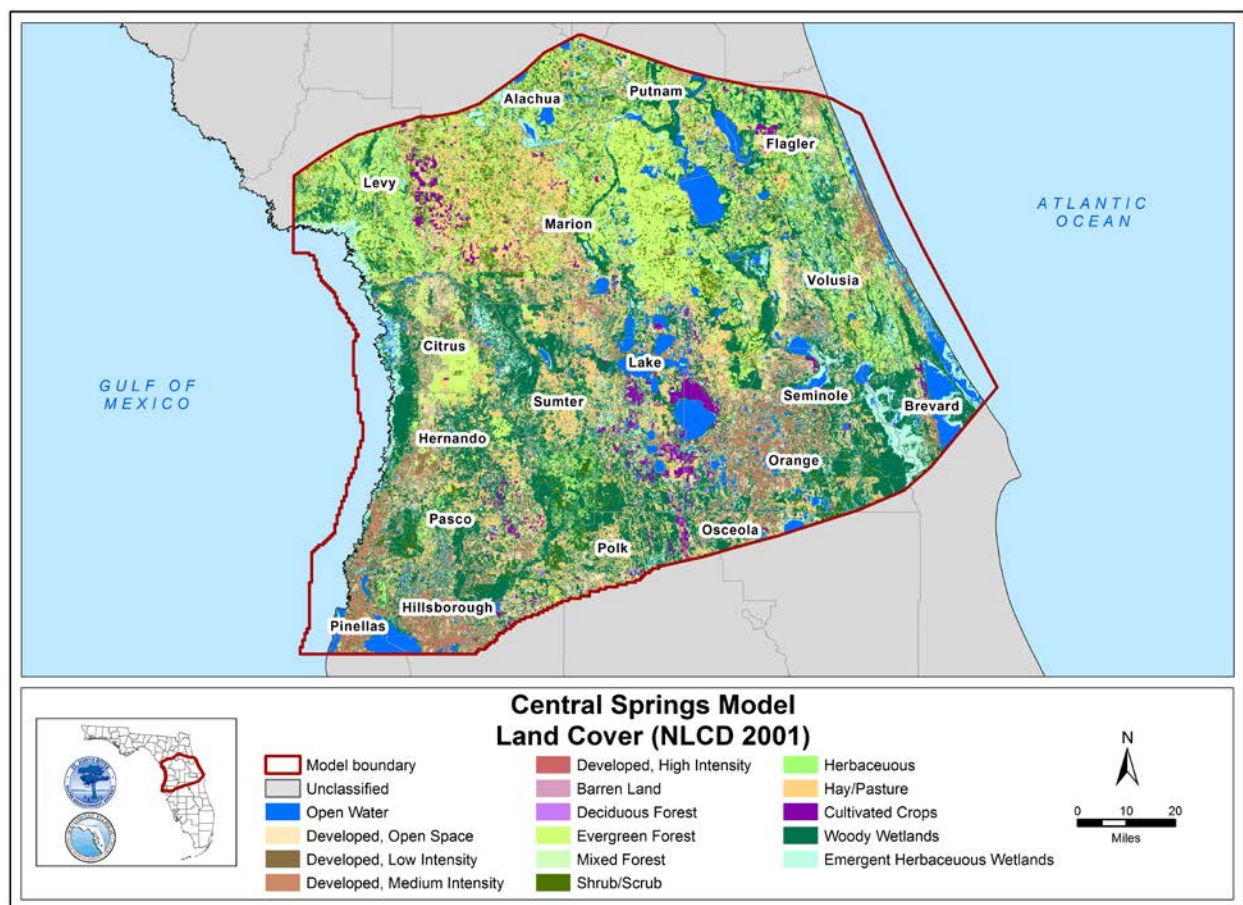


Figure 3-3. Land cover within the Central Springs Model domain (National Land Cover Database 2001)

Water Use

SJRWMD and SWFWMD have individual water use databases that are independently maintained based on information provided by permittees as a condition of their consumptive/water use permits (CUP/WUP). The Districts also maintain water use estimates for non-permitted water consumption, such as withdrawals from domestic private wells and small agricultural and public supply operations that are below permitting thresholds. For the CSM, the water use data from each District between 2005 to 2018 (simulation period) was compiled into a single database and categorized as agricultural (AG), commercial/institutional/industrial (CII), mining/dewatering (MD), domestic self-supply (DSS), landscape/recreational/aesthetic (LRA), and public supply (PS). Water use is summarized by year and type in Table 3-1 and Table 3-2.

The CSM domain extends into adjacent water management districts where the corresponding water use was also incorporated into the model. The SRWMD portion of the domain contributed approximately 1.9 million gallons per day (mgd) and the SWFWMD portion contributed approximately 71.3 mgd of average groundwater withdrawals annually from 2005 to 2018, in addition to the total SJRWMD and SWFWMD withdrawals presented in Table 3-1 and Table 3-2.

Table 3-1. Summary of groundwater withdrawals in the SJRWMD portion of the Central Springs Model domain (million gallons per day)

Year	AG	CII	MD	LRA	PS	DSS	Total
2005	55.6	12.0	9.3	4.1	381.8	38.7	501.5
2006	95.9	12.0	5.8	7.6	414.6	40.0	576.0
2007	72.2	11.8	6.3	5.3	414.7	39.9	550.1
2008	68.6	11.3	5.3	4.6	385.9	37.8	513.4
2009	78.9	11.4	3.9	11.4	363.4	35.2	504.2
2010	95.5	13.2	4.6	12.4	364.4	39.8	529.9
2011	70.5	12.3	4.4	13.8	368.7	38.9	508.6
2012	78.6	11.9	5.0	13.3	359.0	37.1	504.9
2013	74.7	12.5	4.8	12.2	352.6	25.3	482.2
2014	67.9	13.0	5.0	10.1	345.2	26.5	467.7
2015	75.9	13.9	6.0	10.8	352.8	27.3	486.6
2016	78.6	6.9	6.8	9.0	367.6	30.0	498.9
2017	72.3	7.2	6.0	7.5	369.4	28.7	491.1
2018	65.4	7.0	5.2	6.1	356.4	25.3	465.3

Note: AG = agricultural
 CII = commercial/industrial/institutional
 MD = mining/dewatering
 LRA = landscape/recreational/aesthetic
 PS = public supply
 DSS = domestic self-supply

Table 3-2. Summary of groundwater water withdrawals in the SWFWMD portion of the Central Springs Model domain (million gallons per day)

Year	AG	CII_MD	LRA	PS	DSS	Total
2005	42.5	27.4	26.0	206.0	45.7	347.6
2006	72.1	26.2	29.8	240.0	53.4	421.5
2007	68.7	24.4	34.9	224.5	48.2	400.7
2008	50.2	18.6	35.9	190.5	47.3	342.5
2009	66.5	15.0	30.4	192.7	43.4	348.0
2010	60.0	17.7	24.8	194.0	42.0	338.5
2011	46.4	17.0	25.3	190.9	42.2	321.8
2012	58.0	14.1	24.7	182.9	40.4	320.1
2013	48.1	13.6	22.3	189.3	39.1	312.4
2014	42.1	14.9	19.7	174.6	36.4	287.7
2015	38.2	15.8	17.9	188.8	37.7	298.4
2016	38.3	14.7	22.6	196.2	39.3	311.1
2017	42.2	15.4	23.6	195.9	40.8	317.9
2018	41.8	15.1	20.2	191.6	39.0	307.7

Note: AG = agricultural
 CII_MD = commercial/industrial/institutional and mining/dewatering
 LRA = landscape/recreational/aesthetic
 PS = public supply
 DSS = domestic self-supply

HYDROLOGY

(This section is adopted and modified from Appendix C of the HGL 2023 report)

Rainfall

The subtropical climate within the CSM domain is characterized by warm, normally wet summers and mild, dry winters. Maximum temperatures usually exceed 90 degrees Fahrenheit during the summer but may fall below freezing for several days in the winter.

During the summer and early fall, tropical storms and hurricanes can produce substantial rainfall within the project area. Hurricane Wilma in October 2005 and Hurricane Irma in September 2017 passed through the region during the model simulation period, resulting in significant storm rainfall. Winter rainfall is generally associated with large frontal systems that move from the northern latitude southward.

The spatial and temporal distribution of rainfall throughout the simulation period was a key hydrologic parameter that influenced other variables in the model. Rainfall data was sourced from the Next Generation Weather Radar (NEXRAD). For the CSM, NEXRAD data was used to develop rainfall input to the HSPF models, which were used to derive recharge rates and maximum groundwater ET rates for the MODFLOW recharge and ET packages, respectively. The NEXRAD average 2005 to 2018 annual rainfall distribution in the CSM domain is shown on Figure 3-4. The mean annual rainfall for the model domain is 51.3 inches from 2005 to 2018.

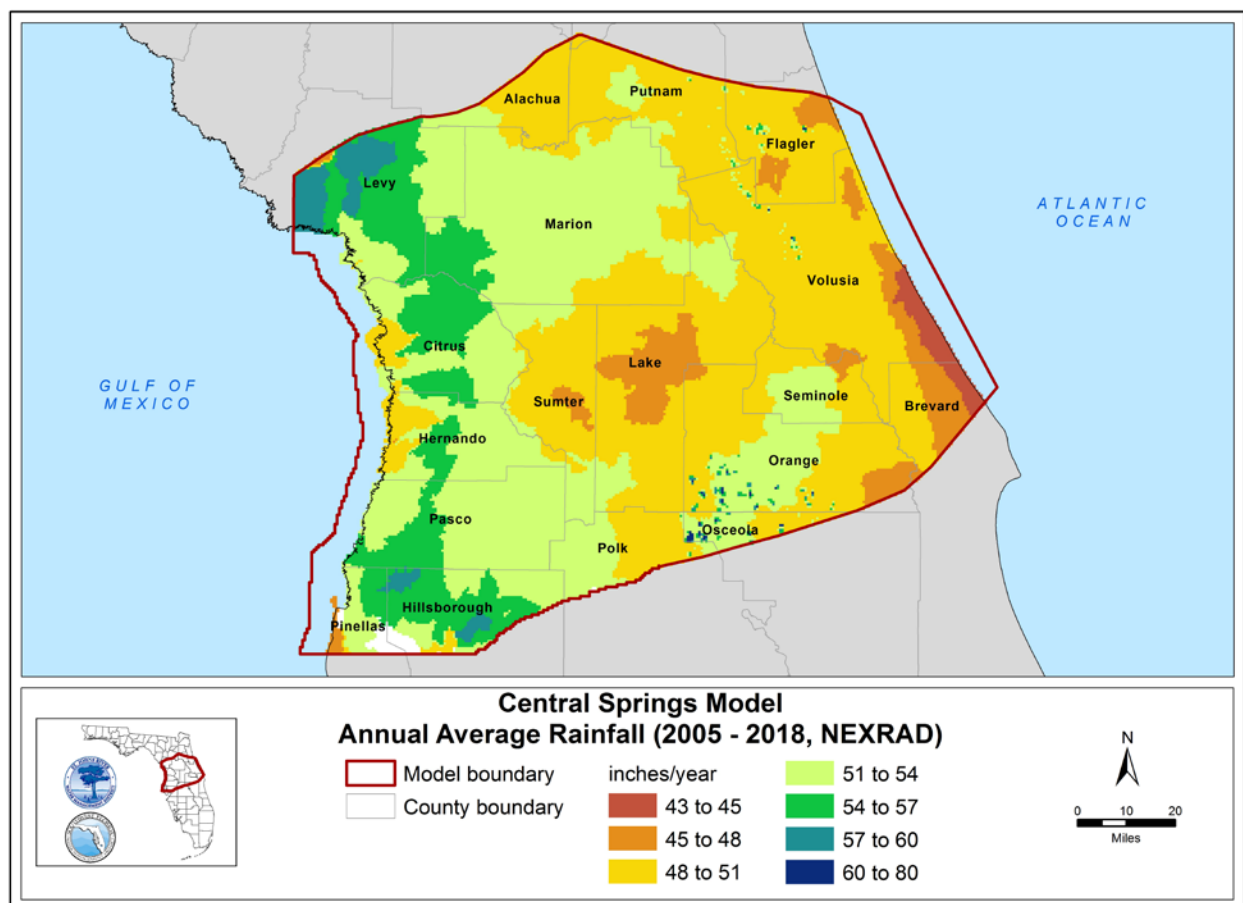


Figure 3-4. Annual average rainfall (2005 to 2018) within the Central Springs Model domain (NEXRAD radar rainfall)

Evapotranspiration

Evapotranspiration is a physical process that represents the combined loss of water through both evaporation from soil and water surfaces and transpiration from plant systems to the atmosphere. Evapotranspiration represents the largest contribution to water loss throughout the model domain. On average, ET represents approximately half to three-quarters of the annual rainfall amount. However, ET can exceed the amount of rainfall during dry periods and for large, open water bodies in the region.

Potential evapotranspiration (PET) is the theoretical maximum rate of ET that could occur from a surface that has unlimited water and is determined by the climate and other environmental factors such as solar radiation, temperature, wind, and humidity. The USGS calculates PET from weather station and satellite data using the insolation-ET algorithm. For this effort, USGS daily PET data from 2005 to 2018 at a 2 kilometer (km) spatial resolution was used as an input to the HSPF models to estimate the actual ET from surface water and groundwater.

Actual evapotranspiration (AET) is the amount of water loss that occurs through ET and is dependent on environmental factors like soil moisture, plant cover, and atmospheric conditions. The monthly AET rate in Florida from 2000 to 2017 was estimated by Sepúlveda (2021) using the Operational Simplified Surface Energy Balance (SSEBop) model with bias-correction based on field measurements at micrometeorological stations. The dataset was used as a qualitative reference in calibrating the AET in the HSPF models. The average annual AET from 2005 to 2017 within the CSM domain is illustrated on Figure 3-5.

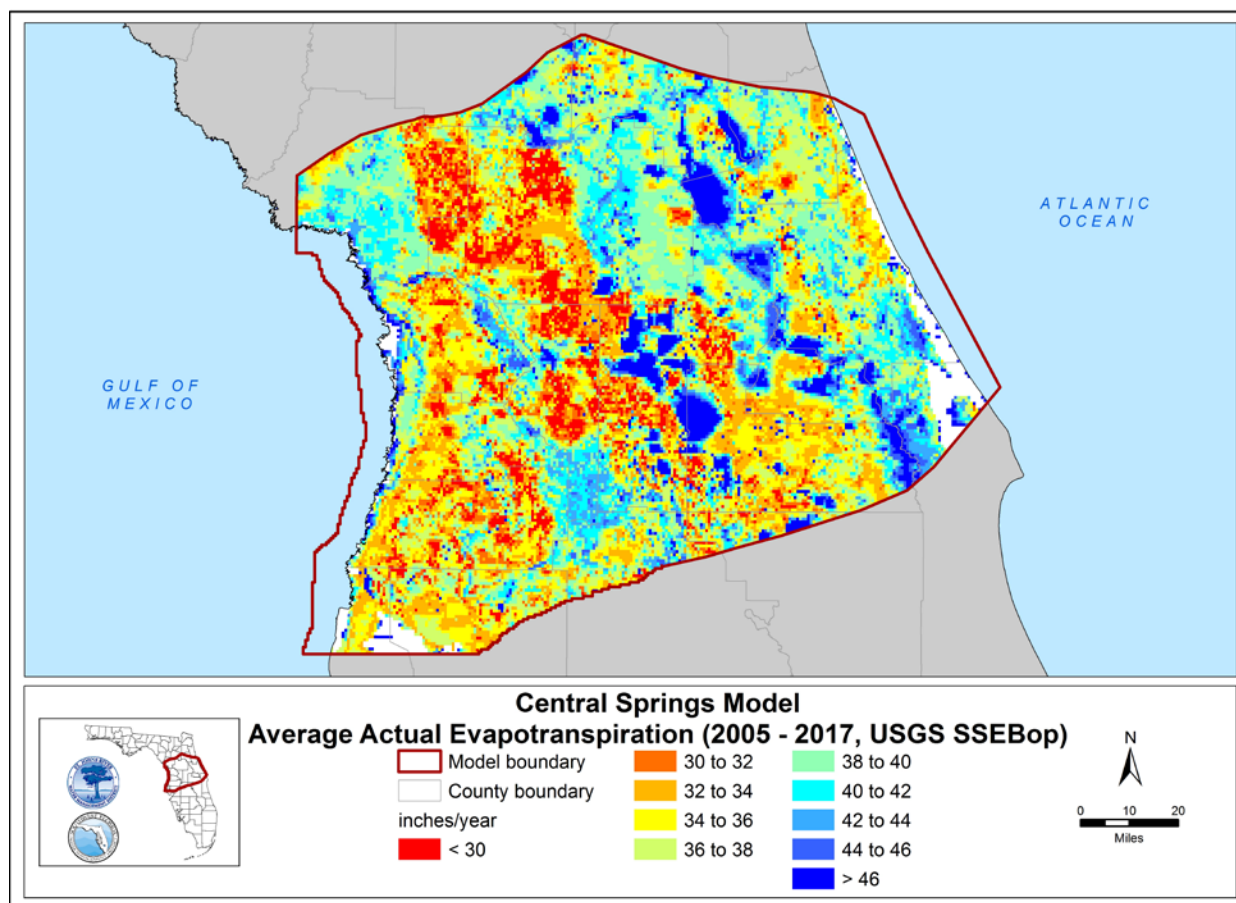


Figure 3-5. Average actual evapotranspiration (2005 to 2017) within the Central Springs Model domain calculated using SSEBop model after bias corrections by the USGS (Sepúlveda, 2021)

Note: SSEBop = Operational Simplified Surface Energy Balance

Rivers

Major rivers in the CSM domain include the St. Johns, Withlacoochee, and Hillsborough (Figure 3-6; FMRI, 1989). The St. Johns River is approximately 310 miles long and flows north from marshy headwaters in the counties of Indian River and Brevard before emptying into the Atlantic Ocean near Jacksonville. Major tributaries to the St. Johns River include the Wekiva, Econlockhatchee, and Ocklawaha rivers. The St. Johns River watershed covers approximately 6,400 square miles in the eastern portion of the model domain.

Headwaters for the Withlacoochee and Hillsborough rivers originate in the Green Swamp in Hernando, Lake, Pasco, Polk, and Sumter counties in the western part of the model area. The Withlacoochee River is approximately 160 miles long and flows north from the Green Swamp before eventually discharging into the Gulf of Mexico near Yankeetown, Florida (Hood et al, 2010). The Withlacoochee River watershed covers approximately 2,100 square miles throughout parts of Citrus, Hernando, Lake, Levy, Marion, Pasco, Polk, and Sumter counties. The Hillsborough River is approximately 54 miles long, drains an area that is approximately 675 square miles, and discharges into Tampa Bay (SWFWMD, 2006). Flow in both the upper and lower reaches of the Hillsborough River is partially derived from spring discharges.

Lakes

Many natural lakes within the model domain are sinkhole lakes, which result from depressions that occur due to the collapse of cavities in the limestone of the underlying UFA. Resistance to downward vertical leakage due to the presence of the ICU helps to retain water in the depressions, forming lakes. Large numbers of sinkhole lakes are found in central Florida and the surrounding area. The location of major lakes is shown on Figure 3-6 (FDEP, 2002). Sinkhole lakes can act as sources of relatively concentrated recharge to the underlying UFA in recharge areas. Leakage rates through these lakes to the UFA are often enhanced by the development of fractures or thinning of the ICU during sinkhole formation.

A potentiometric high is formed along the Lake Wales Ridge in Polk County where recharge rates are enhanced by vertical leakage from numerous sinkhole lakes. This potentiometric high is centered near Polk City and extends south-southeast along the center of the state, forming a hydrologically important feature of the FAS. Many relict sinkhole lakes are prevalent in the Winter Haven Ridge and Lake Wales Ridge areas. Other relict sinkhole lakes occur in the Orlando area, where the UFA is semi-confined. Large lakes, such as Tsala-Apopka in Citrus County, are directly connected to the unconfined UFA, with a lake stage close to the level of the potentiometric surface of the UFA.

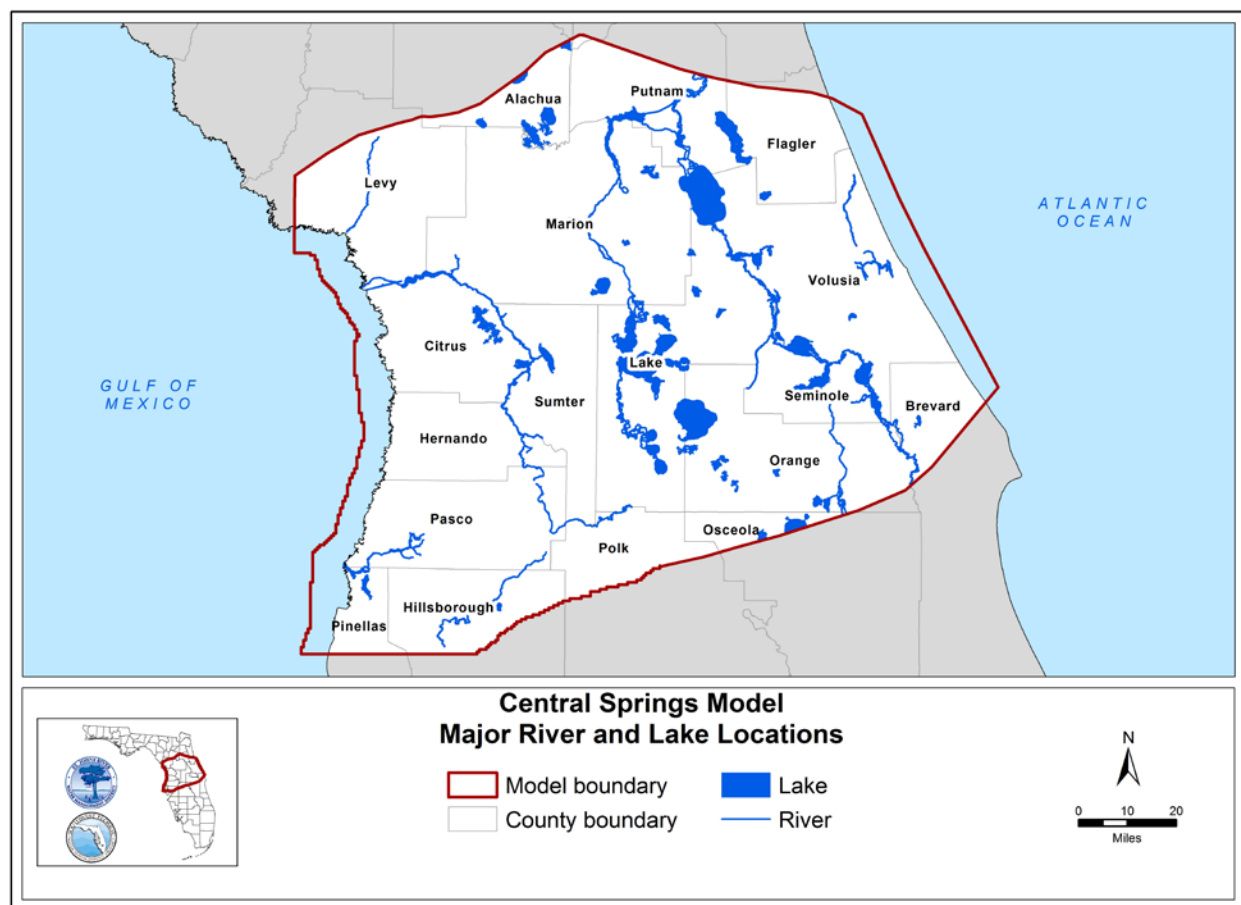


Figure 3-6. Major rivers and lakes within in the Central Springs Model domain (FMRI, 1989 and FDEP, 2002)

Wetlands

Wetlands are shown on Figure 3-7. There are two main types of wetlands in the project area, including isolated wetlands and riverine wetlands connected to river systems. Isolated wetlands consist of cypress wetlands or shallow wet prairie marshes. Riverine wetlands are located within the flood plains of rivers and creeks and generally consist of wetland hardwood forests. The Green Swamp is the largest region of wetlands within the model domain and consists of a largely undeveloped system of cypress domes, hardwood forests, and wet prairies.

Wetlands are related to the hydrogeology of the groundwater system in several ways. In recharge areas, flat terrain decreases surface runoff. If the UFA is confined, vertical leakage to the underlying groundwater system will also be impeded, causing wetlands to form. Swamps can also form in recharge areas where the UFA is unconfined if vertical and horizontal hydraulic conductivities are low.

Wetlands can form in coastal discharge zones where the UFA is unconfined and the potentiometric surface elevation is above land surface. This creates artesian discharge to relatively flat land and results in the pooling of the discharged water onto the land surface, resulting in swamp formation.

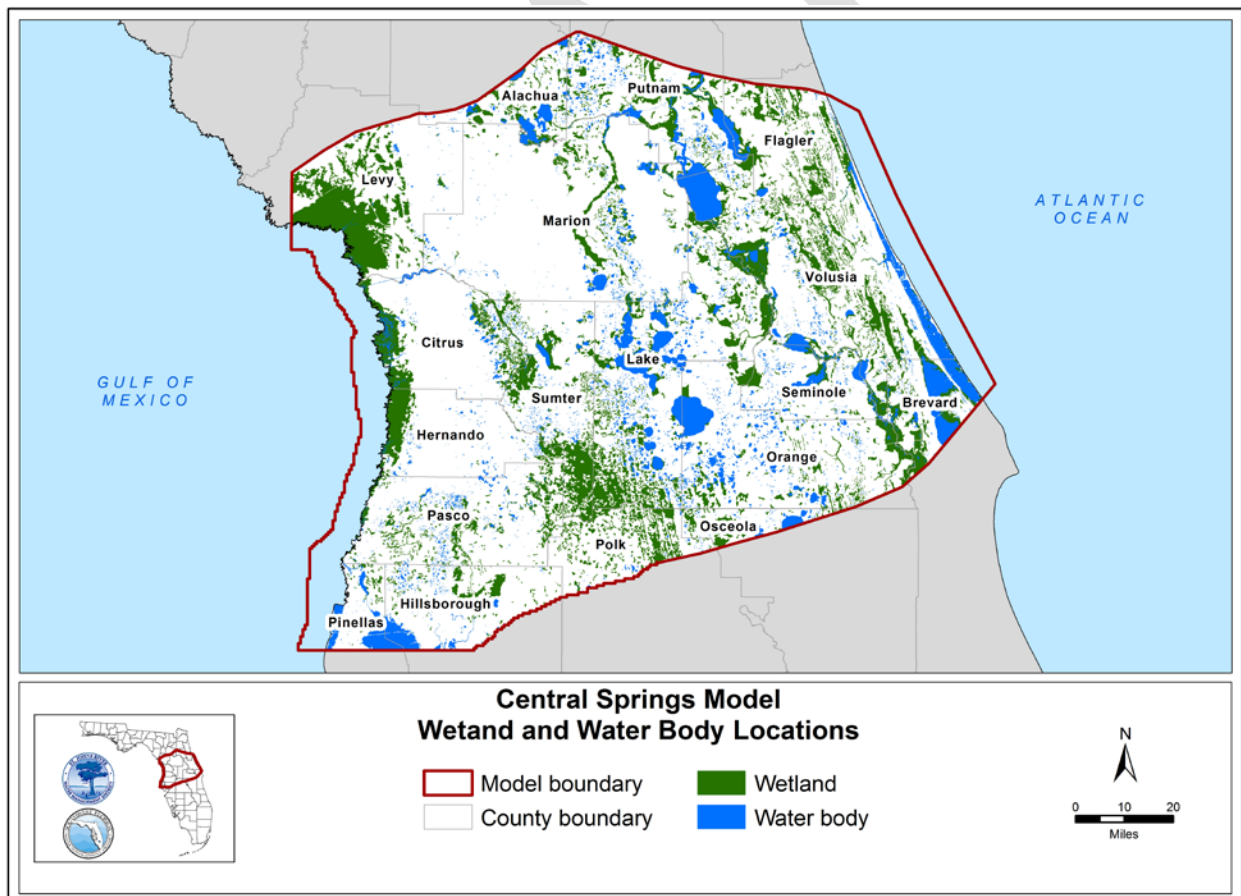


Figure 3-7. Wetlands and other water bodies within the Central Springs Model domain (Wetlands USGS 100k topo)

REGIONAL HYDROSTRATIGRAPHY

(This section is adopted and modified from Appendix B of the HGL 2023 report)

Hydrogeologic Framework

As described in Chapter 2, the conceptualized regional hydrogeologic framework generally follows the hydrogeologic units described by Miller (1986a), Arthur et al. (2005), and Copeland et al. (2010) and includes the SAS, ICU, UFA, MCU I, MCU II, and the LFA. These units are shown in descending order on Figure 3-8. The lithology of each formation is provided in Table 3-3.

Table 3-3. Stratigraphy and generalized lithology of the geologic units within the Central Springs Model domain

System	Series	Formation/Group	Lithology
Quaternary	Holocene and Pliocene	Undifferentiated	Sand and clay
Tertiary	Miocene	Hawthorn Group	Clay, sand, and carbonate
	Oligocene	Suwannee Limestone	Limestone
	Eocene	Ocala Limestone	Limestone
		Avon Park Formation	Dolostone, limestone, and some gypsum
		Oldsmar Formation	Limestone, dolostone, and some gypsum
	Paleocene	Cedar Keys Formation	Limestone, dolostone, and gypsum

Series/Stage		Formation	Aquifers				
			West-central Florida	Southwest Florida	East-central Florida	Hydrogeologic Unit	
Holocene to Pliocene		Undifferentiated	Surficial Aquifer				
Miocene		Hawthorn Group	Intermediate Confining Unit				
		Tampa Limestone (where present)	Upper Floridan			Suwannee Ocala Permeable Zone (SWOCpz)	
Oligocene	Suwannee Limestone						
Eocene	Late	Ocala Limestone					Ocala Avon Park Low Permeable Zone (OCAPlpz)
	Middle	Avon Park Formation					Avon Park Permeable Zone (APpz)
			Middle Confining Unit	Middle Semiconfining Unit	Middle Confining Unit I		
	Early	Oldsmar Formation	Lower Floridan				
Paleocene		Cedar Keys Formation	Sub-Floridan Confining Unit				

Figure 3-8. Regional hydrogeologic framework within the Central Springs Model domain (HGL, 2023)

Surficial Aquifer System

The SAS is conceptualized as a near-surface permeable unit that is either continuously or intermittently saturated with rainfall recharge. The SAS is present in the southern and eastern portions of the project area and is comprised of undifferentiated sands and clays of Pleistocene/Pliocene age. Where the SAS is continuously saturated, it is assumed to be underlain by the less permeable Miocene or late Pliocene soils of the ICU. Soils in the SAS may be dry in areas where the ICU is absent or where the ICU is sufficiently altered through karst activity that results in effective leakage to the underlying UFA.

Intermediate Confining Unit

The ICU is predominantly comprised of interbedded clays, shells, and sands of the Miocene age Hawthorn Group. Areas where the ICU is sufficiently thick corresponds to areas of a semi-confined UFA recharge region. The effective leakage of the ICU is likely to be much higher in areas where active karst activity occurs. The ICU is assumed to be absent or provide little-to-no confinement in karst terrain found in the counties of Citrus, Hernando, Levy, western and central Marion, and most of the northern portion of Sumter, where the hydraulic head difference between the water level in the SAS (if present) and the UFA is less than 0.5 ft. There are two areas within the model domain where the demarcation between the confined and unconfined regions is uncertain: central Hernando County over the Brooksville Ridge and a region covering south-central Marion, northwestern Lake, and northeastern Sumter counties.

Upper Floridan Aquifer

The UFA within the CSM domain is comprised of the Suwannee Limestone (Oligocene), Ocala Limestone (Eocene), and the upper portion of the Avon Park Formation (Eocene). Most groundwater extraction within the model domain occurs from the UFA. The UFA is conceptualized as consisting of three flow zones (layers) with different hydraulic properties: SWOCpz, OCAPlpz, and APpz.

The Suwannee Limestone is found within the southwestern portion of the model domain and is comprised of Oligocene age rocks. The absence of the Suwannee Limestone over most of the model domain is likely the result of chemical and physical erosion during a period of karstification at the end of the Oligocene (Miller, 1986).

The Eocene age rocks within the UFA include the Ocala Limestone (youngest) and the Avon Park Formation (oldest). The Ocala Limestone is absent in parts of Levy and Citrus counties to the west, and in parts of Lake, Seminole, Volusia, Orange, and Osceola counties to the east. The absence of the Ocala Limestone is likely the result of chemical and physical erosion during the period of karstification at the end of the Oligocene after removal of the overlying Suwannee Limestone (Miller, 1986).

The Avon Park Formation was deposited during the Eocene and has varying lithology throughout the model domain. In the western portion of the project area, the Avon Park Formation is mainly a dolostone with scattered gypsum nodules in its lower section (Miller, 1986; Hickey, 1990). The formation has also been observed to contain both dolostone and limestone without gypsum in the northwest portion of Marion County (Janosik, 2011). The Avon Park Formation was initially deposited as a limestone with numerous interbedded peat

layers, with subsequent dolomitization and diagenetic alteration during the Oligocene (Randazzo, 1997). A relatively thick section of fractured, crystalline dolostone occurs in the upper part of the Avon Park Formation above the scattered gypsum nodules in the southwestern part of the project area (Wolansky et al., 1980; Hickey, 1982). Fractured crystalline dolostones are reported to occur in the upper and lower parts of the Avon Park Formation in the eastern part of the project area (O'Reilly et al., 2002).

Middle Confining Units

Two confining units, described by Miller (1986) as MCU I and MCU II, occur within the Avon Park Formation and separate the UFA and LFA (Figure 3-9 and Figure 3-10). The MCU I occurs in the eastern part of the model area and consists of shallower, soft, fine-grained limestones of moderate-to-low permeability without the presence of gypsum nodules. The MCU II occurs in the western part of the model area and consists of deeper, hard gypsiferous dolostone of very low permeability that is hundreds of feet thick.

The units are vertically offset, with MCU I slightly higher in elevation than MCU II. The lateral extents of MCU I and MCU II overlap in parts of Marion, Sumter, and Lake counties; however, the exact location of this overlap is still ambiguous in many areas.

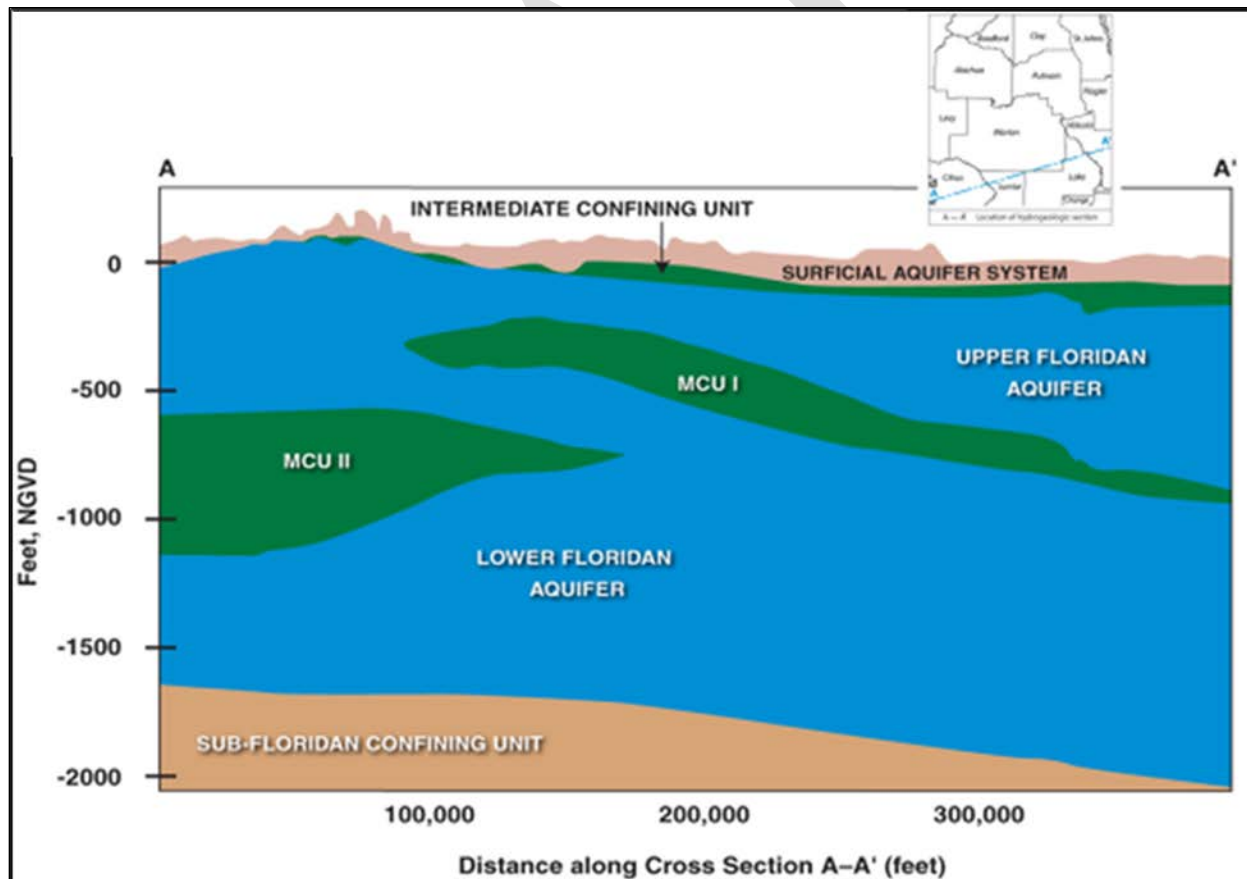


Figure 3-9. Cross-section showing the transition between Middle Confining Units I and II (HGL, 2023)

Note: NGVD = National Geodetic Vertical Datum of 1929

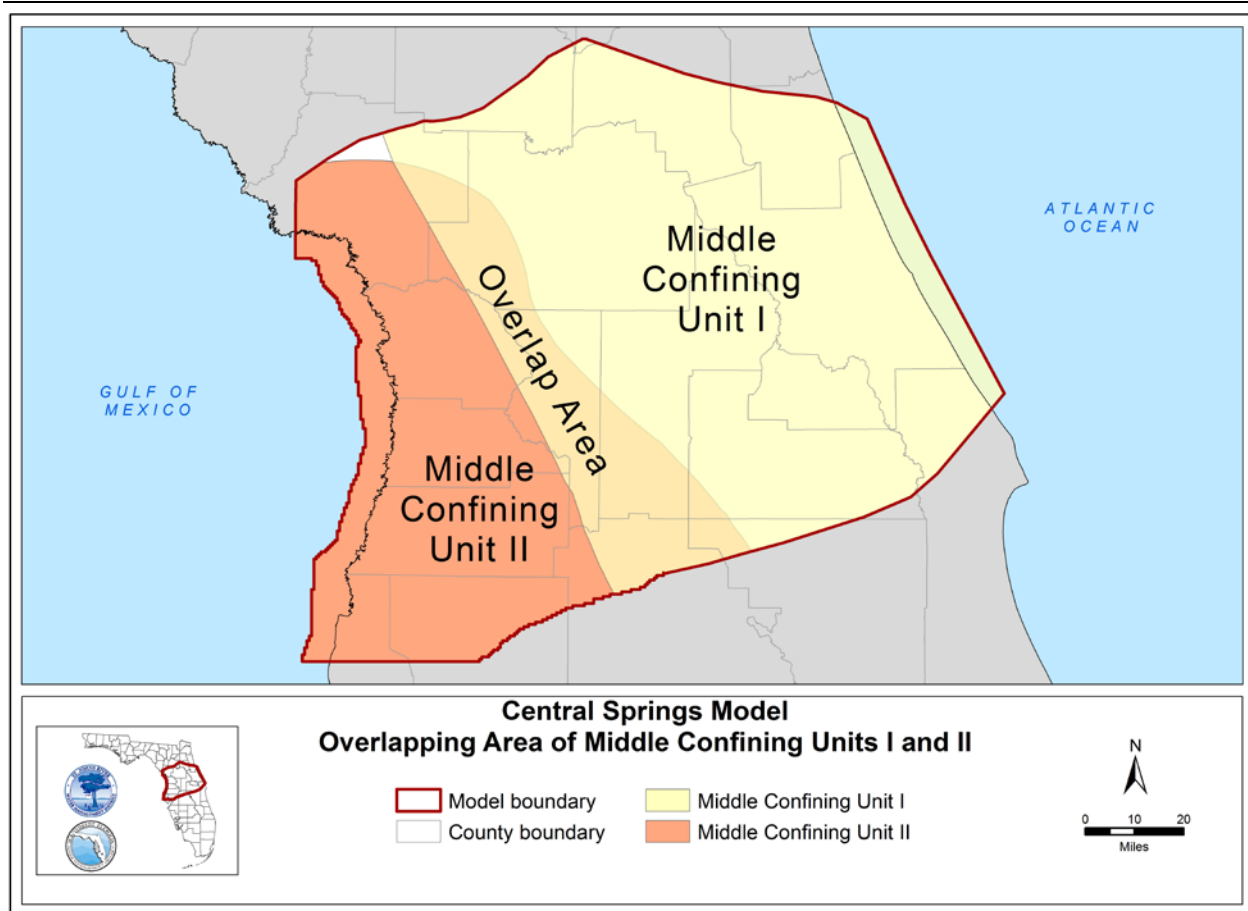


Figure 3-10. Overlapping area of Middle Confining Units I and II (HGL, 2023)

Note: There is an area in the northwestern portion of the model domain where both Middle Confining Units I and II are absent (Miller, 1986).

Lower Floridan Aquifer

The top of the LFA consists of the lower part of the Avon Park Formation and the Oldsmar Formation (Figure 3-8). The base of the LFA is the Cedar Keys Formation (Miller, 1986a). The Oldsmar Formation and Cedar Keys Formation are present only in the subsurface. The Oldsmar Formation in the western part of the project area is composed of both limestone and dolostone and contains scattered gypsum nodules and brines (Hickey, 1982; 1990; Miller, 1986; and Randazzo, in Geology of Florida, 1997). However, in the north-central part of the project area, the Oldsmar Formation is likely a fractured, crystalline dolostone (Janosik, 2011). The Cedar Keys Formation is mainly composed of dolostone and contains brine within gypsum and anhydrite beds throughout the project area (Janosik, 2011; Hickey and Wilson, 1982; Miller, 1986a).

Layer Thickness

The CSM is discretized into seven vertical layers, with each layer representing hydrostratigraphic units of similar hydraulic properties. Where MCU I and MCU II overlay, the LFA is subjacent to the MCU I and superjacent to the eastern edge of MCU II (Figure 3-9). Therefore, in the overlap area, lateral flow can occur to or from the UFA through the LFA. A visual representation and description of the seven model layers are provided on Figure 3-11.

Layer No	SWFWMD		SJRWMD
1	Surficial Sand/Aquifer		Surficial Aquifer
2	Thin Layer Upper Floridan Aquifer/Intermediate Confining Unit*		Intermediate Confining Unit
3	Suwannee Limestone/Thin Layer Upper Floridan Aquifer**		Suwannee/Ocala Limestone
4	Ocala Limestone/Avon Park Formation - upper		Ocala Limestone/Avon Park Formation - upper
5	Avon Park Form.	Middle Confining Unit I	Middle Confining Unit I
6	Avon Park Formation – middle & bottom	Lower Floridan Aquifer I	Lower Floridan Aquifer I
7	Middle Confining Unit (MCU) II		MCU II Lower Floridan Aquifer I

Figure 3-11. Visual representation and description of the layers in the Central Springs Model

* Where the UFA is regionally unconfined, the ICU is converted to a thin limestone layer.

** Where the Suwannee Limestone is absent, layer 3 was converted to a thin limestone layer.

The thickness of model layers varies based on the geospatial position and the hydrogeologic unit that a layer represents. A compilation of layer thickness data from investigative reports and previous models was compared during model development. Thicknesses compiled in USGS professional paper 1807 (Williams and Kuniansky, 2016) and USGS data series 926 (Williams and Dixon, 2015) were used with modifications based on data utilized for the NDM. The thicknesses of the SAS (layer 1) and ICU (layer 2) were taken from the USGS database. The UFA (layer 3 and layer 4) was mostly based on thicknesses from the NDM with smoothing using a 5 by 5 grid moving window. The thickness of MCU I in layer 5 was taken from the USGS database. The thickness of the LFA below MCU I in layer 6 was based on the previous NDM conceptualization. The thickness of MCU II in layer 7 was based on data available from the USGS. The refined thickness and top elevations in the CSM were compared with the USGS report to ensure values were similar to the hydrogeologic conceptualization. The areal distribution of layer thicknesses is depicted on Figure 3-12 through Figure 3-18.

The top and bottom elevations of each layer were calculated after the thickness of each layer was determined. The top elevation of layer 1, which was based on the USGS 10-meter DEM, is represented on Figure 3-19. The top elevations of layer 2 to layer 7 and the bottom elevation of layer 7, as shown on Figure 3-20 to Figure 3-26, were calculated from the top elevation and thickness of each layer.

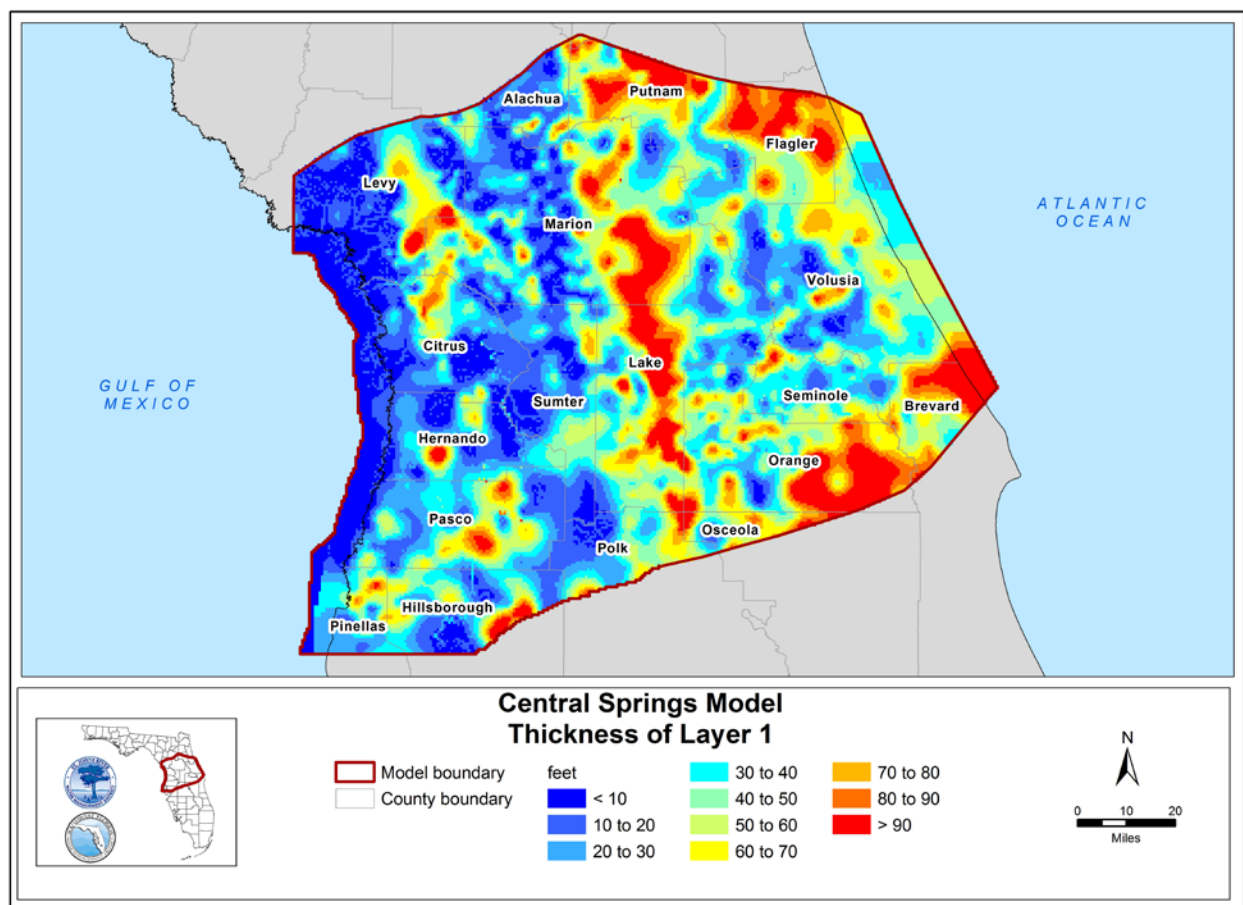


Figure 3-12. Thickness of layer 1 within the Central Springs Model domain

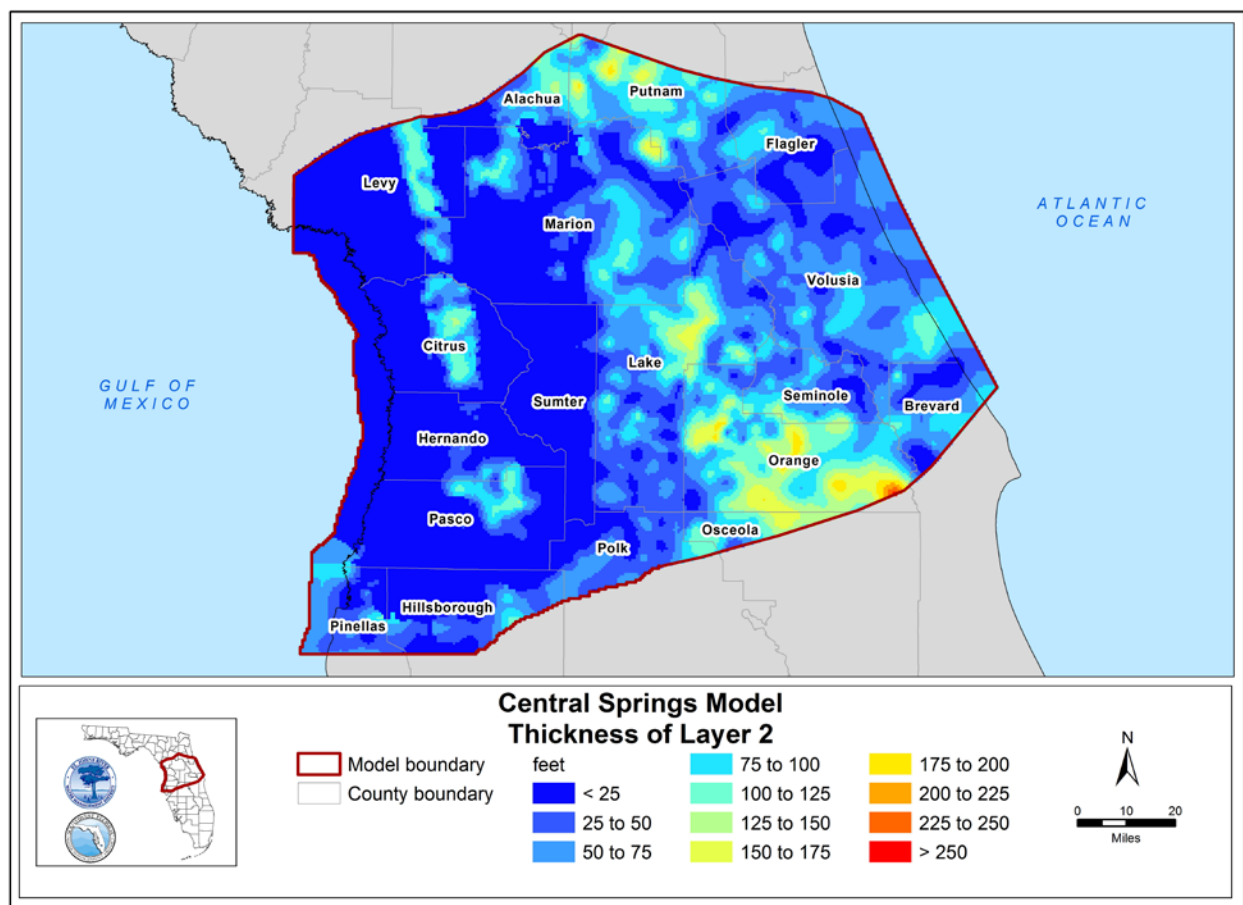


Figure 3-13. Thickness of layer 2 within the Central Springs Model domain

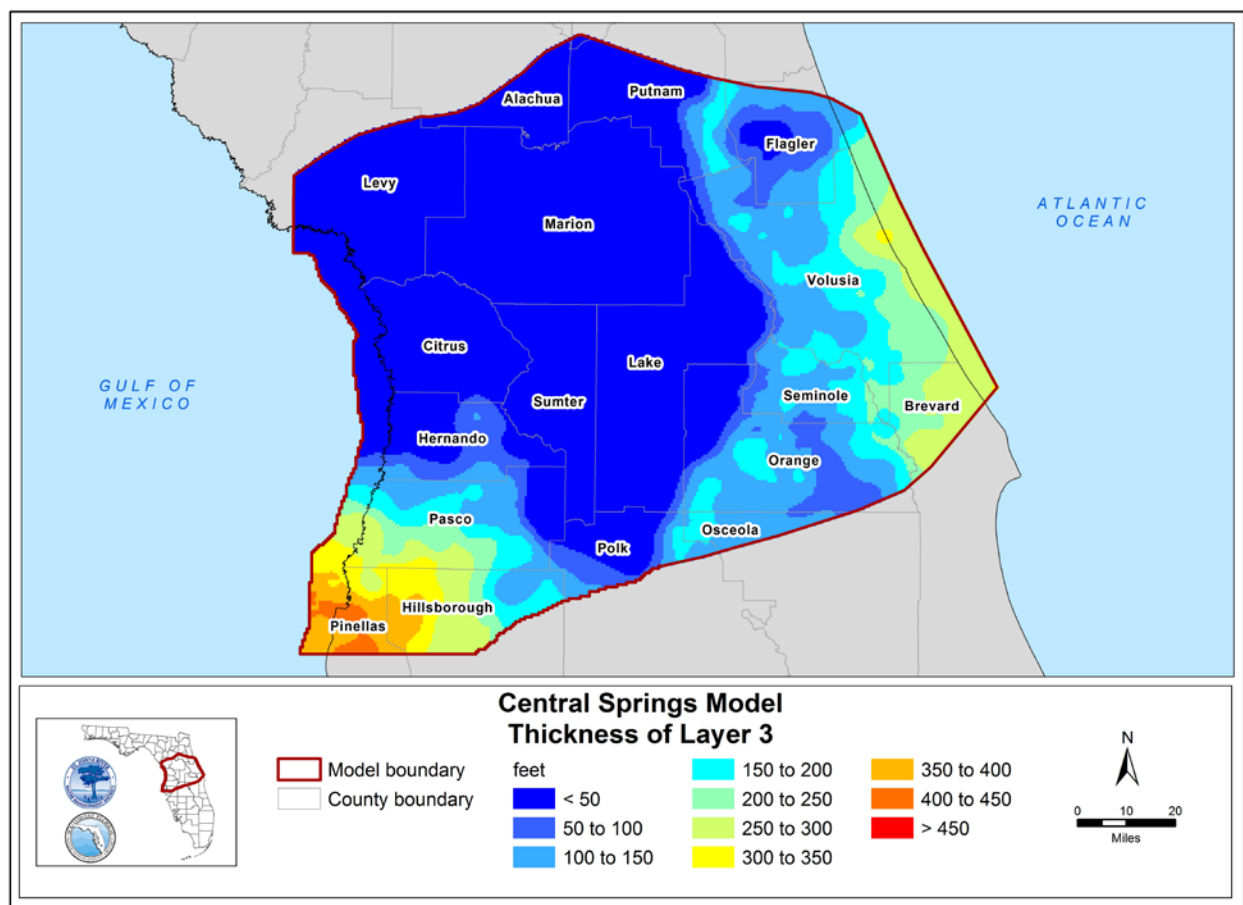


Figure 3-14. Thickness of layer 3 within the Central Springs Model domain

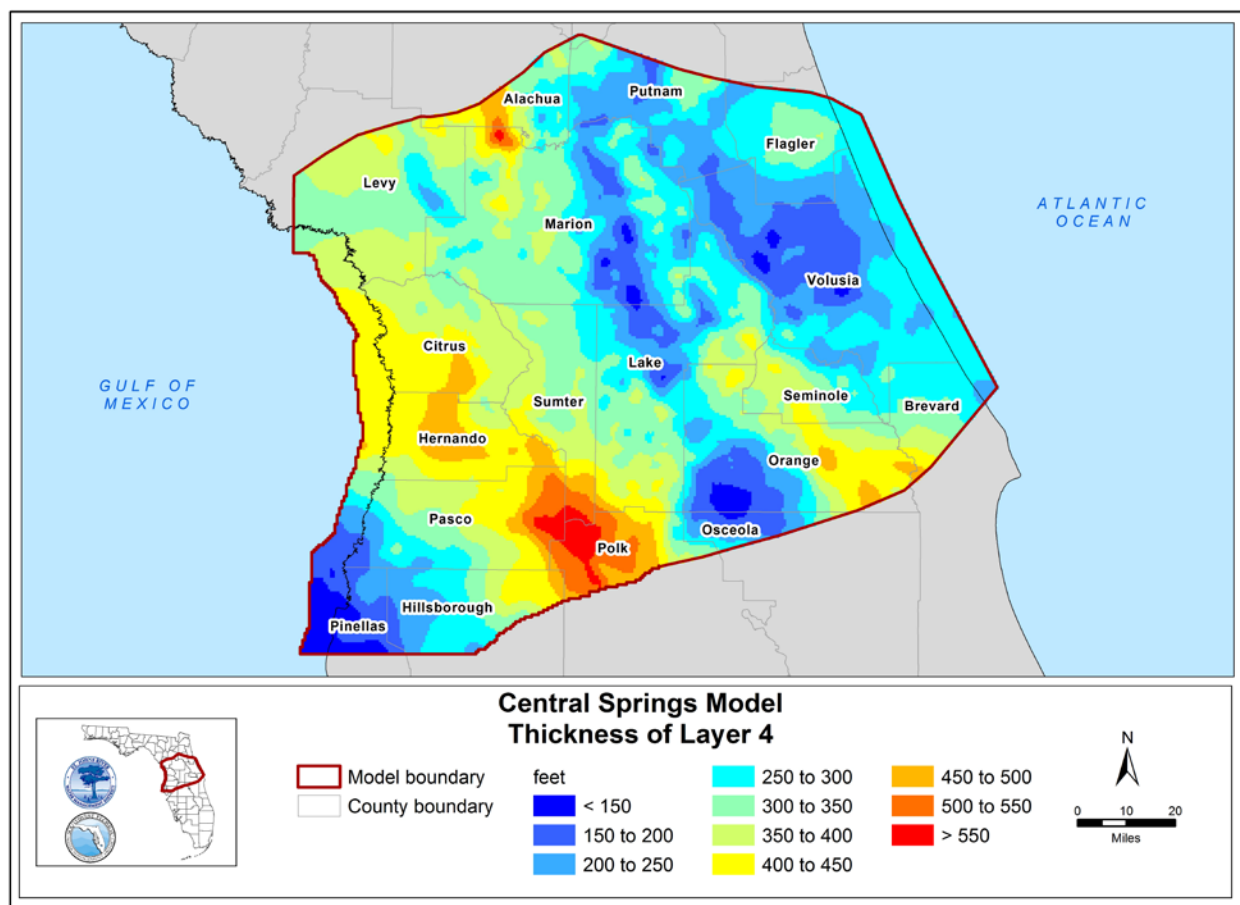


Figure 3-15. Thickness of layer 4 within the Central Springs Model domain

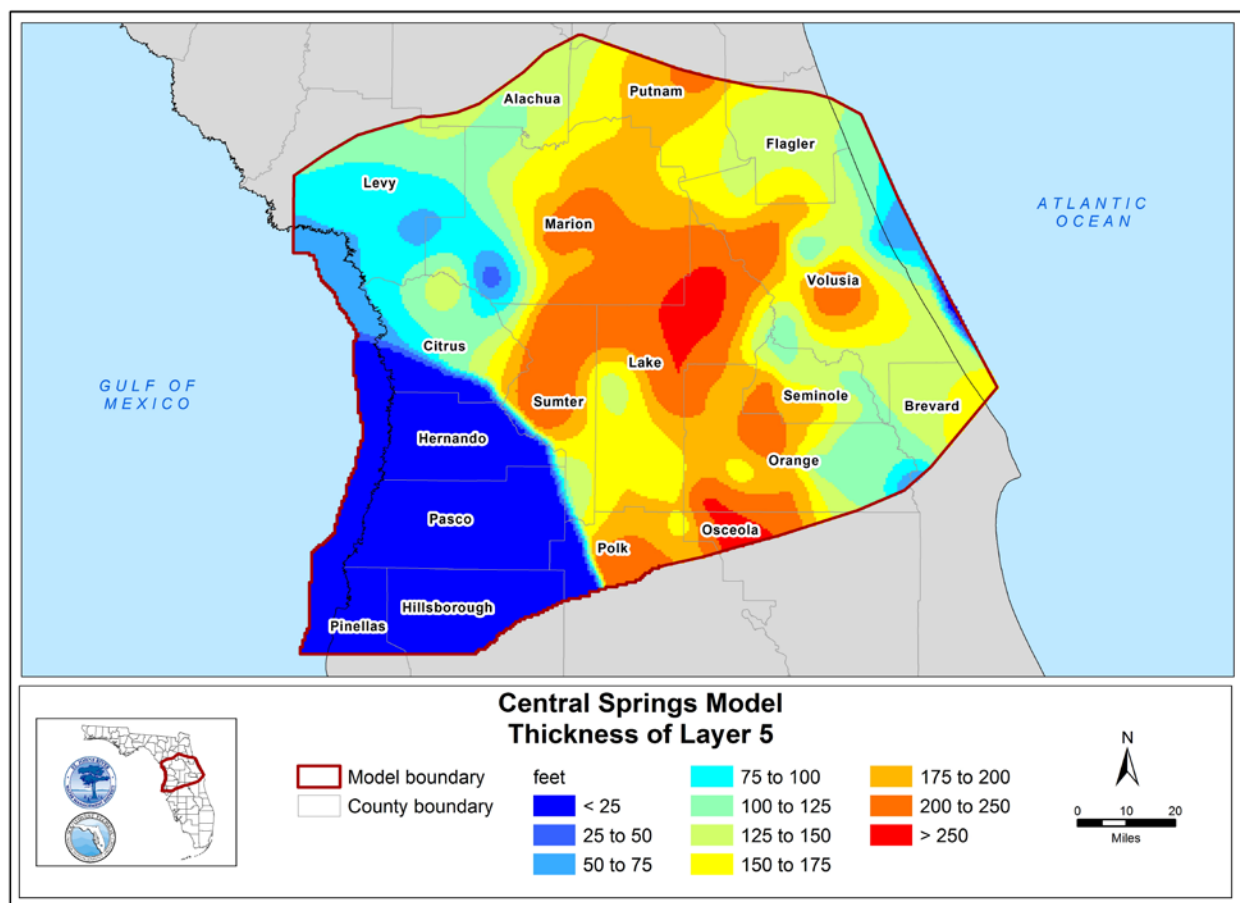


Figure 3-16. Thickness of layer 5 within the Central Springs Model domain

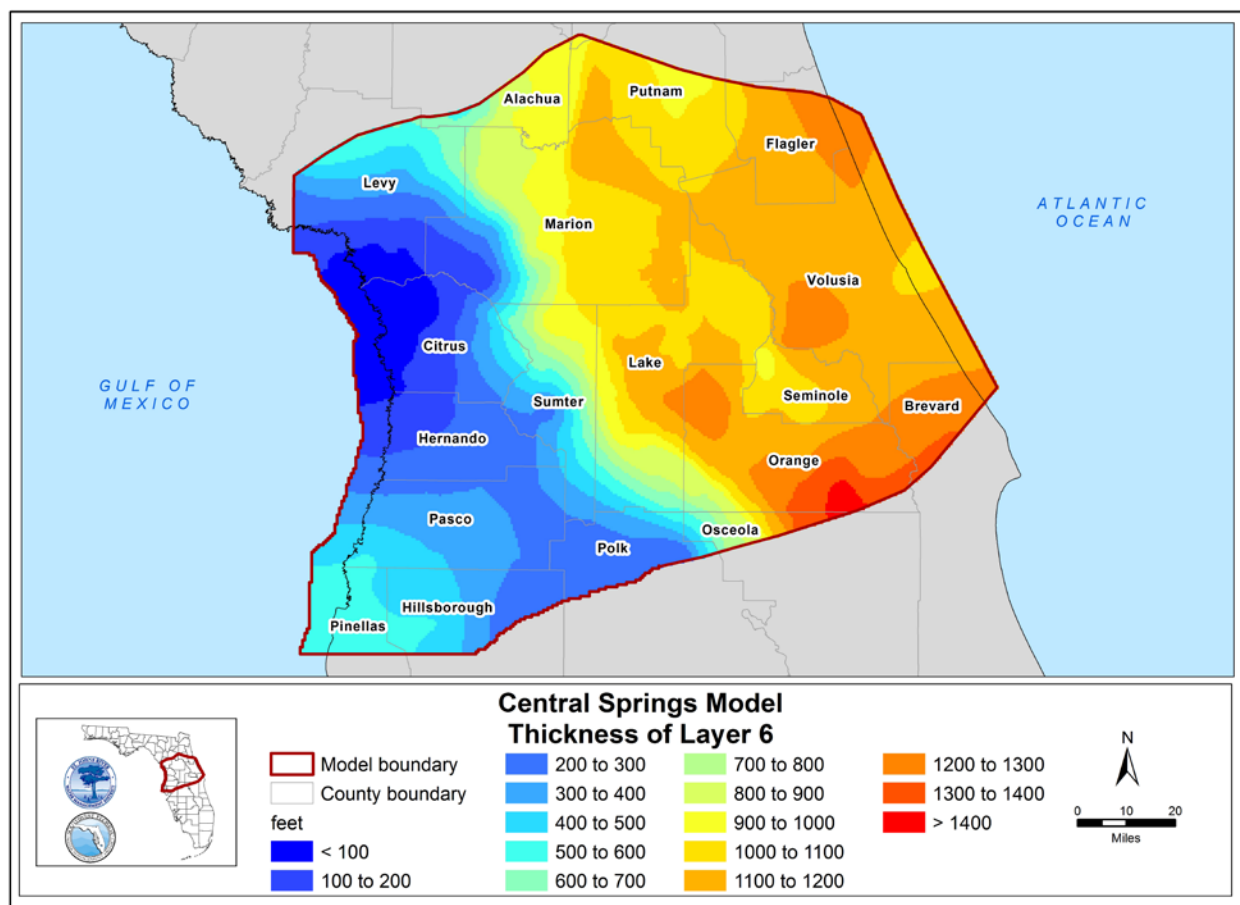


Figure 3-17. Thickness of layer 6 within the Central Springs Model domain

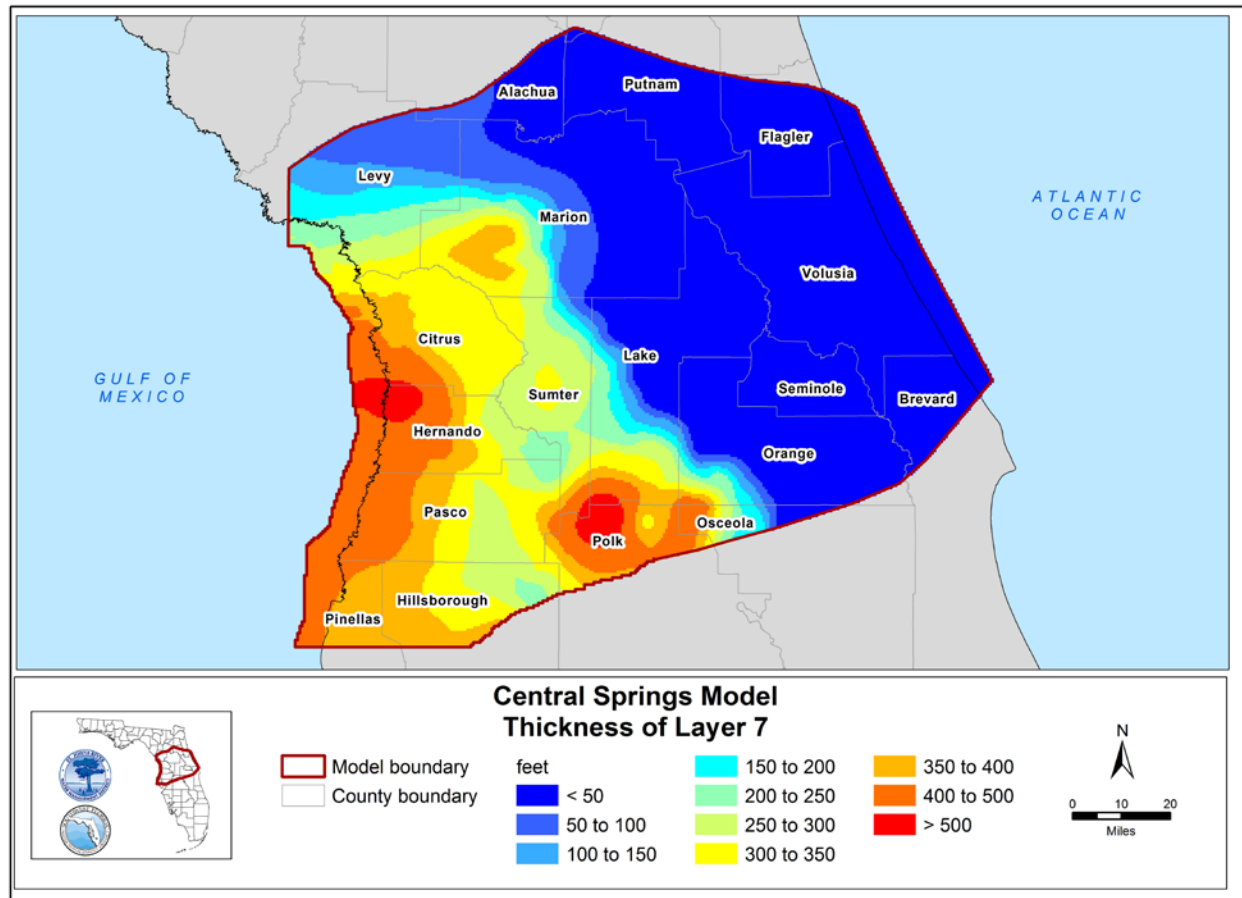


Figure 3-18. Thickness of layer 7 within the Central Springs Model domain

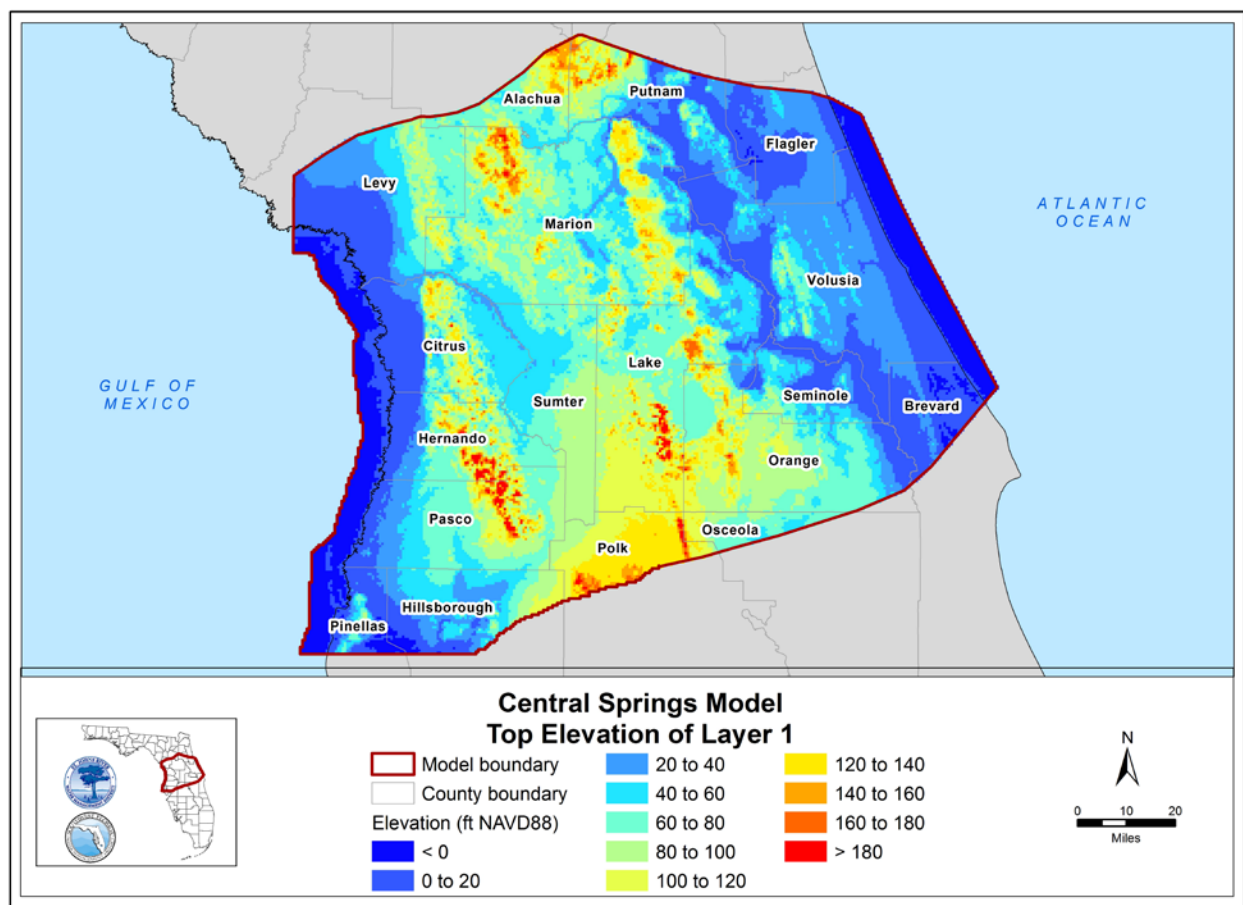


Figure 3-19. Top elevation of layer 1 within the Central Springs Model domain (ft NAVD88)

Note: ft NAVD88 = feet relative to the North American Vertical Datum of 1988

Note: ft NAVD88 = feet relative to the North American Vertical Datum of 1988

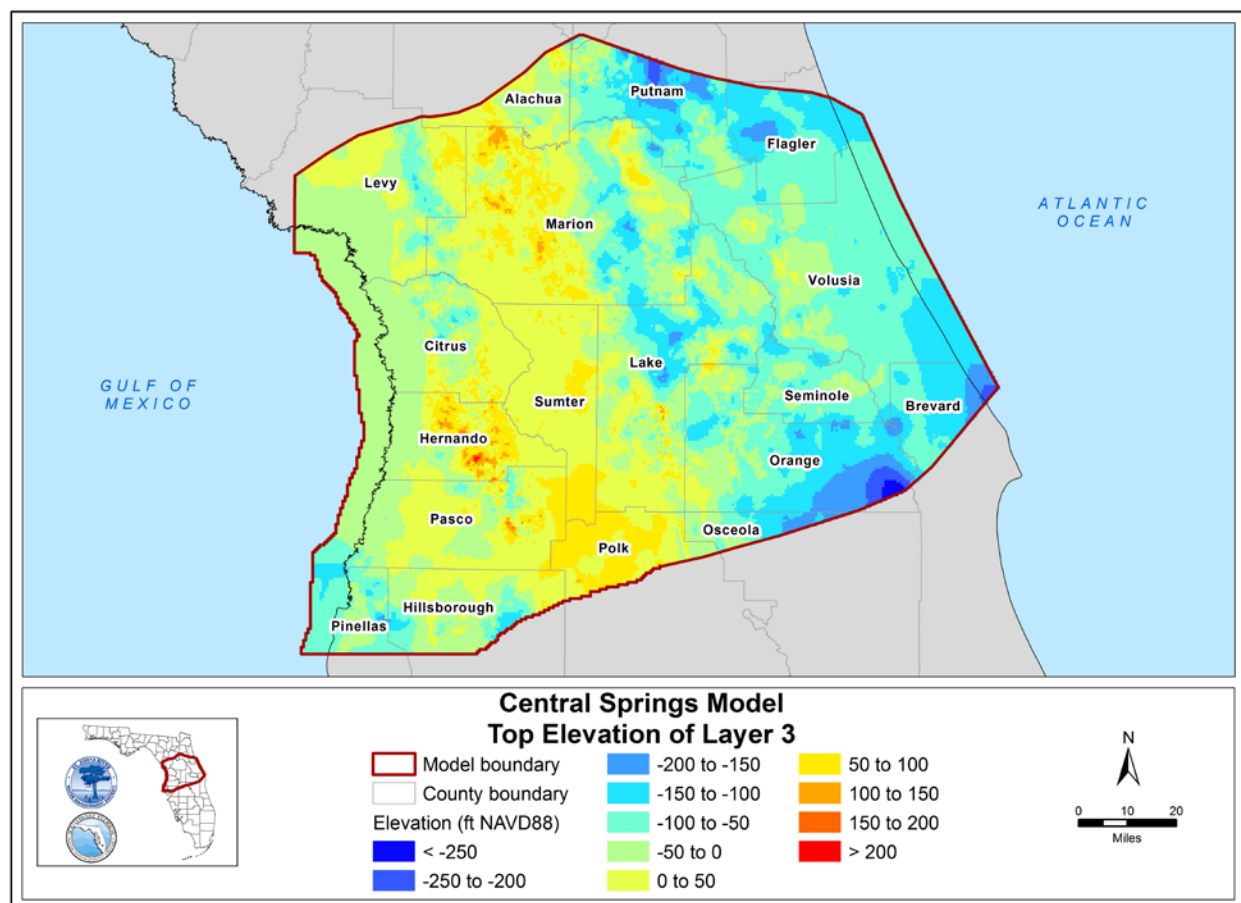


Figure 3-21. Top elevation of layer 3 within the Central Springs Model domain (ft NAVD88)

Note: ft NAVD88 = feet relative to the North American Vertical Datum of 1988

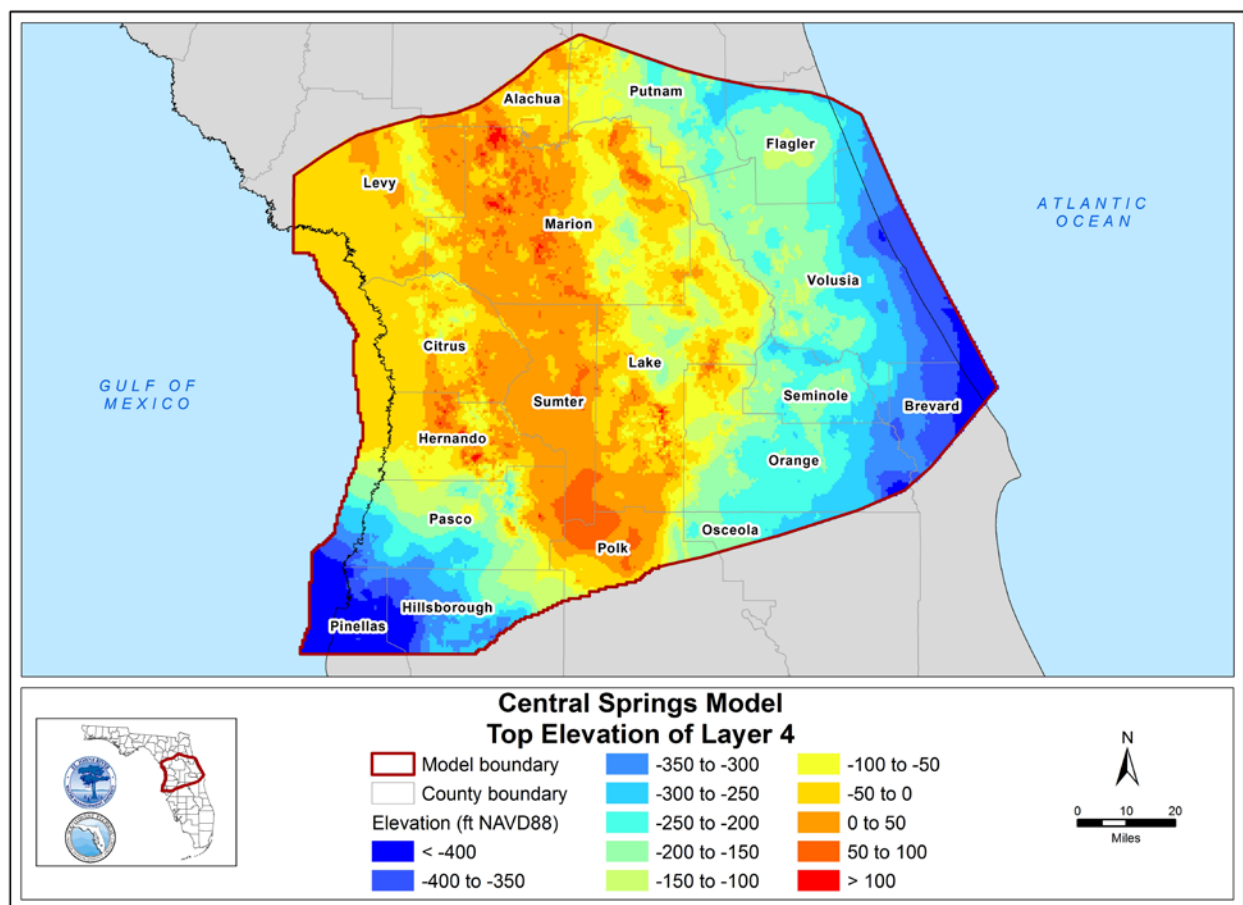


Figure 3-22. Top elevation of layer 4 within the Central Springs Model domain (ft NAVD88)

Note: ft NAVD88 = feet relative to the North American Vertical Datum of 1988

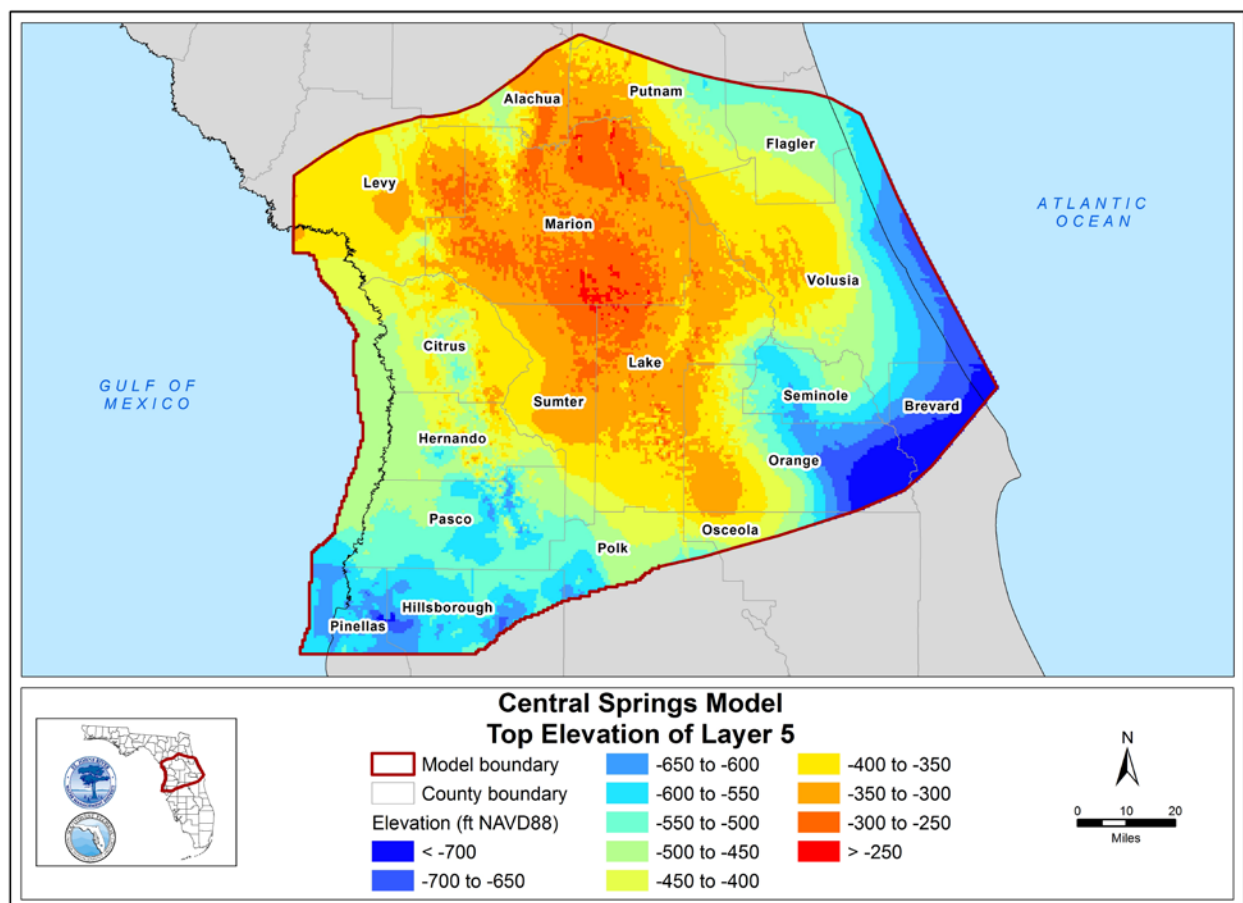


Figure 3-23. Top elevation of layer 5 within the Central Springs Model domain (ft NAVD88)

Note: ft NAVD88 = feet relative to the North American Vertical Datum of 1988

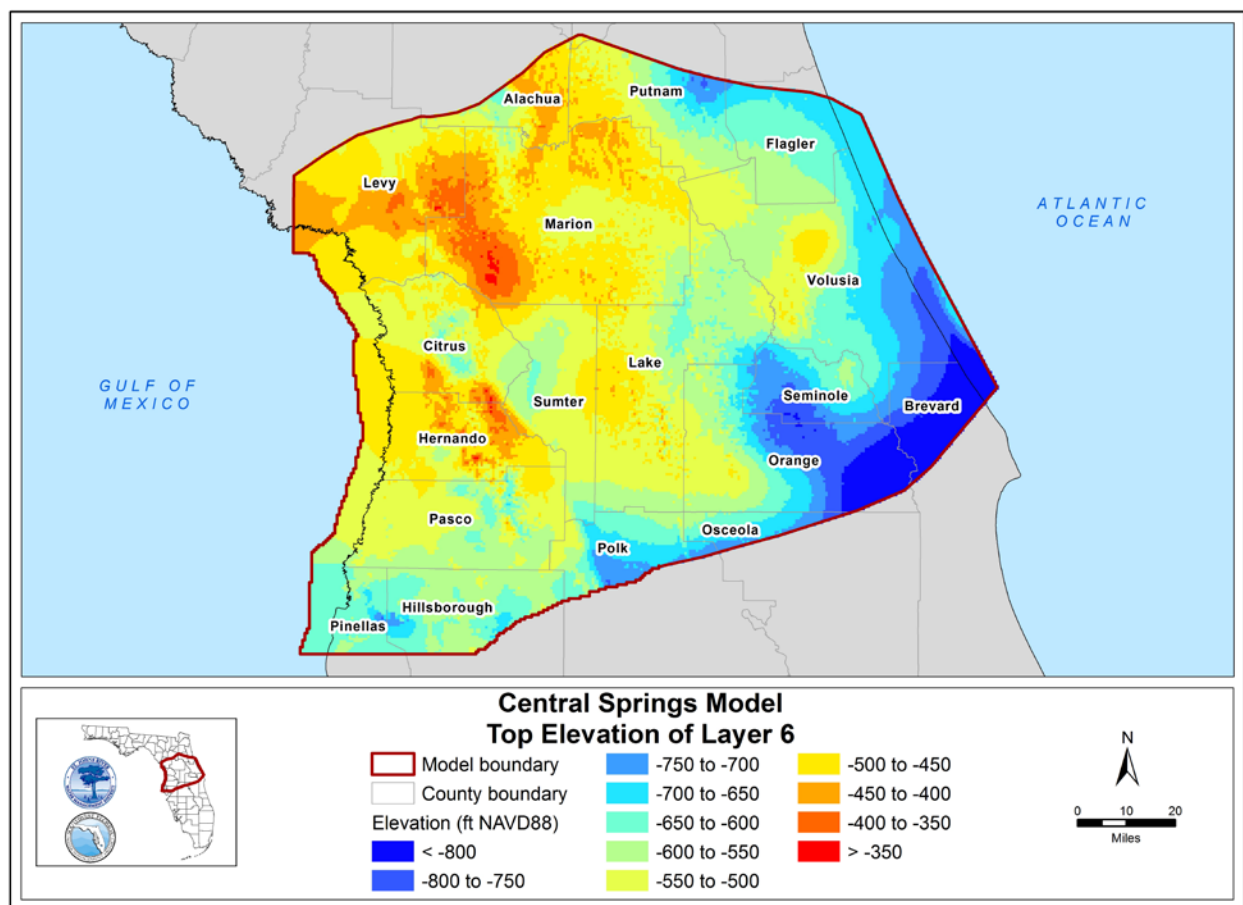


Figure 3-24. Top elevation of layer 6 within the Central Springs Model domain (ft NAVD88)

Note: ft NAVD88 = feet relative to the North American Vertical Datum of 1988

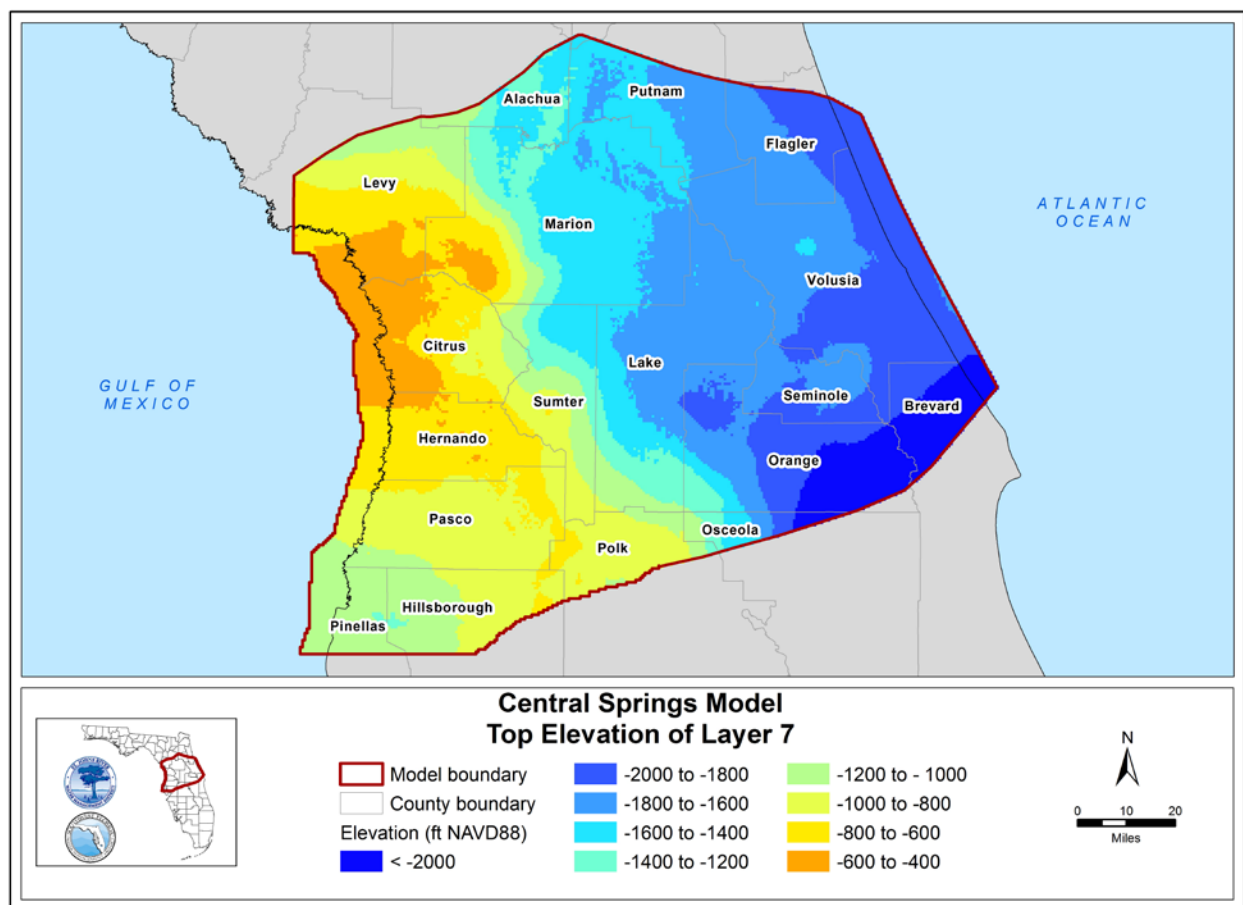


Figure 3-25. Top elevation of layer 7 within the Central Springs Model domain (ft NAVD88)

Note: ft NAVD88 = feet relative to the North American Vertical Datum of 1988

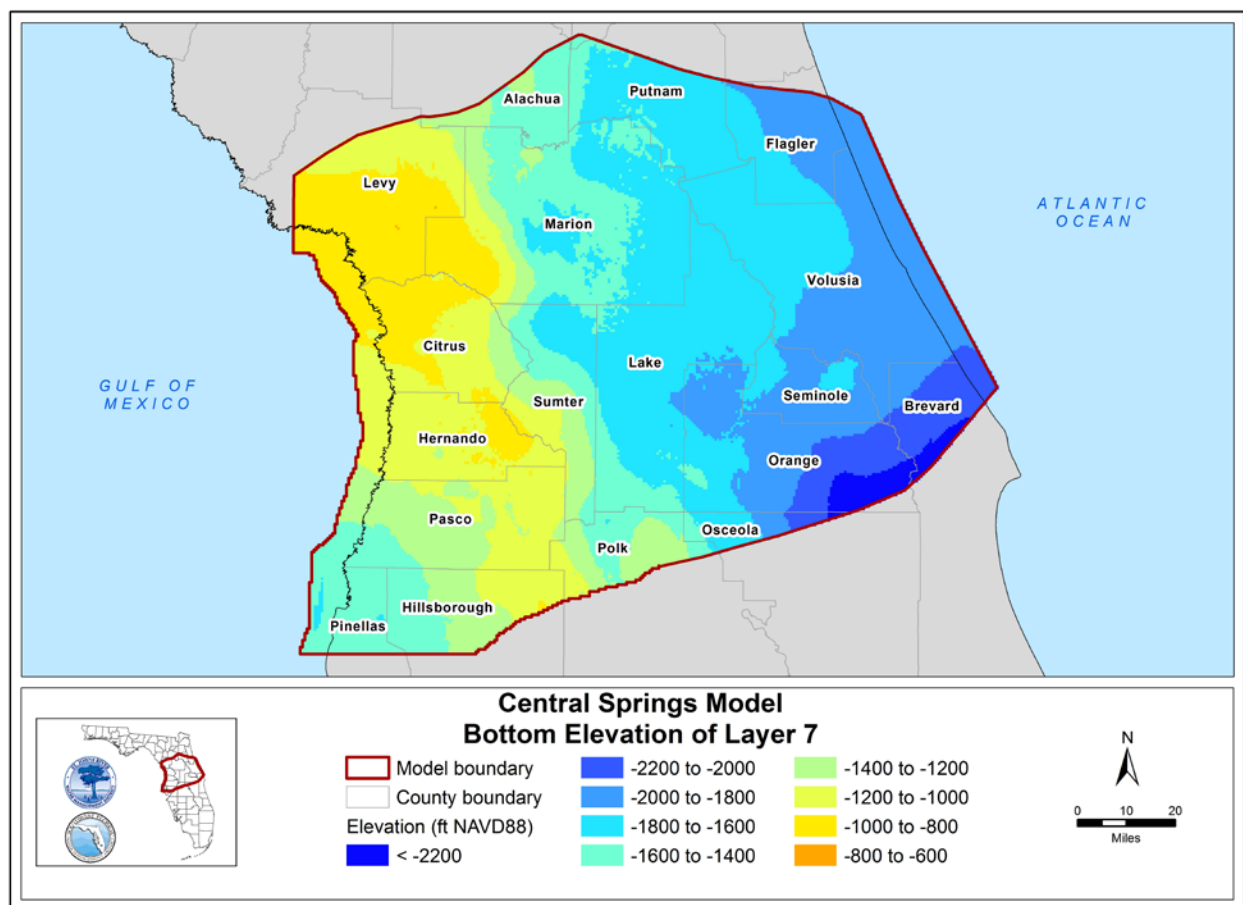


Figure 3-26. Bottom elevation of layer 7 within the Central Springs Model domain (ft NAVD88)

Note: ft NAVD88 = feet relative to the North American Vertical Datum of 1988

SPRINGS

Springs within the CSM domain predominately discharge water from the UFA. The location of identified springs, including vents that belong to a spring group, within the CSM domain are shown on Figure 3-27 (FDEP, 2017). Of the identified springs, only those with flow data were simulated in the model. A list of simulated springs is included in Appendix A. First magnitude (discharge greater than 100 cubic feet per second (cfs)) and second magnitude (discharge between 10 and 100 cfs) springs are shown on Figure 3-28. Certain spring locations represent the general location of a group of springs located within a limited geographic area. For example, the Homosassa Springs location, shown on Figure 3-28, is the general location of discharge from four springs: Halls River Head Spring, Homosassa Spring, Trotter Spring, and Hidden River (Knochenmus and Yobbi, 2001).

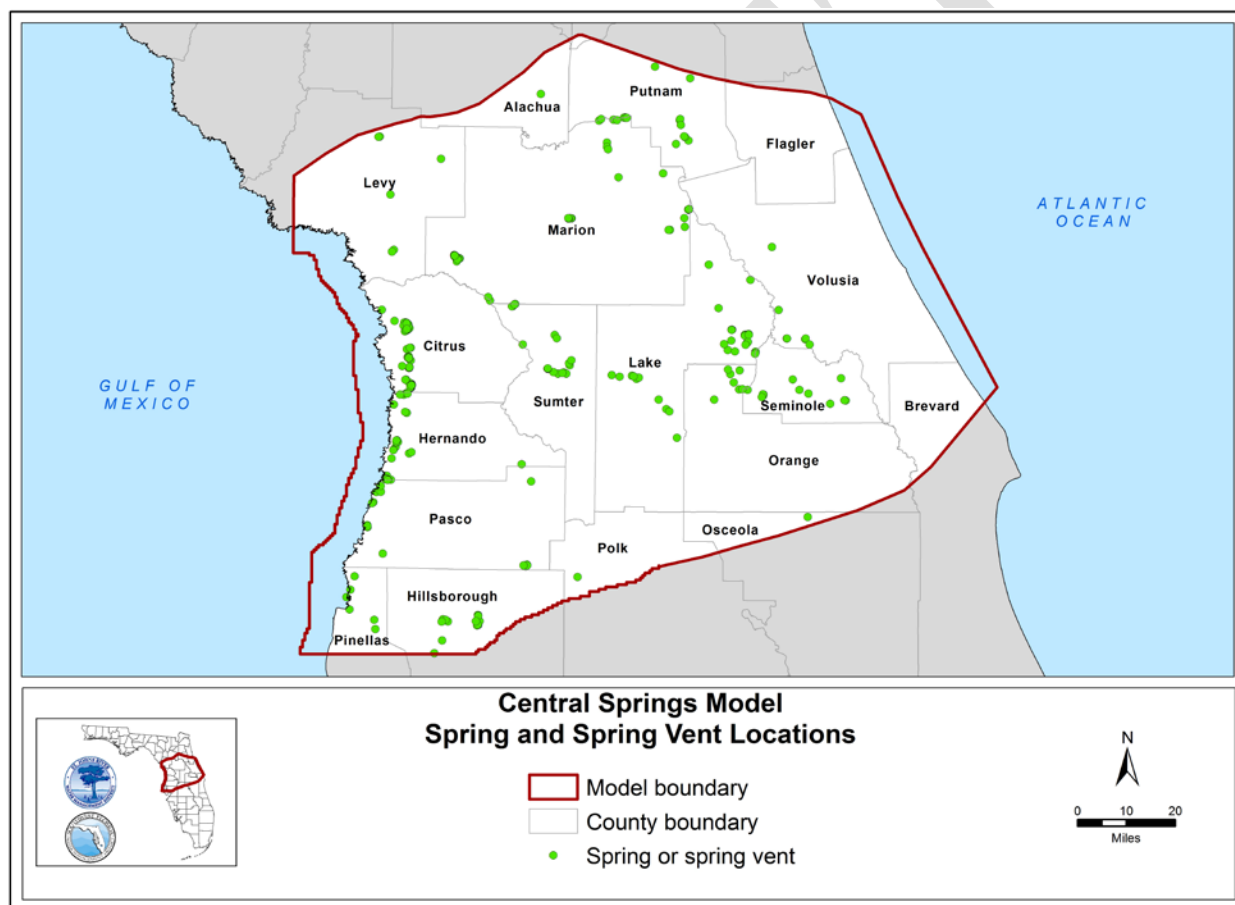


Figure 3-27. Spring and spring vent locations within the Central Springs Model domain (FDEP, 2017)

Note: There is significant overlap of spring points in many areas of the map due the map scale.

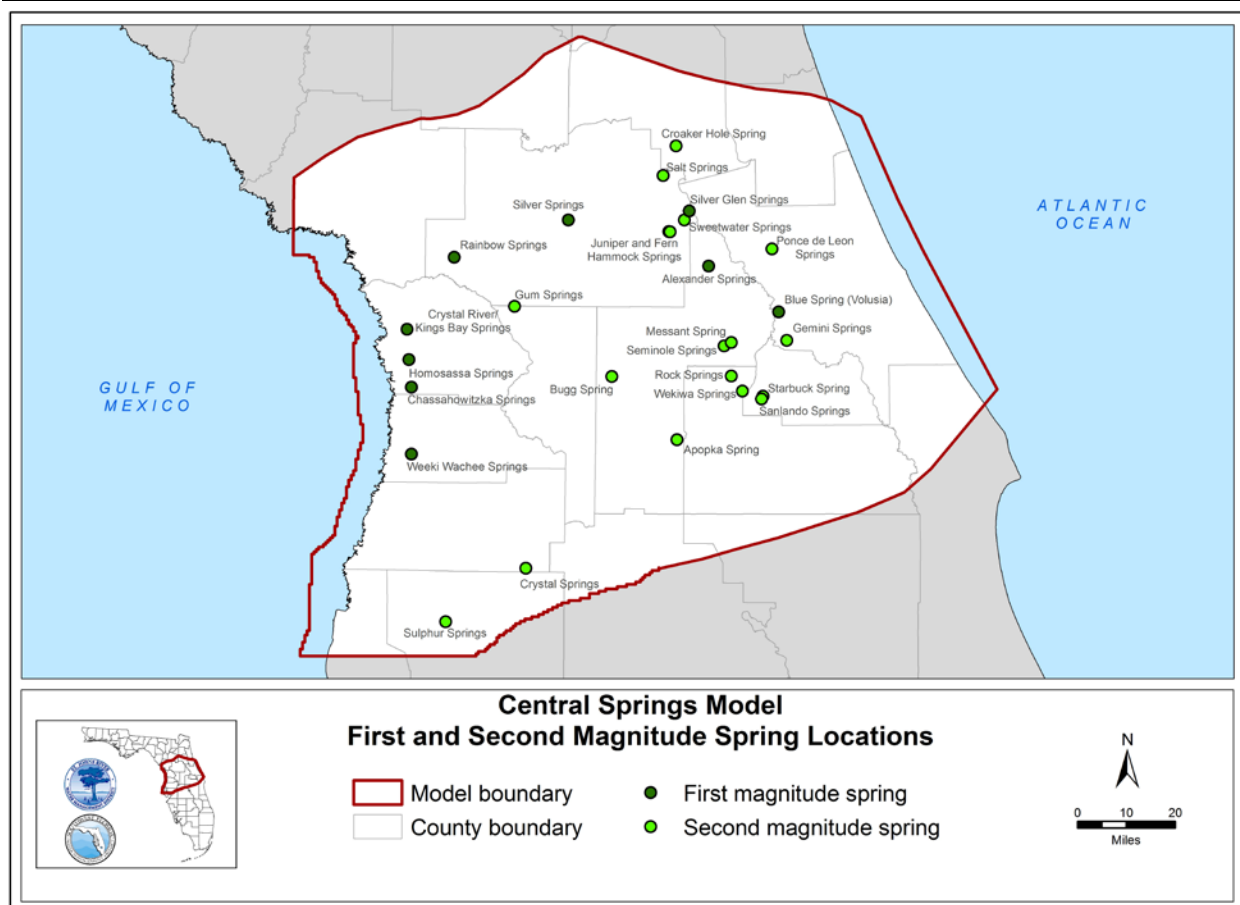


Figure 3-28. First and second magnitude spring locations within the Central Springs Model domain

Rainbow Springs and Silver Springs

Rainbow Springs and Silver Springs have the highest flows of all the first magnitude springs in the model domain. Hydrologic analysis of long-term monitoring data showed that the Rainbow Springs Group and Silver Springs Group had average annual discharges of 677 cfs (average 1965 to 2015) and 700 cfs (average 1947 to 2010), respectively (Sutherland et al., 2017; Holzward et al., 2017). The calculated correlation coefficient between the annual discharge rates from Rainbow and Silver springs over this period was 0.94, indicating potential hydrological interaction between these two major springs in the region.

Water chemistry and isotope data have been interpreted to indicate that Rainbow Springs and Silver Springs discharge groundwater mainly from the Ocala Limestone and possibly from the contiguous upper part of the Avon Park Formation, both of which may constitute the shallow part of the UFA in the springs area (Faulkner, 1976; Phelps, 2004). The upper part of the Avon Park Formation that is contiguous with the Ocala Limestone in south-central Marion County appears to have secondary porosity. Based upon a mass balance using sulfate concentrations, Faulkner (1976) proposed that approximately 8 to 14 percent of Silver Springs discharge included water from the Avon Park Formation, which contains elevated sulfate concentrations.

Gulf Coastal Springs

The springs within the Coastal Discharge Region include Crystal River Springs (also known as Kings Bay Springs), Homosassa Springs, Chassahowitzka Springs, Weeki Wachee Springs, and Aripeka Springs. Aside from Aripeka Springs, these are all classified as first magnitude springs. Tidal changes in the Gulf of Mexico generally affect spring discharge at all locations except Weeki Wachee (Knochenmus and Yobbi, 2001), indicating they are in the saltwater-freshwater transition zone of the UFA within the Coastal Discharge Region (SWFWMD, 1997). As observed, except for Weeki Wachee, spring discharge is generally a mixture of saltwater and freshwater (Knochenmus and Yobbi, 2001; 1997; Rosenau et al, 1977).

Tsala-Apopka Spring Group

The springs within the Tsala-Apopka area include Fenney Springs, Gum Springs, (Citrus) Blue Springs, and Wilson Head Springs. Fenney Springs discharges into Lake Panasoffkee (Rosenau et al., 1977), which in turn discharges into the Withlacoochee River. The remaining springs discharge directly into the Withlacoochee River. The discharge from these springs, including from Lake Panasoffkee, accounts for part of the downstream increase in Withlacoochee River streamflow in the Tsala-Apopka area. Average annual discharge from Lake Panasoffkee, which is primarily groundwater flow with a small surface-water component, was 168 cfs between 1971 and 2000. The average sulfate concentration in water that discharges from Lake Panasoffkee is currently approximately 30 mg/L. Roseneau et al. (1977) reported that sulfate concentrations in discharge from Fenney Spring, Gum Springs, (Citrus) Blue Springs, and Wilson Head Springs were 2 mg/L, 41 mg/L, 7 mg/L, and 7 mg/L, respectively.

Central Springs Group

Springs in the eastern part of the project area are mostly located within the St. Johns River drainage area. These springs include:

In Lake County:

- Alexander Springs
- Blackwater Springs
- Camp la No Che Spring
- Droty Spring
- Messant Spring
- Seminole Springs

In Marion County:

- Silver Springs
- Jupiter Springs
- Blue Spring
- Morman Branch Springs
- Orange Spring
- Salt Springs
- Silver Glen Springs
- Sweetwater Springs
- Tobacco Patch Landing Springs

In Seminole County:

- Wekiwa Springs
- Miami Springs
- Palm Springs
- Starbuck Spring

- Sanlando Springs

In Volusia County:

- Blue Spring in Orange City
- Gemini Springs
- Ponce de Leon Springs

In Orange County:

- Rock Springs
- Sulphur Spring
- Witherington Spring

First magnitude springs within the Central Springs Group include Silver Springs, Blue Spring in Orange City, Silver Glen Springs, and Alexander Springs.

Between 2004 and 2007, hydrologic, physicochemical, and aquatic community data were collected by the USGS for three of the springs in the western model area (Alexander, Rock, and Silver Glen) and six springs within the St. Johns River drainage area as part of an effort to establish or evaluate minimum flows and levels (Walsh et al., 2009). Results from the study indicate the springs in north-central Florida are represented by a wide range of physical, chemical, and biological characteristics.

MODEL PARAMETERIZATION

Initial hydraulic conductivities across the seven layers were transferred from the existing models described in Chapter 2 of this report, including the NDM, the NFSEG Version 1.1, the Volusia County model, and the ECFTX Version 2.0.

MODEL BOUNDARY CONDITIONS

(This section is adopted and modified from Appendix C of the HGL 2023 report)

The lateral and lower model boundaries are assigned CHD (prescribed head), GHB, or no-flow boundary conditions. The approach in assigning these conditions is described below.

Constant Head Boundaries

Flowlines at the seawater-freshwater interface are narrow due to seawater intrusion at the bottom of the aquifer along the coastal boundaries of the Atlantic Ocean, the Gulf of Mexico, and Tampa Bay. Since the less-dense freshwater flow occurs on top of the more-dense seawater, the changes of interface elevation in the coastal region must be reflected in model simulations.

Boundary conditions in coastal environments can be approximated in a groundwater flow model using equivalent freshwater heads specified over the full thickness of the aquifer at the coastal boundary (Motz, 2009). In the CSM, equivalent freshwater heads were assigned as CHD boundaries and estimated assuming a freshwater density of 1 gram per milliliter (g/mL) and a saltwater density of 1.025 g/mL. Constant head boundaries were applied to layer 1 at Tampa Bay, the Indian River Lagoon, and at the model cells extending from the coast to 5 miles into the Gulf of Mexico or the Atlantic Ocean (Figure 3-29). In layer 2 through layer 7, CHD boundaries were applied to the model cells located 5 miles offshore (Figure 3-30).

Non-Coastal General-Head Boundaries

Non-coastal boundaries are the boundaries along the northern and southern model boundary where time-dependent groundwater heads vary throughout the simulation period. Boundary locations were determined by using the potentiometric flowlines in the UFA, as shown on Figure 3-31. The boundaries are approximately perpendicular to the potentiometric contours and may be regarded as no-flow boundaries. General head boundaries were assigned to these model cells due to seasonal variations in the potentiometric surface. General head boundaries are flexible and can be reverted to no-flow boundaries by setting boundary conductance values to zero. The hydraulic head values assigned at these locations were obtained through interpolation between observed groundwater levels in wells immediately external and internal to the boundaries. General head boundaries were applied to layers 3, 4, and 6.

Non-Coastal No-Flow Boundaries

All remaining lateral boundaries were assigned no-flow boundaries, including finite-difference cells located in layer 1 and layer 2, where the flow is assumed to be vertical within the ICU layer. No-flow boundary conditions were assigned to represent competent confining units, which restrict vertical groundwater flow. This occurs in the western portion of the model domain at the base of layer 6 (MCU II) where it is assumed that the underlying Oldsmar

Formation has permeability similar to MCU II. No-flow boundary conditions were also assigned to the bottom of layer 7.

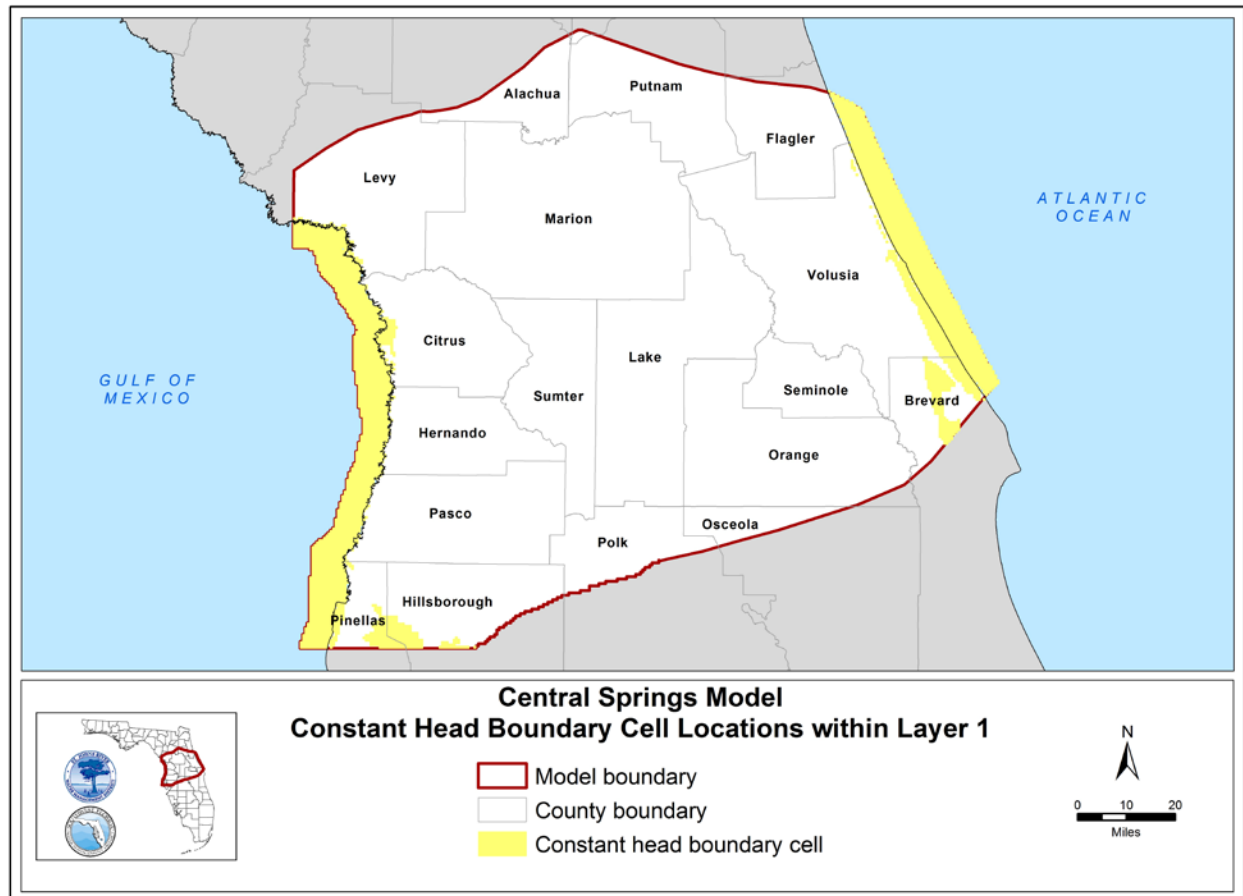


Figure 3-29. Constant head boundary cell locations within layer 1 of the Central Springs Model domain

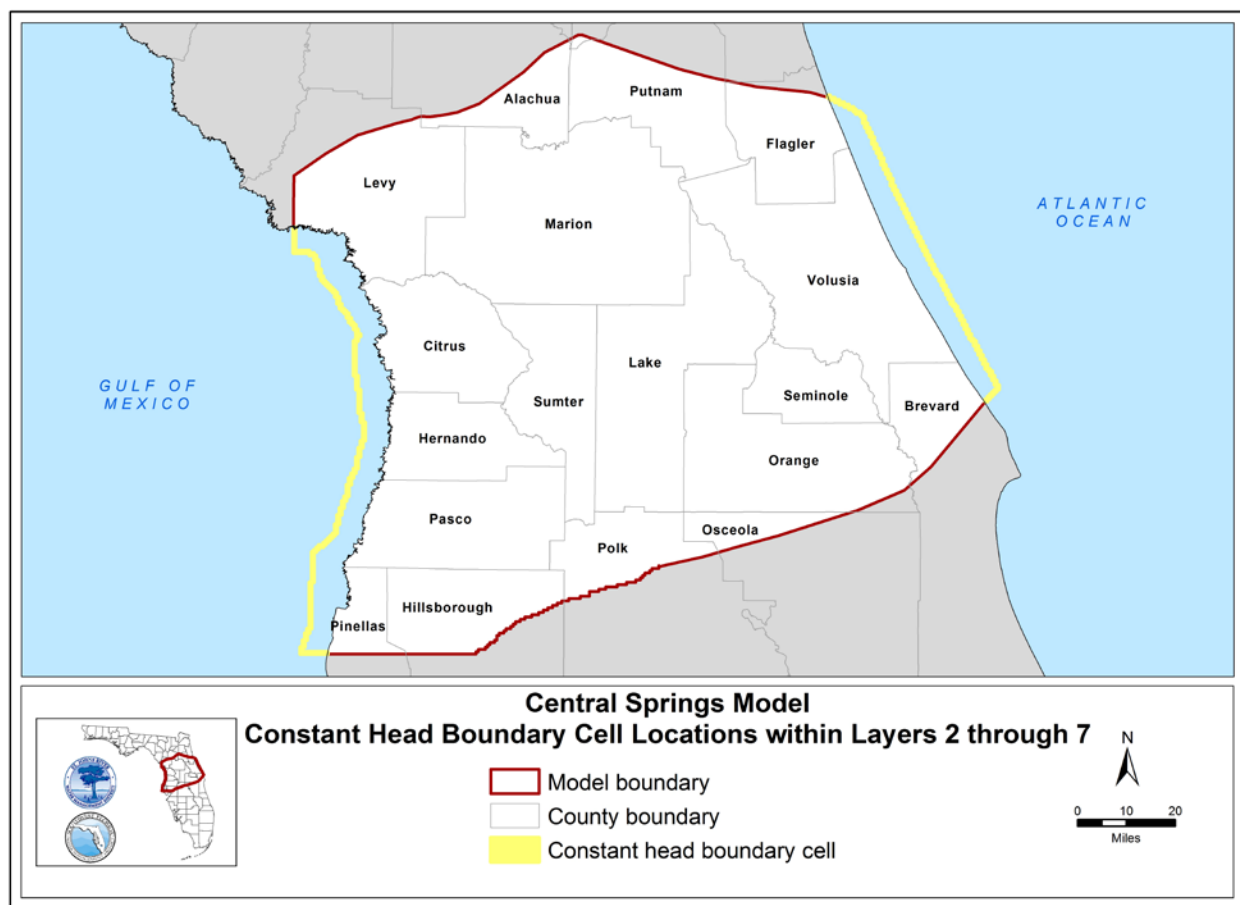


Figure 3-30. Constant head boundary cell locations within layers 2 through 7 of the Central Springs Model domain

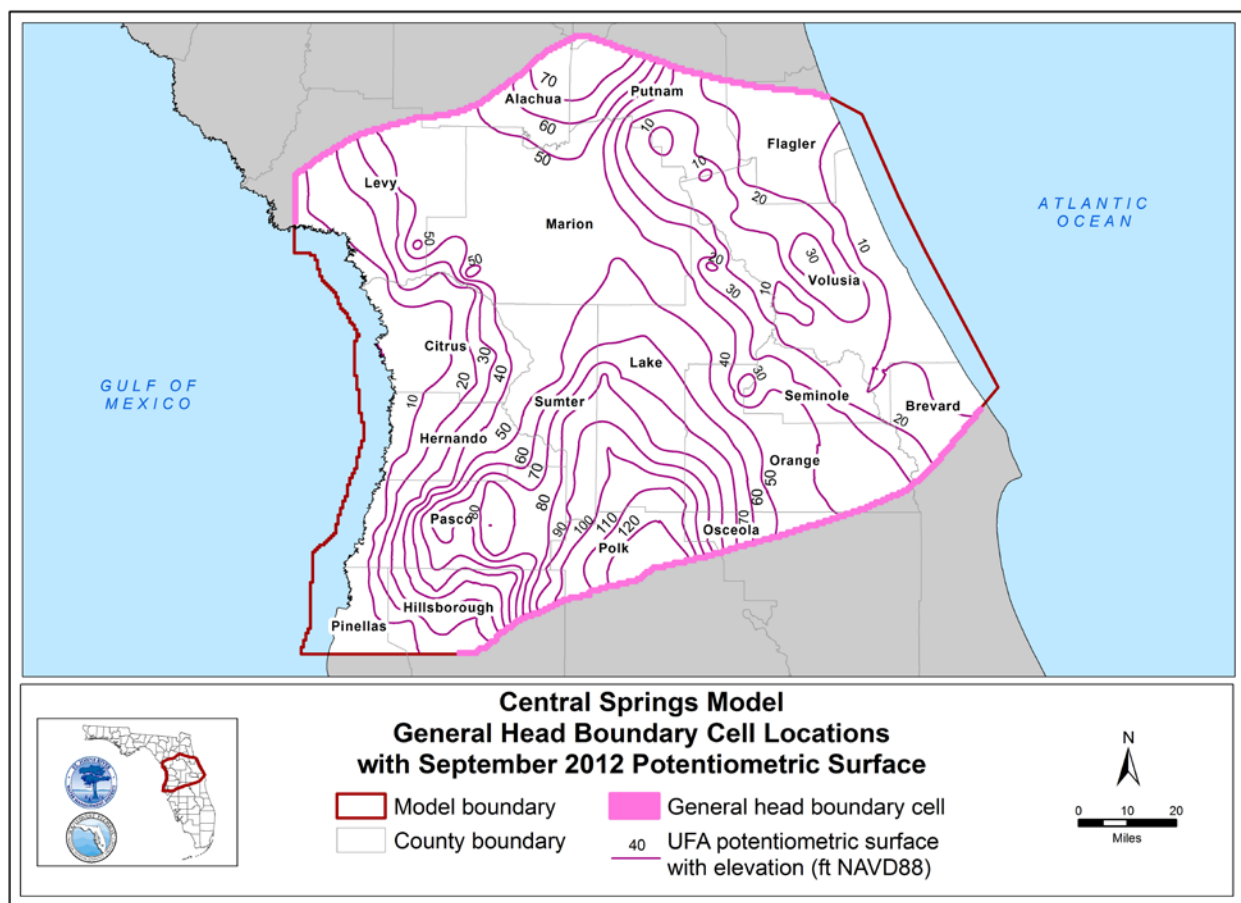


Figure 3-31. General head boundary cell locations within layer 3, layer 4, and layer 6 of the Central Springs Model domain with September 2012 Upper Floridan Aquifer (UFA) potentiometric surface (FDEP, 2014)

Note: ft NAVD88 = feet relative to the North American Vertical Datum of 1988

Rivers and Streams

Rivers were characterized based on flowlines and associated Strahler orders indicated by the National Hydrography Dataset Plus (Moore et al., 2019). Streams of Strahler orders of 2 or greater are likely perennial and were represented by river cells. Streams of Strahler order 1 are smaller and potentially intermittent streams and were included as drain cells. River cell locations are shown on Figure 3-32. Stage and discharge data were gathered from District databases. Baseflow separation analysis of the discharge data was conducted using the Perry Method (Perry, 1995) and the methods in the USGS Groundwater Toolbox (Barlow et al., 2014).

The stream stage at each river cell was found by interpolating observed stages between two adjacent gages. Flow width, flow depth, and river bottom elevation (*RBOT*) of each cell was determined using the following empirical correlations (Moore, 2007):

$$W = 11.95 \times Q^{0.47} \times 3.28083 \text{ (feet/meter, ft/m)} \quad (3-1)$$

$$D = 0.28 \times Q^{0.22} \times 3.28083 \text{ (ft/m)} \quad (3-2)$$

$$RBOT = Stage - D - Th \quad (3-3)$$

Where:

- W = stream width (ft)
- D = stream depth (ft)
- Q = stream discharge (m³/s)
- $RBOT$ = river bottom elevation (ft)
- $Stage$ = stream stage elevation
- Th = thickness of sediment or river bottom layer (ft)

In headwater areas upstream of the upstream-most gage, *Stage* was estimated by assuming the stage was 1 to 2 ft below the mean topographic elevation at the cell. Stream depth *D* was assumed to be equal to the river depth at the upstream-most gage. These assumptions were reasonable for locations where data was not available. *Th* was assumed to be 2 ft based on typical characteristics of the streams in central Florida. *RBOT* may change between stress periods since stream stage and discharge vary with time. *RBOT* at a given river cell is based on the lowest elevation between 2005 and 2018. For rivers with surveyed bathymetry data, *RBOT* was adjusted to the surveyed bottom elevation.

Initial river conductance was estimated using the following equation:

$$CD_{River} = \frac{K_{River} \Delta x W}{Th} \quad (3-4)$$

Where:

- CD_{River} = river conductance (feet squared per day; ft²/day)
- K_{River} = vertical hydraulic conductivity of river bottom (feet/day; ft/day)
- Δx = cell size = 2,500 ft

K_{River} was assumed to be 2 ft/day (HGL, 2016). CD_{River} values were modified during calibration using estimated baseflow. Stream width *W* varies with time due to its dependence on discharge.

CD_{River} varies with discharge across different stress periods. Final CD_{River} values were determined by model calibration.

Lakes

All MFL lakes and lakes with an area greater than half a grid cell (3,125,000 square feet) were included in the model. Many small lakes were excluded as they are considered insignificant in terms of local and overall water budgets.

Lakes were represented using river cells. The rivers and lakes were defined with time-varying input for each stress period. Locations of river cells in the model domain are shown on Figure 3-32. Available lake stages, bathymetry data, leakance values, and leakage rates (from observations and water balance calculations) were compiled and used to develop the RIV package for use in MODFLOW.

Initial lake conductance was estimated using the following equation:

$$CD_{Lake} = \frac{f_{Lake} K_{Lake} \Delta x^2}{Th} \quad (3-5)$$

Where:

CD_{Lake} = lake conductance (ft²/day)

f_{Lake} = fraction of the cell occupied by lake (dimensionless)

K_{Lake} = vertical hydraulic conductivity of lake bottom (ft/day)

Th = thickness of sediment or lake bottom layer (ft)

Δx^2 = grid cell area

K_{Lake} was assumed to be 0.02 ft/day, which falls within the range of values noted by Motz (1998) for karst lakes in peninsular Florida. Final CD_{Lake} values were determined by model calibration.

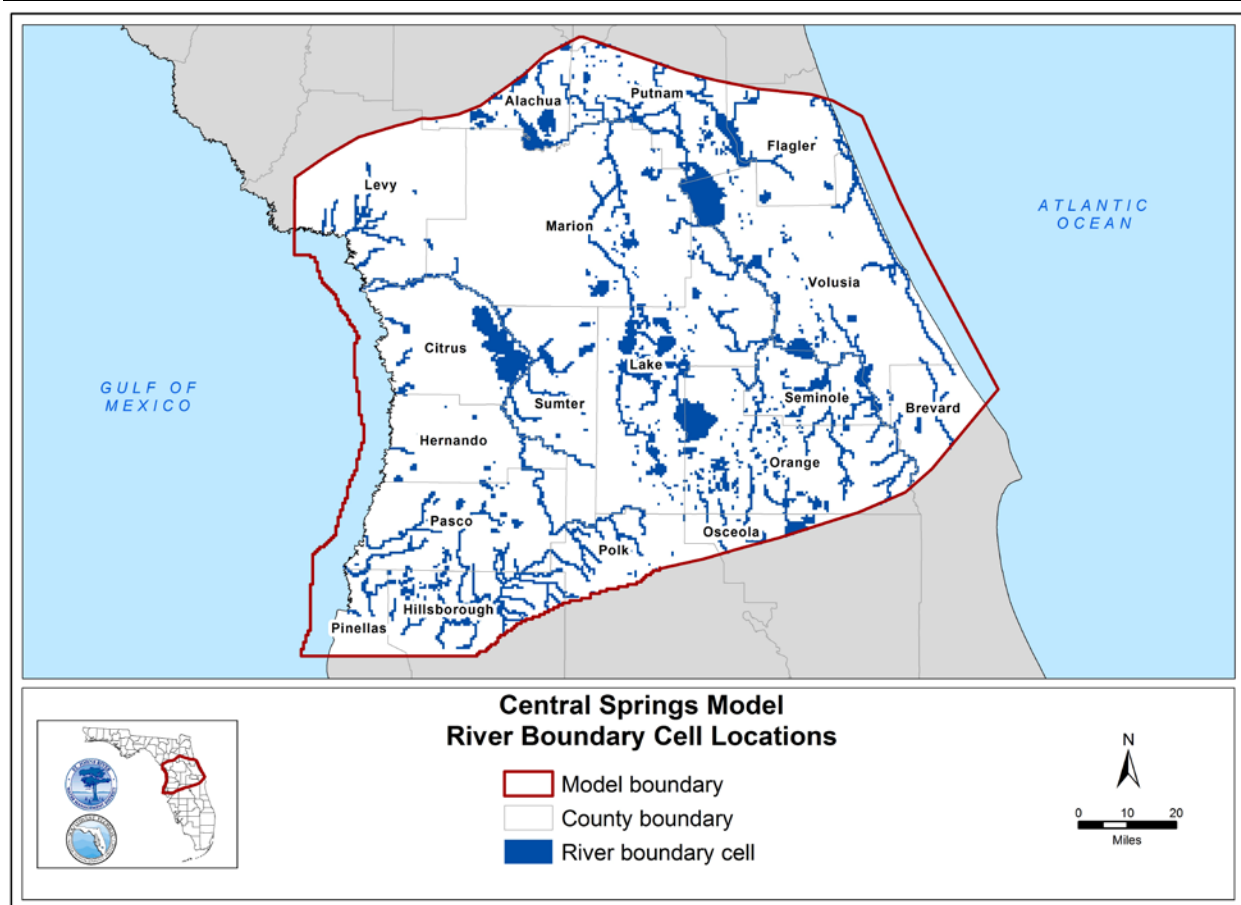


Figure 3-32. River boundary cell locations within the Central Springs Model domain

Wetlands, Small Lakes, and Head Streams

Mapped coastal and interior wetland areas, in addition to streams of Strahler order 1 and some small lakes (less than one half of a grid cell), are represented in the model by drain cells in layer 1 (Figure 3-33). Note that not all small lakes were represented in the model; only those that were critical for preventing flooded cells. Waterbody stage within each drain cell was assumed to be equal to the mean topographic elevation within that cell. Initial conductance values were estimated using Equation (3-5) with a cell fraction of one, hydraulic conductivity of 0.002 ft/day, and a thickness of 2 ft. Final conductance values were determined by model calibration.

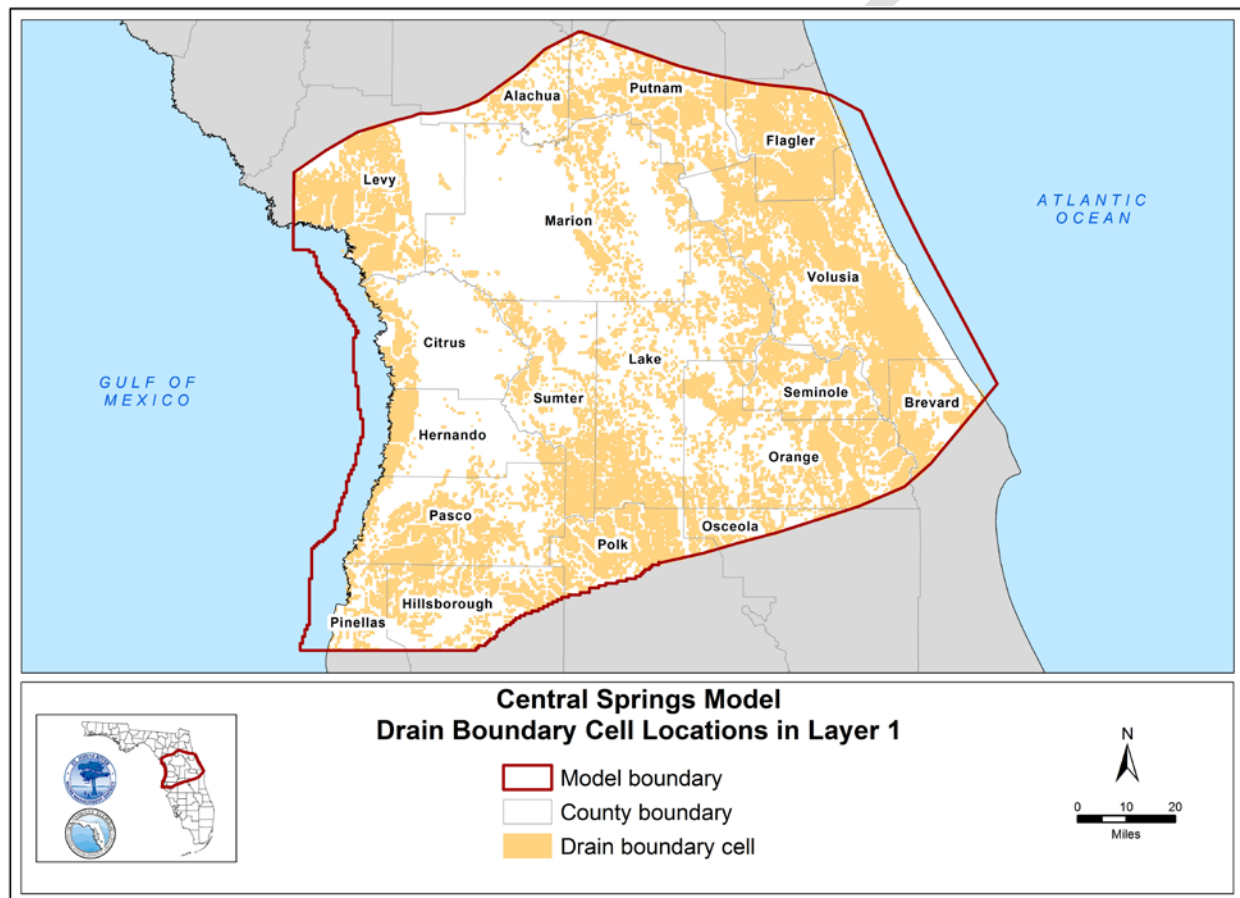


Figure 3-33. Drain boundary cell locations within layer 1 of the Central Springs Model domain

Springs

Springs locations within the model domain are shown on Figure 3-27. Springs were characterized using data from the Florida Department of Environmental Protection (FDEP), SJRWMD, and SWFWMD. Small seeps were excluded from the model. The quality and quantity of spring stage and discharge data varied between spring locations. A list of springs included in the model is provided in Appendix A.

All springs included in the existing models have gone through a rigorous vetting process with extensive data quality review and analysis. All MFL springs and springs with known discharge are included in the CSM. Springs are represented by drain cells. The springs are defined with time-varying pool elevations for each stress period. For springs without pool elevation data, elevations were deduced from mean topographic elevations. For springs with pool elevation and discharge data, initial conductance was estimated using the following equation and adjusted during model calibration:

$$CD_{Spring} = \frac{Q_{Spring}}{\Delta H} \quad (3-6)$$

Where:

CD_{Spring} = spring conductance (ft²/day)

Q_{Spring} = mean spring discharge (ft³/day)

ΔH = mean head difference between aquifer potentiometric elevation and spring pool elevation (ft)

PUMPING AND RECHARGE WELLS

Four categories of groundwater pumping and recharge wells were included in the model, including permitted wells, DSS wells, sink flows/drainage wells, and rapid infiltration basins (RIBs). Well locations and monthly pumping data from 2005 to 2018 were collected from District databases. Locations and rates of land-based applications of excess daily flows and reclaimed water through RIBs and drainage wells were provided by the SJRWMD. Locations of permitted wells, DSS, RIBs, and drainage wells are shown on Figure 3-34 to Figure 3-37. Return flows from agricultural, recreational, and mining land applications were sourced from the HSPF models and included as recharge. Reuse proportions were collected from the reuse inventory report based on water use types (FDEP, 2020) and applied to the HSPF models.

Permitted Wells

Figure 3-34 shows the locations of permitted wells within the model domain, including wells that are associated with a CUP/WUP. Permitted wells also include subthreshold agricultural and public supply wells (well associated with small operations that do not require a permit). Some permitted wells are open across more than one model layer. A well that penetrates multiple model layers was represented by multiple layer-specific wells corresponding to the number of layers in which the well is open. Each layer-specific well is assigned to a single layer in MODFLOW using the WEL package (Harbaugh, 2005). Initially, the extraction rate for each layer was assumed to be equally distributed between the layers to which the well is open. After calibration, the layer-specific extraction rate for each well was apportioned from the total extraction rate by flow fraction, which is defined as the ratio of the product of hydraulic conductivity and well-opening length in the layer over the sum of the products from all layers connected to that well. Each well was assigned with a time-varying rate based on pumping records.

Domestic Self-Supply Wells

Domestic self-supply water use is calculated by the Districts using a county-wide residential per capita rate and an estimate of DSS population for each respective county. For SJRWMD and SFWMD, DSS water use was distributed equally among all DSS locations at the county-wide level. For SWFWMD, DSS wells were aggregated by grid cell into one point in the center of the grid.

The locations of DSS wells are shown on Figure 3-35. Domestic self-supply wells are relatively shallow compared to agricultural and public supply wells and were assigned to a single layer in either the SAS or UFA depending on the local aquifer and well depth (Harbaugh, 2005). Each well was assigned a time-varying rate.

Sink Flows/Drainage Wells

Sink flows were approximated as runoff to closed basins in HSPF and applied uniformly to natural sinkhole locations within each basin (Durden et al., 2019). Each sink was represented as an injection well open to the UFA using the WEL package (Harbaugh, 2005).

Drainage wells are designed to remove excess stormwater and contribute to aquifer recharge. Locations of the drainage wells were obtained from FDEP and are shown on Figure 3-36.

Drainage well flux was estimated from each HSPF model. Each drainage well was assigned as an injection well to a single layer in which the well is open using the WEL package (Harbaugh, 2005). Each well was assigned with a time-varying rate based on HSPF model estimates.

Rapid Infiltration Basins

Rapid infiltration basins are permeable earthen basins constructed to disperse reclaimed water that has undergone advanced secondary treatment. Locations of RIBs within the CSM domain are shown on Figure 3-37. Water is applied to RIBs at land surface and flow is usually directed to the SAS. Therefore, RIBs are represented by injection wells in model layer 1.

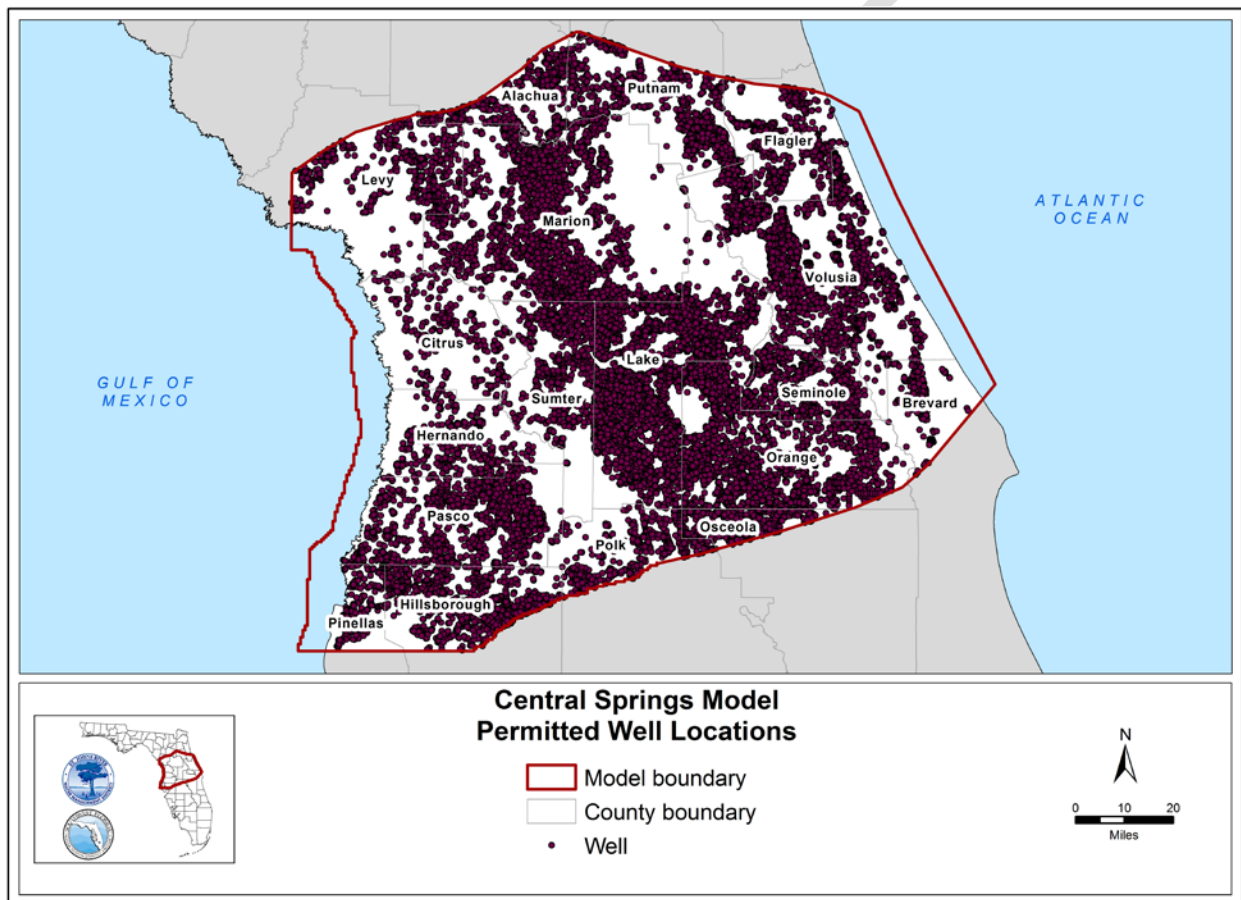


Figure 3-34. Permitted well locations in the Central Springs Model domain

Note: Permitted wells include agricultural and public supply wells with total groundwater withdrawals below permitting thresholds.

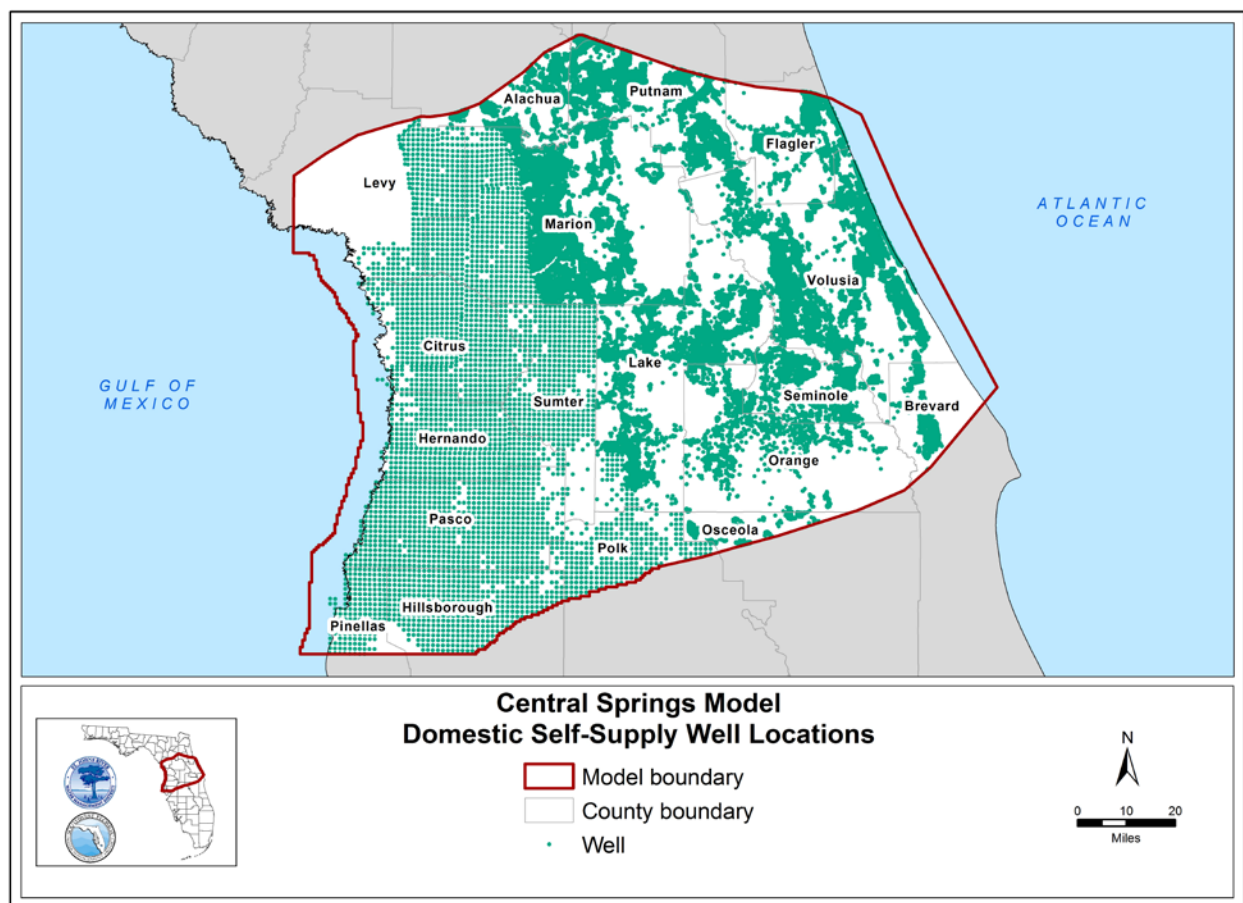


Figure 3-35. Domestic self-supply well locations within the Central Springs Model domain

Note: Domestic self-supply wells in the Southwest Florida Water Management District were not represented individually, but instead were aggregated by grid cell into a single point in the center of the cell.

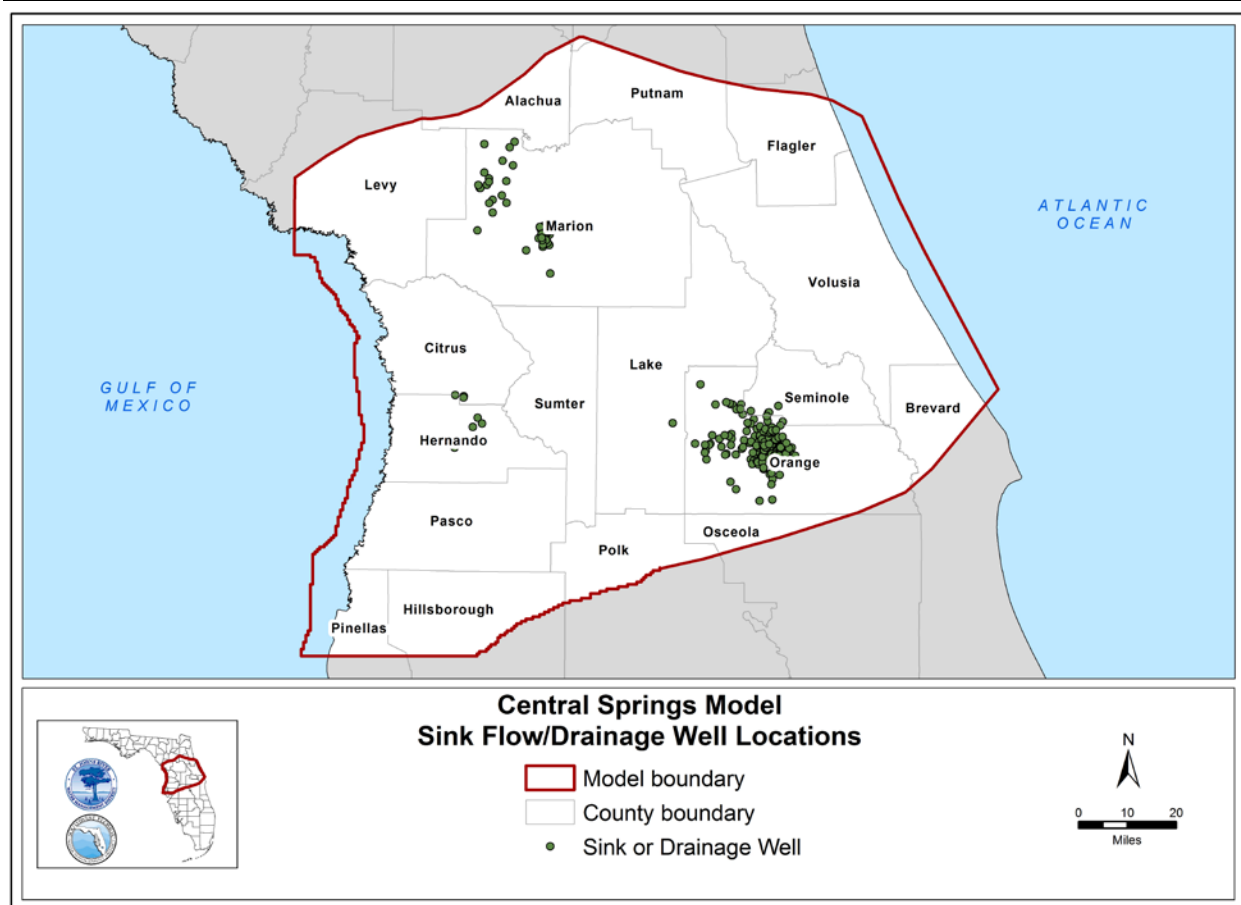


Figure 3-36. Sink flow and drainage well locations within the Central Springs Model domain

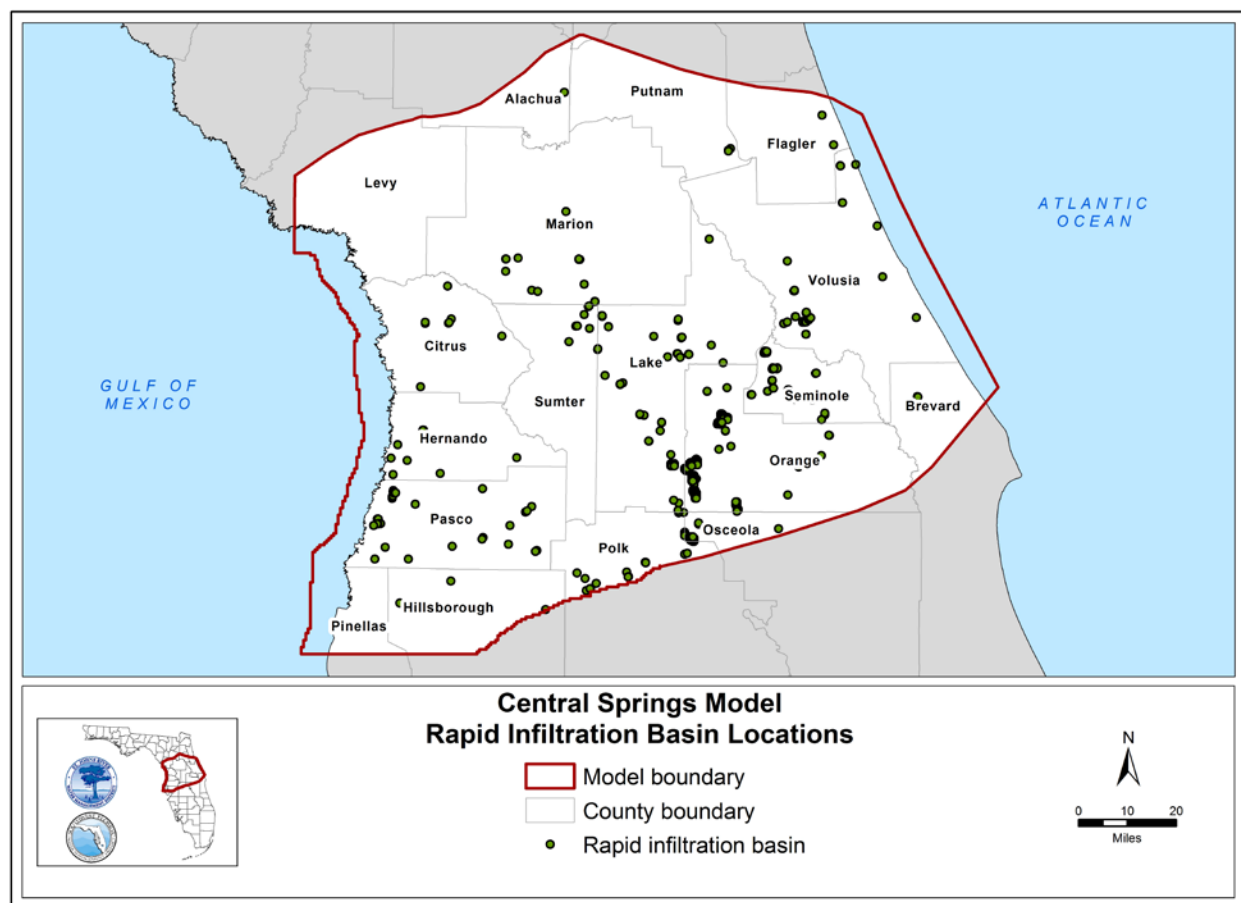


Figure 3-37. Rapid infiltration basin locations within the Central Springs Model domain

RECHARGE AND EVAPOTRANSPIRATION

HSPF Model Development

HSPF models are comprehensive, interconnected representations of the surface-water and near-surface groundwater flow systems (Bicknell et al., 2001). Their calibrated-constrained estimates of recharge and maximum saturated evapotranspiration are components of a complete and internally consistent water budget. As part of this effort, HSPF models simulated the surface water hydrology for all surface water basins within and flowing into the groundwater model domain to generate recharge and maximum saturated evapotranspiration (ETSatMax) estimates for input into the CSM. The HSPF model boundaries were set to the USGS hydrologic unit code (HUC) 8 watershed boundaries shown on Figure 3-38. There are 13 primary watersheds within the CSM domain, therefore 13 HSPF models were generated during development of the CSM. Rainfall and PET data are key inputs to the HSPF models. Sources for these inputs were discussed previously in the Hydrology section of this chapter.

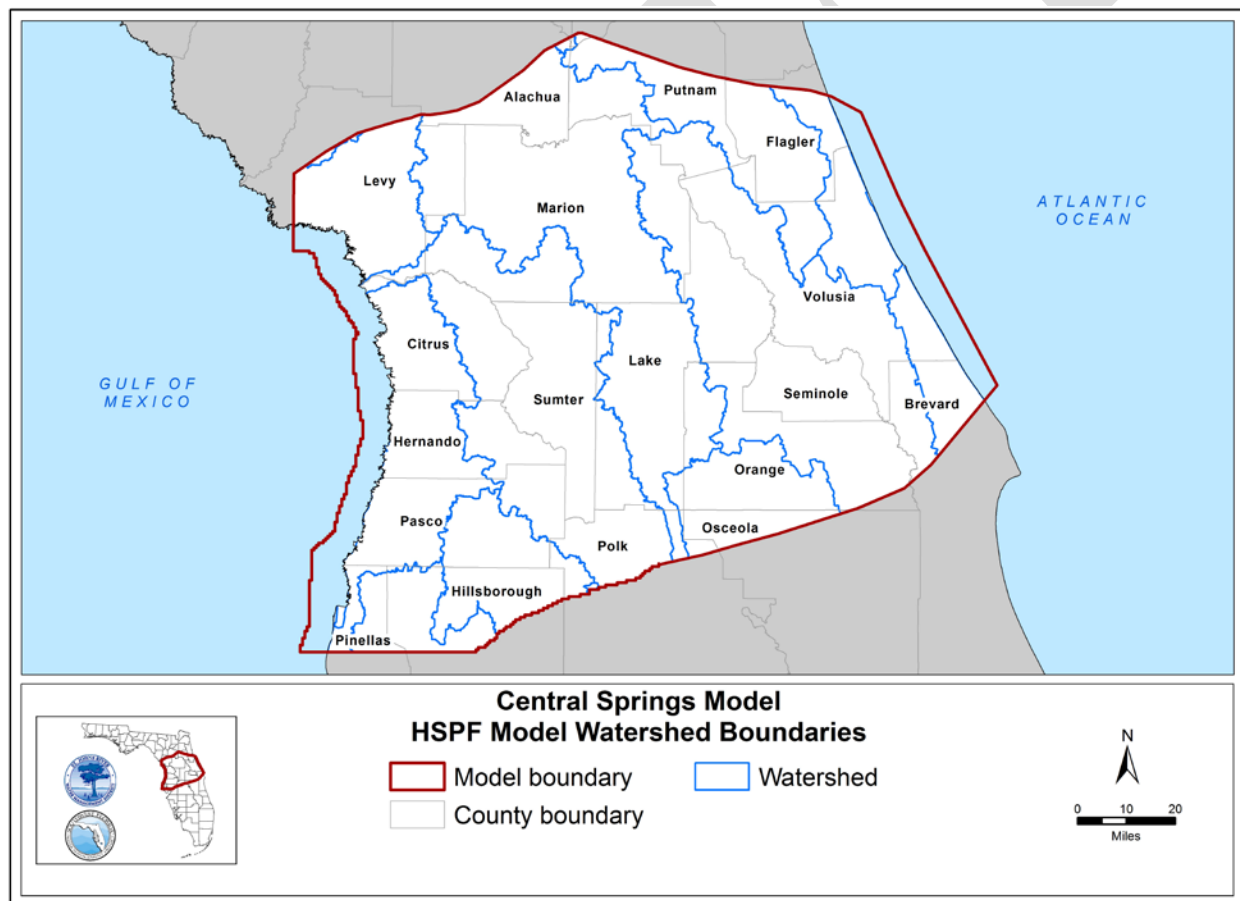


Figure 3-38. HSPF model watersheds within the Central Springs Model domain
 Note: HSPF = Hydrological Simulation Program-FORTRAN

Recharge Calculation

Monthly and annual cell-specific recharge from January 2005 to December 2018 were obtained from the calibrated HSPF models (Cera et al., 2018). Recharge that enters the water table is expressed in terms of the following HSPF variables:

$$R = AGWI + IGWI + SURET \quad (3-7)$$

Where:

R = recharge to water table

$AGWI$ = inflow to the active groundwater storage at the water table

$IGWI$ = inflow to the inactive groundwater storage at the water table

$SURET$ = evapotranspiration from surface water storage

$SURET$ is included in total recharge to account for infiltration from wetlands, which is also subject to ET abstraction in MODFLOW. By including $SURET$, ET abstraction was prevented from occurring twice by HSPF and MODFLOW. Land-applied water quantities (irrigation, septic tanks, etc.) for the model domain from 2005 to 2018 were obtained from SJRWMD and SWFWMD data and were added to rainfall as input to the HSPF models. Examples of monthly and annual recharge are shown on Figure 3-39 and Figure 3-40, respectively.

Sink flows, drainage wells, and RIB flows were not considered in recharge calculations since they were represented within the MODFLOW well package.

Groundwater Evapotranspiration

The CSM utilized the MODFLOW ET package to actively simulate groundwater ET. The MODFLOW ET package requires input for SURF (ET surface elevation), EXDP (extinction depth), and EVTR (maximum evapotranspiration from the saturated zone; same as ETSatMax).

ETSatMax may be expressed in terms of HSPF's variables as follows:

$$ETSatMax = PET - CEPE - UZET - LZET \quad (3-8)$$

Where:

$ETSatMax$ = maximum evapotranspiration from the saturated zone

PET = evapotranspiration potential

$CEPE$ = ET from the interception storage

$UZET$ = ET from the upper zone storage

$LZET$ = ET from the lower zone storage

Maximum saturated evapotranspiration is equal to the difference between PET and above-the-water table ET and consists of ET from the interception storage, the upper zone storage of the vadose zone, and the lower zone storage of the vadose zone. Monthly and annual ETSatMax for the model domain from 2005 to 2018 were provided by the HSPF models (Cera et al., 2018). Examples of monthly and annual ETSatMax estimates are shown on Figure 3-41 and Figure 3-42, respectively.

Extinction depth is the depth below ground surface where ET from groundwater diminishes. The extinction depth represents the vertical extent over which soil moisture content declines from saturation at the water table to a “wilting point” moisture content at which plant roots cannot extract moisture. Extinction depths for the CSM domain were estimated by SJRWMD using soil characteristics and vegetation type from land cover (Shah et al., 2007; Freese, 2019) (Figure 3-43).

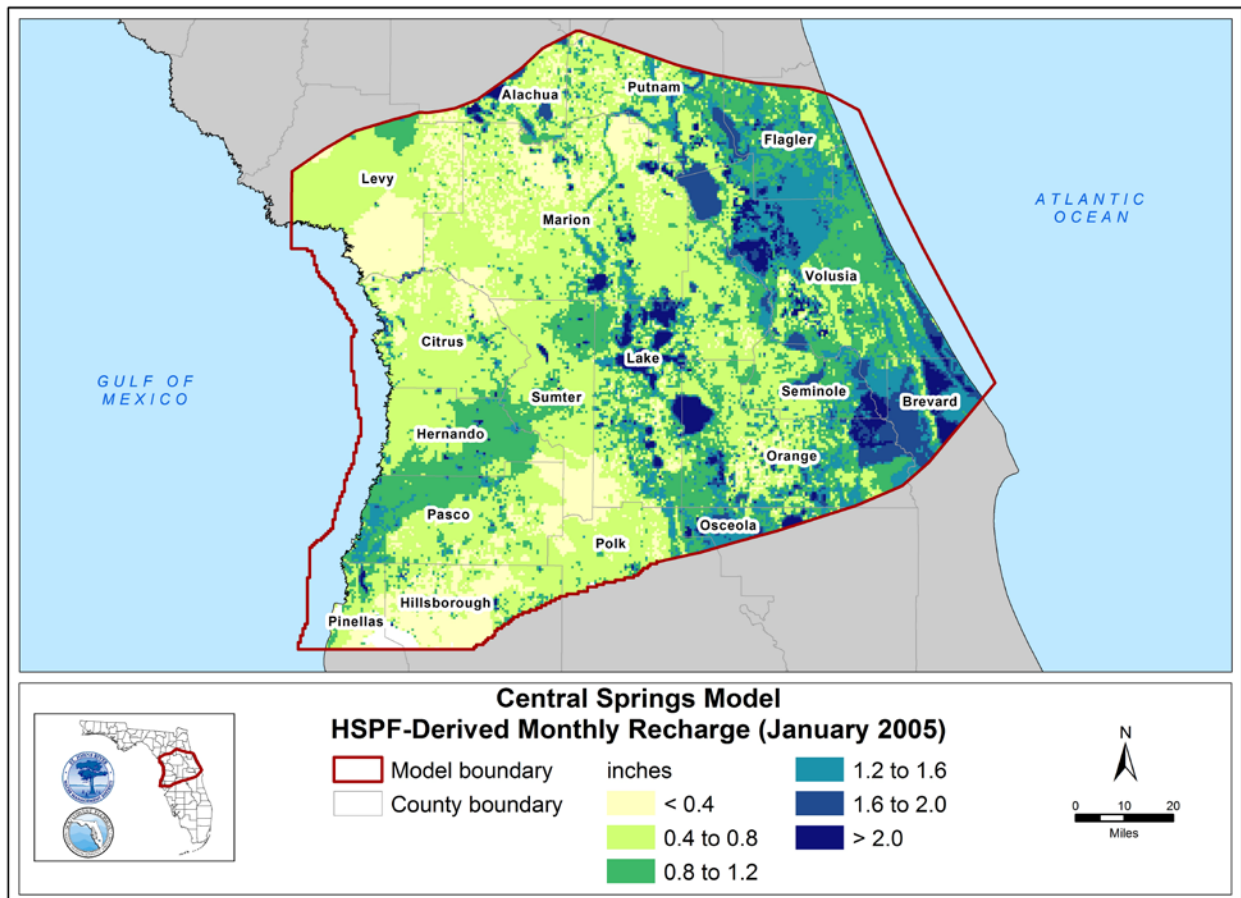


Figure 3-39. HSPF-derived monthly recharge rates within the Central Springs Model domain for January 2005
 Note: HSPF = Hydrological Simulation Program-FORTRAN

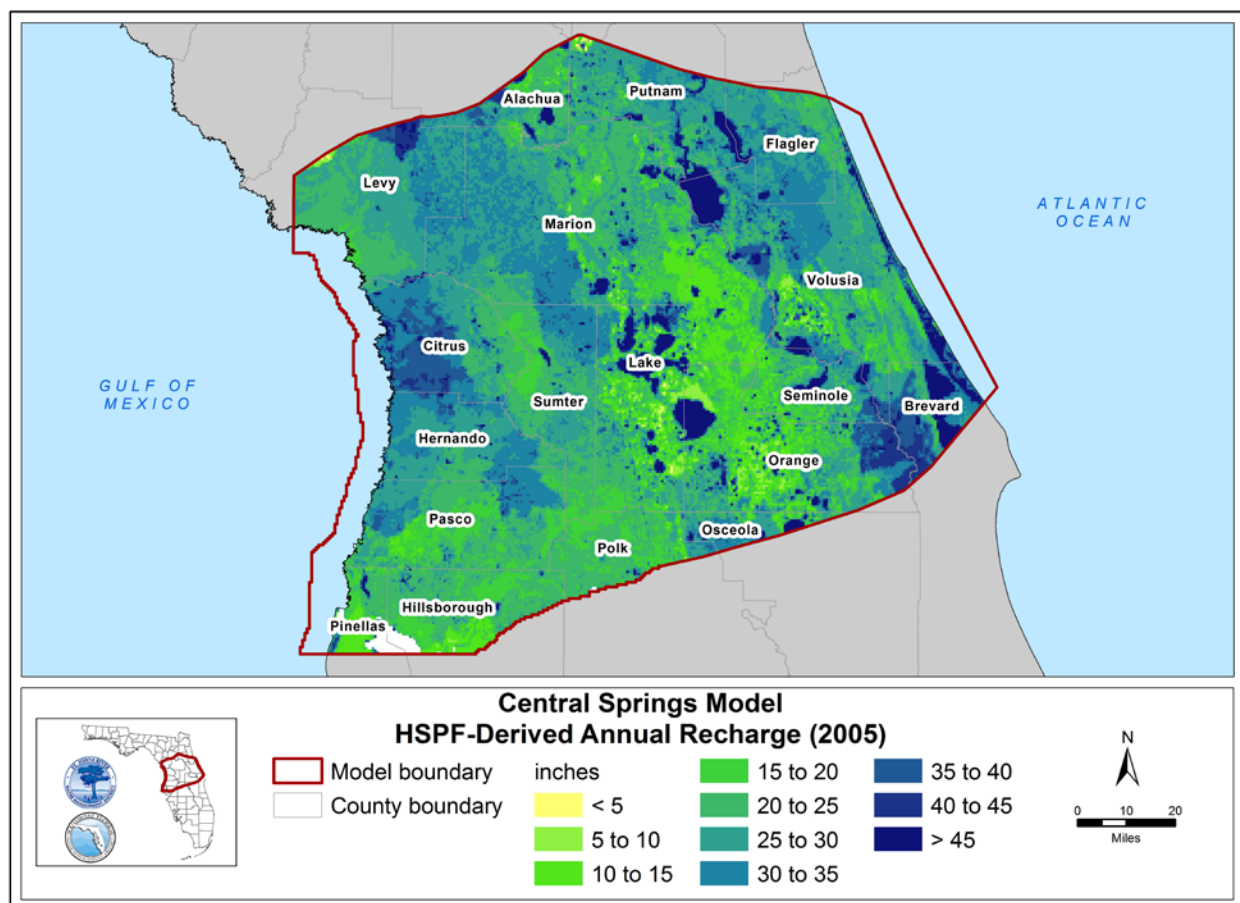


Figure 3-40. HSPF-derived annual recharge rates within the Central Springs Model domain for 2005
Note: HSPF = Hydrological Simulation Program-FORTRAN

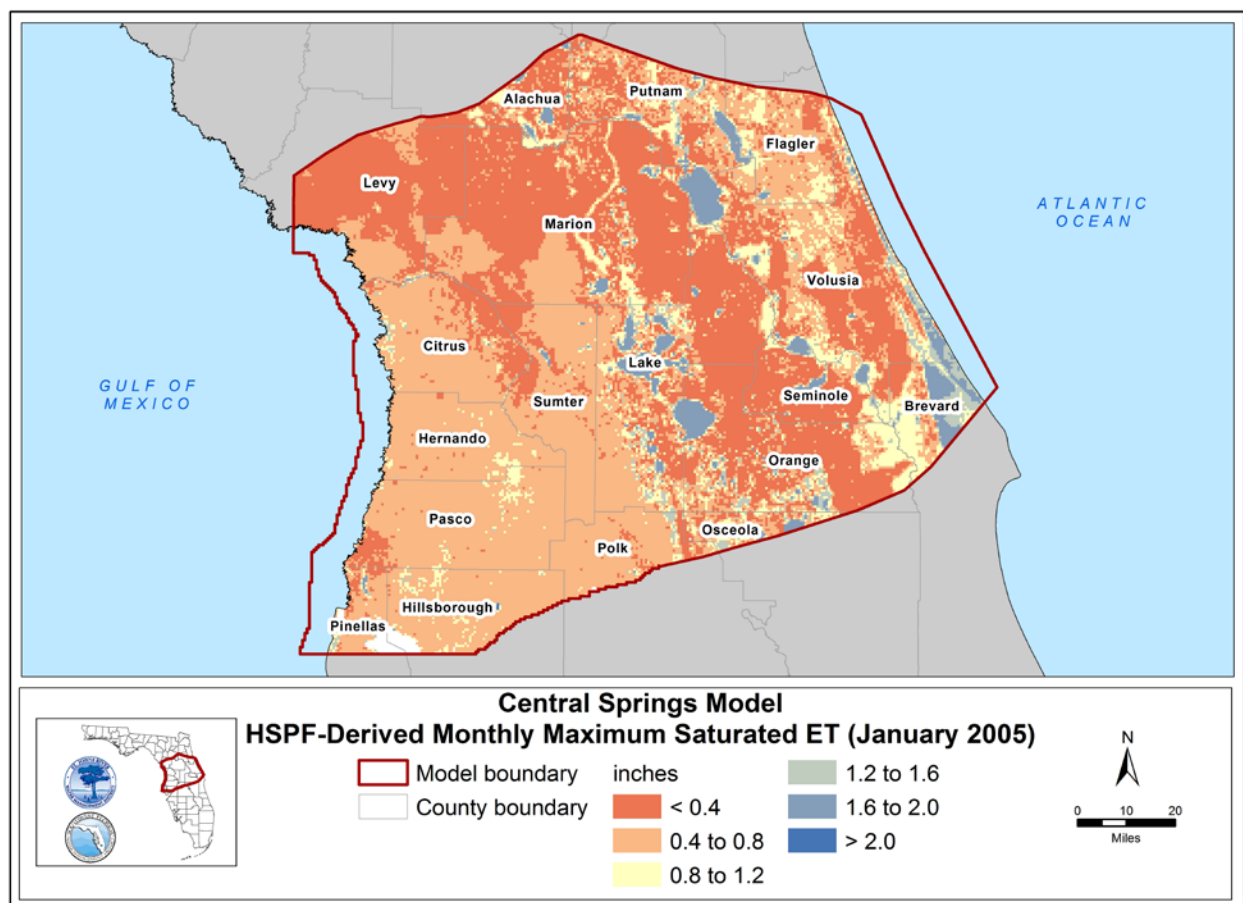


Figure 3-41. HSPF-derived monthly maximum saturated evapotranspiration rates within the Central Springs Model domain for January 2005

Note: HSPF = Hydrological Simulation Program-FORTRAN, ET = evapotranspiration

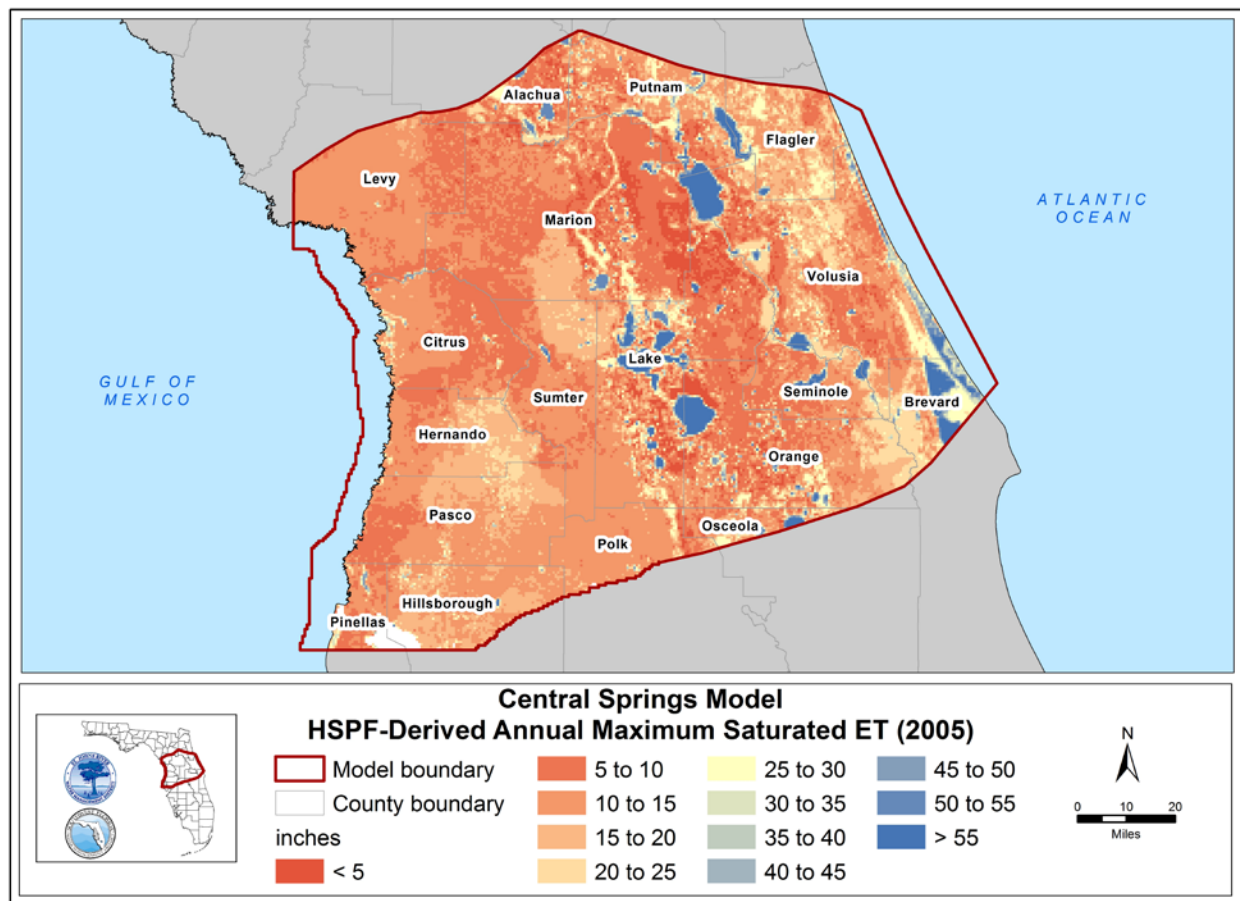


Figure 3-42. HSPF-derived annual maximum saturated evapotranspiration rates within the Central Springs Model domain for 2005

Note: HSPF = Hydrological Simulation Program-FORTRAN, ET = evapotranspiration

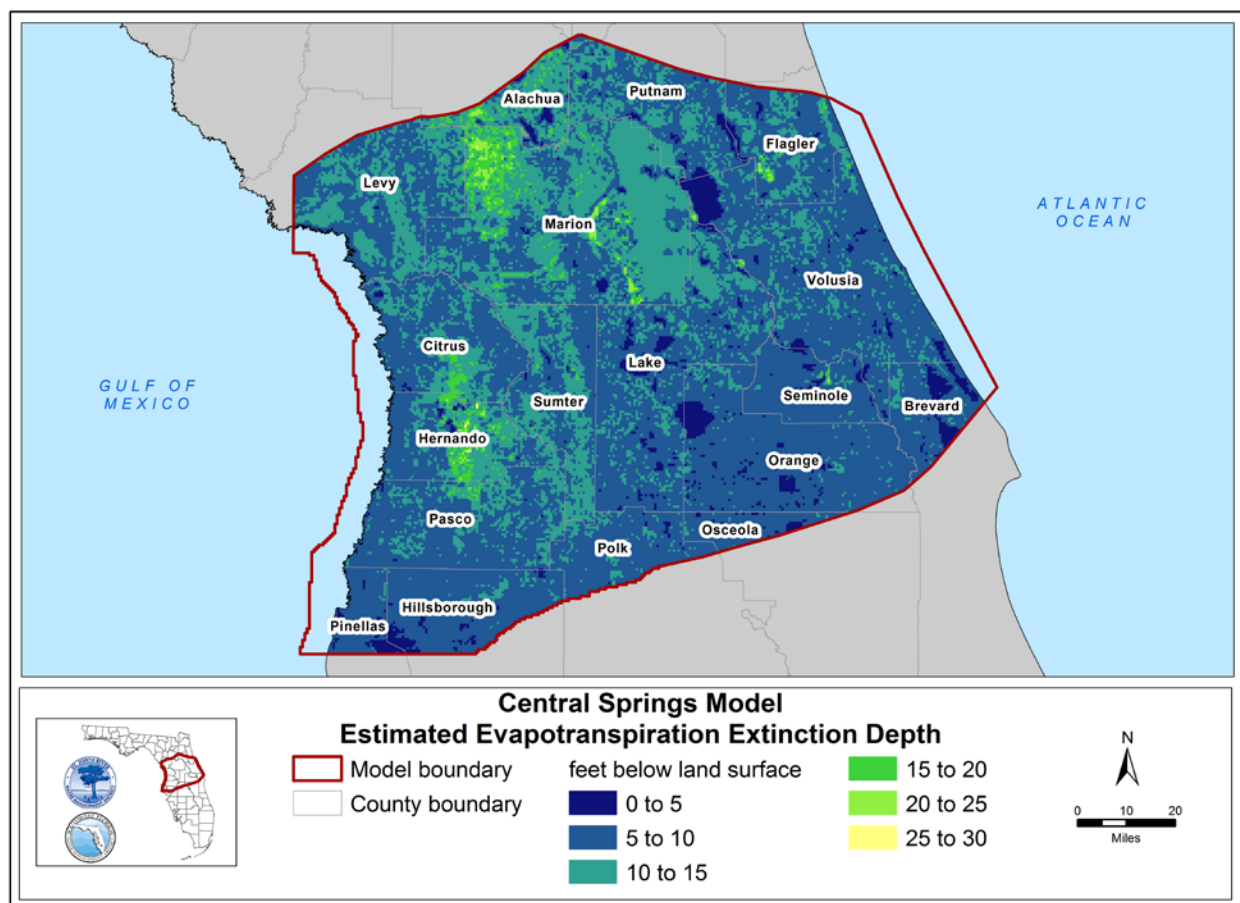


Figure 3-43. Estimated evapotranspiration extinction depth within the Central Springs Model domain

4. MODEL CALIBRATION

Model calibration is the process in which model parameters and/or boundary conditions are adjusted to obtain a satisfactory match between simulated and observed hydrologic conditions (Anderson and Woessner, 1992). Parameter ESTimation code (PEST; Doherty, 2010) was used to assist in calibration of the CSM.

CALIBRATION PROCEDURE

(This section is adopted and modified from Appendix E of the HGL 2023 report)

The CSM was calibrated using a variety of observed hydrologic data, including measured groundwater levels, differences in groundwater levels across confining units, and observed discharges at springs. Because of the difficulty in using PEST for transient calibration due to very long computational time, the CSM calibration was performed in two steps. Initially, the CSM was calibrated to a steady-state condition representing average 2005 to 2018 hydrological and pumping conditions using PEST. Later, the model properties obtained from the steady-state calibration were input into the transient model for testing and refinement. A schematic of the general approach is shown on Figure 4-1. The two-step approach is described as follows.

- Step 1 – Automated steady-state calibration using PEST to calibrate the average 2005 to 2018 steady-state model to determine hydraulic properties.
- Step 2 – Manual transient calibration limited to adjustment of storage properties using hydraulic parameters from Step 1. After reviewing transient calibration results, additional steady-state PEST calibration was conducted as needed.

The process went through several iterations to achieve the pre-determined calibration criteria.

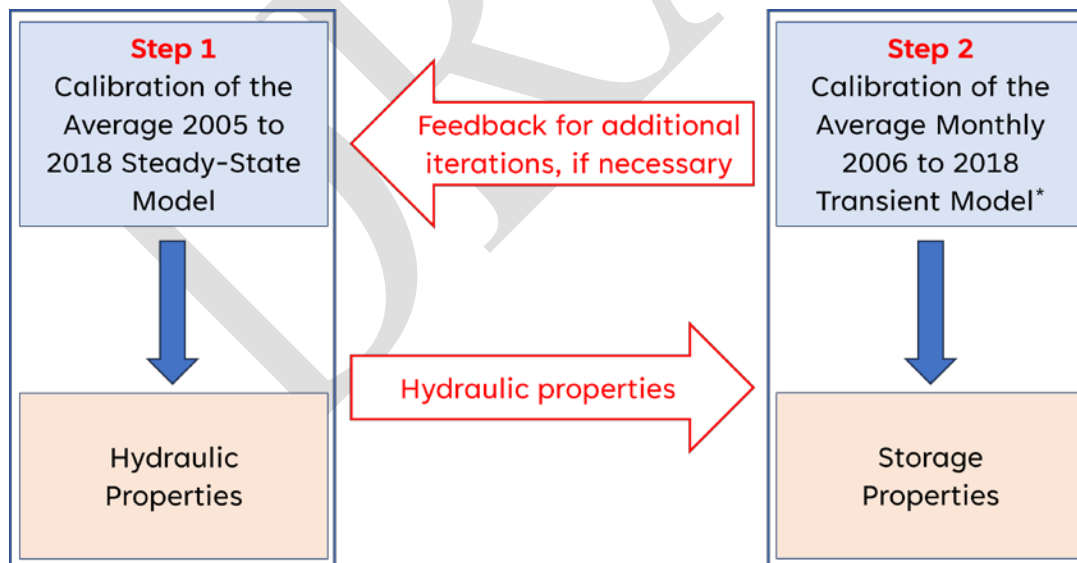


Figure 4-1. Central Springs Model calibration approach (HGL, 2023)

* With 2005 average annual conditions used as initial conditions

Steady-State Model Calibration

Prior to the automated PEST calibration, an initial manual adjustment was performed to achieve reasonable starting conditions in the steady-state model. PEST was then used to estimate hydraulic properties by minimizing residuals to satisfy calibration criteria. Residuals are defined as follows.

$$\text{Residual} = \text{simulated value} - \text{observed value} \quad (4-1)$$

The following hydraulic properties were estimated:

- Hydraulic conductivity
- River conductance
- Lake conductance
- Drain conductance
- Spring conductance

Observed or estimated variables used as part of the PEST calibration process included the following:

- Groundwater levels
- Groundwater level differences across confining units
- Spring discharges
- Baseflows (qualitative)
- Vertical lake leakages (qualitative)

The metrics and calibration criteria that were identified for the steady-state model are described in the Metrics and Criteria section.

Transient Model Calibration

The transient model calibration was conducted using hydraulic properties derived from PEST calibration of the steady-state model. Therefore, the transient model can be viewed as an extensive verification of the PEST calibration. Storage properties including specific yield (Sy) and specific storage (Ss) were assigned based on typical reported values estimated in the hydrogeologic layers.

Model simulated monthly hydrographs of groundwater heads at monitoring wells and springs were plotted and compared with measured hydrographs. Statistical parameters including mean residual, coefficient of determination (R^2), and Nash-Sutcliffe efficiency coefficient (NSE) were calculated for each hydrograph. Summary statistics for the SAS, UFA, LFA, and springs were calculated and compared with the identified metrics and criteria that are described in the following section. The transient simulation results provided guidance to the PEST calibration process to further refine and constrain hydraulic parameters.

An interactive web application (<https://waterapp.shinyapps.io/CentralSpringModel/>) was developed using the open-source R-language code packages Shiny and Leaflet to visualize and assist the transient calibration process. The locations of target monitoring wells, springs, river

gages, and lakes were plotted on interactive maps within the application. Users can view a comparison of the simulated and measured hydrographs by clicking on an individual target location. Summary statistics for each category of calibration targets are automatically calculated and reported on the “Data Explorer” dashboard. Users can download the graphs and data from the web application for further analysis. Figure 4-2 shows a screenshot of the web application.

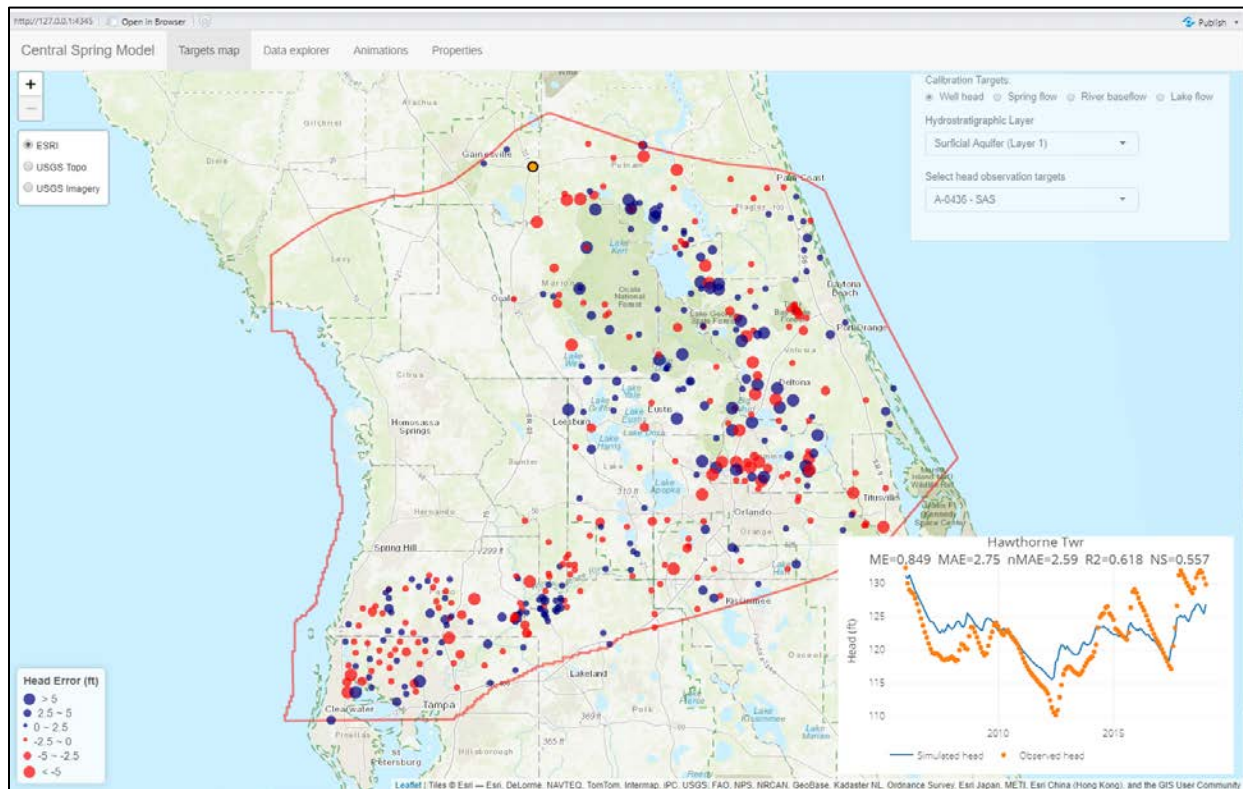


Figure 4-2. Central Springs Model interactive web application (shinyapps.io) for the visualization of transient model outputs (<https://waterapp.shinyapps.io/CentralSpringModel/>)

METRICS AND CRITERIA

The CSM calibration was based on three quantitative calibration targets, including:

- Groundwater level residuals
- Vertical head differences across confining units
- Spring discharges

The statistical metrics utilized in the CSM calibration criteria are defined below.

Mean Error (ME): The mean value of the squared differences between simulated and observed values, calculated as

$$ME = \left[\frac{1}{n} \sum_{i=1}^n (s_i - x_i)^2 \right] \quad (4-2)$$

Where:

x_i = observed value

s_i = simulated value

n = number of observations (targets)

The ME is used to measure the collective discrepancy between modeled and observed values and indicates the bias in simulated results. A value close to zero indicates no bias and reflects better model performance.

Mean Absolute Error (MAE): The mean value of the squared differences between simulated and observed values, calculated as:

$$MAE = \left[\frac{1}{n} \sum_{i=1}^n |s_i - x_i| \right] \quad (4-3)$$

The MAE is used to measure the collective discrepancy between modeled and observed values and indicates the closeness between the simulated results and the observations. Smaller values represent modeled data closer to the observed data and reflect better model performance.

Percent Bias (PBIAS): The percent bias measures the average tendency of the simulated data to be larger or smaller than the observed data and is calculated as:

$$PBIAS = \left[\frac{\frac{1}{n} \sum_{i=1}^n (s_i - x_i) \times 100}{\frac{1}{n} \sum_{i=1}^n x_i} \right] \quad (4-4)$$

Coefficient of Determination/Pearson Product-Moment Correlation Coefficient (R^2) between simulated and observed values is calculated as:

$$R^2 = \left[\frac{\sum (x_i - x_m)(s_i - s_m)}{(\sum (x_i - x_m)^2 \sum (s_i - s_m)^2)^{0.5}} \right]^2 \quad (4-5)$$

Where:

x_m = mean of observed data

s_m = mean of simulated data

R^2 is the measure of the degree of linear association between simulated and observed values and represents the amount of variability between them. The R^2 value can vary from 0 to 1, with 1 indicating a perfect fit between simulated and observed values.

Ratio of Root-Mean-Square Error and Standard Deviation of Observed Data (RSR) is calculated as:

$$RSR = \frac{\sqrt{\sum (s_i - x_i)^2}}{\sqrt{\sum (x_i - x_m)^2}} \quad (4-6)$$

RSR is the ratio of root mean square errors of residuals over the standard deviation of observations. It incorporates the benefits of error index statistics and includes a scaling/normalization factor so that the resulting statistic and reported values can apply to various constituents. RSR varies from an optimal value of 0, which indicates zero residual variation and therefore perfect model simulation. The lower RSR, the lower the RMS error and the better the model simulation performance.

Nash-Sutcliffe Efficiency Coefficient (NSE) between simulated and observed values is calculated as:

$$NSE = 1 - \frac{\sum (s_i - x_i)^2}{\sum (x_i - x_m)^2} \quad (4-7)$$

Like the R^2 discussed above, NSE is another indicator of goodness of fit and has been recommended by the American Society of Civil Engineers (ASCE, 1993) for use in hydrologic studies. A value equal to 1 indicates a perfect fit between simulated and observed values, and values equal to zero indicate that the model is predicting no better than using the average of the observed data. Therefore, any value above zero suggests that the model has some utility, with higher values indicating better performance. Generally, the R^2 values tend to be higher than NSE values because an outlying value on a single event will significantly lower NSE while only slightly affecting R^2 . Further, the NSE value favors high flows while sacrificing low flows; hence, it is a measure of a good match to the high flows.

Metrics and criteria for the steady-state and transient targets are summarized in Table 4-1 and Table 4-2, respectively.

Table 4-1. Steady-state calibration criteria (spatial statistics)

Category	Metric	Calibration Criteria
Groundwater levels	ME	$< \pm 0.5$ ft
	MAE	All layers - 50% of MAE < 2.5 ft and 80% of MAE < 5 ft SAS - evaluate depth to water table qualitatively
	R ²	> 0.85 (UFA/LFA) > 0.75 (SAS)
Spring discharges	MAE	First magnitude springs $< 5\%$ of observed flow Second magnitude springs $< 10\%$ of observed flow Second magnitude springs (with limited data) $< 20\%$ of observed flow Third or higher magnitude springs – within the same order of magnitude of observed flow
	R ²	> 0.75
Baseflows	NA	Within the range of baseflow estimated by several methods
Vertical head difference residuals (ICU and MCU)	NA	The same flow direction for targets ≤ 5 ft Simulated is larger than 50% and smaller than 150% of observed for targets > 5 ft

Notes: ft = feet
 ICU = Intermediate Confining Unit
 LFA = Lower Floridan Aquifer
 MAE = mean absolute error
 MCU = Middle Confining Unit
 ME = mean error
 NA = not applicable
 R² = coefficient of determination
 SAS = Surficial Aquifer System
 UFA = Upper Floridan Aquifer

Table 4-2. Transient calibration criteria (temporal statistics)

Category	Metric	Calibration Criteria
Groundwater levels	PBIAS	$< \pm 10$ (UFA/LFA) $< \pm 15$ (SAS)
	MAE	All layers - 50% of MAE < 2.5 ft and 80% of MAE < 5 ft
	ME	$< \pm 0.5$ ft
	RSR	≤ 0.5 (UFA/LFA) ≤ 0.7 SAS
	R ²	> 0.85 (UFA/LFA) > 0.75 (SAS)
Spring discharges	MAE	First magnitude springs $< 5\%$ of observed flow Second magnitude springs $< 10\%$ of observed flow Second magnitude springs (with limited data) $< 20\%$ of observed flow Third or higher magnitude springs – within the same order of magnitude of observed flow
	R ²	> 0.6 (springs > 10 cfs)
Baseflows	NA	Within the range of baseflow estimated by several methods
Vertical head difference residuals (ICU and MCU)	NA	The same flow direction for targets ≤ 5 ft Simulated is larger than 50% and smaller than 150% of observed for targets > 5 ft

Notes: ft = feet

ICU = Intermediate Confining Unit

LFA = Lower Floridan Aquifer

MAE = mean absolute error

MCU = Middle Confining Unit

ME = mean error

NA = not applicable

PBIAS = percent bias

R² = coefficient of determination

SAS = Surficial Aquifer System

UFA = Upper Floridan Aquifer

Groundwater Level Residuals

All observed groundwater levels in the areas of saltwater intrusion/upconing were converted to equivalent freshwater heads before calibration and residual calculation. The equivalent freshwater head is given by the equation:

$$H = z + \frac{\rho_s}{\rho_f} d \quad (4-8)$$

Where:

- H = equivalent hydraulic head (ft)
- z = elevation head (positive vertically upward) (ft)
- d = depth below sea level (ft)
- ρ_s = groundwater density (g/mL)
- ρ_f = freshwater density (g/mL)

In Equation (4-8), d for a given cell was the depth of the cell centroid below sea level, and ρ_s and ρ_f were set at 1.025 and 1.00 g/mL for seawater and freshwater, respectively. Measured groundwater density ρ_s was used for the equivalent freshwater head evaluation when available.

Groundwater level residuals were used to determine the goodness of fit between the simulated and observed water levels. The objective of the calibration effort was to minimize errors between the simulated and observed water levels and to minimize spatial bias in the errors. Calibration goals were set to a ME of less than 0.5 ft and a MAE of less than 2.5 ft for 50 percent of groundwater levels and less than 5.0 ft for 80 percent of groundwater levels.

Vertical Head Differences Across Confining Units

In addition to comparing simulated and observed heads, vertical head difference directions and magnitudes across the confining units were also used to assess the model's ability to simulate the degree of confinement across the ICU and MCU I. The general requirement was similarity in terms of direction and magnitude of head differences. For observed groundwater level differences less than 5 feet, the simulated difference should have the same flow direction. For an observed groundwater level difference greater than 5 feet, the difference between the simulated and observed head differences should be larger than 50 percent and less than 150 percent of the observed groundwater level difference.

Spring Discharges

Model parameters were adjusted to match simulated discharge for each first magnitude spring to within 5 percent of the observed discharge, for each second magnitude spring to within 10 percent of the observed discharge, and for second magnitude springs with limited observations to within 20 percent. The criterion for third magnitude or higher springs was to match simulated discharge to within the same order of magnitude as the observed discharge. The same spring discharge criteria were applied to both the steady-state and transient calibrations.

Qualitative Assessments

Other assessments included comparing estimated and simulated river baseflows, reviewing hydraulic properties from aquifer performance tests (APTs), comparing estimated and simulated lake leakage and depth to water table values, and examining general regional flow patterns in UFA.

Baseflows were estimated using multiple methods. The eight hydrograph techniques in the USGS GW Toolbox (Barlow et al. 2014) and Perry method (Perry, 1995; also known as the “USF method”) were used to separate baseflow from streamflow. The locations of the baseflow gages utilized in the CSM are shown on Figure 4-3. Estimated baseflows derived from the USGS GW Toolbox methods tend to fall within the high range of estimated values, while baseflows estimated by the Perry method generally fall at the low end. Baseflow rates were not estimated for tidally affected sites, sites influenced by structures, or sites missing more than a few daily flow measurements throughout the simulation period.

Properties determined from APTs were used qualitatively to evaluate the reasonableness of calibrated aquifer parameters, such as transmissivity. It was a goal during calibration to match simulated aquifer transmissivities to within one order of magnitude of the APT values.

Estimated vertical leakages from lakes with local water budget analyses were compared against simulated vertical lake leakages. In addition, lake leakage was limited to within ± 20 in/yr to help to constrain leakage rates to reasonable values. Long-term depth to water table values from SAS monitoring wells were also compared qualitatively to simulated values.

Simulated potentiometric head distributions in the UFA were compared against those provided by the USGS to ensure that regional groundwater flow directions and potentiometric contours were simulated reasonably well.

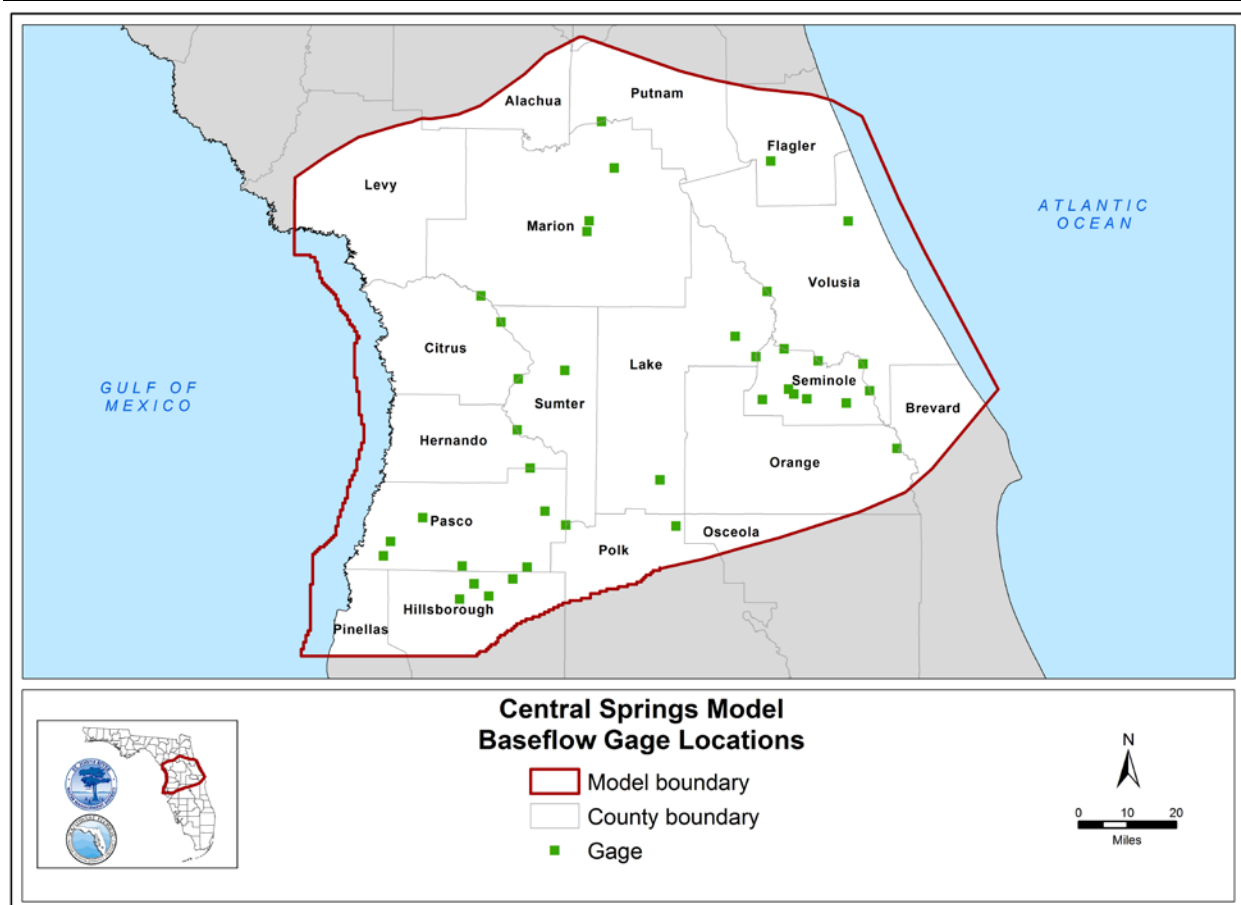


Figure 4-3. Baseflow gage locations within the Central Springs Model domain

PRE-CALIBRATION SENSITIVITY ANALYSIS

(This section is adopted from Appendix D of the HGL 2023 report)

A parameter sensitivity analysis was conducted prior to calibration to rank the degree of model sensitivity to changes in each hydrologic parameter. The sensitivity analysis was conducted by systematically varying one parameter or boundary condition, while keeping the others constant. Thirteen parameters that appreciably affect groundwater flow in the model domain were included in the sensitivity analysis as shown in Table 4-3. The perturbation of each parameter was based on the expected range of variability of that parameter. The first 11 parameters were investigated using steady-state simulations, while the last two (Sy and Ss) were subject to transient simulations.

Sensitivity Analysis Results

Results of relative sensitivity for the SAS, the UFA, and the LFA are shown in Table 4-4, Table 4-5, and Table 4-6, respectively. Mean absolute error was used as the primary sensitivity metric. Relative sensitivity is defined as the difference in MAE between the perturbed sensitivity case and a base case using a multiplicative factor of one and an additive factor of zero. The results for the most sensitive parameters for the SAS, the UFA, and the LFA are graphically summarized on Figure 4-4, Figure 4-5, and Figure 4-6, respectively.

Sensitivity Discussion

The sensitivity analysis indicated that groundwater levels were more sensitive to changes in recharge and hydraulic conductivity. They were relatively insensitive to changes in river stage and conductance, spring/drain pool elevation and conductance, and GHB elevation and conductance although these parameters could be important for simulating spring flows and baseflows.

Table 4-3. List of parameters and perturbation types

Number	Parameter	Perturbation Type
1	Hydraulic conductivity of the UFA	Multiplicative
2	Hydraulic conductivity of the LFA	Multiplicative
3	River/lake conductance	Multiplicative
4	River/lake stage	Additive
5	Spring/drain conductance	Multiplicative
6	Spring/drain pool elevation	Additive
7	Leakance of the ICU	Multiplicative
8	Leakance of the MCU	Multiplicative
9	Recharge	Multiplicative
10	GHB conductance	Multiplicative
11	GHB elevation*	Additive
12	Specific yield	Multiplicative
13	Storage coefficient	Multiplicative

Note: * Applicable to the northern, eastern, and southern boundaries of the UFA

GHB = General head boundary
 ICU = Intermediate Confining Unit
 LFA = Lower Floridan Aquifer
 MCU = Middle Confining Unit
 UFA = Upper Floridan Aquifer

Table 4-4. Relative sensitivity for the Surficial Aquifer System (HGL, 2023)

Parameter	Change in Mean Absolute Error		
	Multiplier		
	0.20	1.00	5.00
Upper Floridan Aquifer hydraulic conductivity	1.13	0.00	2.13
Lower Floridan Aquifer hydraulic conductivity	0.46	0.00	0.51
River conductance	0.38	0.00	0.06
Drain conductance	0.16	0.00	0.17
Intermediate Confining Unit leakance	2.69	0.00	3.21
Middle Confining Unit leakance	0.00	0.00	0.28
General head boundary conductance	0.03	0.00	-0.01
Specific yield	0.94	0.00	-0.26
Storage coefficient	0.17	0.00	-0.17
Parameter	Multiplier		
	0.80	1.00	1.25
Recharge	0.58	0	2.38
Parameter	Added stage (feet)		
	0.00	1.00	
River stage	0.00	0.05	
Drain stage	0.00	0.02	
General head boundary level	0.00	-0.01	

Table 4-5. Relative sensitivity for the Upper Floridan Aquifer (HGL, 2023)

Parameter	Change in Mean Absolute Error		
	Multiplier		
	0.20	1.00	5.00
Upper Floridan Aquifer hydraulic conductivity	3.53	0.00	3.65
Lower Floridan Aquifer hydraulic conductivity	0.81	0.00	1.24
River conductance	0.12	0.00	0.05
Drain conductance	0.50	0.00	0.19
Intermediate Confining Unit leakance	1.09	0.00	0.46
Middle Confining Unit leakance	0.08	0.00	0.40
General head boundary conductance	0.02	0.00	0.00
Specific yield	0.15	0.00	-0.11
Storage coefficient	0.05	0.00	-0.04
Parameter	Multiplier		
	0.80	1.00	1.25
Recharge	0.24	0.00	1.03
Parameter	Added stage (feet)		
	0.00	1.00	
River stage	0.00	0.03	
Drain stage	0.00	0.09	
General head boundary level	0.00	0.01	

Table 4-6. Relative sensitivity for the Lower Floridan Aquifer (HGL, 2023)

Parameter	Change in Mean Absolute Error		
	Multiplier		
	0.20	1.00	5.00
Upper Floridan Aquifer hydraulic conductivity	1.67	0.00	4.33
Lower Floridan Aquifer hydraulic conductivity	1.79	0.00	2.93
River conductance	0.05	0.00	-0.06
Drain conductance	-0.19	0.00	0.73
Intermediate Confining Unit leakance	1.75	0.00	-0.1
Middle Confining Unit leakance	2.85	0.00	1.19
General head boundary conductance	0.11	0.00	0.00
Specific yield	0.01	0.00	-0.08
Storage coefficient	-0.02	0.00	0.02
Parameter	Multiplier		
	0.80	1.00	1.25
Recharge	0.71	0.00	0.24
Parameter	Added stage (feet)		
	0.00	1.00	
River stage	0.00	-0.09	
Drain stage	0.00	-0.05	
General head boundary level	0.00	0.01	

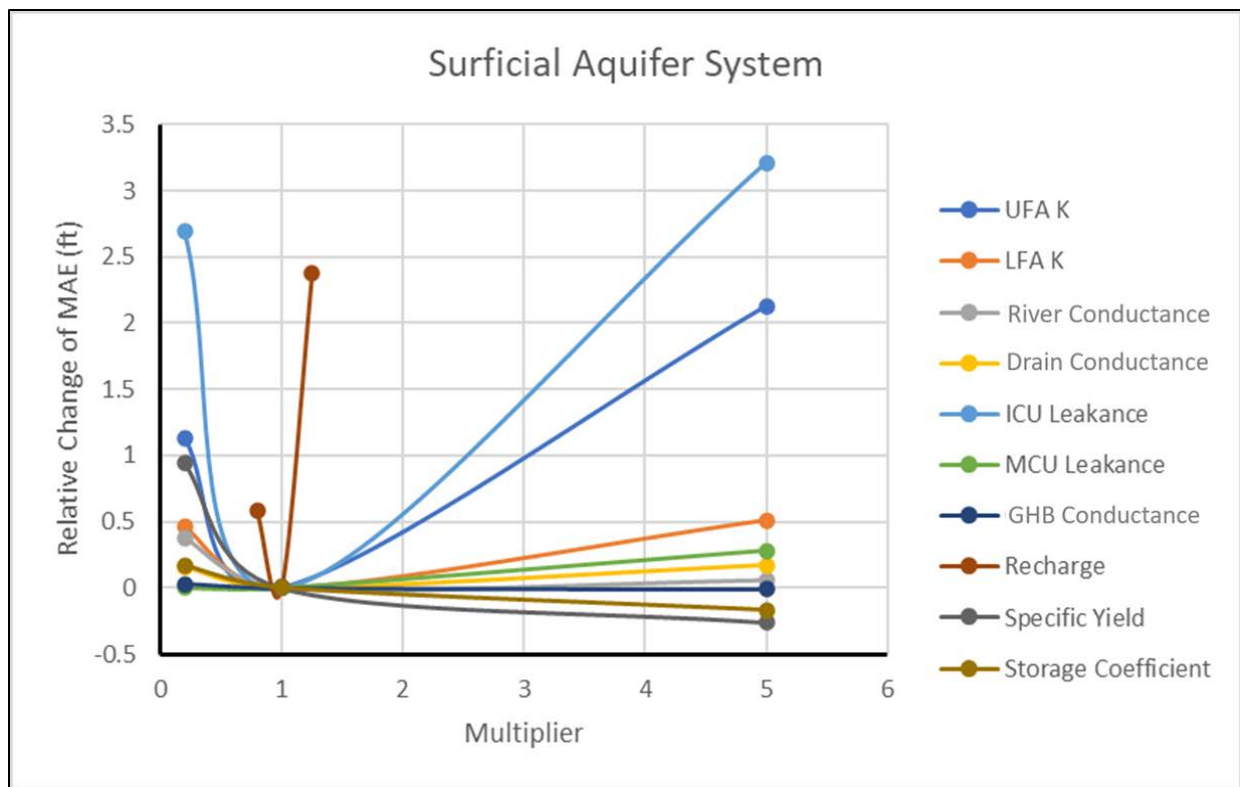


Figure 4-4. Relative sensitivity for the Surficial Aquifer System (HGL, 2023)

Note: ft = feet

GHB = General head boundary

ICU = Intermediate Confining Unit

K = hydraulic conductivity

LFA = Lower Floridan Aquifer

MAE = mean absolute error

MCU = Middle Confining Unit

UFA = Upper Floridan Aquifer

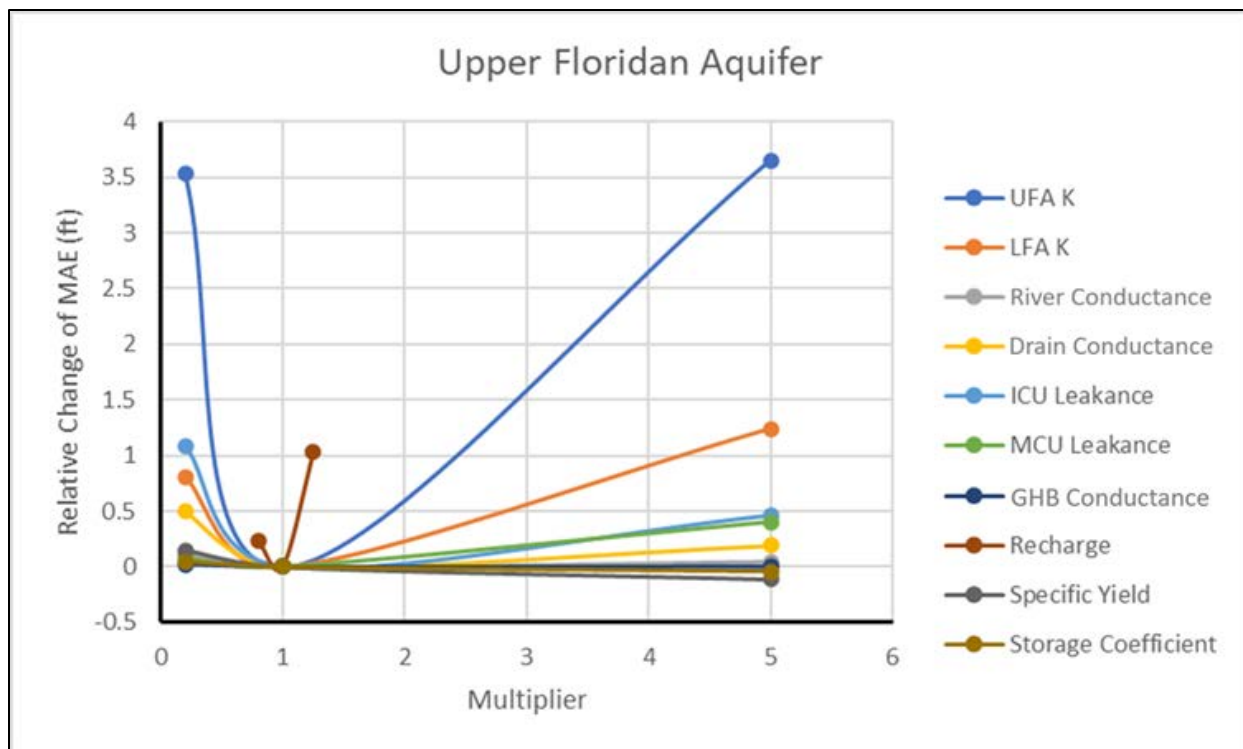


Figure 4-5. Relative sensitivity for the Upper Floridan Aquifer (HGL, 2023)

Note: ft = feet

GHB = General head boundary

ICU = Intermediate Confining Unit

K = hydraulic conductivity

LFA = Lower Floridan Aquifer

MAE = mean absolute error

MCU = Middle Confining Unit

UFA = Upper Floridan Aquifer

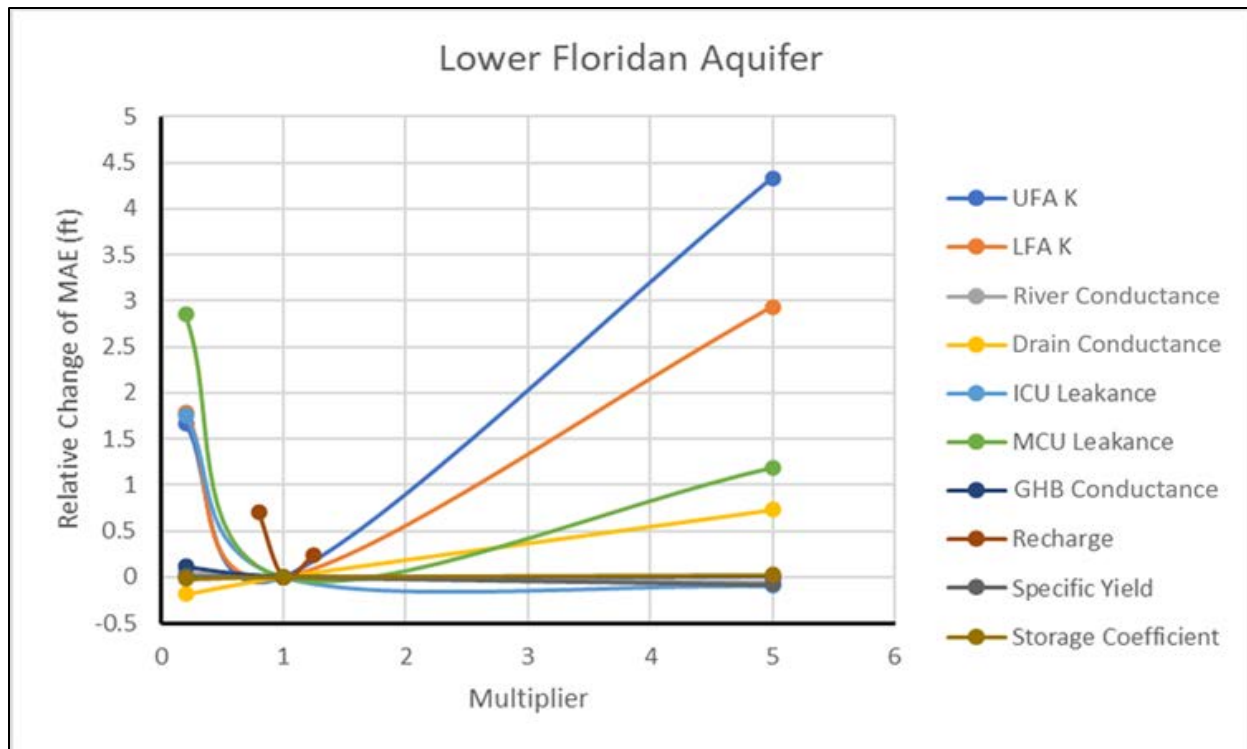


Figure 4-6. Relative sensitivity for the Lower Floridan Aquifer (HGL, 2023)

Note: ft = feet

GHB = General head boundary

ICU = Intermediate Confining Unit

K = hydraulic conductivity

LFA = Lower Floridan Aquifer

MAE = mean absolute error

MCU = Middle Confining Unit

UFA = Upper Floridan Aquifer

5. STEADY-STATE CALIBRATION

The steady-state model was calibrated to average hydrologic and pumping conditions from 2005 to 2018 utilizing PEST. As described in Chapter 4, a sensitivity analysis was conducted prior to calibration to understand how the model responded to changes in hydraulic conductivity and other parameters. Upon completion of the sensitivity analysis, an initial manual calibration was conducted to test the model numerical requirements, numerical stability and performance of MODFLOW-NWT, and response of the hydrological system to changes in model parameters. Following the initial manual calibration, a number of automated PEST calibrations were performed by adjusting hydraulic parameters, which were then input to the transient model in an iterative fashion as described in Chapter 4. This iterative process helped refine the steady-state model and its PEST calibration configuration based on insights and understandings obtained from the transient simulations.

PEST CALIBRATION

PEST Approach

PEST calibration is organized around two primary groups of data, including observation groups and calibration (adjustable) parameter groups. Observation groups are comprised of empirical or estimated groundwater levels and flows. Adequate simulation of observation group measurements is the primary objective of the calibration process. PEST facilitates calibration through a process of systematic adjustment of the various model parameters that constitute the calibration parameter groups to minimize the objective function.

The PEST objective function is defined as follows (Doherty, 2010):

$$\Phi = \sum_{i=1}^n (w_i R_i)^2 \quad (5-1)$$

Where:

Φ = PEST objective function, equal to the summation of the squares of the products of w_i and corresponding value of R_i , summed over n observations

w_i = assigned to the residual of observation i

R_i = difference between the value of observation i and its model simulated counterpart

n = number of all observations comprising the various observation groups.

PEST utilizes numerous model runs and optimization iterations with the goal of minimizing the value of the objective function while maintaining the values of the various calibration parameters within user-specified ranges. For each iteration, prior to estimating a set of parameter values, PEST constructs a Jacobian matrix, which contains the derivative of each observation with respect to each adjustable model parameter. PEST uses the Jacobian matrix to obtain an improved parameter data set by adjusting hydrogeologic parameter values at the beginning of the iteration within the user-specified ranges.

PEST users can integrate their expert knowledge into the calibration process through specification of initial hydrogeologic parameter values, minimum and maximum values that

represent the acceptable ranges of the calibration parameters, and weights assigned to residuals of observations, with residuals representing the difference between simulated and observed data.

Observation Data Groups

The steady-state model was calibrated to the arithmetic mean of observed water levels and spring discharge rates for the years 2005 to 2018. A detailed listing of the observation groups utilized in the PEST calibration process is provided in Table 5-1. The observation groups can generally be placed into one of two categories. The first category consists of measured or derived values, including:

- Groundwater levels
- Groundwater level differences across confining units
- Spring discharges

It should be noted that there were relatively few monitoring wells available for use as calibration targets in the LFA below MCU I (layer 6). The LFA wells within the SWFWMD jurisdiction were mostly constructed in the last decade and little data was available over the calibration period. A time-series evaluation showed a strong correlation in observed groundwater levels between wells in the UFA and LFA. Therefore, a linear regression methodology was implemented to develop a synthesized time-series of LFA target well water levels using available long-term monitoring data from UFA monitoring wells. The average 2005 to 2018 groundwater levels were calculated using this synthetic data and used for calibration of the steady-state model.

PEST calibration requires specification of weights assigned to the residuals of observation parameter groups. The assigned weights, provided in Table 5-1, help PEST prioritize its optimization strategy for each observation group.

A series of penalty groups was included with the observation groups to prevent excessive flooding in the SAS and constrain fluxes from the boundary conditions to reasonable ranges based on professional judgement. Penalty groups used during calibration of the CSM include:

- Flooding penalty (constrained by layer 1 top elevations by minimizing the difference between simulated SAS head and layer 1 top elevation at flooded cells)
- CHD flux penalty (constrained by ± 100 in/yr)
- GHB flux penalty (constrained by ± 100 in/yr)
- RIV flux penalty (constrained by ± 20 in/yr)

The flooding penalty was incorporated to help prevent excessive flooding in layer 1 during the simulation. Penalties for CHD, GHB, and river cell fluxes were gradually implemented and adjusted to ensure the simulated water budget remained within a reasonable range. The weights of the flux penalties were also adjusted during this process to minimize the likelihood of individual boundary condition cells becoming unreasonable sources or sinks in the overall water budget. The final weights for the penalty groups are listed in Table 5-1.

Table 5-1. PEST observation groups

Observation Group Name	Description	Weight Assigned to Observation Group Residual
h_1, h_3, h_4, h_5, h_6	Heads in layers 1, 3, 4, 5, and 6	1
vdf_sas_ufa	Vertical head differences between SAS and UFA	1
vdf_ufa_lfa	Vertical head differences between UFA and LFA	1
spfobs	Springflows	1E-4
fp	Flooding penalty	5E-2
chdqp	CHD flux penalty	5E-3
ghbqp	GHB flux penalty	5E-3
rivqp	RIV flux penalty	1E-1

Note: SAS = Surficial Aquifer System
 LFA = Lower Floridan Aquifer
 UFA = Upper Floridan Aquifer
 CHD = Constant head
 GHB = General head boundary

Calibration Parameter Groups

PEST calibration requires input of user-specified initial values and upper and lower bounds for each member of the calibration parameter groups, as shown in Table 5-2. The calibration parameter groups are categorized as follows:

- Hydraulic conductivity
 - horizontal hydraulic conductivity (Kh) for layers 1, 3, 4, 6 and 7
 - vertical hydraulic conductivity (Kv) for layers 2 and 5
- General head boundary conductance
- Drain conductance to represent springs or spring groups
- River/drain conductance multipliers by HSPF subbasin
- Lake/stream zone multipliers for adjustment of Kv in layer 2 to constrain leakage rates to the UFA from lakes and streams
- Recharge multipliers

A description of each calibration parameter group is provided in the following section.

Table 5-2. PEST calibration parameter groups

Parameter Group Name	Parameterization Device	Description
kh1	Pilot points	Layer 1 horizontal hydraulic conductivity
kz2	Pilot points	Layer 2 vertical hydraulic conductivity
kh3	Pilot points	Layer 3 horizontal hydraulic conductivity
kh4	Pilot points	Layer 4 horizontal hydraulic conductivity
kz5	Pilot points	Layer 5 vertical hydraulic conductivity
kh6	Pilot points	Layer 6 horizontal hydraulic conductivity
kh7	Pilot points	Layer 7 horizontal hydraulic conductivity
rchm	Sub-basins	Recharge multiplier; not activated
rivdrn_m	Sub-basins	RIV and DRN conductance multiplier
riv2kz	Specified layer 2 zones beneath RIV cells	kz2 (layer 2 vertical k) multiplier for layer 2 cells beneath RIV
spc	Spring vents	Spring conductance

CALIBRATED PARAMETERS

Initial estimates of parameter values were assigned based on previous modeling efforts, with additional consideration of field measurements and existing knowledge of the hydrogeologic system. The model parameters produced during PEST calibration were reviewed after application to the transient model. Quantitative targets, qualitative targets, and the water budget were used to gauge model performance during different PEST configurations. The iterative approach illustrated on Figure 4-1 was used to guide the PEST calibration process.

Hydraulic Conductivity

Hydraulic conductivity is the most important input parameter of a groundwater model. It represents the aquifer's ability to transmit water under a hydraulic gradient. Hydraulic conductivity values are given in the horizontal and vertical flow direction. The horizontal hydraulic conductivity (Kh) value establishes how water flows between each cell within a given model layer, while the vertical hydraulic conductivity (Kv) value establishes the rate of vertical flow through model layers. Hydraulic conductivity values are necessary to calculate other model parameters such as leakance, transmissivity, and GHB conductance.

Horizontal hydraulic conductivity values for layers 1, 3, 4, 6, and 7 and Kv values for layers 2 and 5 were estimated directly at pilot point locations in the PEST calibration process. Pilot points are user specified points at which the values of parameters are adjusted during the PEST calibration process. Once Kh and Kv are optimized, the ordinary kriging spatial interpolation method employed by PEST is used to distribute values of hydraulic conductivity to individual grid cells by interpolating between pilot points. The pilot points were located uniformly using a distance of 10 grid cells (25,000 ft). Figure 5-1 depicts pilot point locations within the CSM domain. The final calibrated Kh and Kv values for layer 1 through layer 7 are provided in Figure 5-2 through Figure 5-8.

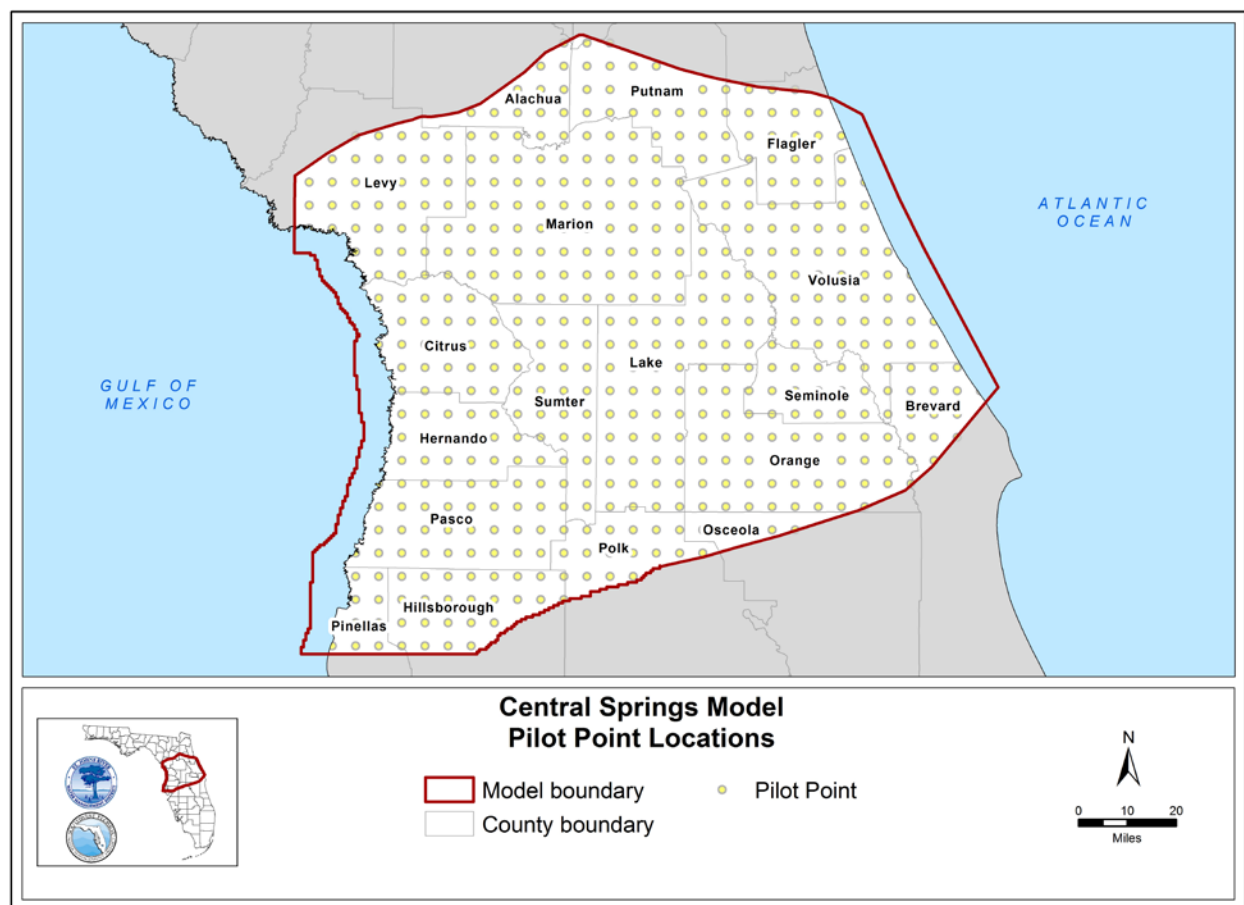


Figure 5-1. Pilot point locations within the Central Springs Model domain

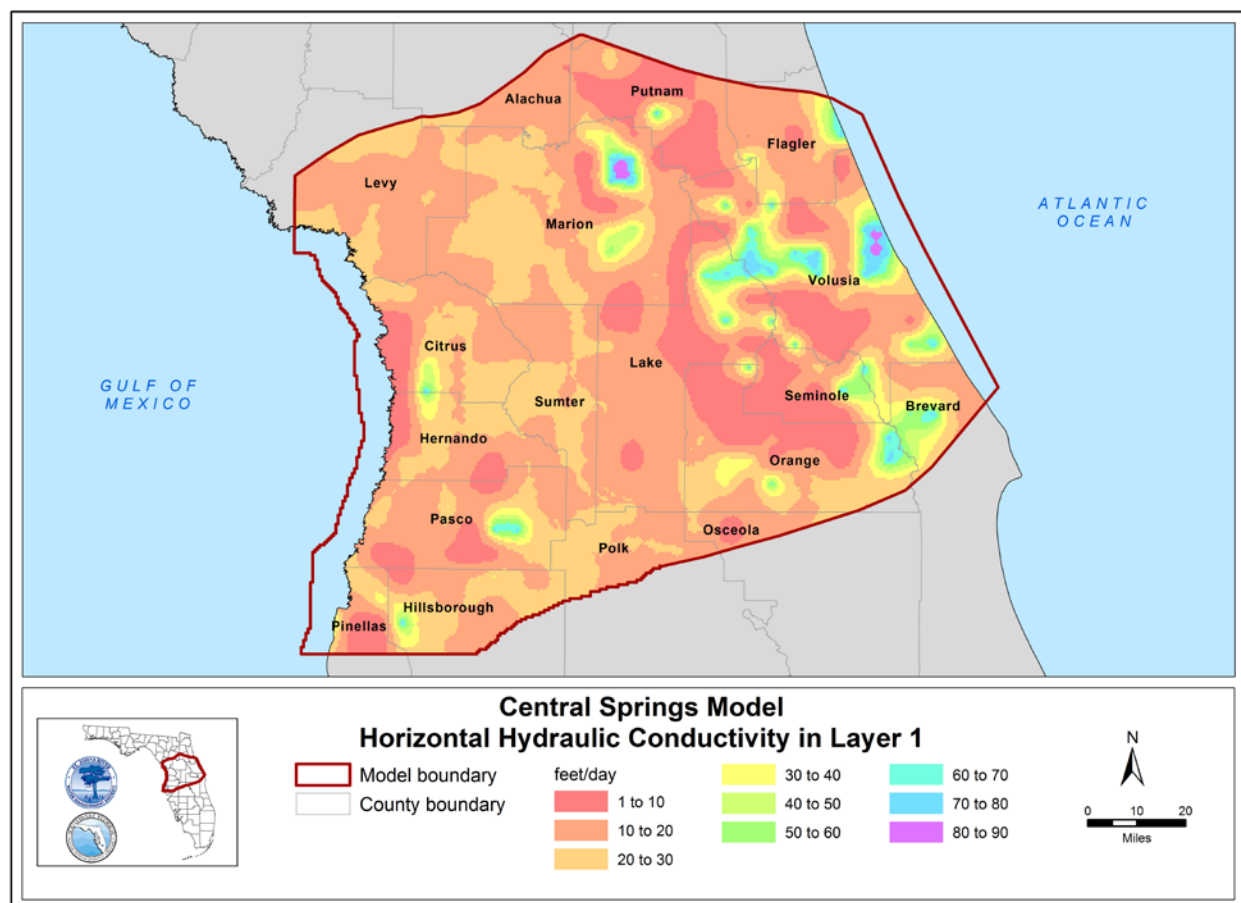


Figure 5-2. Horizontal hydraulic conductivity in layer 1 within the Central Springs Model domain

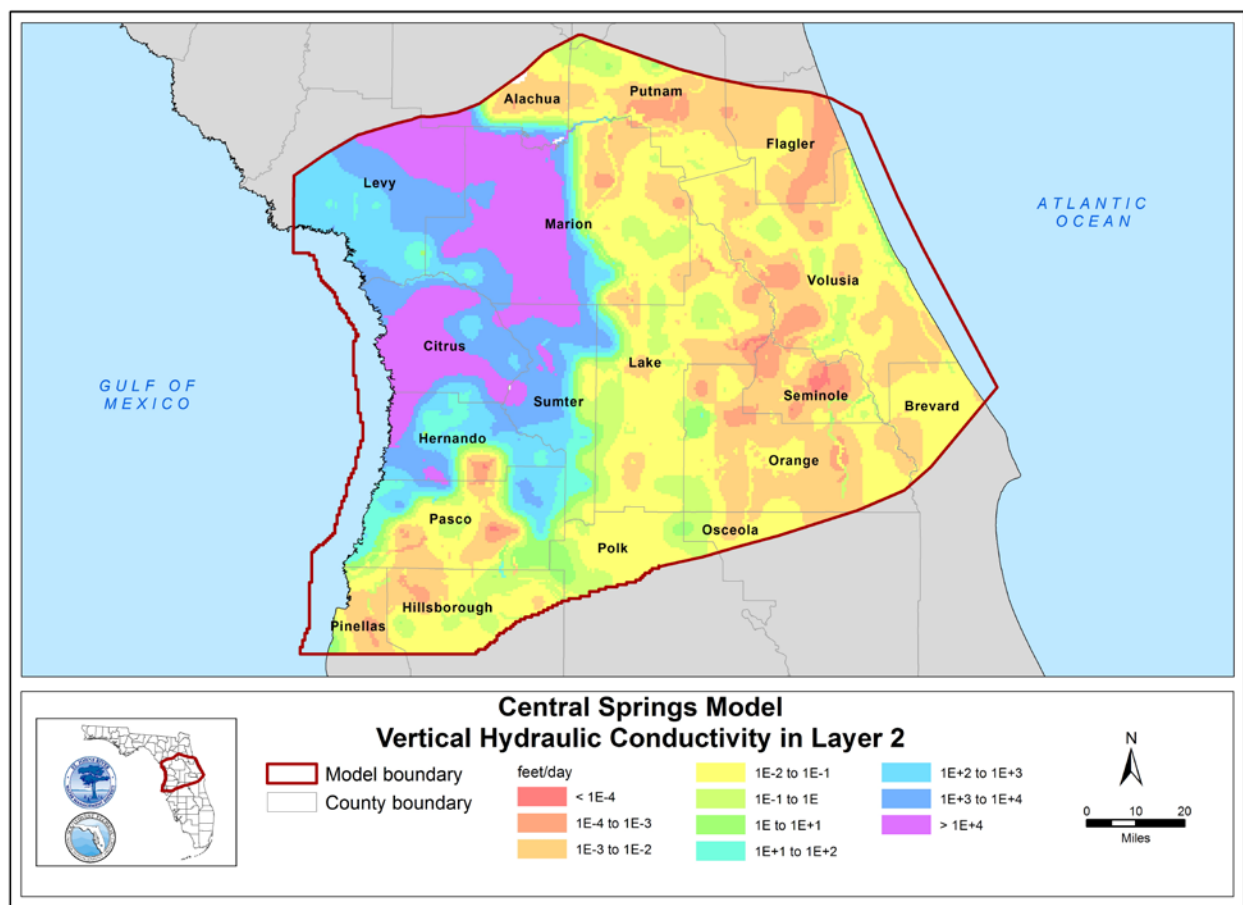


Figure 5-3. Vertical hydraulic conductivity in layer 2 within the Central Springs Model domain

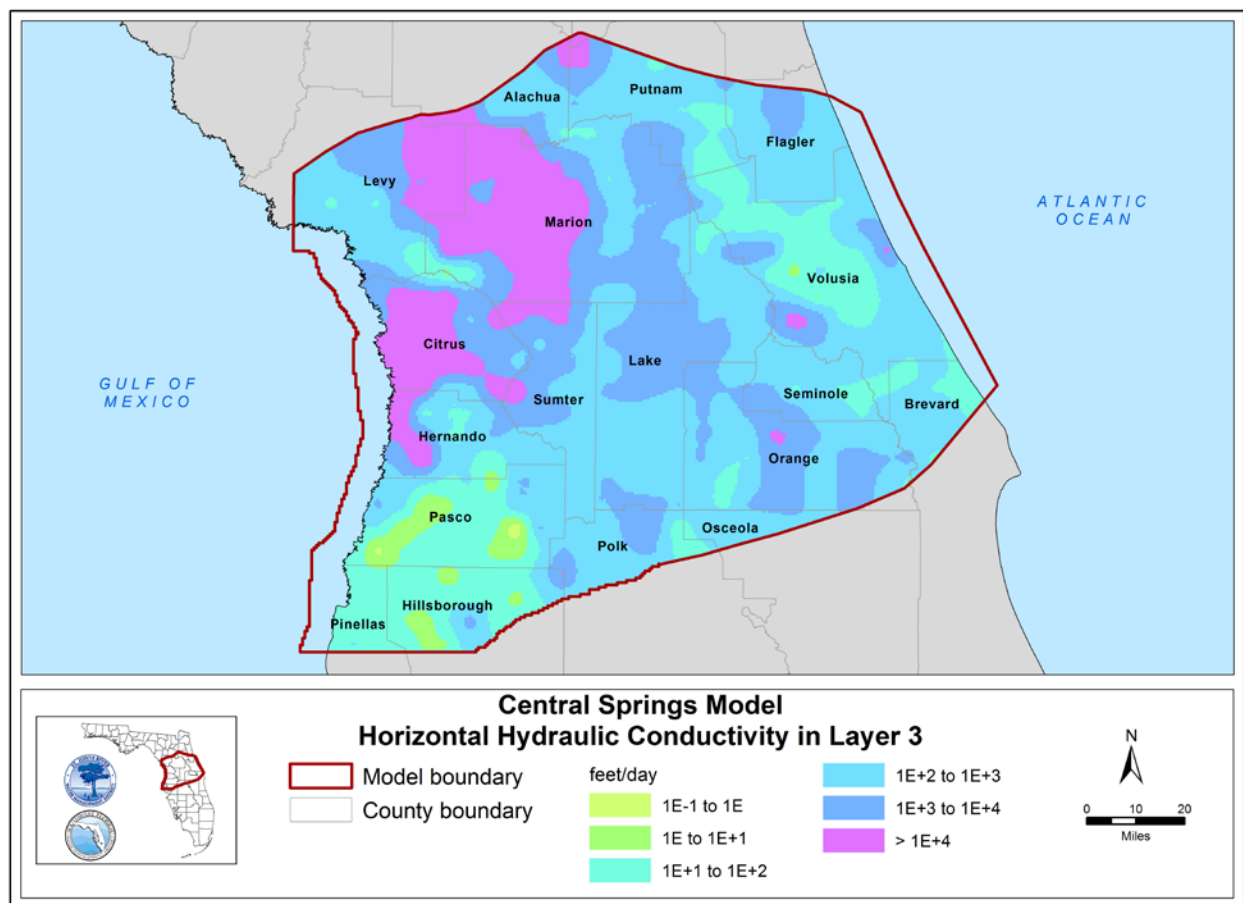


Figure 5-4. Horizontal hydraulic conductivity in layer 3 within the Central Springs Model domain

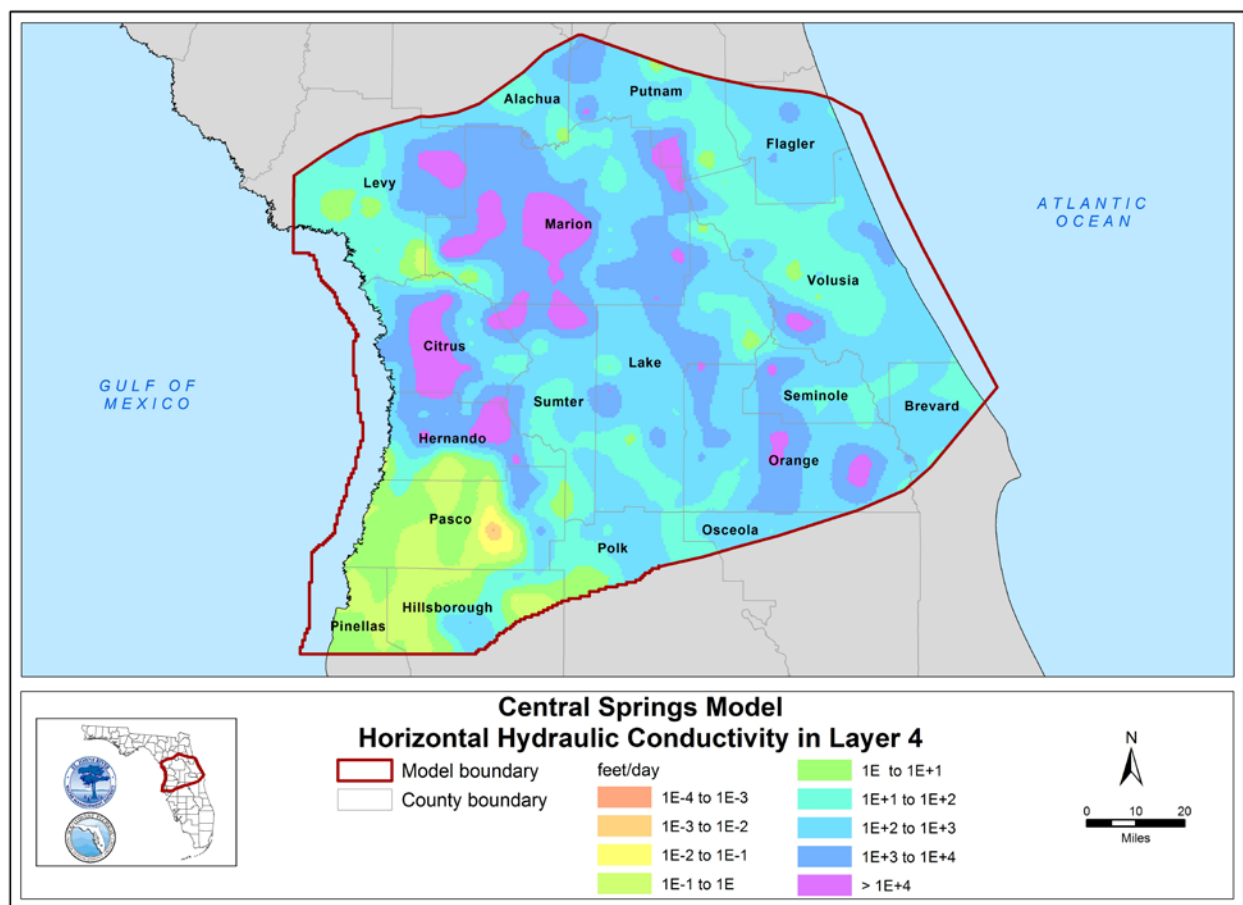


Figure 5-5. Horizontal hydraulic conductivity in layer 4 within the Central Springs Model domain

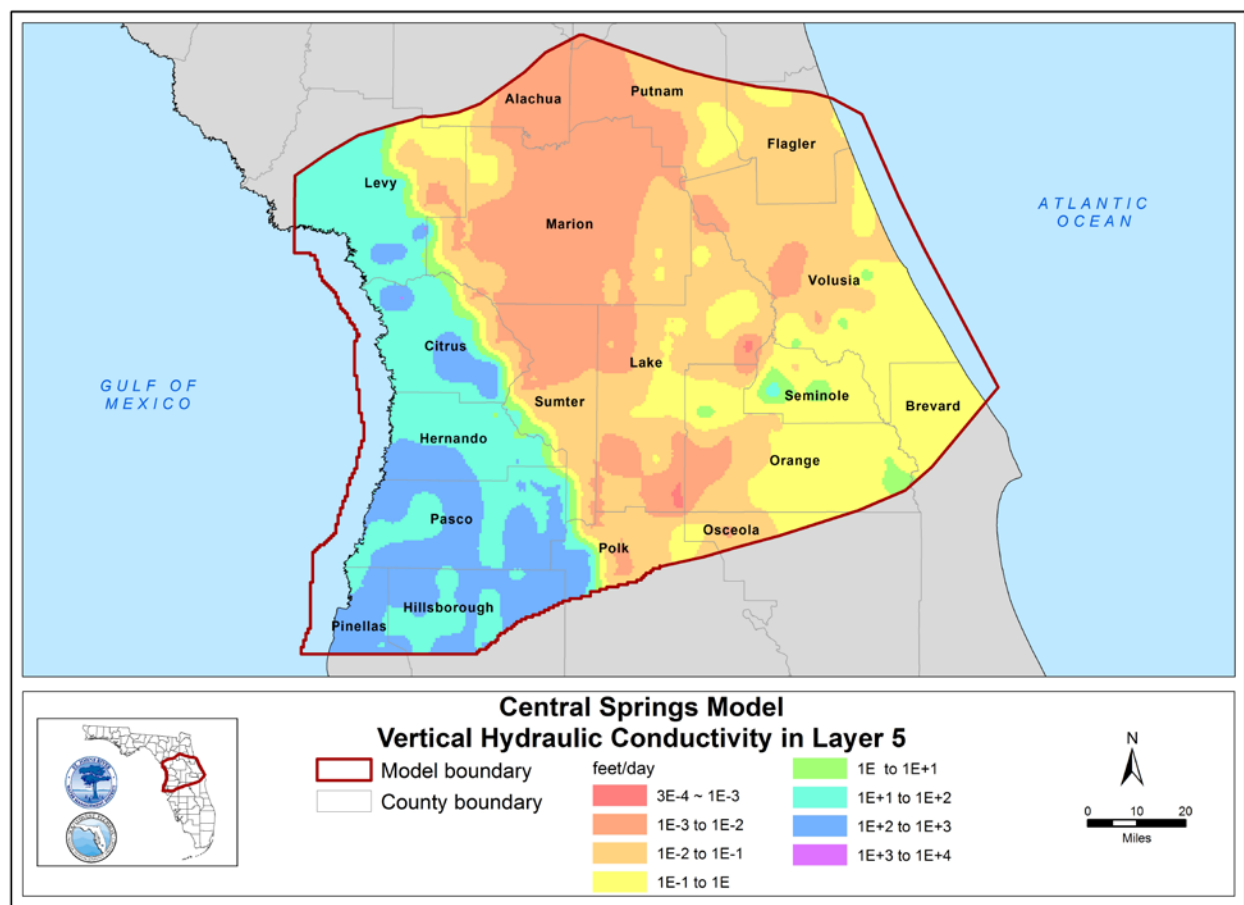


Figure 5-6. Vertical hydraulic conductivity in layer 5 within the Central Springs Model domain

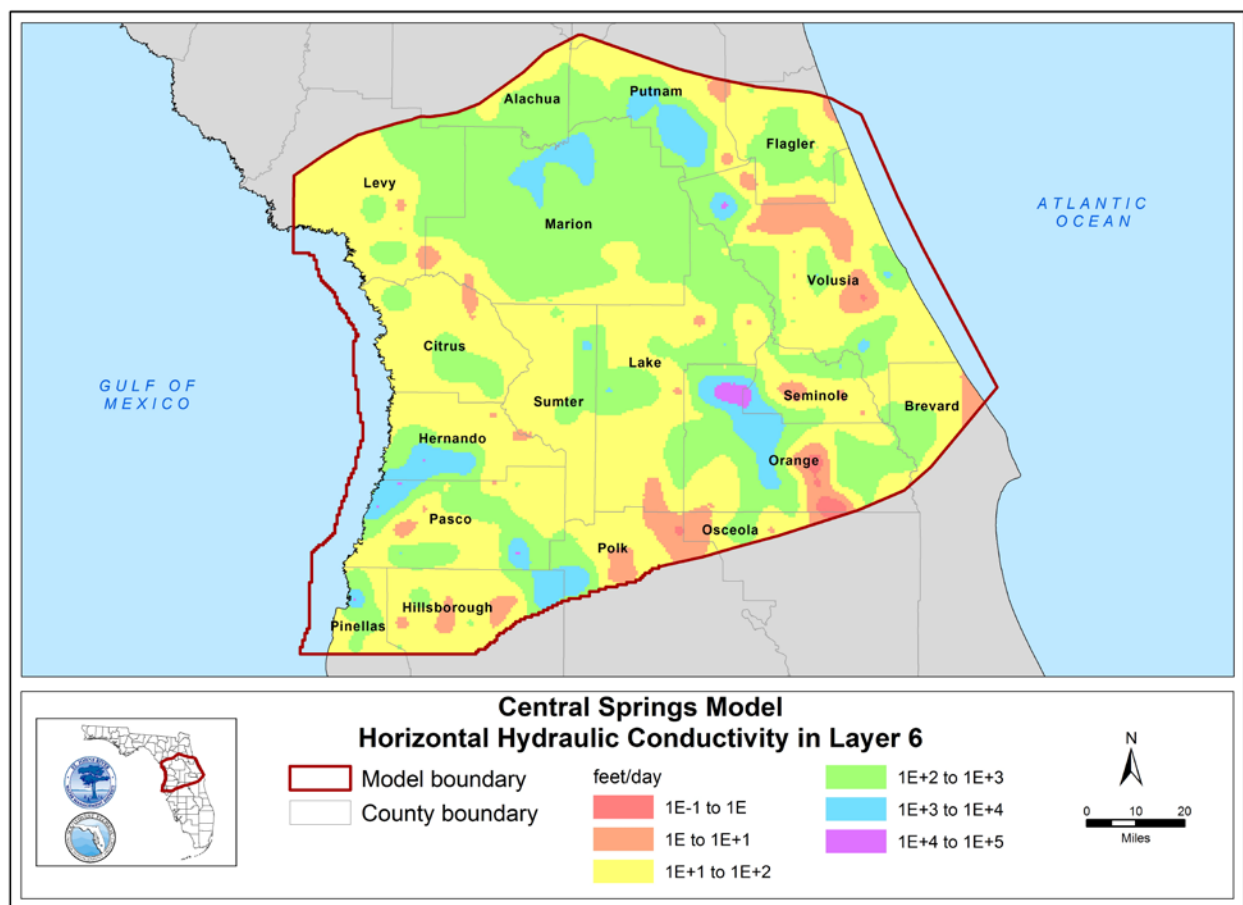


Figure 5-7. Horizontal hydraulic conductivity in layer 6 within the Central Springs Model domain

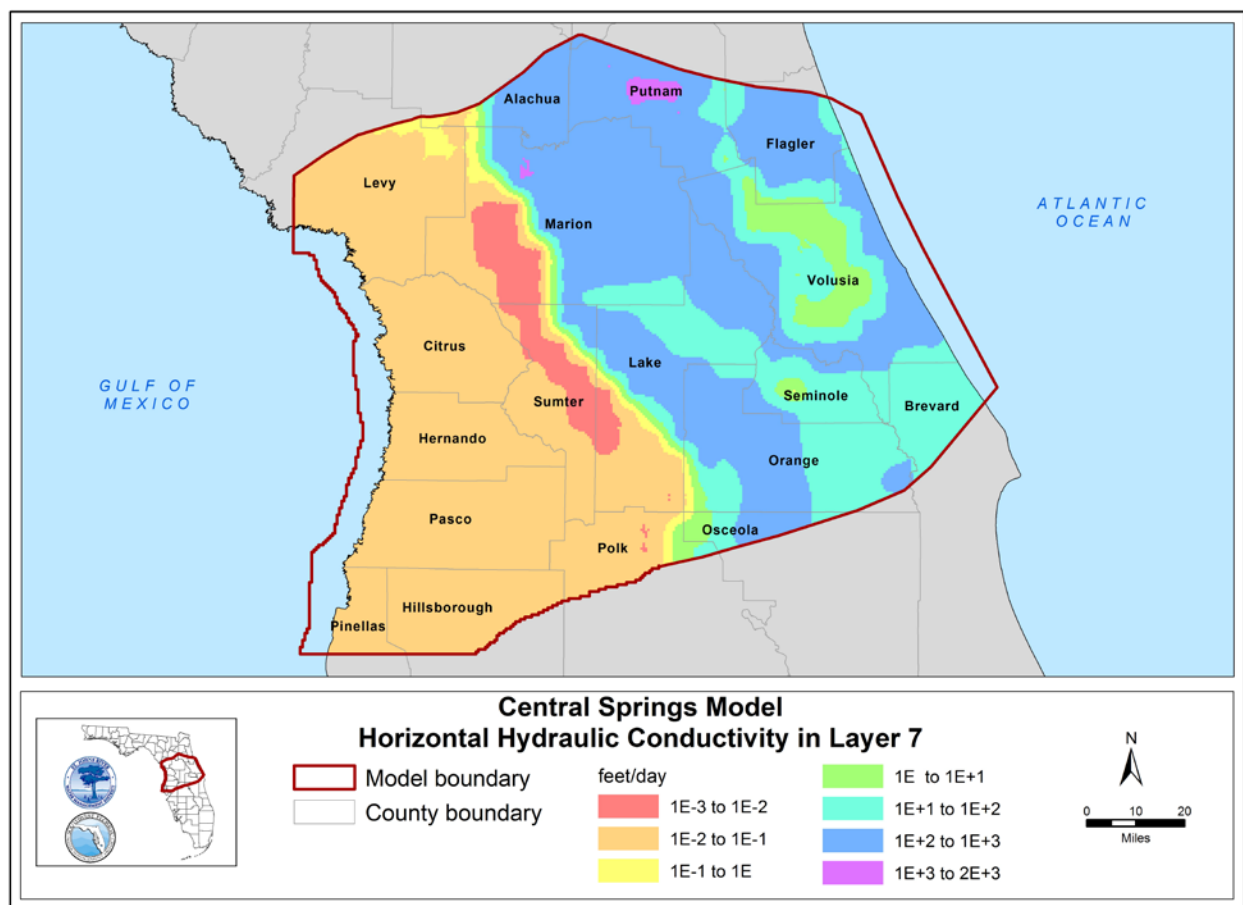


Figure 5-8. Horizontal hydraulic conductivity in layer 7 within the Central Springs Model domain

Vertical Anisotropy

Vertical anisotropy is characterized as the ratio of K_h to K_v within a cell (K_h/K_v). Due to the high uncertainty of anisotropy within each hydrostratigraphic unit, fixed anisotropy ratios were assigned based on the hydrogeological framework provided in Chapter 3. Anisotropy ratios were not modified during the PEST calibration process, which substantially reduced the number of adjustable hydraulic parameters. Vertical hydraulic conductivity values for layers 1, 3, 4, 6, and 7 were calculated by dividing calibrated K_h values by the corresponding anisotropy ratio. For confining layers 2 and 5, K_h was calculated by multiplying the calibrated K_v values by the corresponding anisotropy ratio.

A K_h/K_v of 1:1 was used for hydrostratigraphic units simulated as aquifers throughout the model domain (layers 1, 3, 4, 6 and 7) to allow for principal flow in both the vertical and horizontal directions. As shown on Figure 5-9, layer 2 was separated into 3 different zones with a zonal K_h/K_v of 1:1 for unconfined regions, 10:1 for semi-confined regions, and 25:1 for confined regions. The spatial coverage of confinement was based on the ICU thickness provided in USGS professional paper 1807 (Williams and Kuniandy, 2016) and USGS data series 926 (Williams and Dixon, 2015). The higher K_h/K_v used for confined areas was applied to allow principal flow in the horizontal direction. For layer 5, a K_h/K_v of 10:1 was utilized in the eastern and central portion of the model domain where MCU I is present and, and a ratio of 1:1 was utilized in the western portion of the model domain where MCU I is absent (Figure 5-10).

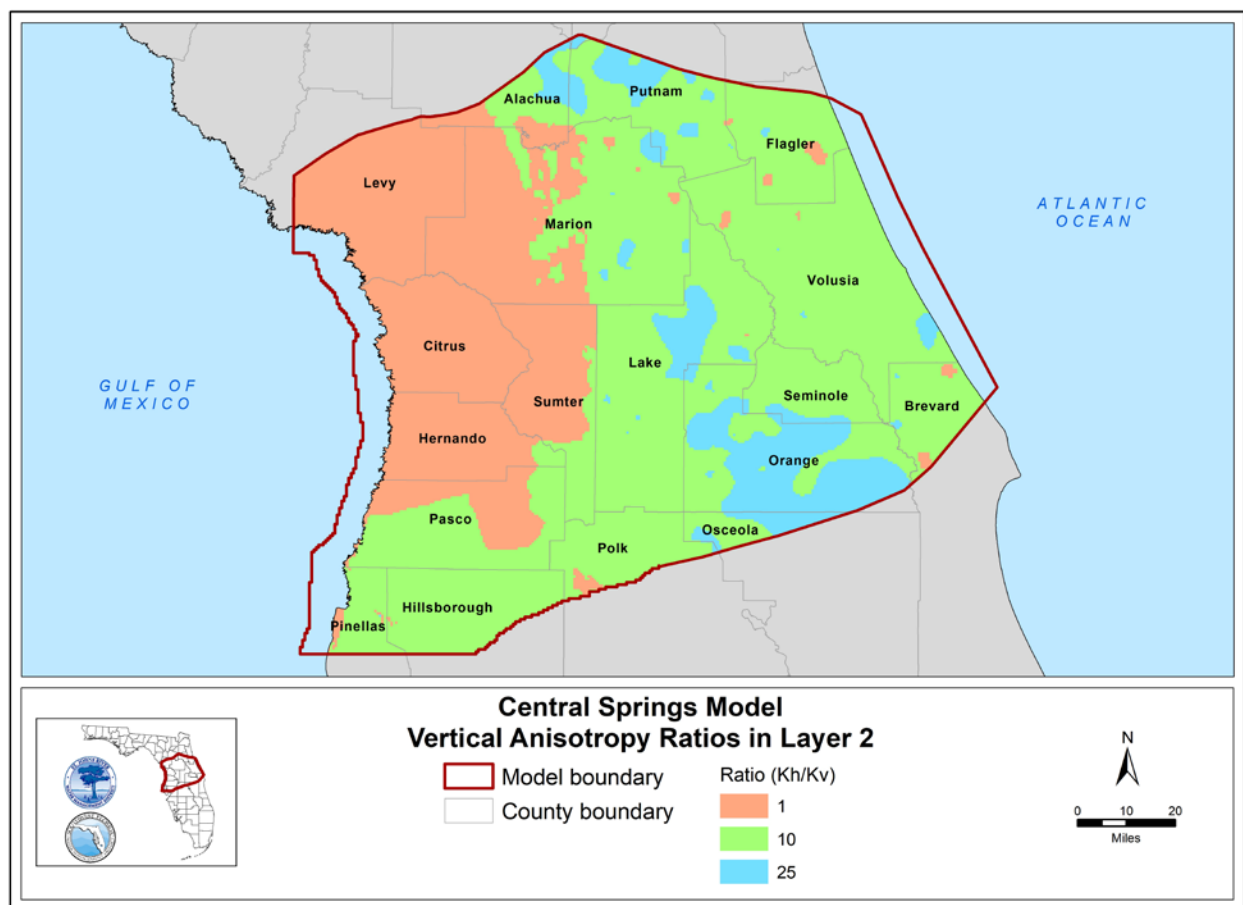


Figure 5-9. Vertical anisotropy ratios in layer 2 within the Central Springs Model domain

Note: Kh = horizontal hydraulic conductivity

Kv = vertical hydraulic conductivity

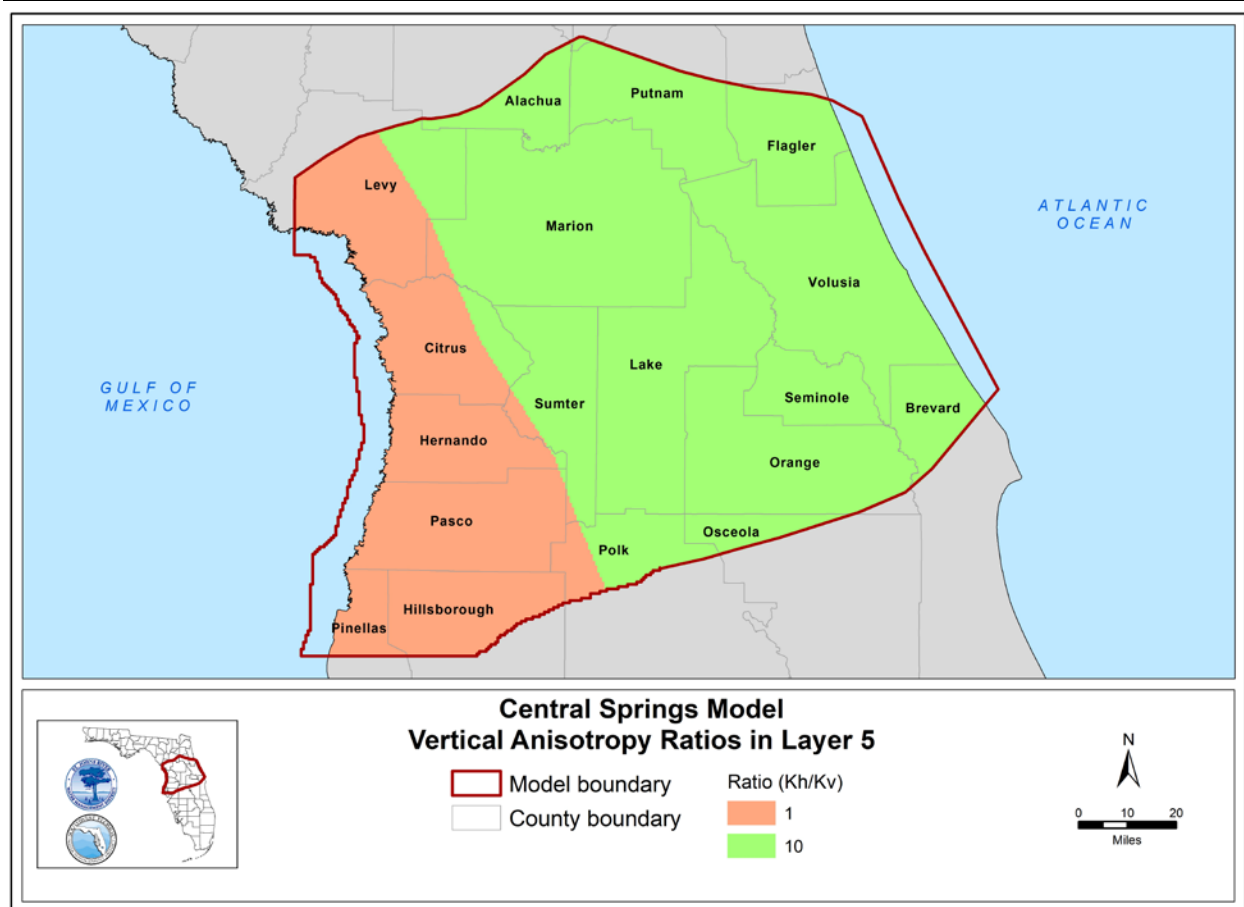


Figure 5-10. Vertical anisotropy ratios in layer 5 within the Central Springs Model domain

Note: K_h = horizontal hydraulic conductivity

K_v = vertical hydraulic conductivity

Leakance

A leakance coefficient value represents the rate of vertical transfer of water between layers and is expressed in ft per day per ft (day^{-1}). Leakance is calculated as K_v divided by the thickness of the confining unit with its value indicating the general degree of confinement (i.e., lower values in areas with a thick confining unit and higher values where the confining unit is thin or absent). Leakance values for the ICU (layer 2) and MCU I (layer 5) are shown on Figure 5-11 and Figure 5-12, respectively. A wide range of leakance values was estimated for the ICU in the CSM and is similar to the ICU leakance range in the regional groundwater models described in Chapter 2. In the eastern portion of the model domain where the UFA is considered confined to semi-confined, layer 2 leakance values are relatively low. Layer 2 leakance values are several orders of magnitude higher in the northwest portion of the model domain where the UFA is considered unconfined and layer 2 constitutes part of the UFA.

Middle Confining Unit I is generally considered a semi-confining unit and the calculated leakance values agree with this conceptualization. Middle Confining Unit I is thickest in the central portion of the model domain and gradually thins to the west and east. The spatial distribution of calculated leakance in layer 5 generally corresponds to the relative magnitude of confinement of MCU I, with lower leakance values in areas of thicker confinement. In the western portion of the model domain where MCU I is absent, layer 5 is simulated as part of the UFA (Figure 3-11).

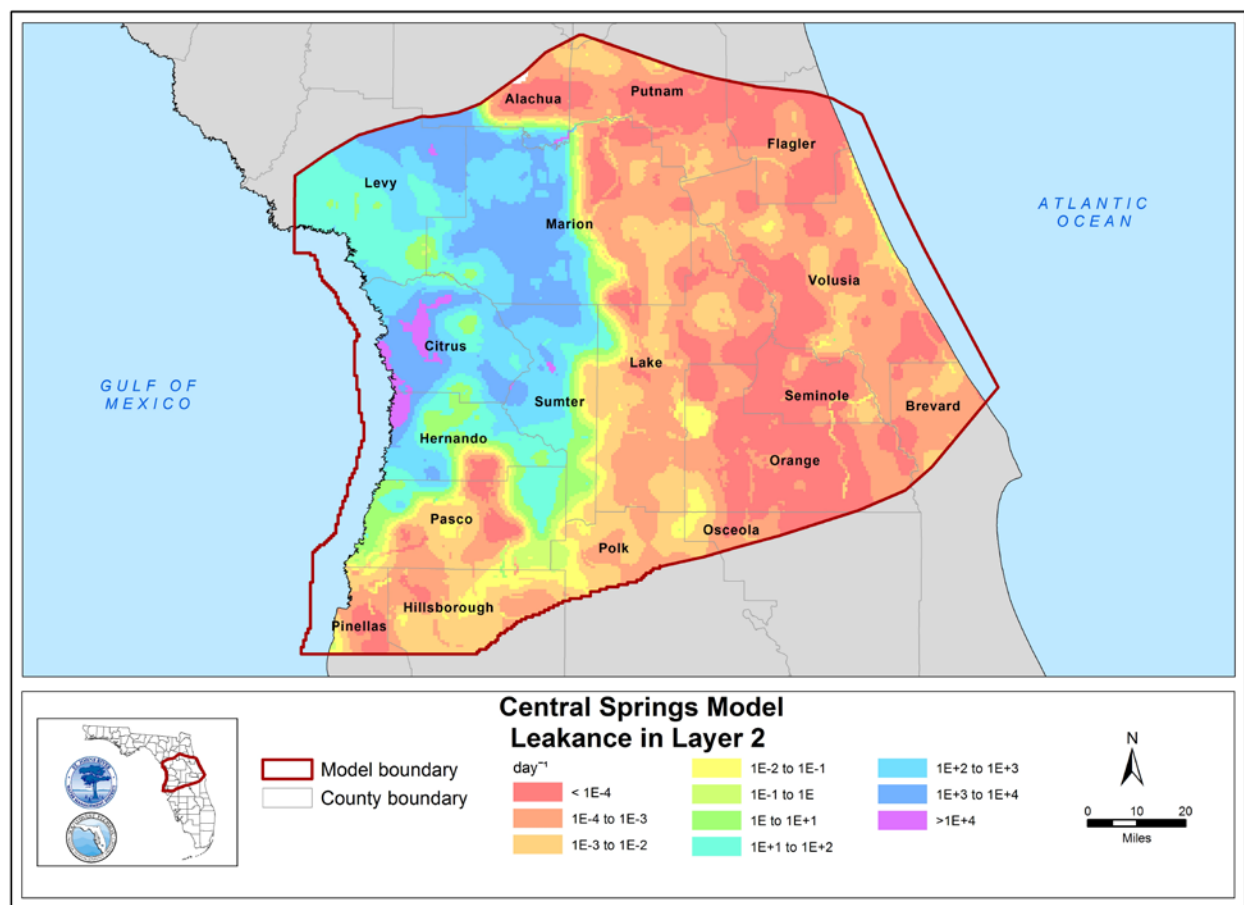


Figure 5-11. Leakance in layer 2 within the Central Springs Model domain

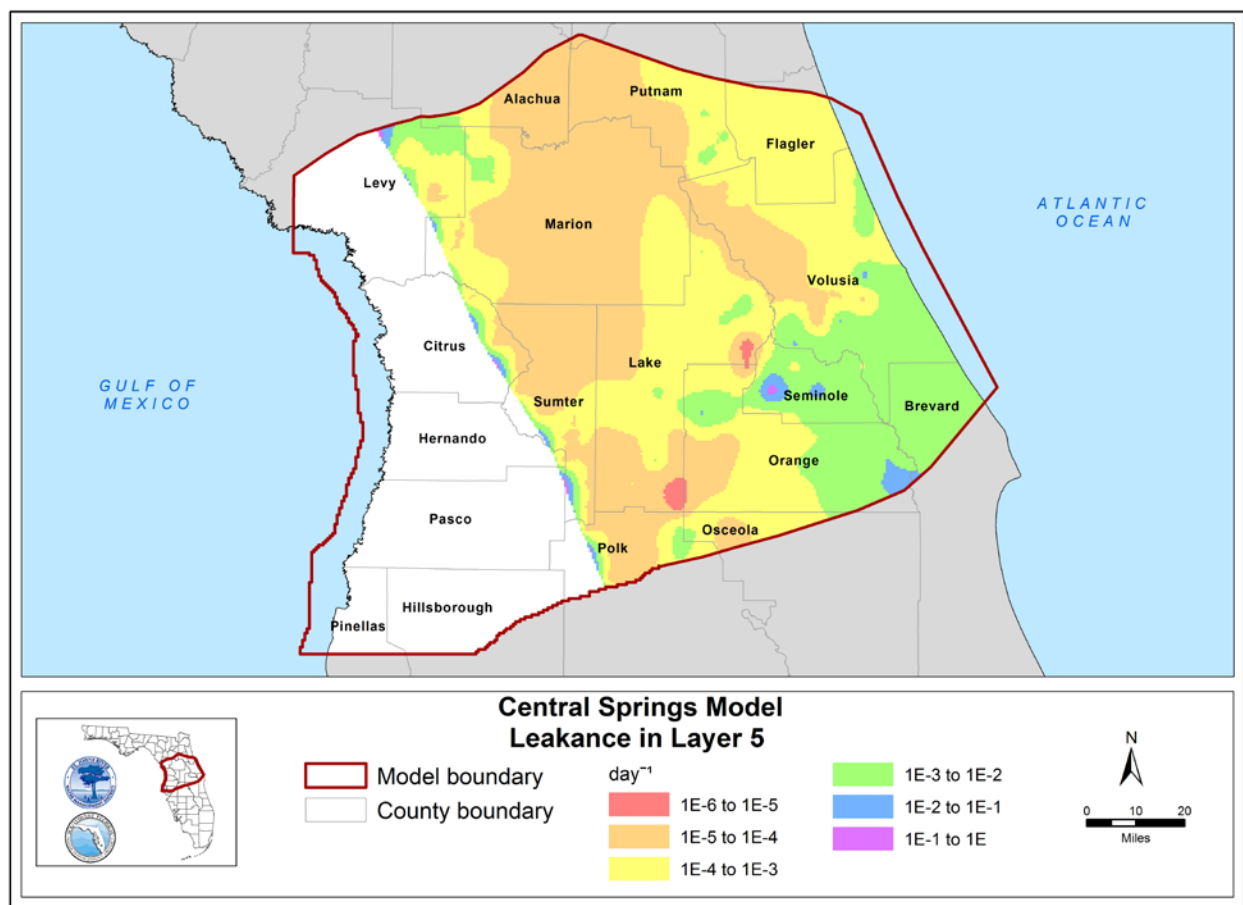


Figure 5-12. Leakance in layer 5 within the Central Springs Model domain

Note: No leakance values are provided in the western portion of the model domain where the Middle Confining Unit I (layer 5) is absent.

Transmissivity

Transmissivity is the rate at which water is transmitted horizontally through an aquifer layer under a hydraulic gradient. Transmissivity is the product of Kh and the saturated thickness of an aquifer layer and is expressed as feet squared per day (ft^2/d). Composite transmissivities for the UFA and LFA, derived from all layers representing each aquifer at any given point within the model domain, are provided on Figure 5-13 and Figure 5-14, respectively.

As shown on Figure 3-11, the UFA in the eastern portion of the model domain is confined between ICU and MCU I and consists of layer 3 and layer 4. In the western portion of the model domain, where the UFA is unconfined and MCU I is absent, the UFA consists of layer 2 through layer 6. In the central portion of the model domain, where the UFA is unconfined at the surface but separated from the LFA by MCU I, the UFA consists of layer 2 through layer 4. For numerical stability, a dummy layer with minimal thickness (10 ft) was used in the model where the confining units (ICU or MCU I) were absent. Aside from these variations, the majority of the UFA within the model domain is comprised of layer 3 and layer 4.

High transmissivity values for the UFA are found in the northwest unconfined karst regions of the model domain. Additional areas of high transmissivity result from known localized karst features in Orange, Seminole, and Volusia counties where several first and second magnitude springs are present. A comparison between UFA transmissivities derived from calibration and those measured from APTs is shown on Figure 5-13. In general, the range of estimated transmissivity values agrees with the APT measurements. In addition, the spatial pattern of UFA transmissivity agrees with the map of UFA transmissivity from Kuniatsky et al. (2012), which was interpolated from measured transmissivity data using geostatistical methods.

The LFA below MCU I is represented in the CSM by layer 6 in the central portion of the model domain and by layer 6 and layer 7 in the eastern portion of the model domain (Figure 3-11). In the western portion of the model domain, the LFA is located subjacent to layer 7 and is not represented in the model. Composite transmissivity of the LFA is shown on Figure 5-14. The LFA is increasingly used as a water source for public supply in the central portion of the model domain. However, for most areas within the model domain, available APT data within the LFA is sparse. A comparison with the limited APT measurements showed that the range of LFA transmissivity values was in general agreement.

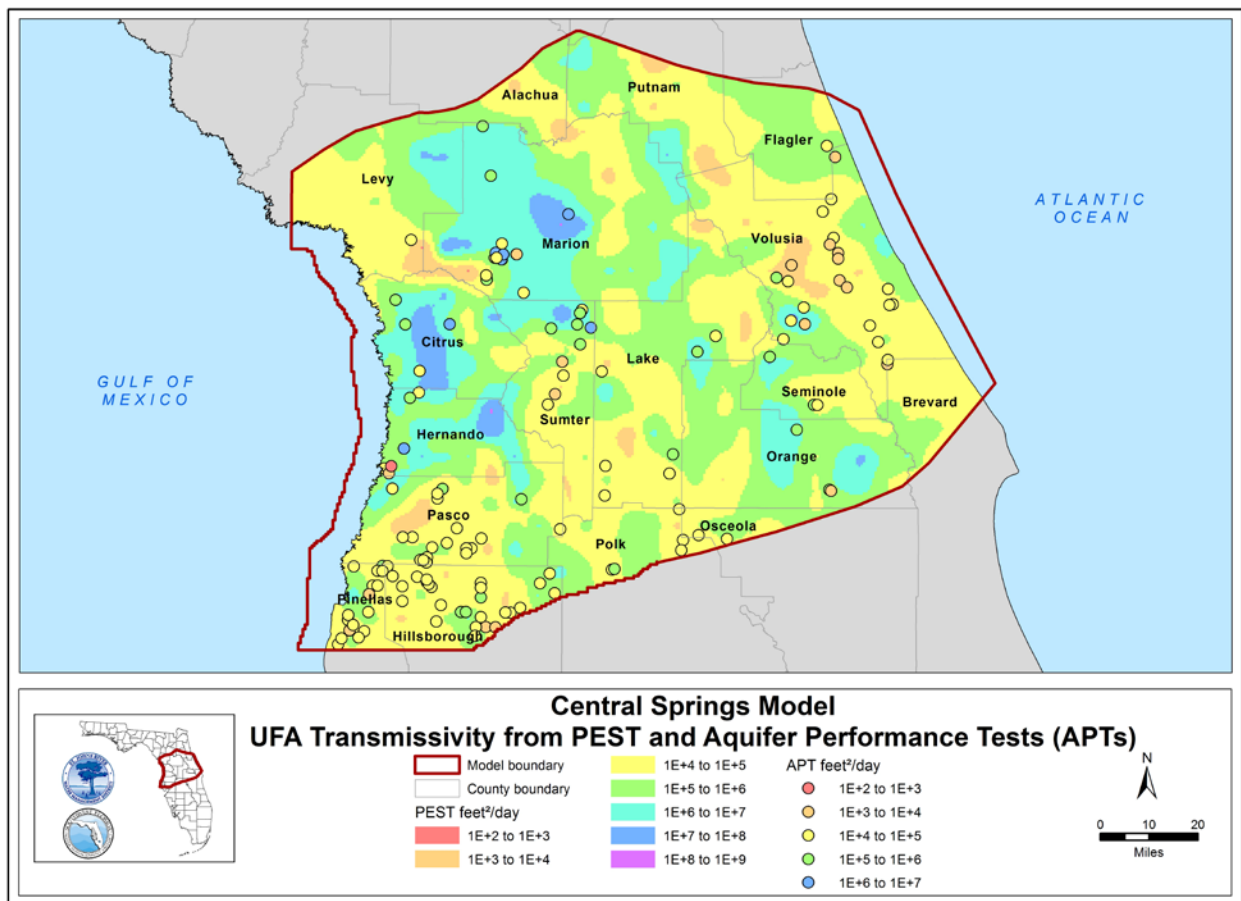


Figure 5-13. Upper Floridan Aquifer (UFA) transmissivity from PEST calibration and aquifer performance tests within the Central Springs Model domain

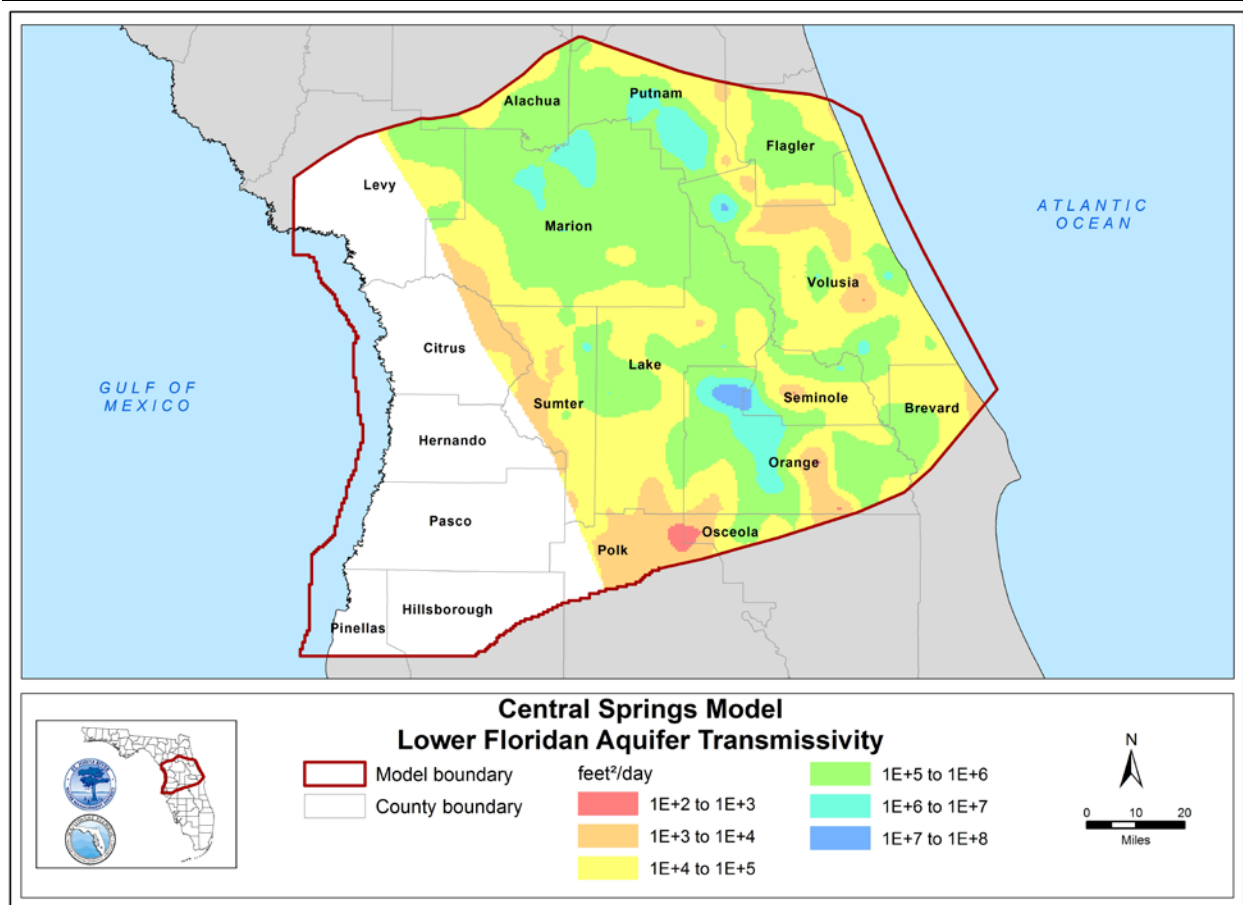


Figure 5-14. Lower Floridan Aquifer transmissivity within the Central Springs Model domain

Note: Transmissivity values are not provided in the western portion of the model domain where the Lower Floridan Aquifer is not present within layers 6 and 7.

General Head Boundary Conductance

General head boundary conductance is the rate at which water is transmitted horizontally through a GHB cell under a hydraulic gradient. In the CSM, GHB conductance was calculated using the following equation:

$$CD_{GHB} = \frac{K_h A}{L} \quad (5-2)$$

Where:

CD_{GHB} = GHB conductance (ft²/day)

K_h = horizontal hydraulic conductivity of GHB model cell (ft/day)

A = GHB cell section area; a product of layer thickness and cell width (ft²)

L = distance between GHB cell and source; half-cell width (ft)

General head boundary conductance was not directly calibrated. It was calculated by inputting the calibrated K_h values from the model cells adjacent to GHBs into Equation (5-2).

Spring Conductance

Spring conductance is defined as the rate at which water is transmitted through a spring vent under a hydraulic gradient. Springs and spring groups were represented in the CSM as DRN cells in layer 4. The conductance of each DRN cell was adjusted by PEST to match springflow targets. The calibrated conductance values for target springs are provided in Appendix A.

River and Drain Conductance Multipliers

The conductance values of river (representing perennial streams and large lakes) and drain (representing non-perennial streams and wetlands) model boundaries were determined as the product of a multiplier estimated in the calibration process and the initial conductance values calculated using the methods described in Chapter 3. The subbasins developed for the HSPF models were used to set up the multipliers. A single multiplier was set for each HSPF subbasin and was assigned to all river and drain boundaries within a given subbasin. The value of each subbasin multiplier was initially set to 1 and later adjusted by PEST during calibration to match calibration targets. Final calibrated river and layer 1 drain cell conductance values are provided on Figure 5-15 and Figure 5-16, respectively.

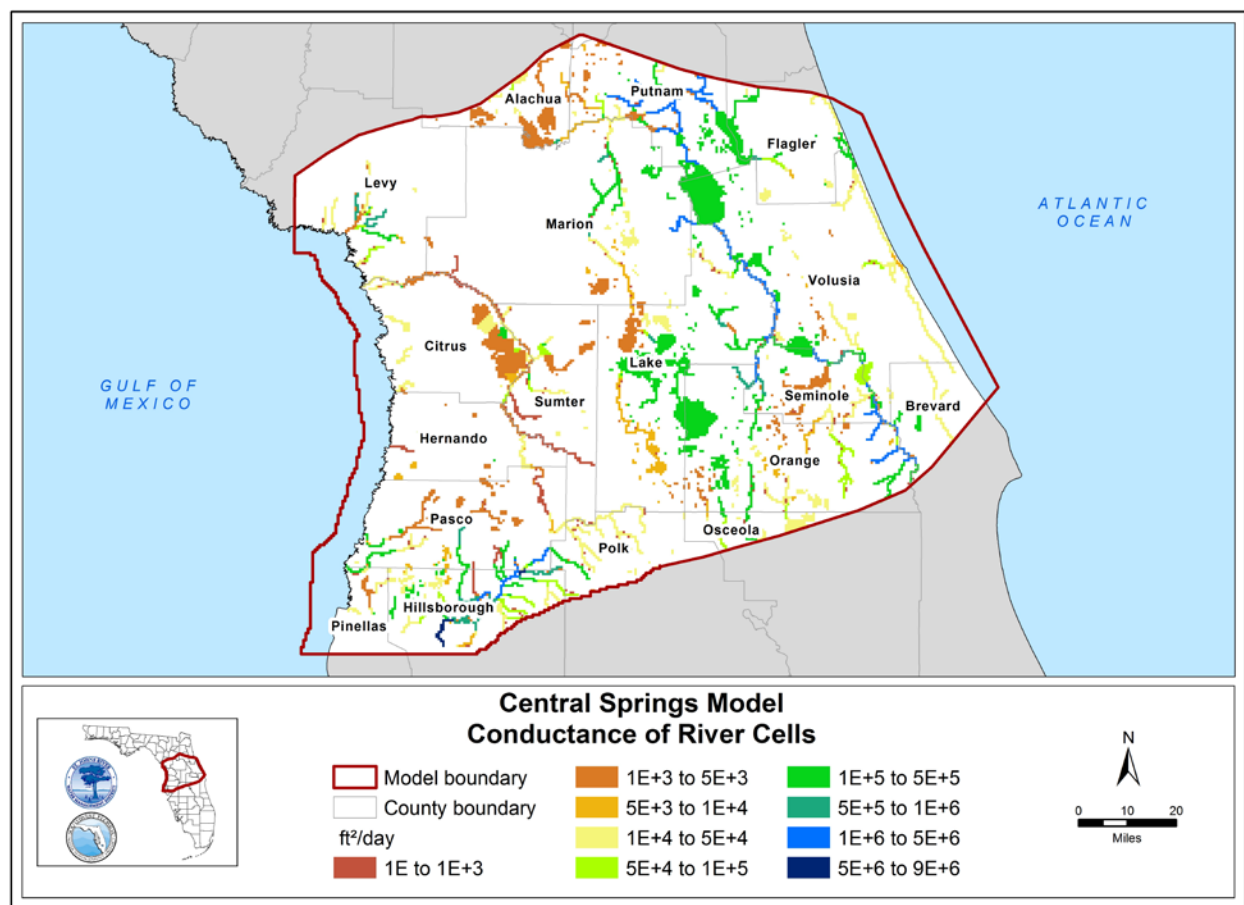


Figure 5-15. River cell conductance within the Central Springs Model domain

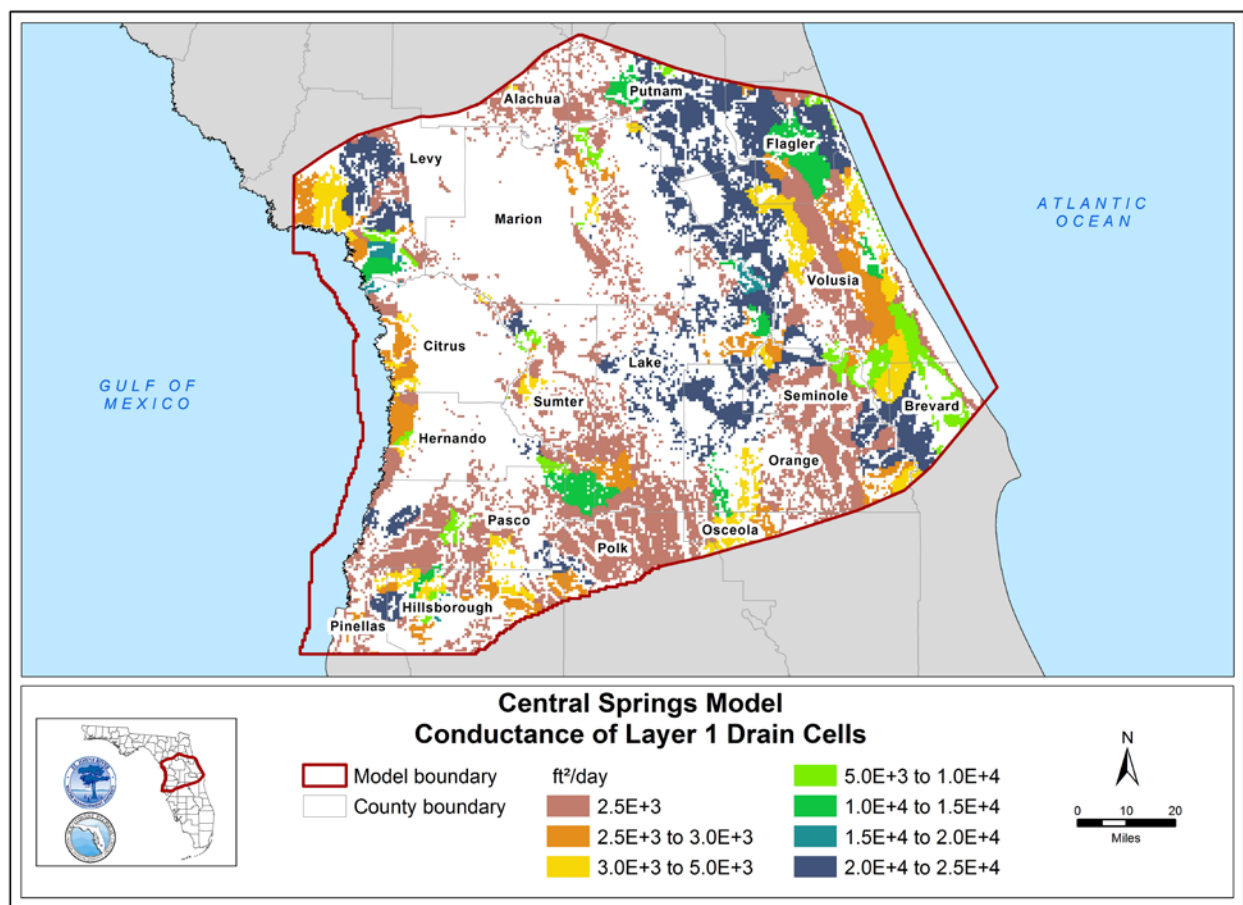


Figure 5-16. Drain cell conductance within layer 1 of the Central Springs Model domain

Lake and Stream Zone Multipliers

Lake and stream zone multipliers were used to help better simulate flow exchange between lakes and streams and the underlying UFA since the degree of connection between a lake or river and the UFA could be different from the surrounding area. A single multiplier was assigned to individual zones of layer 2 grid cells below a give lake or stream, then adjusted by PEST during calibration. Vertical hydraulic conductivity in layer 2 beneath RIV cells representing lakes and streams was calculated as the product of the calibrated Kv value and the calibrated lake and stream zone multiplier. These zone multipliers were used to refine Kv estimates beneath the streams and lakes at a local scale.

Recharge Multipliers

Multipliers to HSPF-derived recharge values were prepared for use during PEST calibration. However, adjustment of other hydrogeologic parameters resulted in adequate calibration and precluded the need to adjust recharge multipliers during calibration. This reinforces the reasonableness and quality of the recharge derived by HSPF as an input to the CSM.

STEADY-STATE SIMULATION RESULTS

The steady-state simulation results were examined in terms of groundwater head, springflow, baseflow, lake leakage, and overall water budget. Following steady-state calibration, a transient calibration was conducted to test and refine the calibrated hydraulic parameters and estimate storage parameters. The steady-state calibration results presented in the following sections are based on the final calibration run. Calibration results for the transient model are presented in Chapter 6.

Groundwater Heads

The groundwater head residual statistics are shown in Table 5-3 and compared with the calibration criteria established in Chapter 4. A total of 410 SAS (layer 1), 601 UFA (layer 3 and 4), and 37 LFA (layer 6) monitoring wells were used as quantitative targets for steady-state calibration. Simulated groundwater heads were compared with average fresh water equivalent heads from 2005 to 2018. All calibration criteria defined in Table 4-1 were met. Note that there were no groundwater head targets in the confining unit layers (layer 2 and layer 5) or layer 7 due to a lack of observed data.

Regression plots of simulated versus observed groundwater heads in the SAS (layer 1) are shown on Figure 5-17. A 1-to-1 line is included on the charts to easily identify any deviations between the simulated and observed data. Surficial Aquifer System residuals exhibited a ME of -0.1 ft and a MAE of 2.0 ft, which is well within the performance evaluation criteria. In addition, the strong correlation ($R^2 = 0.9905$) indicates that the simulated groundwater heads closely mimic the observed groundwater heads. Spatial distribution of the head residuals for SAS target wells, as illustrated on Figure 5-18, indicate there is little spatial bias in the mean error of simulated water levels in the model. Due to the large grid cell size (2,500 ft \times 2,500 ft), surficial groundwater heads in localized, hydraulically steep gradient areas are sometimes difficult to match, resulting in relatively higher simulation residuals for the target wells in those areas.

Regression plots and spatial distributions of groundwater heads for the UFA (layer 3 and layer 4) are illustrated on Figure 5-19 through Figure 5-22, respectively. Calibration target statistics were also achieved for the UFA as demonstrated by the statistics in Table 5-3. The close alignment between the scatter plots and the 1-to-1 lines indicates the good match between model simulated and observed groundwater heads at the target wells. The spatial distribution of simulation residuals appears to have little to no spatial bias.

A regression plot (Figure 5-23) and spatial distribution (Figure 5-24) of groundwater heads in the LFA (layer 6) demonstrate a close match between model simulated and observed groundwater heads at target wells. Calibration target statistics were achieved for the LFA, as demonstrated by the statistics presented in Table 5-3.

Table 5-3. Groundwater head residuals by layer

Metric	Criteria	Layer 1	Layer 3	Layer 4	Layer 6
Number of wells	NA	410	228	373	37
Mean error (ft)	$< \pm 0.5$ ft	-0.1	0.3	0.0	-0.4
Mean absolute error (ft)	NA	2.0	1.6	1.4	1.3
Percent of residual < 2.5 ft	$> 50\%$	74.9%	78.5%	84.5%	89.2%
Percent of residual < 5 ft	$> 80\%$	92.0%	96.9%	97.3%	94.6%
R^2	> 0.75 (SAS) > 0.85 (UFA/LFA)	0.9905	0.9915	0.9937	0.9892

Note: ft = feet

LFA = Lower Floridan Aquifer

NA = not applicable

SAS = Surficial Aquifer System

UFA = Upper Floridan Aquifer

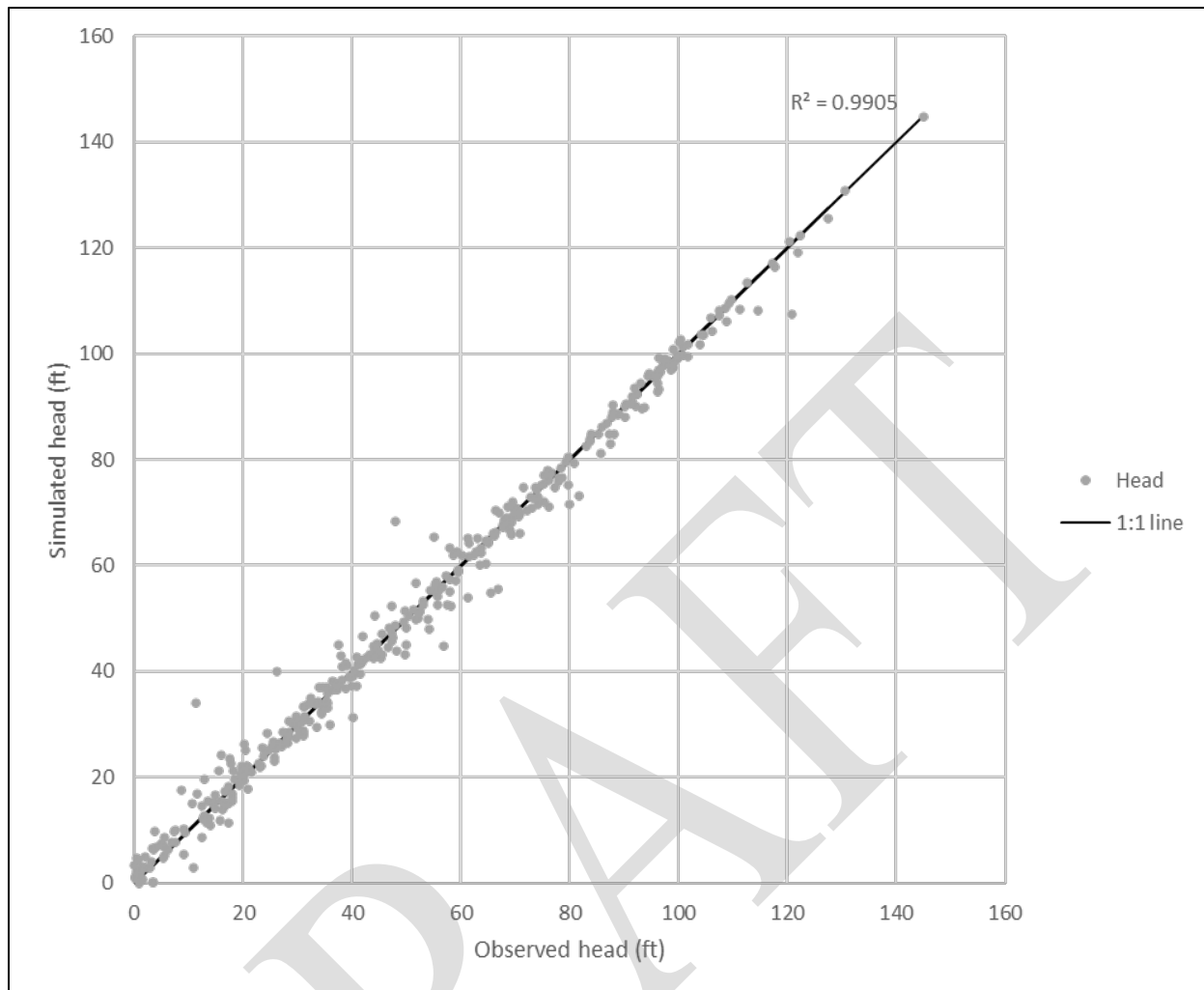


Figure 5-17. Layer 1 (Surficial Aquifer System) head target scatter plot

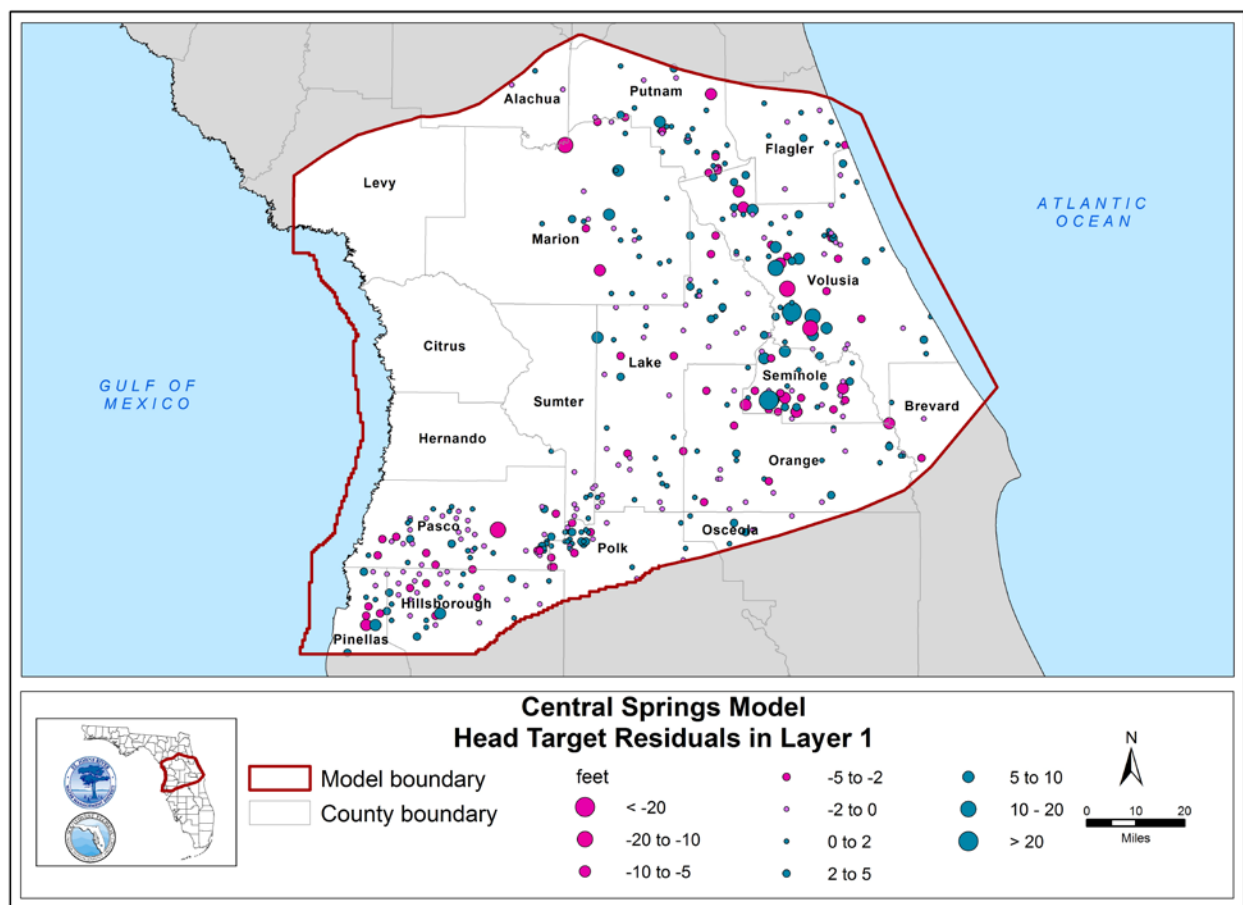


Figure 5-18. Head target residuals in layer 1 within the Central Springs Model domain
 Note: Residual = simulated - observed

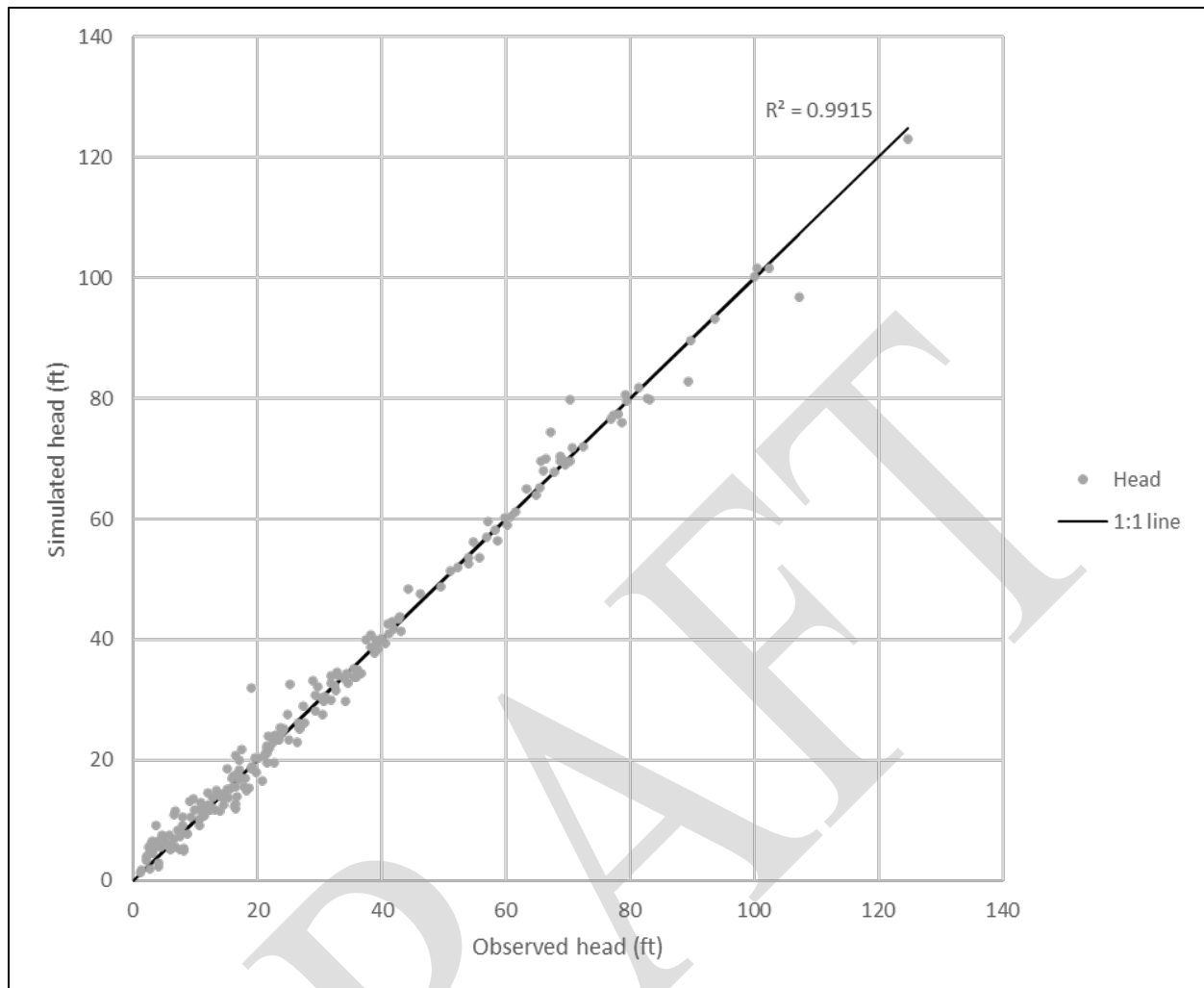


Figure 5-19. Layer 3 (Upper Floridan Aquifer) head target scatter plot

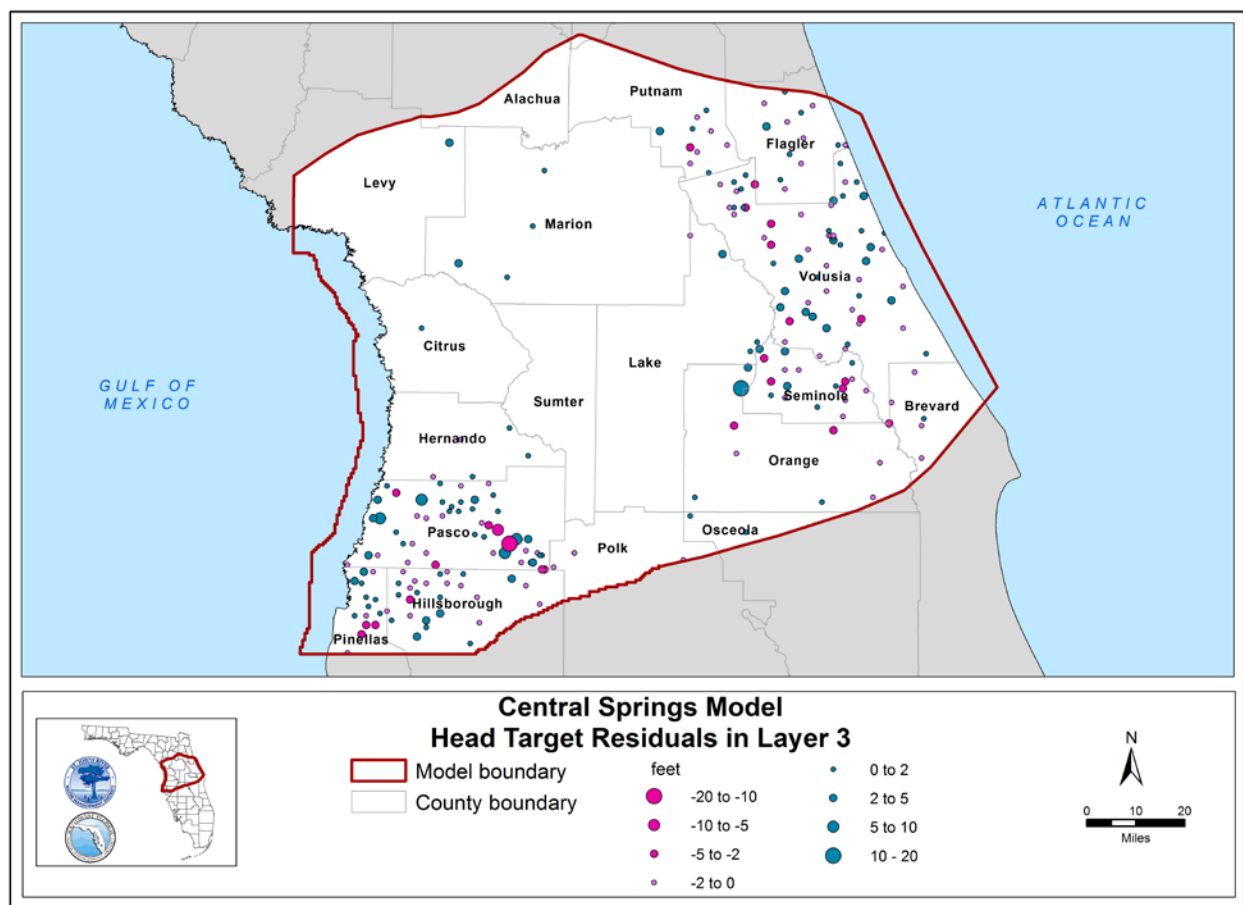


Figure 5-20. Head residuals in layer 3 within the Central Springs Model domain

Note: Residual = simulated – observed

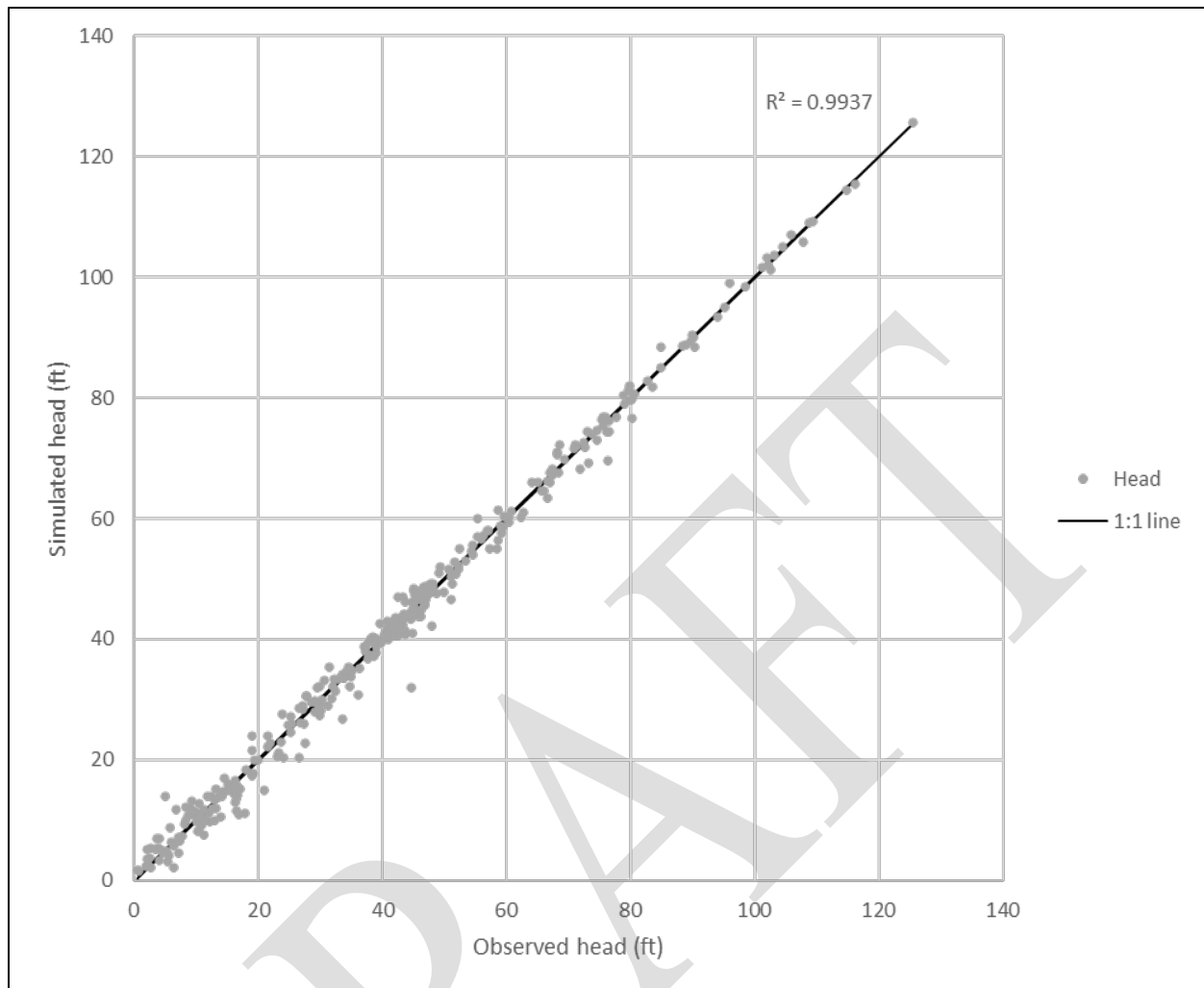


Figure 5-21. Layer 4 (Upper Floridan Aquifer) head target scatter plot

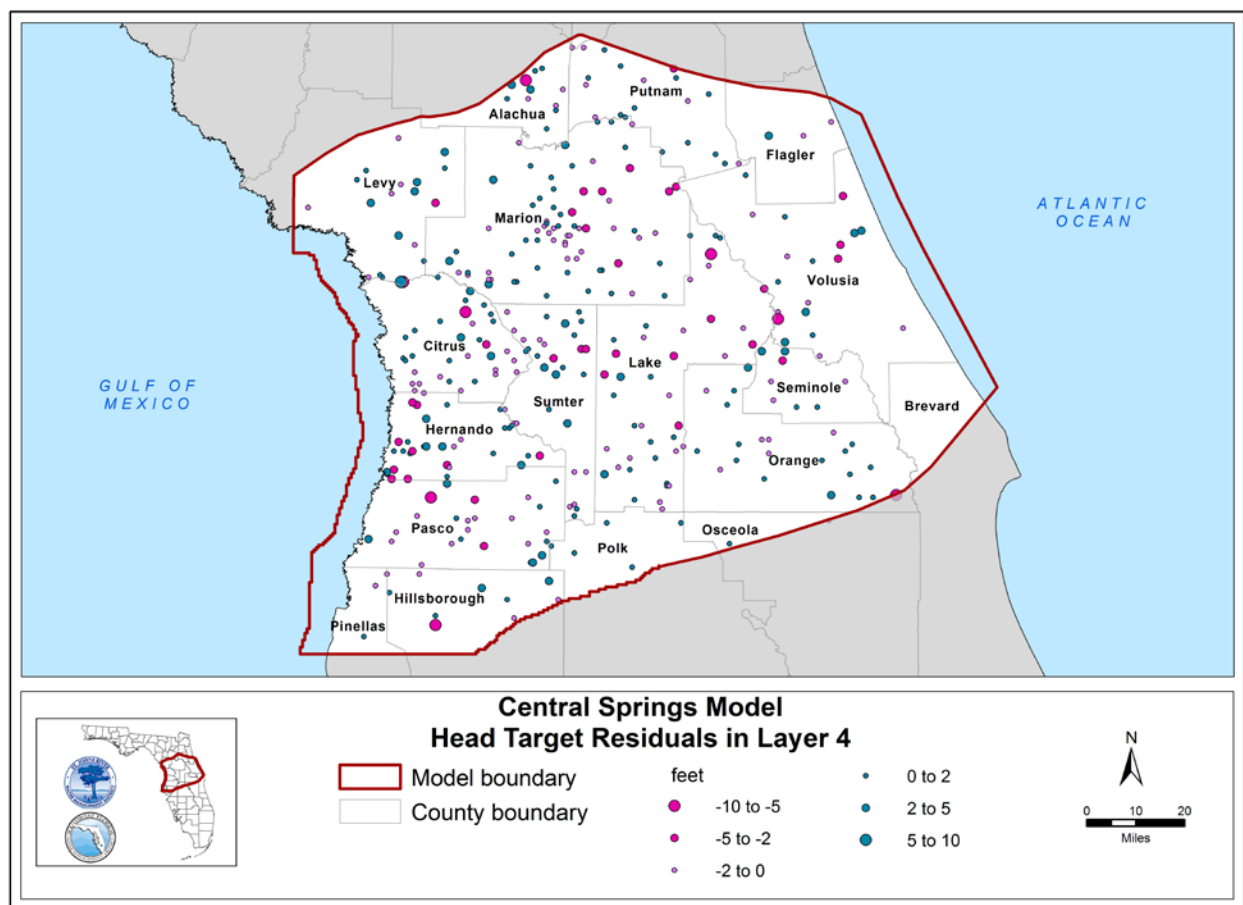


Figure 5-22. Head target residuals in layer 4 within the Central Springs Model domain

Note: Residual = simulated - observed

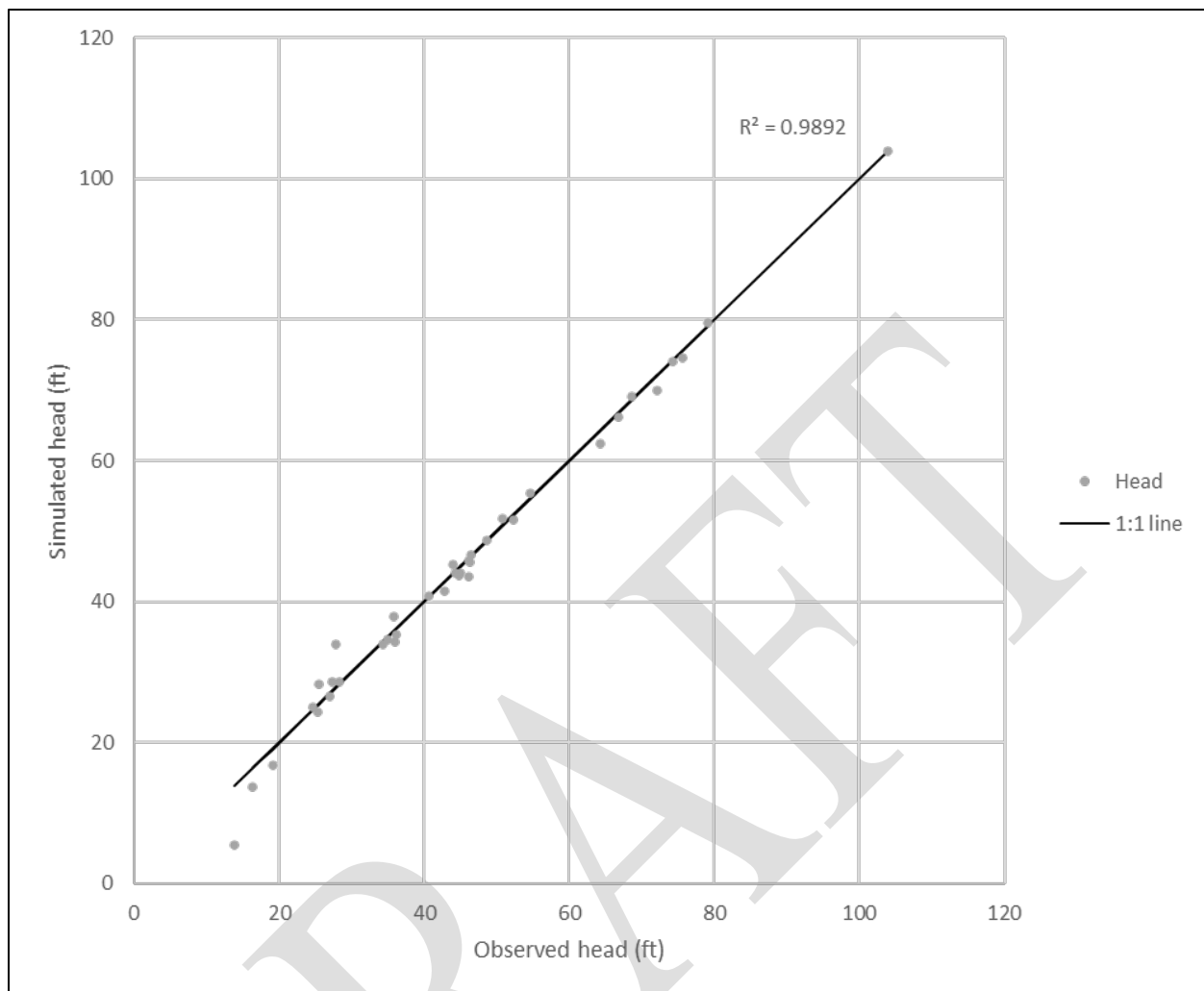


Figure 5-23. Layer 6 (Lower Floridan Aquifer) head target scatter plot

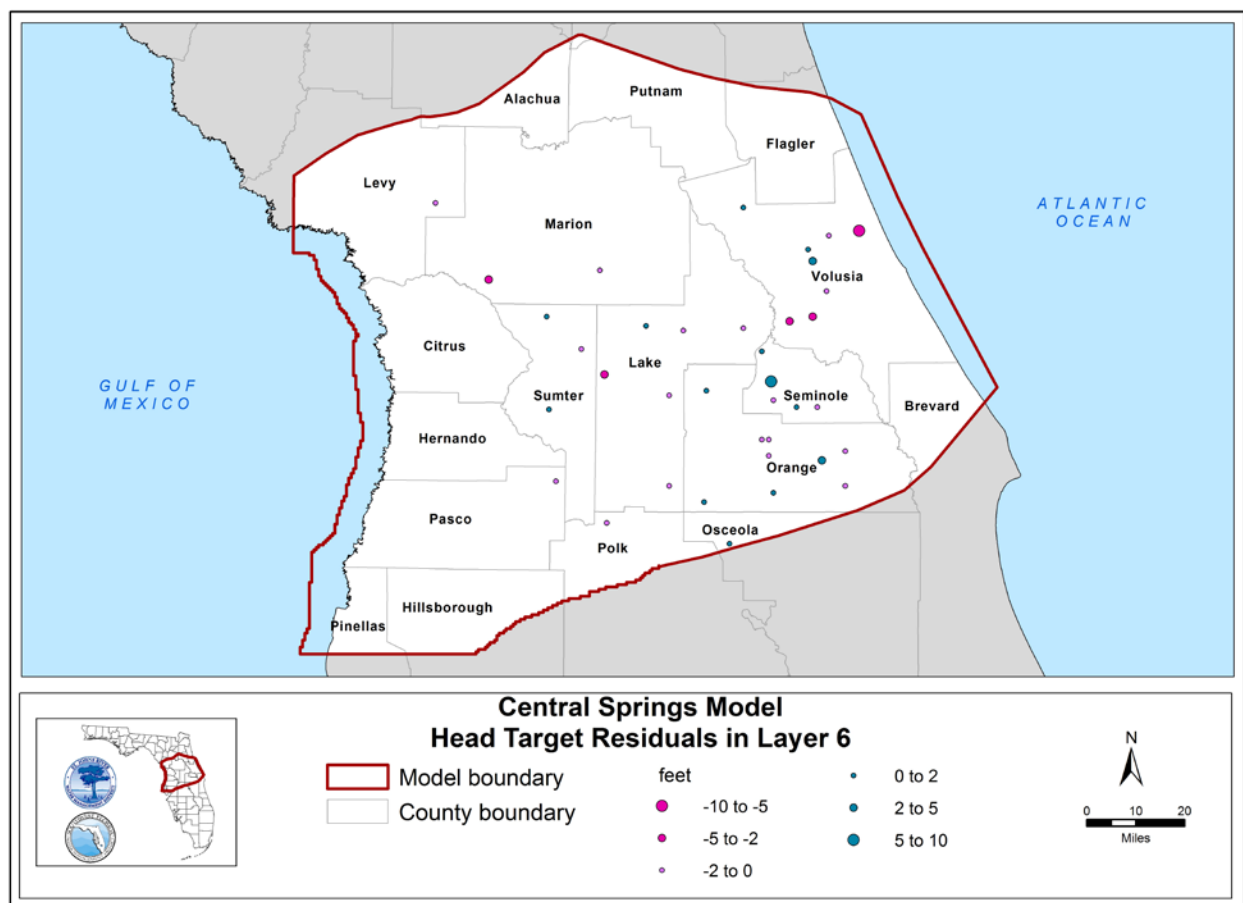


Figure 5-24. Head residuals in layer 6 within the Central Springs Model domain

Note: Residual = simulated - observed

Head Differences Across Confining Units

In addition to comparing groundwater heads within individual model layers, vertical groundwater level differences in SAS-UFA well pairs installed across the ICU and UFA-LFA well pairs installed across the MCU I were also examined. This comparison was used to evaluate the model performance in simulating the degree of confinement across confining units in the model.

The simulation residuals of vertical head differences are illustrated spatially on Figure 5-25 and Figure 5-26 for SAS-UFA and UFA-LFA well pairs, respectively. There appears to be little spatial bias in vertical head difference across the confining units. Scatter plots of head difference residuals are displayed on Figure 5-27 and Figure 5-28. The strong correlation ($R^2 = 0.9613$ for SAS-UFA pairs and $R^2 = 0.8716$ for UFA-LFA pairs) and close match with the theoretical 1-to-1 line suggest that the model adequately simulated the degree of confinement across the confining units. A summary of head difference targets is given in Table 5-4 and Table 5-5 and indicates that most of the calibration criteria were met. The match between the signs of the head difference for most of the target pairs suggests that simulated vertical flux across the confining units were in the same direction as indicated by the observed head difference.

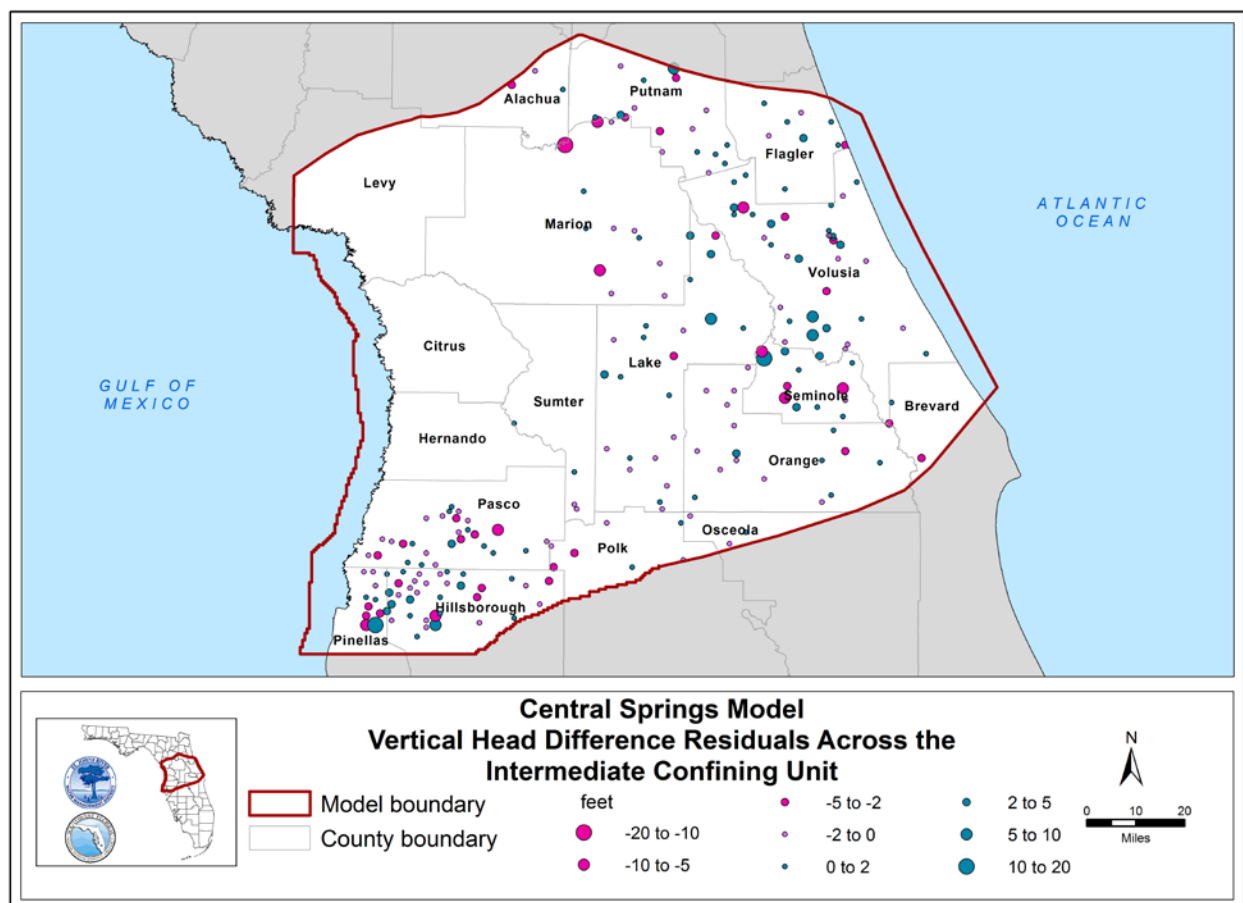


Figure 5-25. Vertical head difference residuals across the Intermediate Confining Unit within the Central Springs Model domain

Note: Residual = simulated - observed

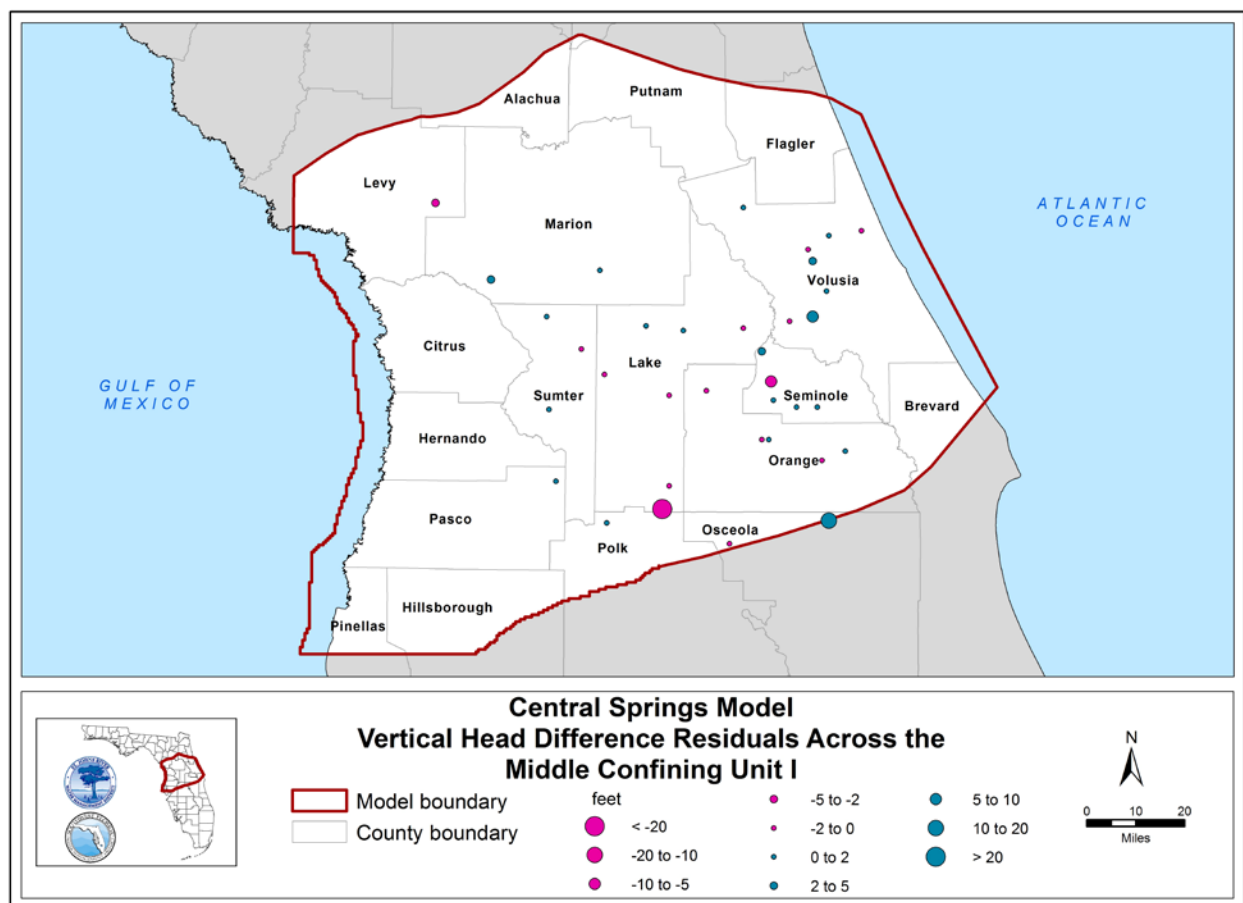


Figure 5-26. Vertical head difference residuals across the Middle Confining Unit I within the Central Springs Model domain

Note: Residual = simulated - observed

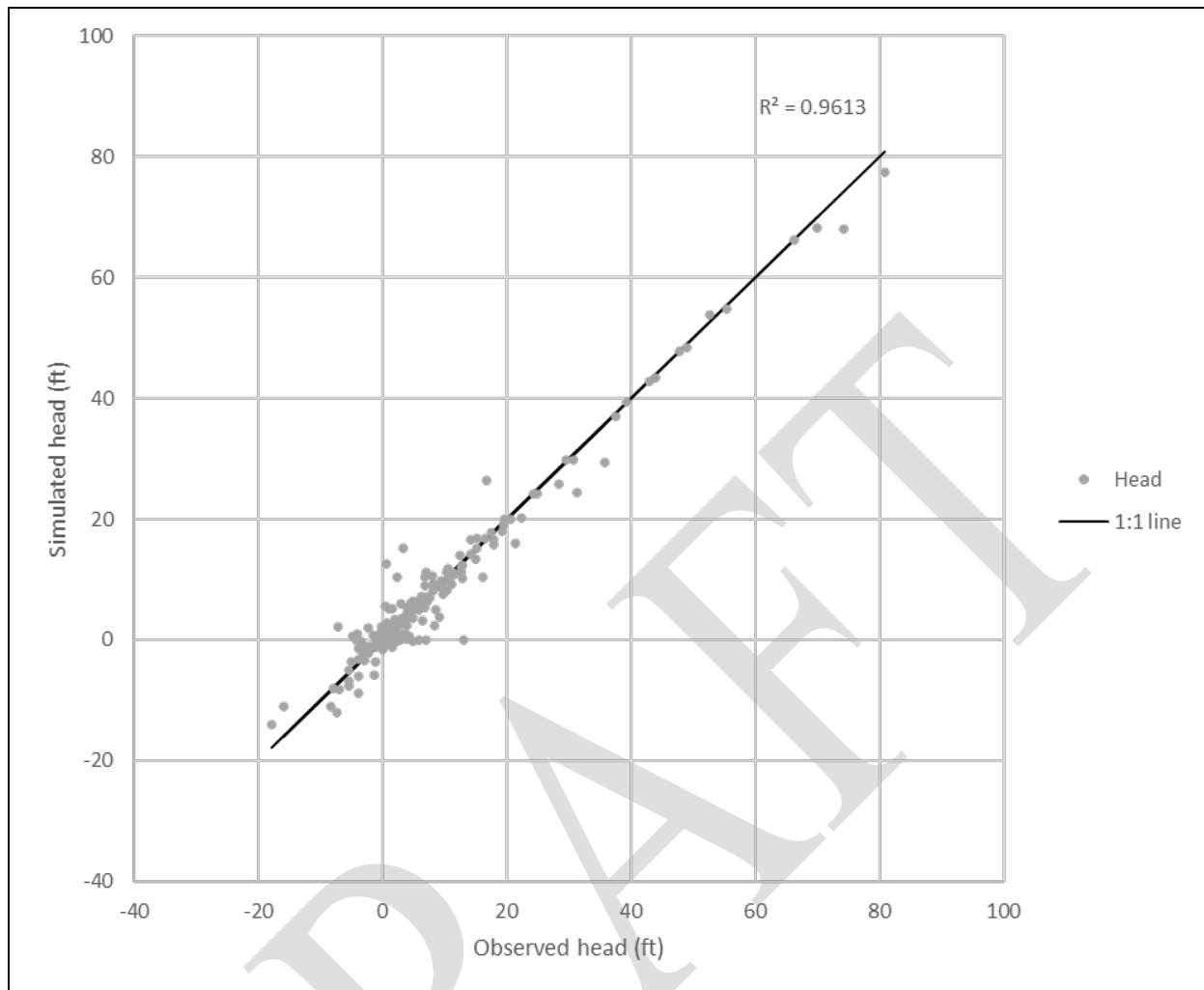


Figure 5-27. Scatter plot of vertical head difference targets across layer 2 (Intermediate Confining Unit)

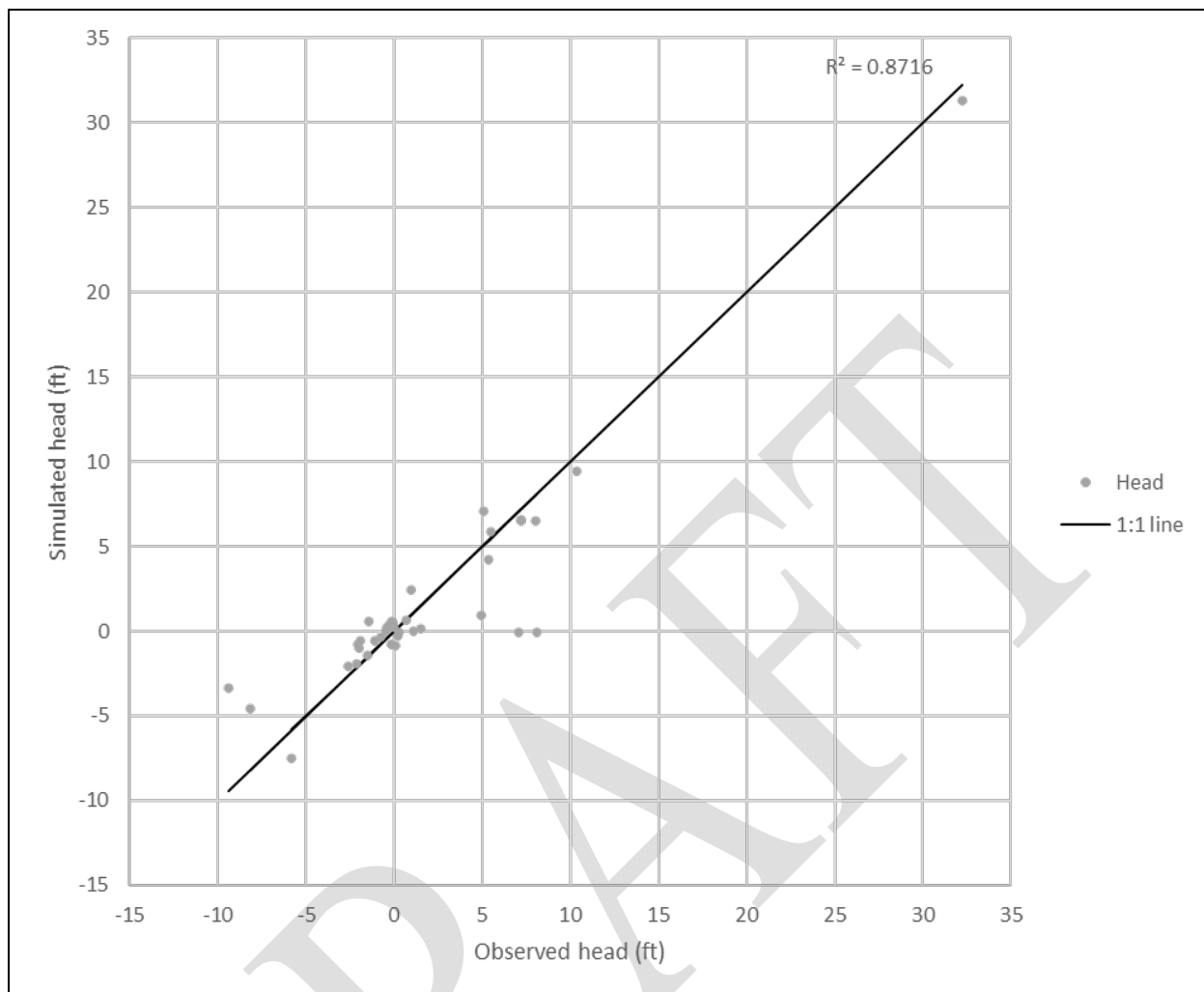


Figure 5-28. Scatter plot of vertical head difference targets across layer 6 (Middle Confining Unit I)

Table 5-4. Vertical head differences across the Intermediate Confining Unit (218 total targets)

Observed Differences	Total	Different Sign	Same Sign	$50\% \leq \Delta s / \Delta \leq 150\%$	Criteria
$\Delta \leq 5$ feet	121	23	98	47	Same flow direction (same sign)
$\Delta > 5$ feet	97	2	95	86	Simulated head difference larger than 50% of observed and smaller than 150% of observed

Note: Δ = observed difference
 Δs = simulated difference

Table 5-5. Vertical head differences across the Middle Confining Unit I (27 total targets)

Observed Differences	Total	Different Sign	Same Sign	$50\% \leq \Delta s / \Delta \leq 150\%$	Criteria
$\Delta \leq 5$ feet	16	0	16	5	Same flow direction (same sign)
$\Delta > 5$ feet	11	2	9	10	Simulated head difference larger than 50% of observed and smaller than 150% of observed

Note: Δ = observed difference
 Δs = simulated difference

Spring Discharges

A total of 185 spring vents/groups were simulated in the model. Average spring discharge between 2005 and 2018 was used as a calibration target for the steady-state model. It should be noted that only a limited set of springs had measured discharge data. The majority of the third magnitude and higher springs had few to no flow measurements. For springs without flow measurements, an estimated flow was used. Appendix A compares the steady-state model simulated spring discharge to observed or estimated spring discharge for all 185 springs.

A critical parameter for calibration of spring discharge is the value of conductance for spring cells represented in the drain package of MODFLOW. The conductance value was adjusted during PEST calibration. The maximum conductance for all simulated springs was limited to $1\text{E}+8$ ft²/day. The upper bound of spring conductance was set based on previous modeling efforts and theoretical calculations of hydraulic conductivity at open spring vents.

Simulated and observed spring discharges and their percent differences are summarized in Table 5-6 for first magnitude springs and Table 5-7 for second magnitude springs. Calibration criteria were met with a R^2 of 0.9999 (Figure 5-29) for all 185 simulated springs and the scatter plot closely matches the 1-1 theoretical line. The MAE of all first magnitude springs is smaller than 5 percent, the MAE of all second magnitude springs is smaller than 10 percent, and simulated flow at third or higher magnitude springs is within the same order of magnitude as observed flow. A map of springflow residuals is presented on Figure 5-30 and suggests there is little spatial bias in modeled springflows.

Table 5-6. Simulated and observed discharge of first magnitude of springs

Spring	Simulated (cfs)	Observed (cfs)	% Difference
Alexander Springs	97.1	97.1	0.0%
Blue Spring Org City	140.6	140.6	0.0%
Chassahowitzka Springs	192.8	192.7	0.1%
Crystal River/Kings Bay	473.9	474.0	0.0%
Homosassa Springs	304.7	304.7	0.0%
Rainbow Springs	672.8	672.6	0.0%
Silver Glen Springs	85.7	85.7	0.0%
Silver Springs	542.8	542.6	0.0%
Weeki Wachee Springs	216.7	216.8	-0.1%

Note: cfs =cubic feet per second

% Difference = (simulated – observed)/observed

Rounding of flows accounts for nominal discrepancies.

Table 5-7. Simulated and observed discharge of second magnitude of springs

Spring	Simulated (cfs)	Observed (cfs)	% Difference
Apopka Spring	23.9	23.8	0.2%
Bugg Spring	10.5	10.5	-0.2%
Croaker Hole Spring	69.3	69.3	0.0%
Crystal Main Spring (Pasco)	46.3	46.3	0.0%
Fern Hammock Springs	11.3	11.3	0.0%
Gemini Spring	9.5	9.6	-1.1%
Gum Springs	73.1	73.2	-0.1%
Juniper Springs	11.1	11.1	0.0%
Messant Spring	14.2	14.2	-0.4%
Ponce De Leon Spring	22.8	22.7	0.1%
Rock Springs	54.9	55.0	-0.1%
Salt Springs	76.5	76.4	0.1%
Sanlando Spring	19.8	19.8	0.0%
Seminole Springs - Lake	35.0	35.1	-0.3%
Starbuck Spring	11.7	11.8	-0.7%
Sulphur Spring (Hillsborough)	20.3	20.2	0.5%
Sweetwater Springs	12.9	12.9	0.0%
Wekiwa Springs	61.1	61.1	0.0%

Note: cfs = cubic feet per second

% Difference = (simulated – observed)/observed

Rounding of flows accounts for nominal discrepancies.

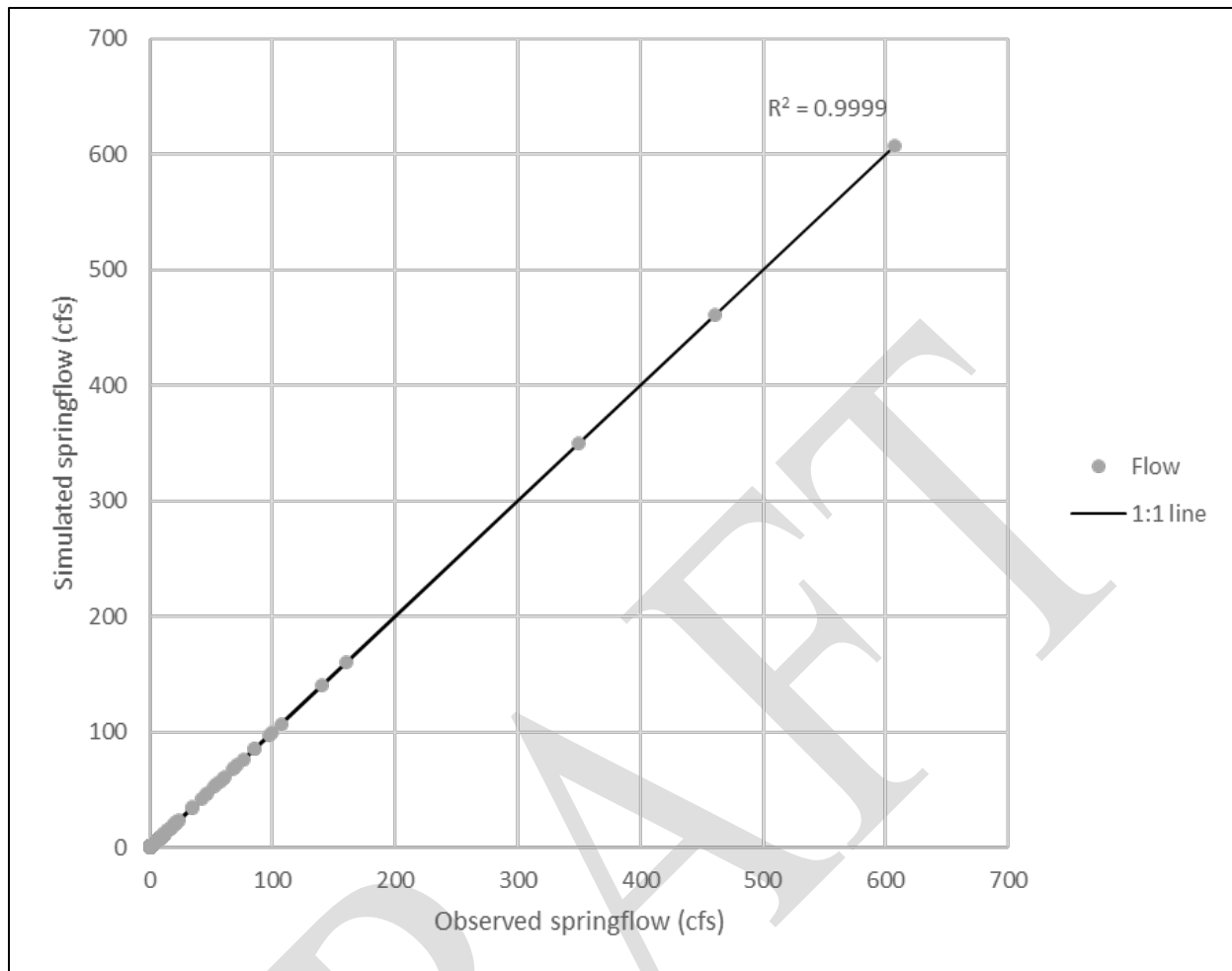


Figure 5-29. Scatter plot of springflow targets

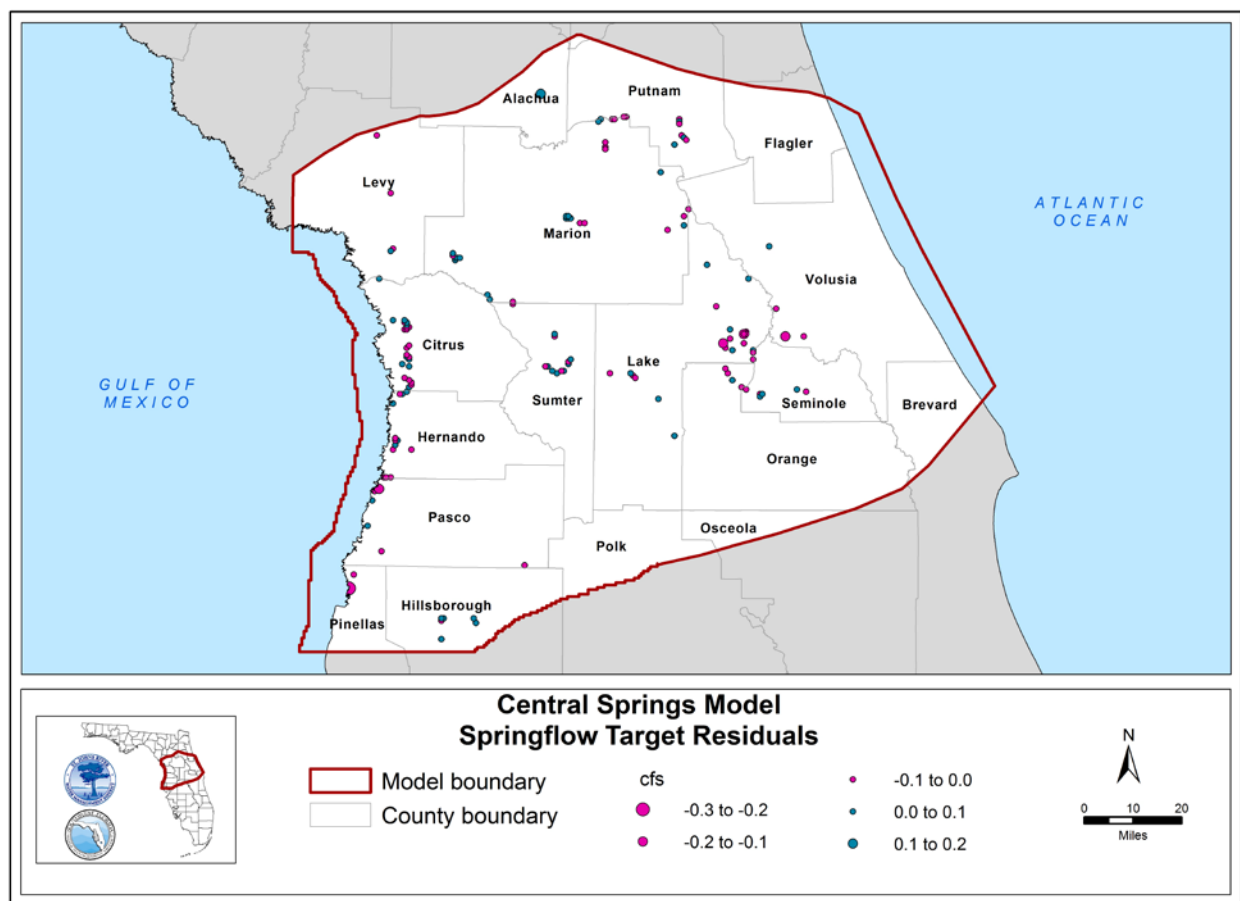


Figure 5-30. Springflow target residuals within the Central Springs Model domain

Water Budgets

Simulated water budgets illustrating hydrologic inflows and outflows by layer are provided in Table 5-8 and Table 5-9. The net fluxes, represented as inflows minus outflows, are well preserved throughout the steady-state simulation (Table 5-10). The net flux for each major component of the water budget during the calibration period includes recharge of 14.2 in/yr, ET of -5.5 in/yr, net discharge to river, lake, and wetland of -1.7 in/yr (summation of River/Lake and Drain), and spring discharge of -4.0 in/yr. Lateral flux through the coastal constant head (CHD) and non-coastal general head (GHB) boundaries are -1.2 in/yr and -0.6 in/yr, respectively. The overall groundwater withdrawal is -1.5 in/yr (outflux) and groundwater recharge through natural sinkholes, drainage wells, and RIBs is 0.2 in/yr (influx), resulting in a net groundwater withdrawal of -1.3 in/yr.

Table 5-8. Boundary condition influx by layer within the steady-state Central Springs Model (inches/year)

Layer	CHD	GHB	Well	River/Lake	Recharge	Vertical (Lower Face)*
1	0.0	-	0.1	1.1	14.2	4.5
2	0.1	-	-	-	-	5.8
3	0.1	0.0	0.1	-	-	5.7
4	0.2	0.1	-	-	-	2.6
5	0.1	-	-	-	-	2.5
6	0.3	0.2	-	-	-	0.2
7	0.1	-	-	-	-	-
Total	0.9	0.3	0.2	1.1	14.2	-

* Flux across layer bottom; positive = downward flux; negative = upward flux

Note: CHD = constant head

GHB = general head boundary

Rounding of fluxes may account for nominal discrepancies.

Table 5-9. Boundary condition outflux by layer within the steady-state Central Springs Model (inches/year)

Layer	CHD	GHB	Well	River/Lake	Drain	Spring	ET	Vertical (Lower Face)*
1	-2.0	-	-	-2.4	-0.4	-	-5.5	-9.7
2	-0.0	-	-	-	-	-	-	-11.0
3	-0.1	-0.3	-0.5	-	-	-	-	-10.4
4	-0.0	-0.3	-0.7	-	-	-4.0	-	-2.5
5	-0.0	-	-0.1	-	-	-	-	-2.4
6	-	-0.2	-0.3	-	-	-	-	-0.1
7	-	-	-	-	-	-	-	-
Total	-2.1	-0.8	-1.5	-2.4	-0.4	-4.0	-5.5	-

* Flux across layer bottom; positive = downward flux; negative = upward flux

Note: CHD = constant head

ET = evapotranspiration

GHB = general head boundary

Rounding of fluxes may account for nominal discrepancies.

Table 5-10. Boundary condition net flux by layer within the steady-state Central Springs Model (inches/year)

Layer	CHD	GHB	Well	River/Lake	Drain	Spring	Recharge	ET	Vertical (Lower Face)*
1	-2.0	-	0.1	-1.3	-0.4	-	14.2	-5.5	-5.2
2	0.1	-	-	-	-	-	-	-	-5.3
3	0.0	-0.2	-0.3	-	-	-	-	-	-4.7
4	0.2	-0.3	-0.7	-	-	-4.0	-	-	0.1
5	0.1	-	-0.1	-	-	-	-	-	0.1
6	0.3	-0.0	-0.3	-	-	-	-	-	0.1
7	0.1	-	-	-	-	-	-	-	-
Total	-1.2	-0.6	-1.3	-1.3	-0.4	-4.0	14.2	-5.5	-

* Flux across layer bottom; positive = downward flux; negative = upward flux

Note: CHD = constant head

ET = evapotranspiration

GHB = general head boundary

Rounding of fluxes may account for nominal discrepancies.

6. TRANSIENT MODEL CALIBRATION

The transient model calibration was conducted using PEST-optimized hydraulic parameters from the steady-state model calibration, described in Chapter 5, and testing storage parameters. The monthly simulation output was compared with measured groundwater levels at monitoring wells, spring discharges, river baseflows, and lake leakages to evaluate the performance of the model. The transient results were used to refine the PEST calibration process and further improve model parameterization through an iterative approach.

Throughout the calibration process, a consistent focus was placed on maintaining the conceptual model of the hydrogeologic system as described in Chapter 3. To this end, parameter values were constrained within sensible ranges informed by prior modeling efforts and existing knowledge of the hydrological system.

Calibration results were visualized on an interactive web application ([Central Spring Model \(shinyapps.io\)](https://shinyapps.io)), where transient hydrographs for target wells, springs, river baseflow, and lake leakage can be viewed by clicking the target locations on the map.

TRANSIENT MODEL PARAMETERS

Storage Parameters

Specific yield (S_y) is a ratio indicating the volume of water an aquifer releases from storage per unit surface area of the aquifer per unit decrease in the water table elevation under the forces of gravity. Specific yield is expressed as a decimal fraction and is the same as effective porosity in an unconfined setting. The S_y in the unconfined SAS (layer 1) was assigned based on geologic and geomorphic setting, with values ranging from 0.10 to 0.20 (Figure 6-1). Ridge areas with a deep water table and mostly sandy soils were assigned a S_y value of 0.20. Specific yield values of 0.10 were assigned to the valley and lowland areas with relatively higher percentages of fine-grained soils. An intermediate value of 0.15 was assigned to the remaining areas.

For a confined aquifer or aquitard, storativity (storage coefficient) is the vertically integrated specific storage (S_s) value. Specific storage is the volume of water a unit volume of saturated aquifer releases from storage for a unit decline in hydraulic head by expansion of water or compression of the rock or soil matrix. Although storage coefficients can be estimated from APTs, measured values are scarcely available, and the reported values can vary by several orders of magnitude. The MODFLOW code requires input of a S_s value, which is calculated by dividing the storage coefficient by the aquifer thickness. For the transient simulation, the S_s values for layer 2 through layer 7 were assigned based on the typical literature values reported for the region and varied based on the confinement of the aquifer layers. A constant S_s value of $1\text{E-}6\text{ ft}^{-1}$ was assigned for confining units. Semi-confining units were assigned a S_s value of $2\text{E-}6\text{ ft}^{-1}$. Unconfined regions of the UFA were assigned a S_s value of $1\text{E-}5\text{ ft}^{-1}$. In confined or semi-confined regions of UFA, S_s values varied between $2\text{E-}6\text{ ft}^{-1}$ and $5\text{E-}6\text{ ft}^{-1}$ based on depth and confinement. The MCU I, MCU II, and the LFA were assigned a uniform

Ss value of $1\text{E-}6\text{ ft}^{-1}$. Specific storage for layer 2 through layer 6 is presented on Figure 6-2 through Figure 6-6.

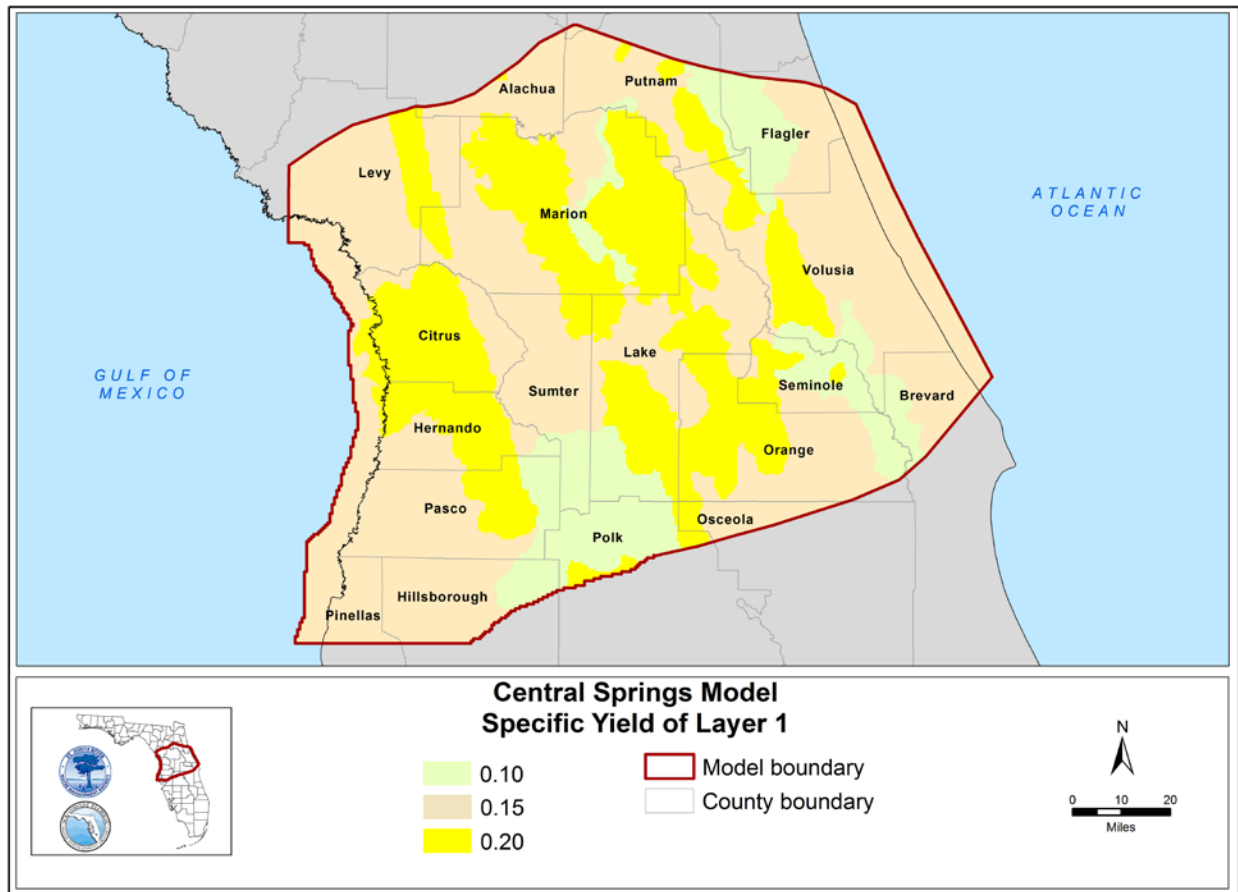


Figure 6-1. Specific yield of layer 1 within the Central Springs Model domain

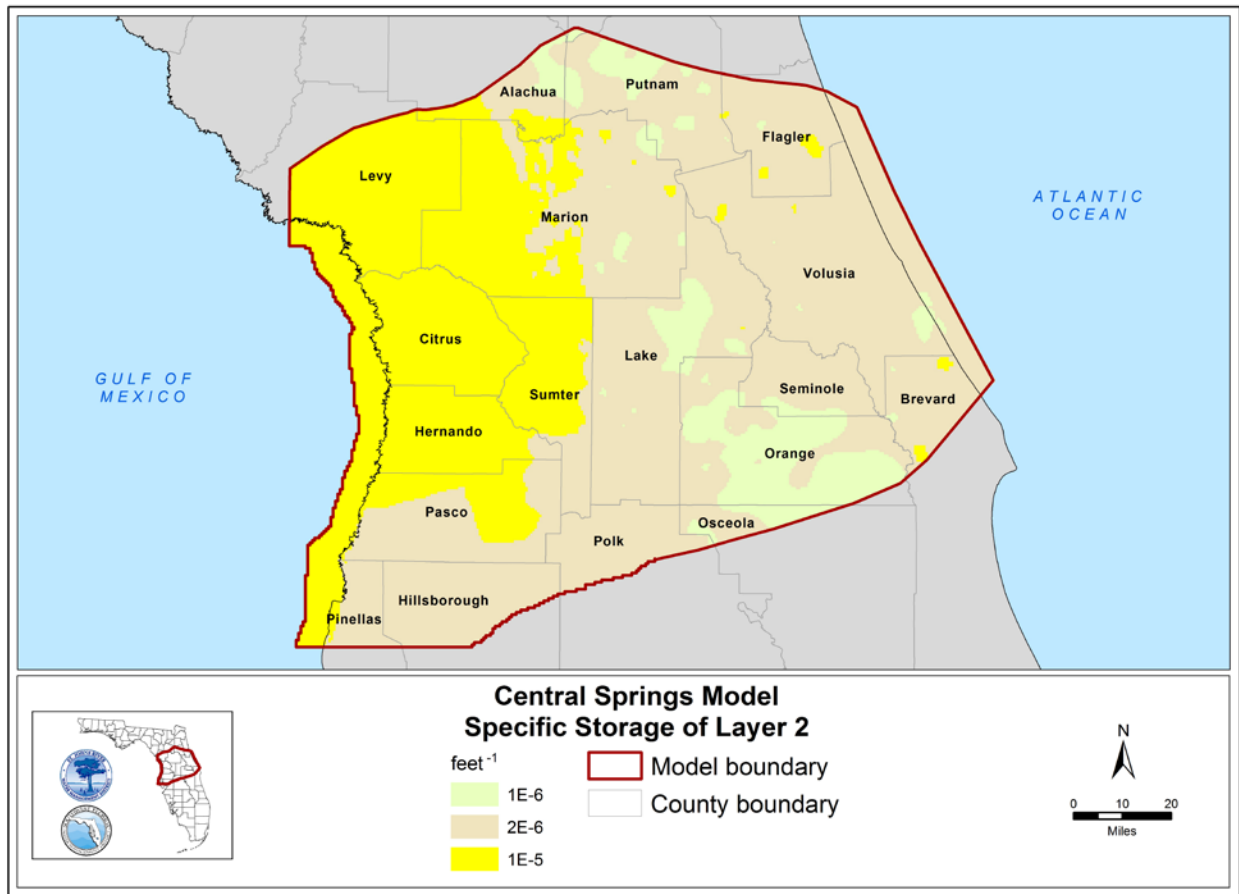


Figure 6-2. Specific storage of layer 2 within the Central Springs Model domain

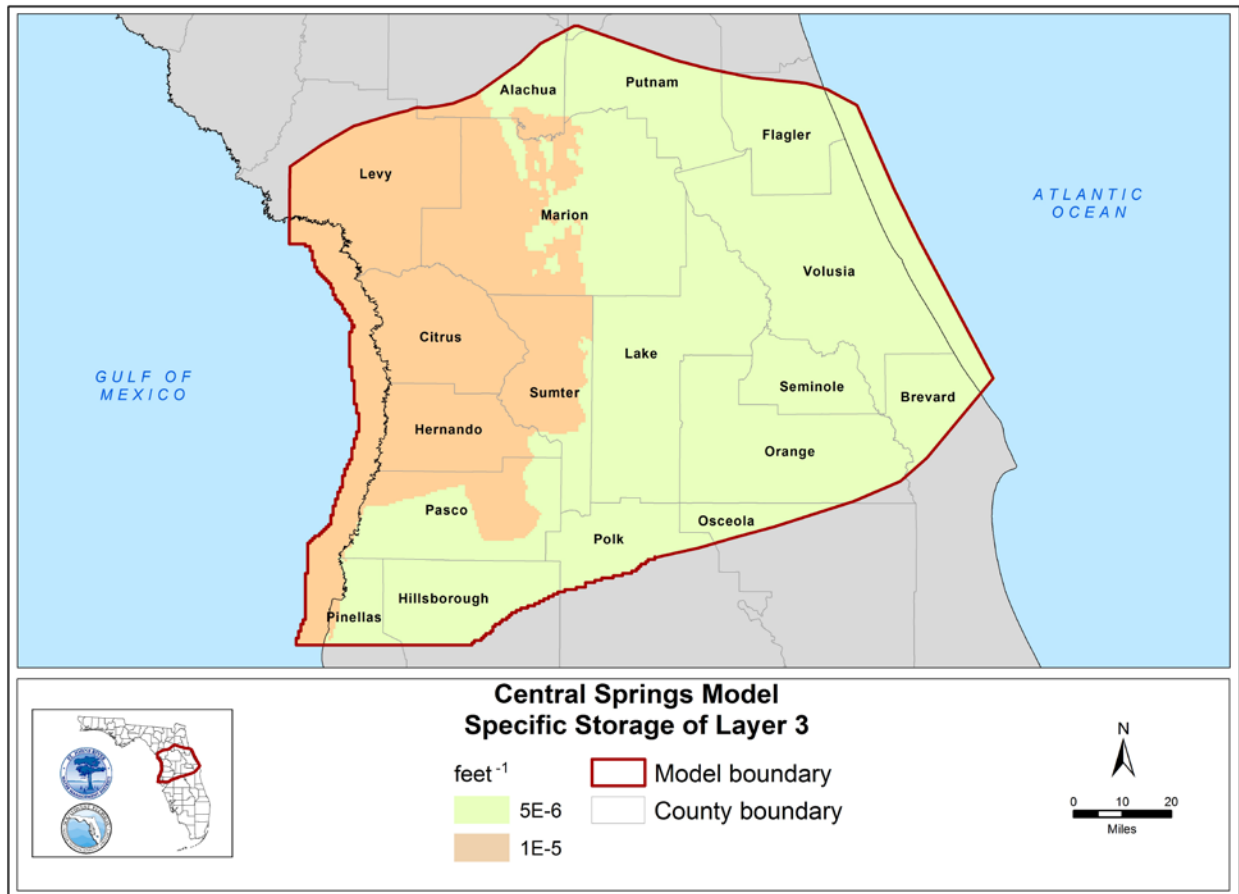


Figure 6-3. Specific storage of layer 3 within the Central Springs Model domain

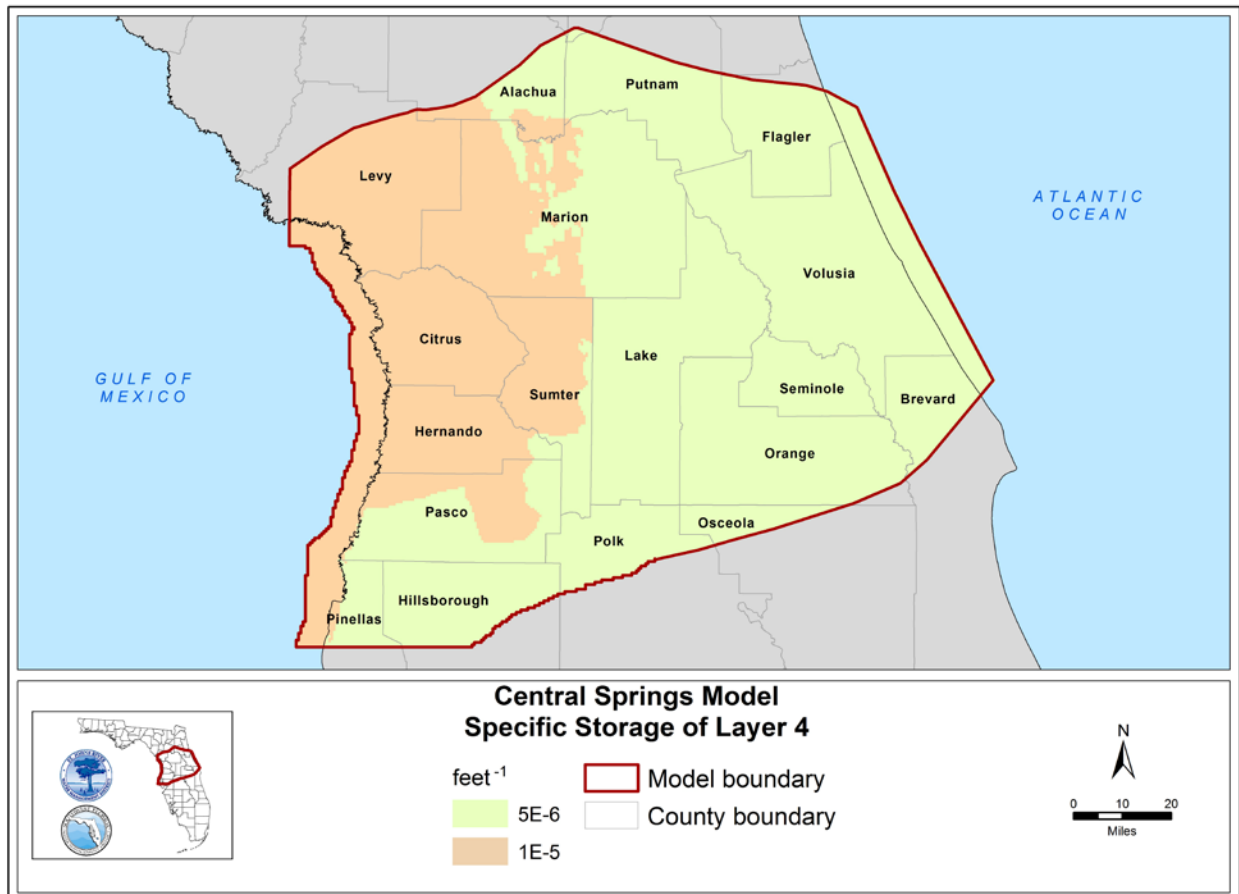


Figure 6-4. Specific storage of layer 4 within the Central Springs Model domain

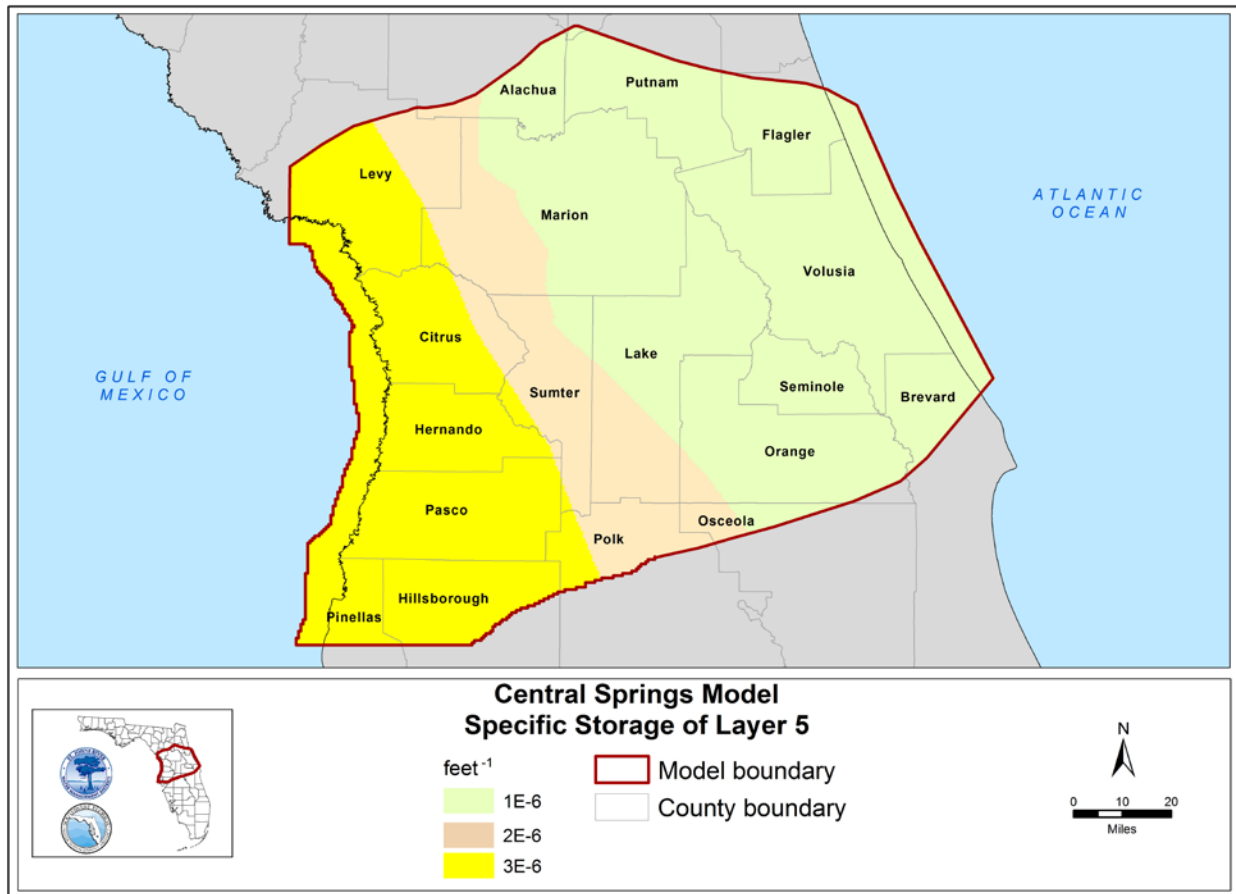


Figure 6-5. Specific storage of layer 5 within the Central Springs Model domain

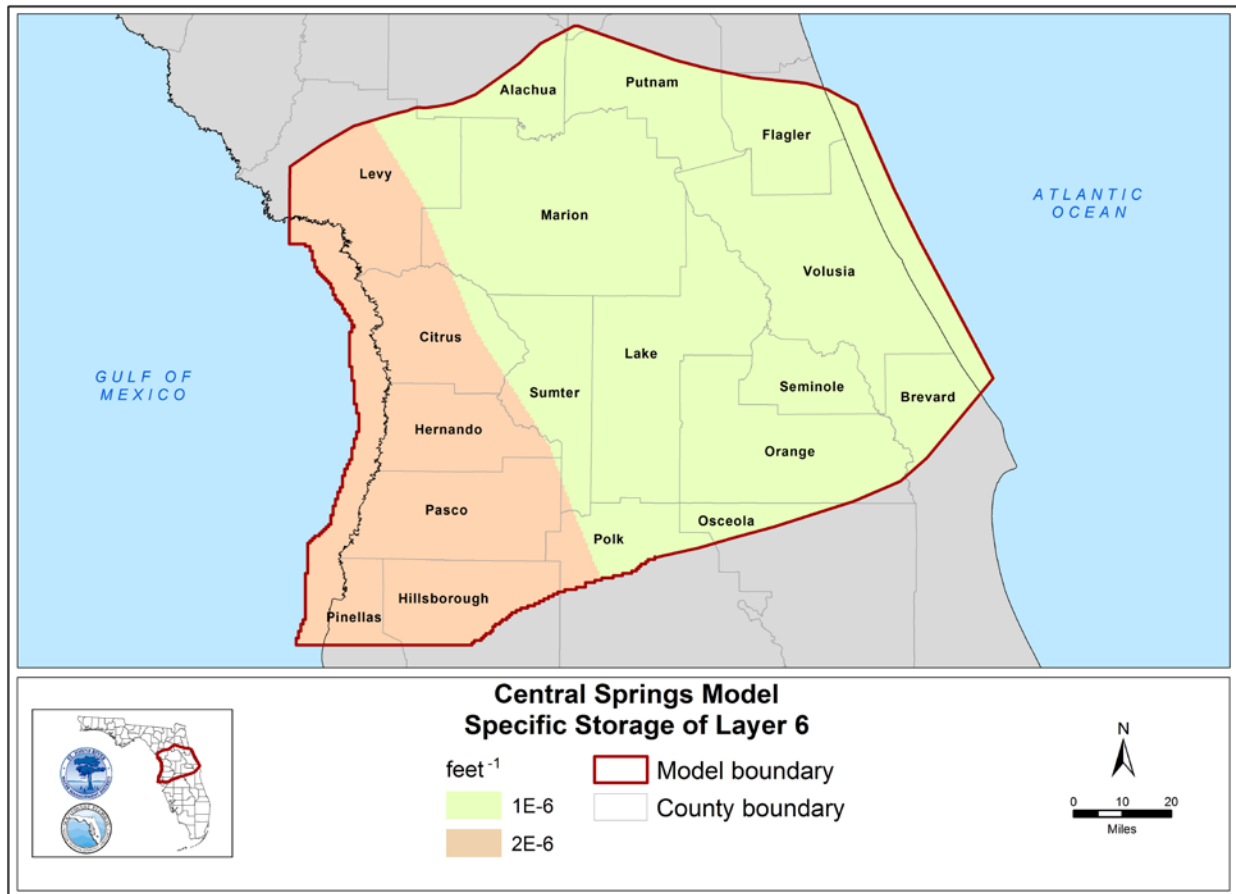


Figure 6-6. Specific storage of layer 6 within the Central Springs Model domain

River and Drain Conductance

According to Equation (3-1) and Equation (3-4) presented in Chapter 3, the conductance of a river varies with river discharge (Q), which is related to geography and seasonal precipitation. River and drain (RIV/DRN) conductance were first calculated during PEST calibration of the steady-state model. For springs, conductance values were consistent with the steady-state model and kept constant throughout the transient simulation period. The conductance of rivers, lakes, and wetlands was adjusted seasonally in the transient model based on the seasonality of the recharge. The seasonally-adjusted conductance accounts for the geometric variations of rivers, lakes, and wetlands during the wet and dry season. For each RIV/DRN cell monthly recharge ratios were computed by dividing the recharge in that month by the average recharge value across the entire simulation period. Subsequently, the conductance of the river and wetland cells was adjusted based on the respective recharge ratio in each cell.

TRANSIENT SIMULATION RESULTS

A diverse set of quantitative and qualitative targets was considered during calibration of the transient model. Groundwater head statistics at target monitoring wells and discharge at first and second magnitude springs with measured discharge data were calculated and compared to the metrics and criteria presented in Chapter 4. Model-simulated river baseflows and lake leakages were calculated and compared with estimated baseflows and reported lake leakage values to ensure that the simulated fluxes were within a reasonable range. Other criteria including depth to water table, vertical head difference across confining units, and flooded and dry cells were examined during the transient calibration process. Semi-annual May and September potentiometric surface maps from the USGS, FDEP and Districts were compared to simulated May and September UFA heads across the model domain during the calibration period as another guide to model calibration.

Groundwater Heads

Monthly average aquifer water levels and available salinity data (chloride concentration, specific conductance, and total dissolved solids) were obtained from recorded observations or approximated during the transient simulation period. Freshwater equivalent heads were calculated based on the USGS method (Kuniansky et al., 2017), as described in Equation (4-2) in Chapter 4. Average monthly equivalent freshwater heads at target monitoring wells for the SAS (layer 1), UFA (layers 3 to 4), and the LFA (layer 6) were assigned as calibration target criteria. Calibration statistics based on groundwater head residuals are presented in Table 6-1. The differences in statistics between Table 5-3 and Table 6-1 are expected. They reflect the differences between steady-state and transient model simulations, with the impacts of starting heads and aquifer storage exhibited in the transient model.

A total of 403 SAS, 601 UFA, and 38 LFA monitoring wells were used as quantitative targets for transient calibration. Simulated groundwater heads were compared with observed monthly average fresh water equivalent heads throughout the model simulation period. The spatial distribution of mean errors for the target wells in the SAS, UFA, and LFA is displayed on Figure 6-7 through Figure 6-9, respectively.

Example hydrographs of simulated groundwater heads versus observed groundwater levels in target wells in the SAS, UFA, and LFA throughout the simulation period are presented on Figure 6-10 through Figure 6-12. Calculated statistics including ME, MAE, R^2 , and NSE are presented for each well. Note that R^2 calculations presented in Chapter 5 included all wells within a model layer, whereas here R^2 calculations are evaluated for individual wells. The percentage of wells with $R^2 > 0.4$ is reported by aquifer in Table 6-1. The complete set of simulated and observed hydrographs for calibration target wells is provided in Appendix B (SAS), Appendix C (UFA), and Appendix D (LFA).

Table 6-1. Transient model calibration statistics of target monitoring wells in the Central Springs Model domain (feet, except where noted)

Metrics	Transient Statistics		
	SAS	UFA	LFA
Mean error	0.5	0.3	-0.3
Error standard deviation	3.6	2.2	2.2
Mean absolute error (MAE)	2.6	1.8	1.7
RMS error	3.6	2.2	2.2
Minimum residual	-12.2	-12.4	-8.4
Maximum residual	24.5	13.1	6.4
Number of observations	403	601	38
Percentage with MAE < 2.5 ft	72.0%	82.7%	89.5%
Percentage with MAE < 5.0 ft	90.6%	96.5%	94.7%
Percentage with $R^2 > 0.4$	59.8%	86.2%	94.7%

Note: Mean error expressed as simulated minus observed.

LFA = Lower Floridan Aquifer

RMS = root mean square

R^2 = coefficient of determination

SAS = Surficial Aquifer System

UFA = Upper Floridan Aquifer

The SAS exhibited the largest simulation bias for groundwater heads within target monitoring wells, with a mean error of 0.5 ft and an RMS error of 3.6 ft. This is a result of the complex surface water-groundwater interaction within the SAS, which is affected by numerous factors and processes including recharge, ET, river/lake exchange, vadose zone processes, and leakage to deeper aquifers. It should be noted that the CSM is intended solely for the simulation of groundwater and lacks the capability to simulate the dynamic interaction between groundwater and surface water. The model relies on recharge and maximum saturated ET input from the HSPF models to simulate the transient variations in influx and outflux.

In addition to evaluating model fit statistics, minimizing excessive flooding peaks and the number of dry cells per month was an important consideration during the calibration process. Figure 6-13 highlights the distribution of flooded cells with simulated heads greater than 5 ft above land surface in layer 1 during September 2017, a stress period characteristic of high rainfall from Hurricane Irma. Although flooding of low land is a naturally occurring phenomenon as part of the hydrologic cycle, unrealistically high peaks of flooding reflect an imbalance in the water budget and need to be accounted for. The calibrated model addressed

the flooding issue and minimized the number of cells with high flooding peaks. Figure 6-14 illustrates the distribution of layer 1 dry cells with simulated heads beneath the bottom elevation of layer 1 in May 2012, which was unusually dry. The large areas of dry cells in the western part of the model domain were expected as the UFA in this area is unconfined and the water table can be greater than one hundred feet below land surface. Model-simulated mean depths-to-water table were compared to observed well data (Figure 6-15). The transient simulation compared favorably to the observed data, indicating a deep water table along the Brooksville Ridge and ridges in the Orlando area.

The UFA target monitoring wells met the calibration criteria set in Chapter 4. The ME for UFA target wells was 0.3 ft, and the RMS error was 2.2 ft. In addition, more than 86 percent of the wells had R^2 values greater than 0.4, which demonstrates reasonable correlation between the seasonal variation of simulated and observed heads.

Simulated heads were compared to observed UFA potentiometric surfaces to examine simulated head distribution during wet and dry periods. Figure 6-16 and Figure 6-17 show the reasonable match between simulated and observed potentiometric surfaces for May 2010 (dry) and September 2014 (wet), respectively, illustrating that the UFA flow field is well represented in the transient model. A complete set of comparisons between simulated and observed UFA potentiometric surfaces is provided in Appendix E. Model-simulated mean SAS-UFA head differences were also compared to observed well pair data (Figure 6-18). As expected, the greatest difference in simulated SAS-UFA heads is in the area where the UFA is tightly confined, whereas the smallest difference is observed where the UFA is unconfined or leaky.

The LFA target monitoring wells also met the preset calibration criteria, with a ME of -0.3 ft and an RMS error of 2.2 ft. With approximately 95 percent of the target wells having a mean error less than 5 ft, the model well represented the LFA groundwater head. Approximately 95 percent of the LFA target wells had an R^2 greater than 0.4, showing a reasonable agreement between simulated and observed temporal trends. In addition, model-simulated mean UFA-LFA head differences were reasonably correlated for most given well pairs (Figure 6-19).

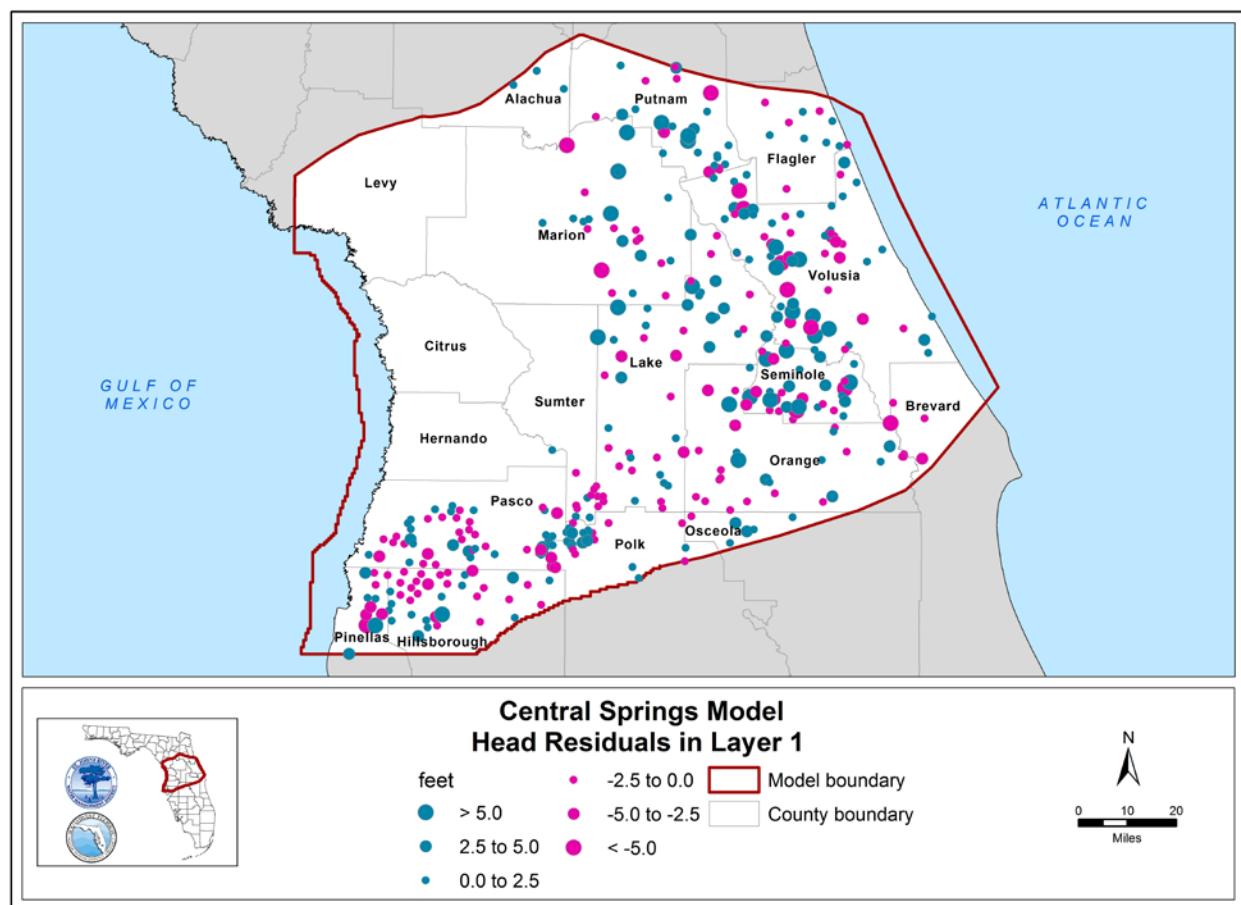


Figure 6-7. Average head residuals over the transient simulation period in layer 1 target wells

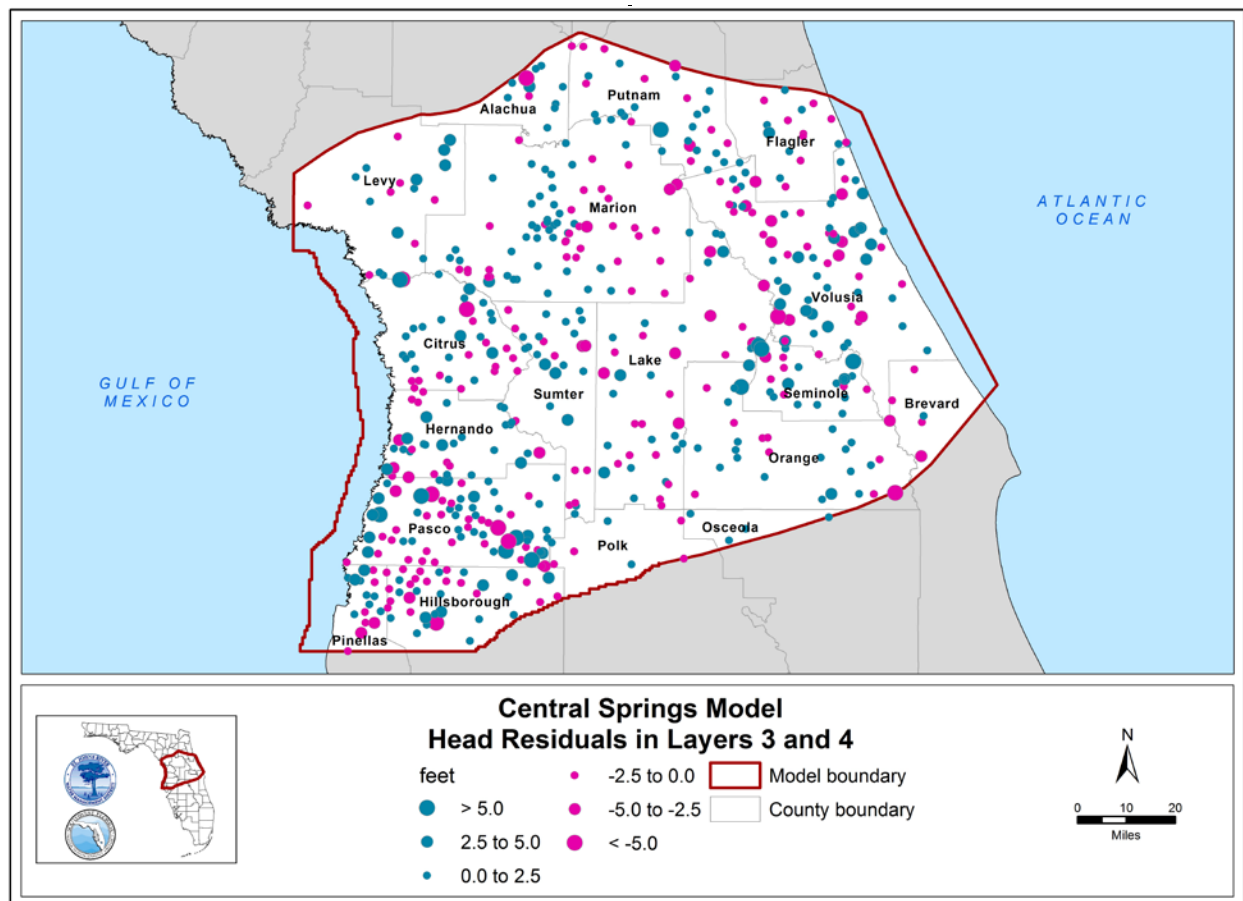


Figure 6-8. Average head residuals over the transient simulation period in layer 3 and layer 4 target wells

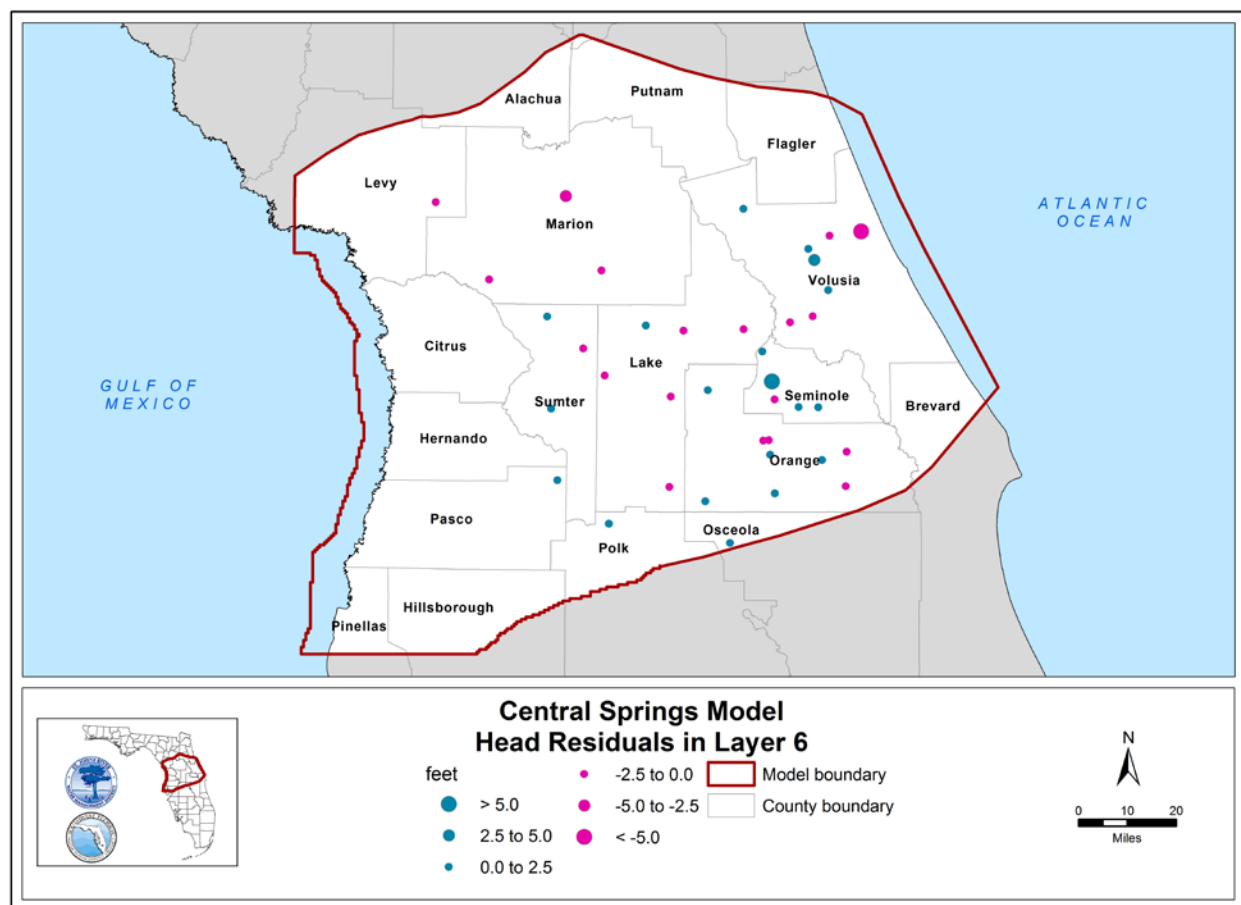


Figure 6-9. Average head residuals over the transient simulation period in layer 6 target wells

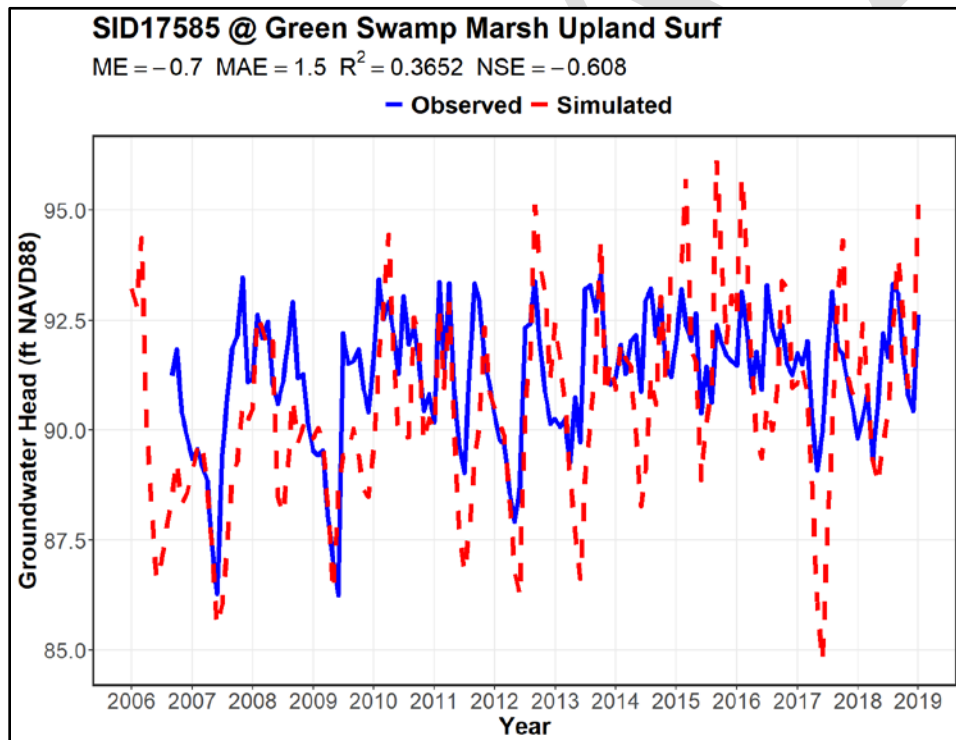
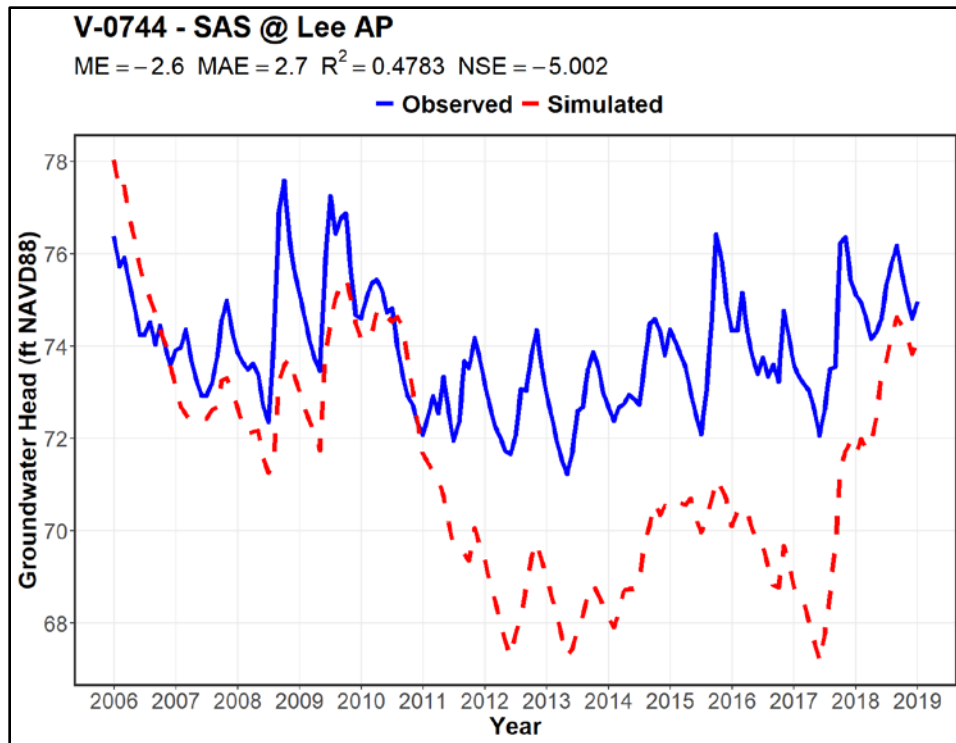


Figure 6-10. Comparison of model-simulated hydrographs to monthly observed groundwater levels at selected target wells in layer 1

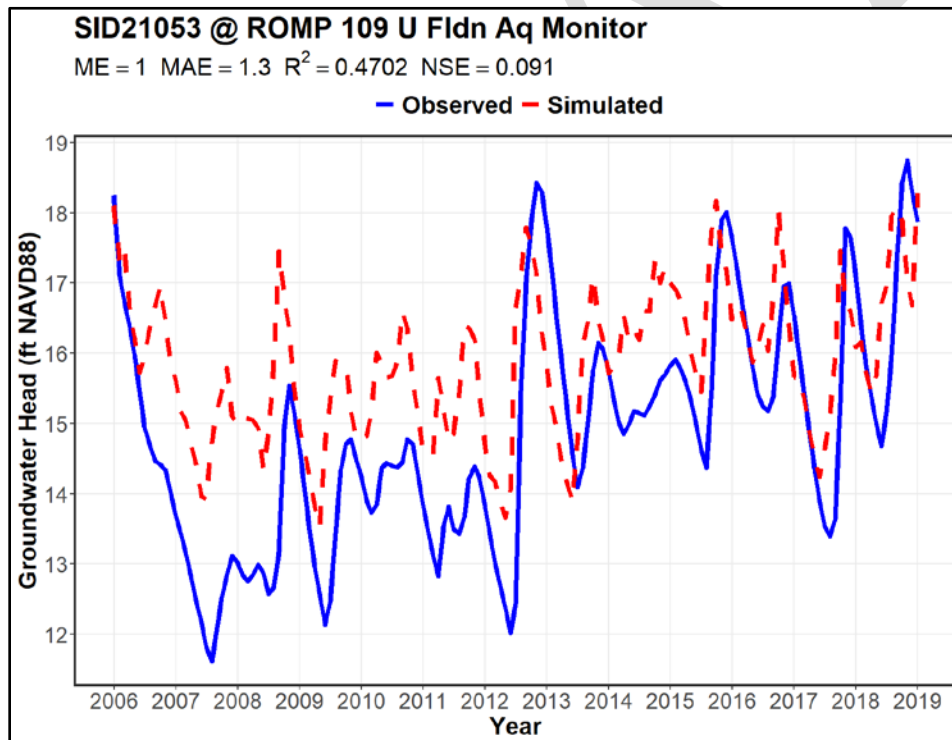
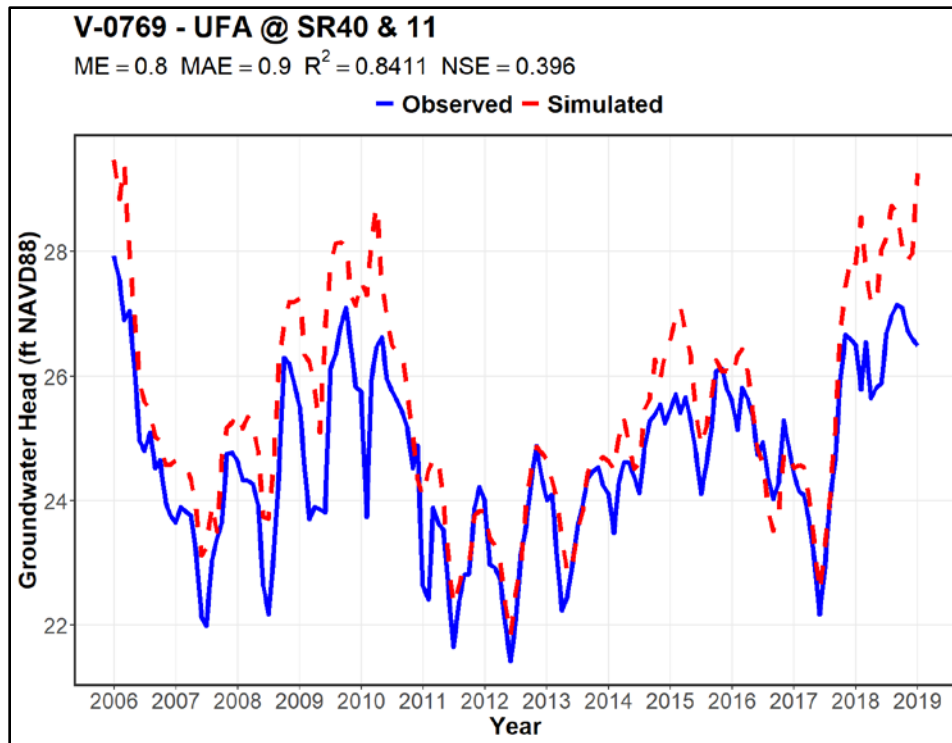


Figure 6-11. Comparison of model-simulated hydrographs to monthly observed groundwater levels at selected target wells in layer 3 and layer 4

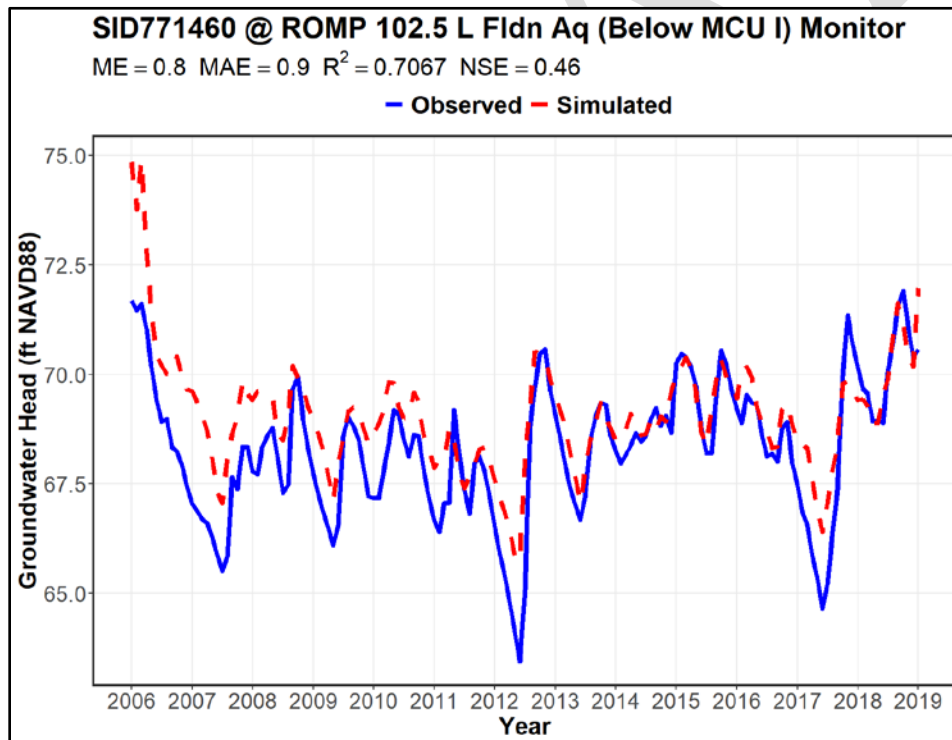
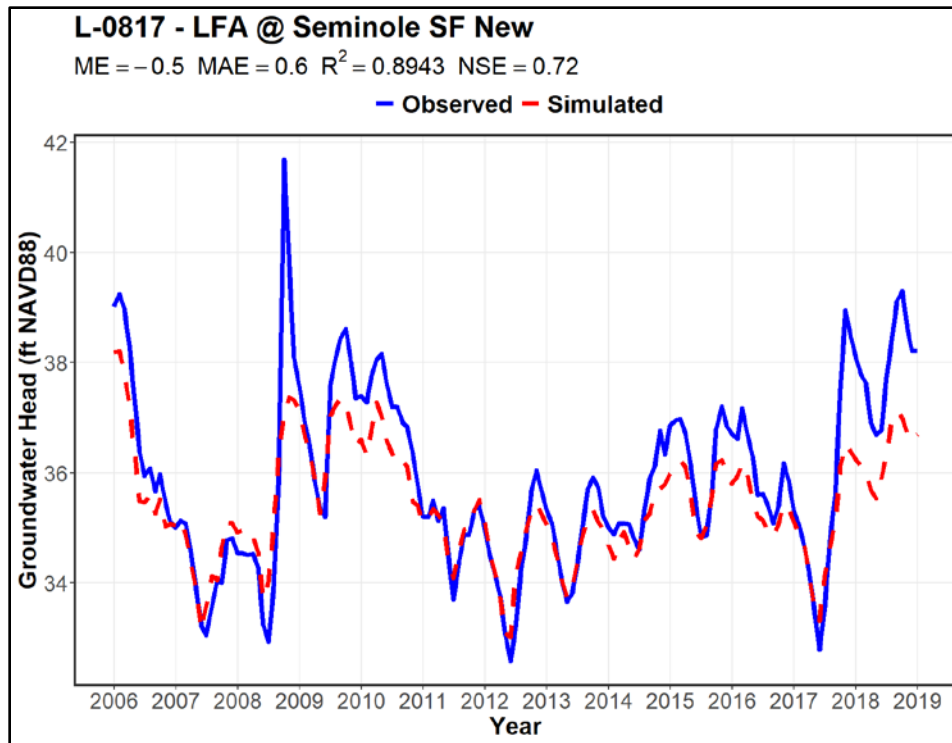


Figure 6-12. Comparison of model-simulated hydrographs to monthly observed groundwater levels at selected target wells in layer 6

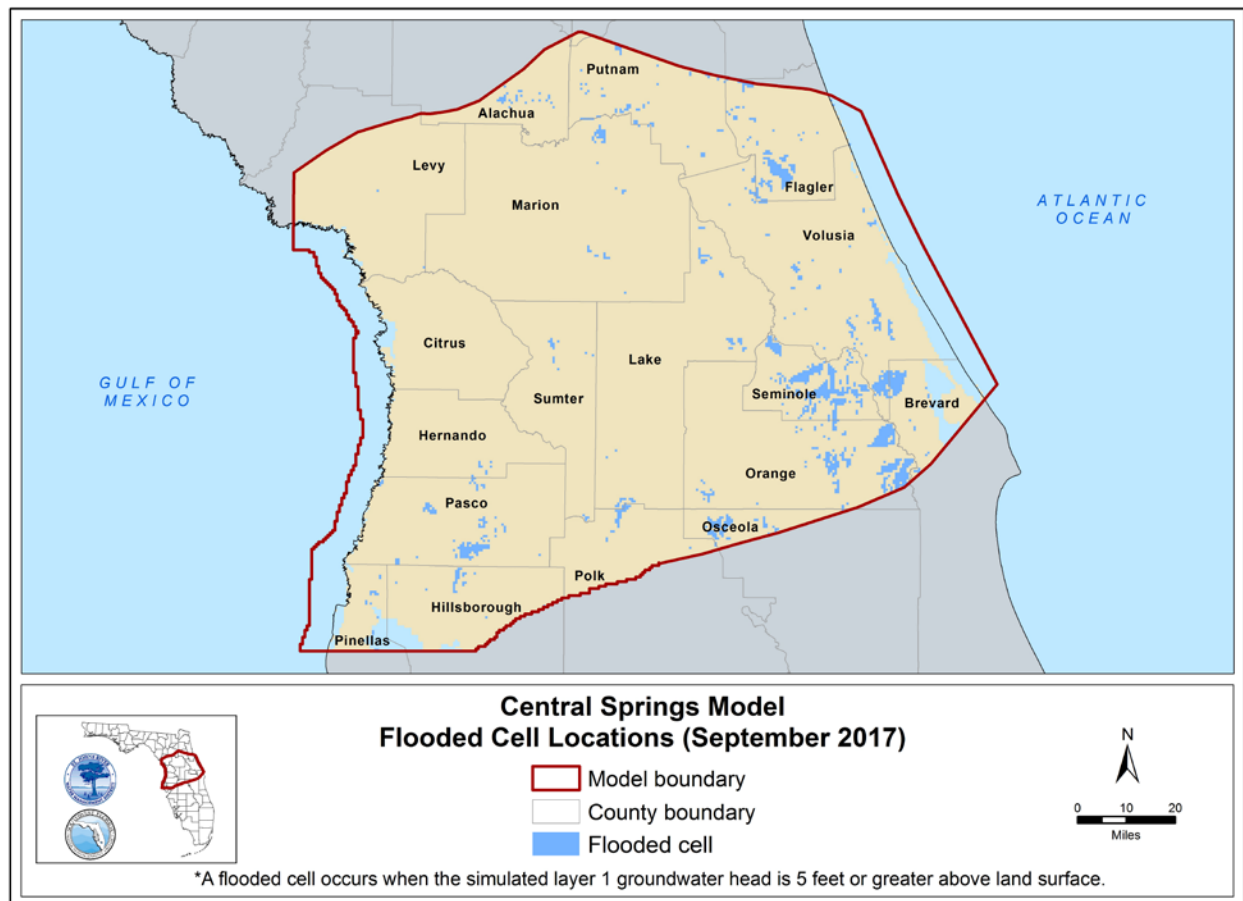


Figure 6-13. Spatial distribution of flooded cells in September 2017

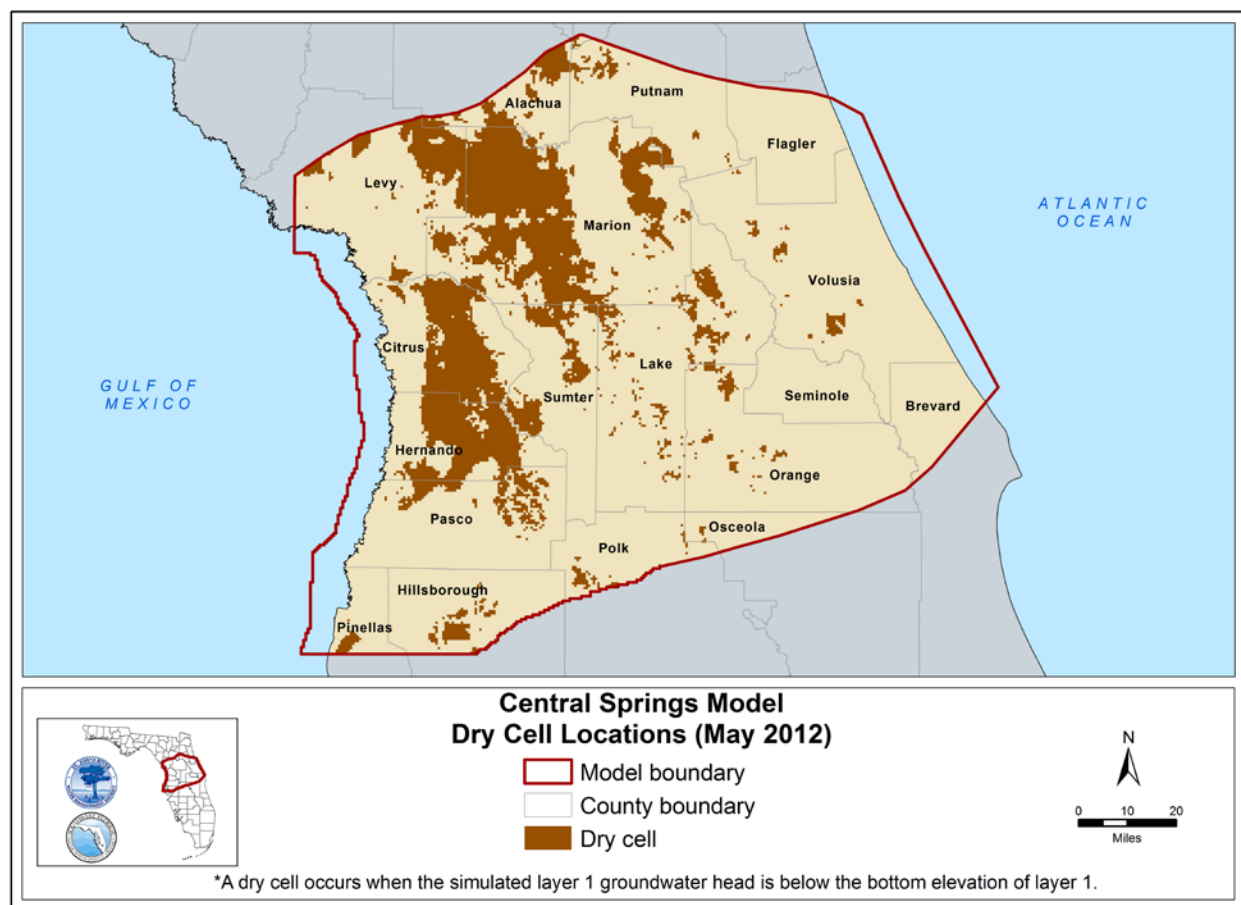


Figure 6-14. Spatial distribution of dry cells in May 2012

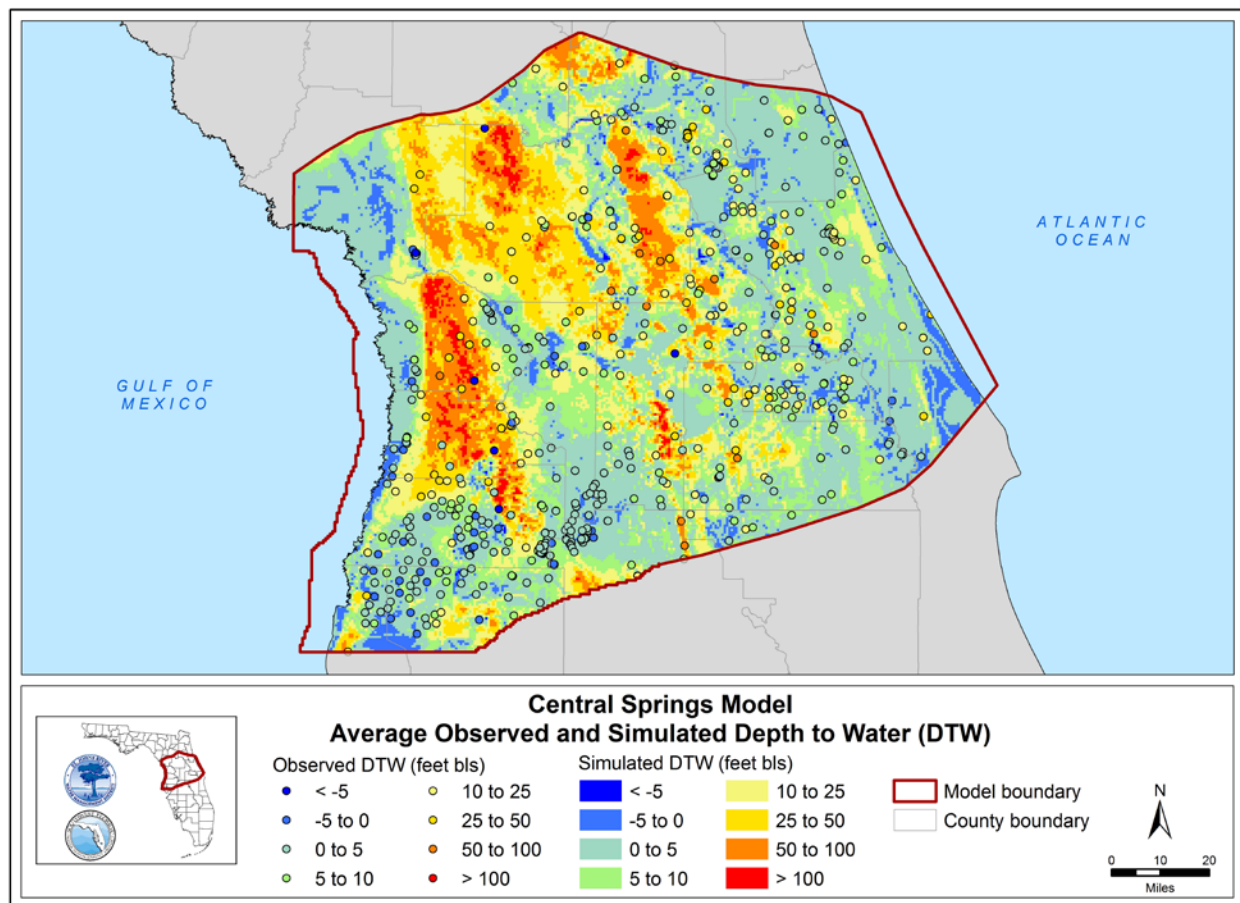


Figure 6-15. Comparison of simulated 2005 to 2018 average depth to water table with observed values in layer 1
 Note: bls = below land surface

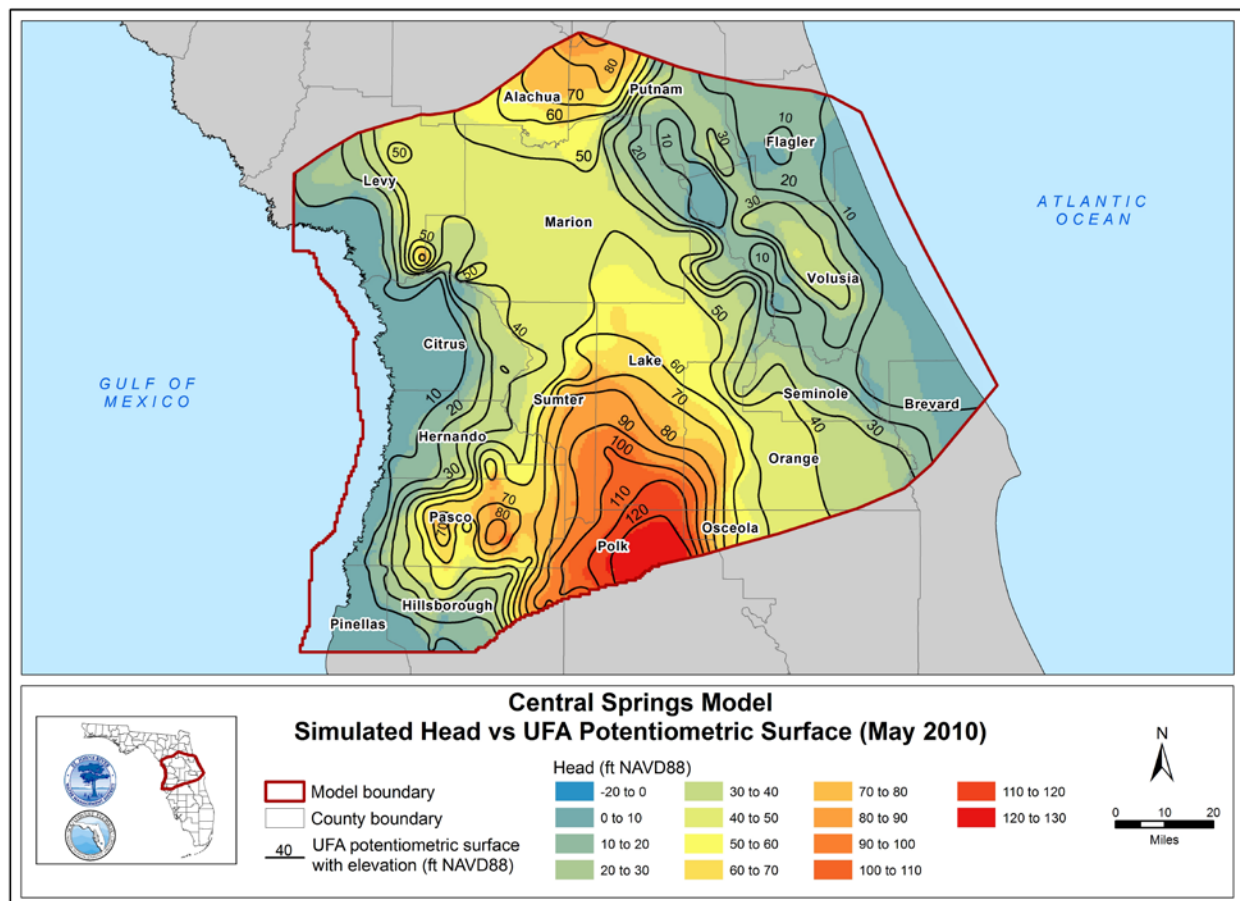


Figure 6-16. Comparison of model-simulated heads in layer 3 and the Upper Floridan Aquifer (UFA) potentiometric surface in May 2010

Note: ft NAVD88 = feet relative to the North American Vertical Datum of 1988

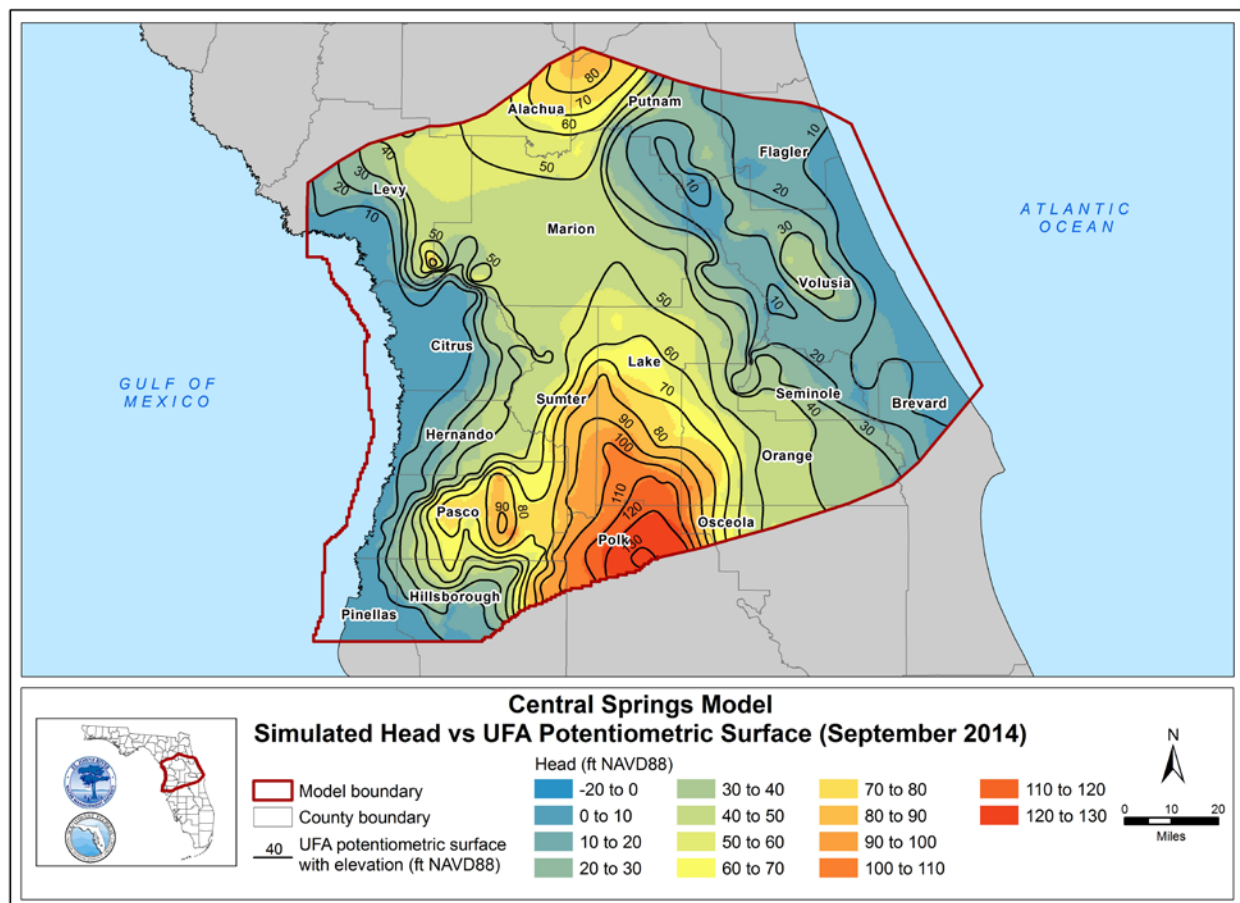


Figure 6-17. Comparison of model-simulated heads in layer 3 and the Upper Floridan Aquifer (UFA) potentiometric surface in September 2014

Note: ft NAVD88 = feet relative to the North American Vertical Datum of 1988

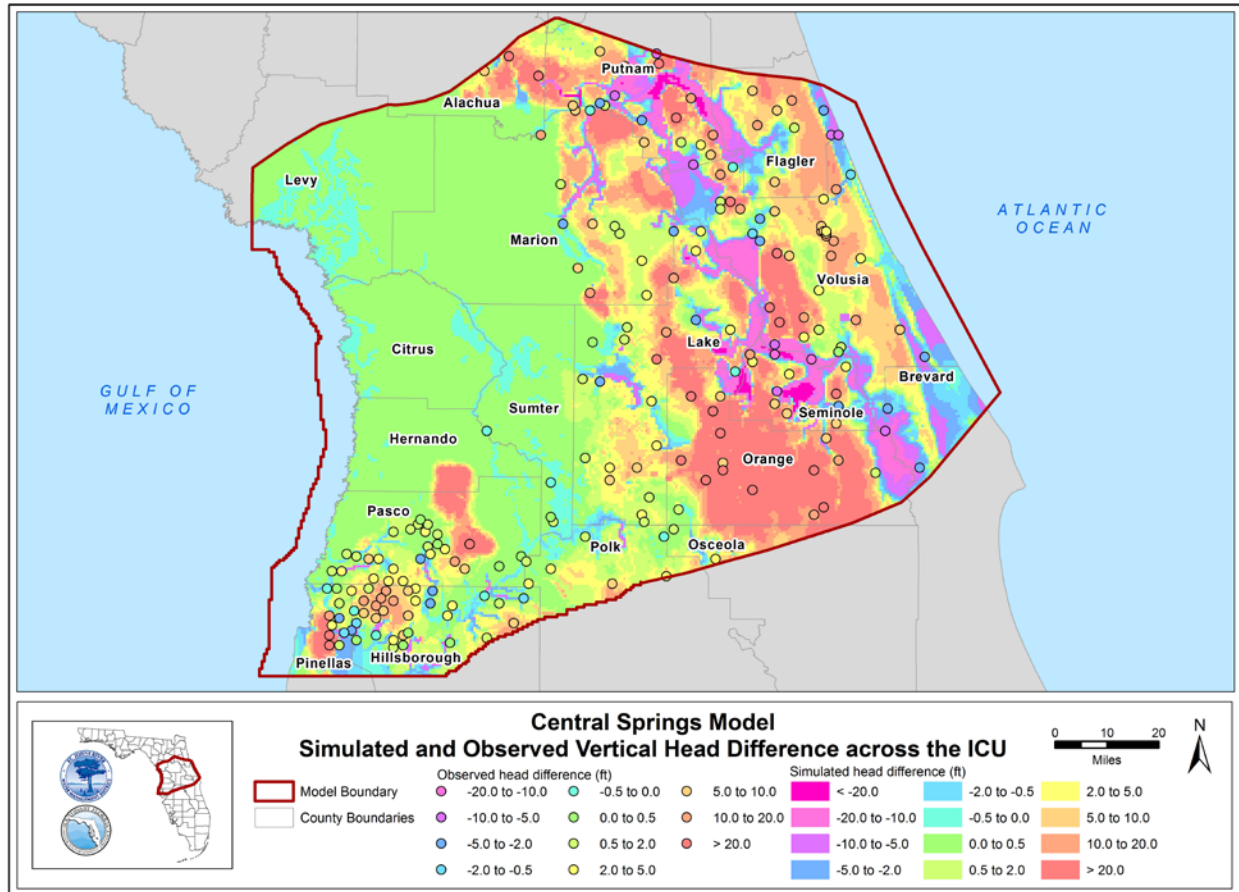


Figure 6-18. Comparison of simulated 2005 to 2018 average vertical head difference across the Intermediate Confining Unit (ICU) with observed values at well pairs

Note: There were no observed vertical head differences less than -20 feet.

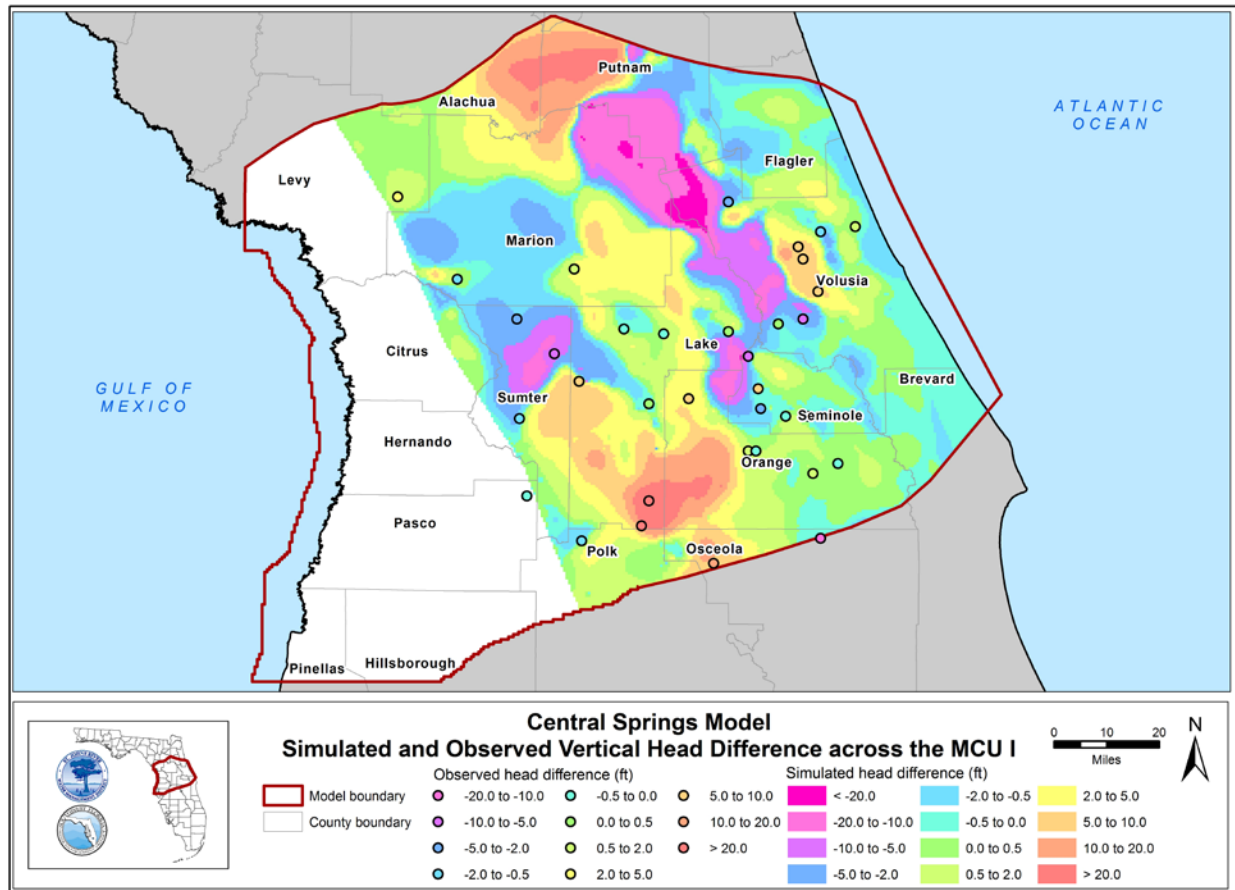


Figure 6-19. Comparison of simulated 2005 to 2018 average vertical head difference across Middle Confining Unit I (MCU I) with observed values at well pairs

Note: There were no observed vertical head differences less than -20 feet.

Spring Discharges

First magnitude (greater than 100 cfs) and second magnitude (10 to 100 cfs) springs in the model domain with flow measurement data during the calibration period served as calibration targets for the transient model. Comparison of simulated and observed spring fluxes averaged through the transient simulation period are provided in Table 6-2 for 27 target springs. Comparisons between the simulated and observed hydrographs for selected first and second magnitude springs are shown on Figure 6-20 through Figure 6-31. A complete set of simulated and observed hydrographs for transient target springs is provided in Appendix F. It is noted that observed springflow data was reported using various springflow measurement methods, which may represent discharge from a single spring vent or cumulative discharge from a group of springs. Substantial efforts were made by the Districts over the years to compile and analyze springflow data and the best available data was used as transient calibration targets. More detailed descriptions of specific measurement methods and hydrologic analysis of springflows are provided in the MFL reports for individual springs.

The springs are simulated as drain cells in the UFA (layer 4). The transient stages of the spring cells were determined using measured pool elevations when available. For smaller springs that lacked field measurements, the stages were estimated using nearby springs or monitoring wells. The steady-state conductance calculated by PEST, as described in Chapter 5, was directly used for transient simulations without any modification.

Most of the target springs met the calibration criteria set in Chapter 4. In addition, the hydrographs illustrate a strong correlation between simulated and observed monthly spring flux, demonstrating that the transient model can predict the temporal variation of spring discharge. Mean errors of all first magnitude spring discharges are within 5 percent of the average observed spring discharge. All target springs except Crystal Spring in Pasco County have a mean error within ± 10 percent of the observed springflow. For Crystal Springs, the transient model-simulated discharge was 15 percent higher than the average measured discharge rate, which overrepresents seasonal variation. However, this spring is located in the northern Tampa Bay area, which is not the focus of this model.

Spring discharge at the third and higher magnitude springs was also calculated from the transient simulation. These smaller springs were not used as calibration targets for the transient model due to limited flow measurements. Best available estimates of springflow were compiled from various sources and used as input for steady-state model calibration, as described in Chapter 5 and provided in Appendix A. For the transient simulation, the cumulative average discharge of all 185 simulated springs was 3,653 cfs, which is less than 0.2 percent lower than the total estimated flow of 3,659 cfs.

Table 6-2. Comparison of average 2005 to 2018 simulated and observed flux of the target springs in the transient Central Springs Model

Spring Name	Simulated Flux (cfs)	Observed Flux (cfs)	% Difference
Alexander Springs	98.5	95.9	2.8%
Apopka Spring	24.1	23.5	2.6%
Blue Spring (Marion)	21.5	20.7	4.0%
Blue Spring (Orange City)	142.5	138.4	3.0%
Bugg Spring	10.4	10.3	1.3%
Chassahowitzka Spring	59.7	59.9	-0.3%
Croaker Hole Spring	71.0	68.7	3.3%
Crystal Spring (Pasco)	52.8	46.0	14.7%
Fern Hammock Springs	11.7	11.1	5.2%
Gum Spring	69.6	64.1	8.6%
Homosassa Springs	83.1	84.5	-1.7%
Juniper Springs	11.4	11.0	3.9%
Levy Blue Spring	8.1	8.1	0.0%
Ponce De Leon Springs	23.1	22.7	1.5%
Rainbow Springs	597.4	601.0	-0.6%
Rock Springs	55.3	54.3	1.9%
Salt Springs	78.0	75.3	3.7%
Sanlando Springs	20.0	19.6	2.0%
Silver Glen Springs	87.4	85.2	2.6%
Silver Springs	531.8	532.9	-0.2%
Starbuck Spring	11.8	11.5	2.6%
Sulphur Spring (Hillsborough)	20.3	20.1	1.1%
Sweetwater Springs	13.3	12.7	4.0%
Weeki Wachee Spring	157.3	158.5	-0.7%
Wekiva Springs (Levy)	51.8	49.1	5.6%
Wekiwa Springs (Seminole)	61.4	60.6	1.3%

Note: cfs =cubic feet per second

% Difference = (simulated – observed)/observed

Rounding of flows accounts for nominal discrepancies

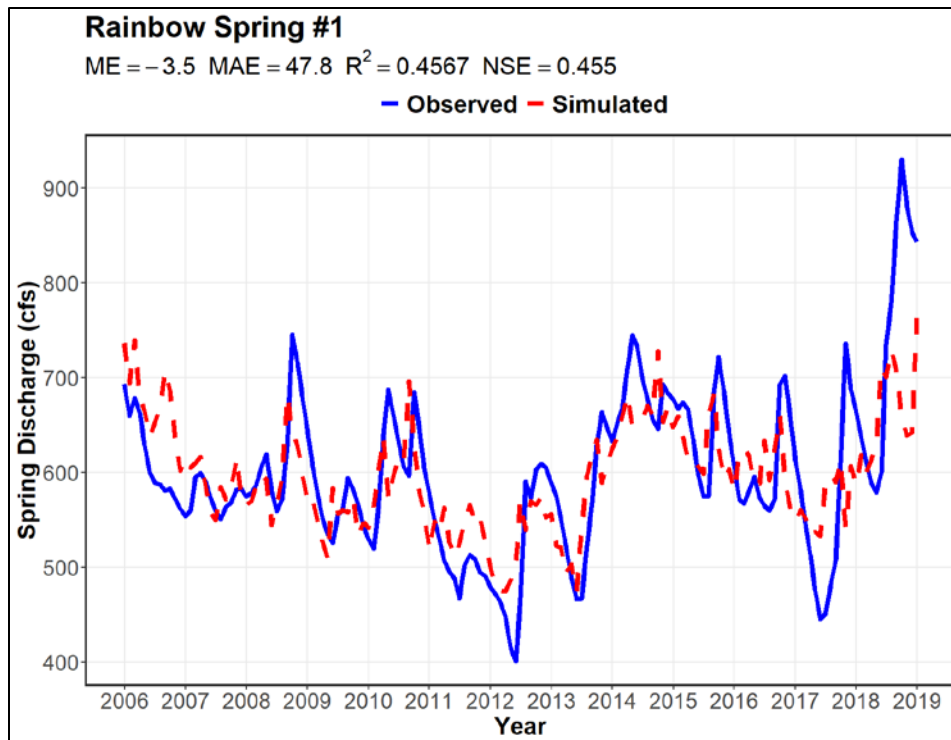


Figure 6-20. Simulated and observed hydrographs for Rainbow Springs #1

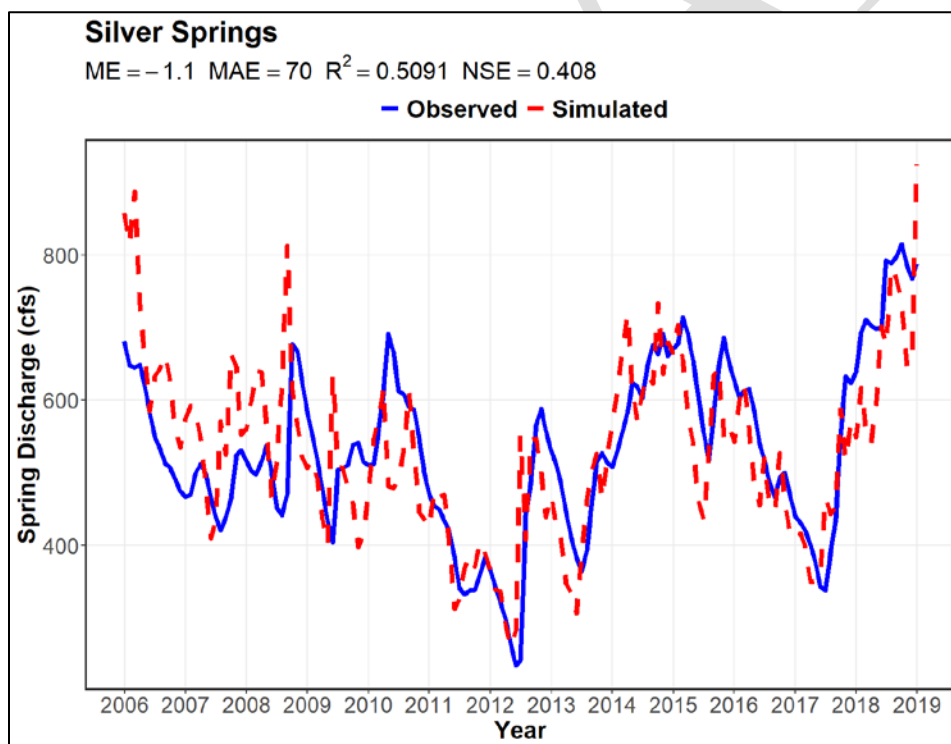


Figure 6-21. Simulated and observed hydrographs for Silver Springs Group

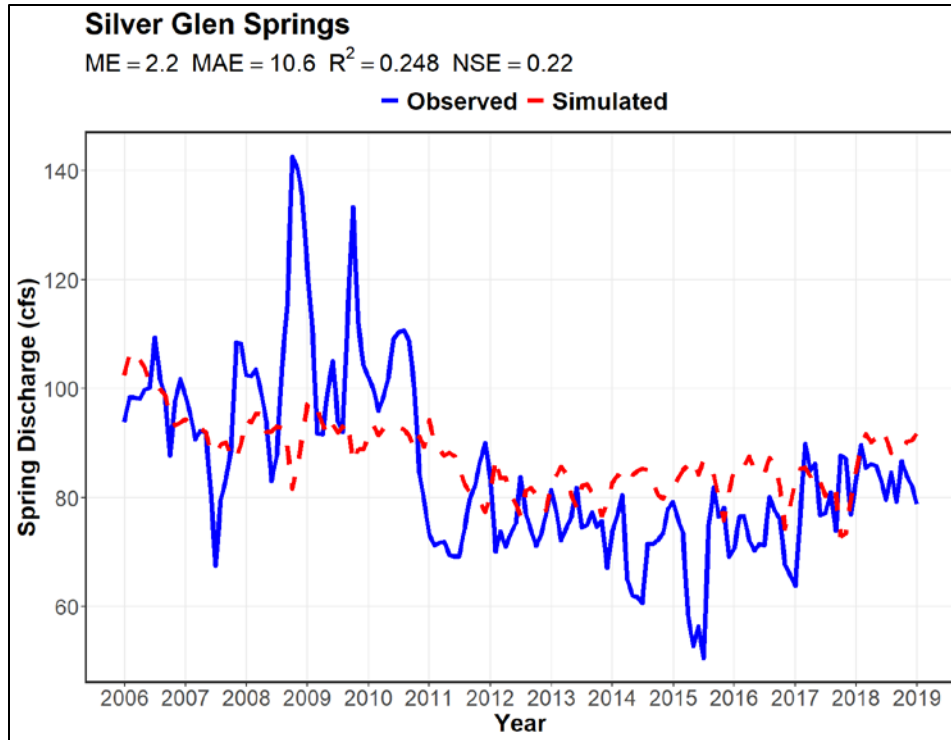


Figure 6-22. Simulated and observed hydrographs for Silver Glen Springs

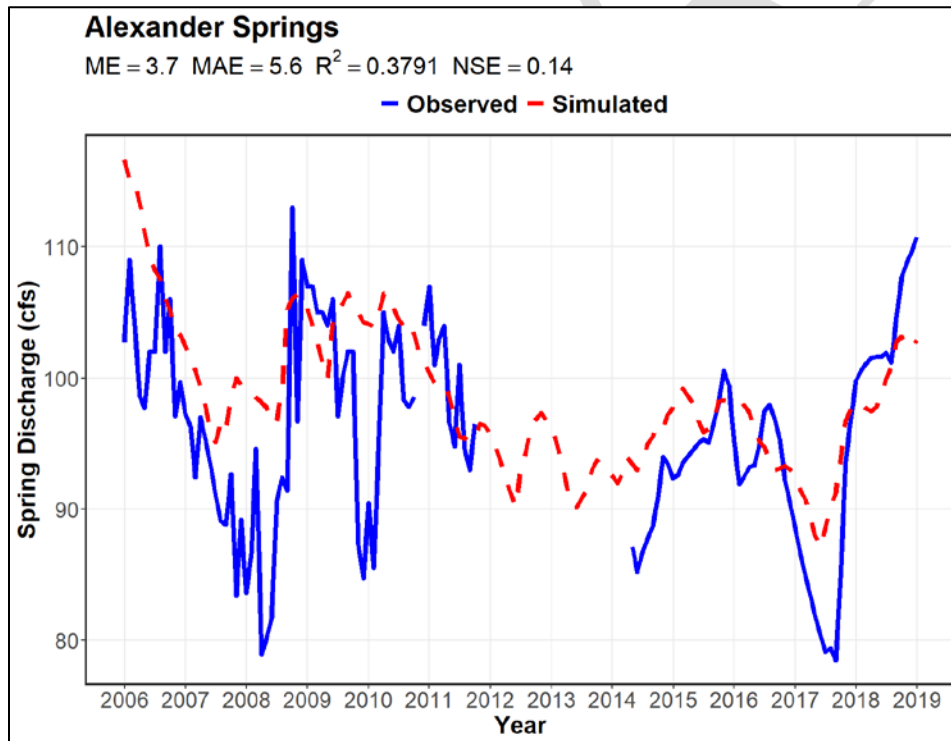


Figure 6-23. Simulated and observed hydrographs for Alexander Springs

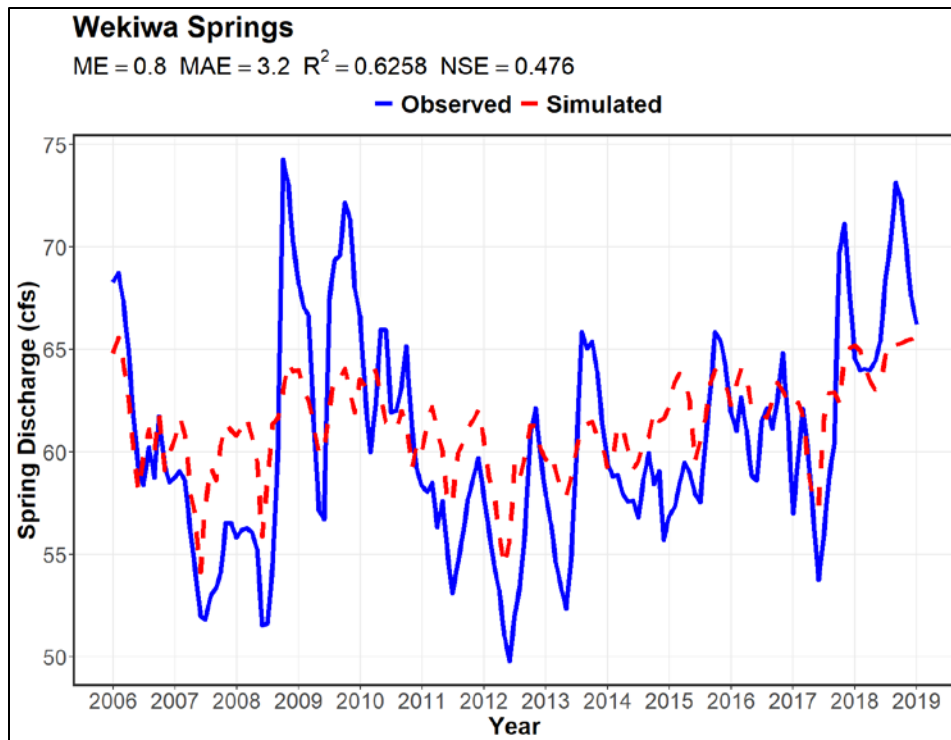


Figure 6-24. Simulated and observed hydrographs for Wekiwa Springs

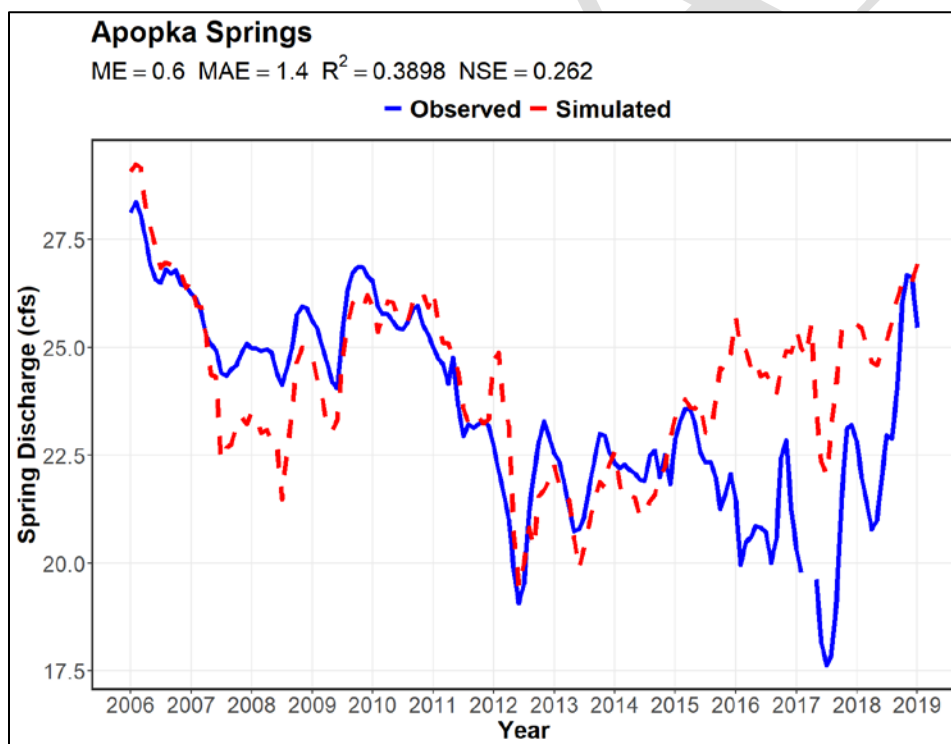


Figure 6-25. Simulated and observed hydrographs for Apopka Spring

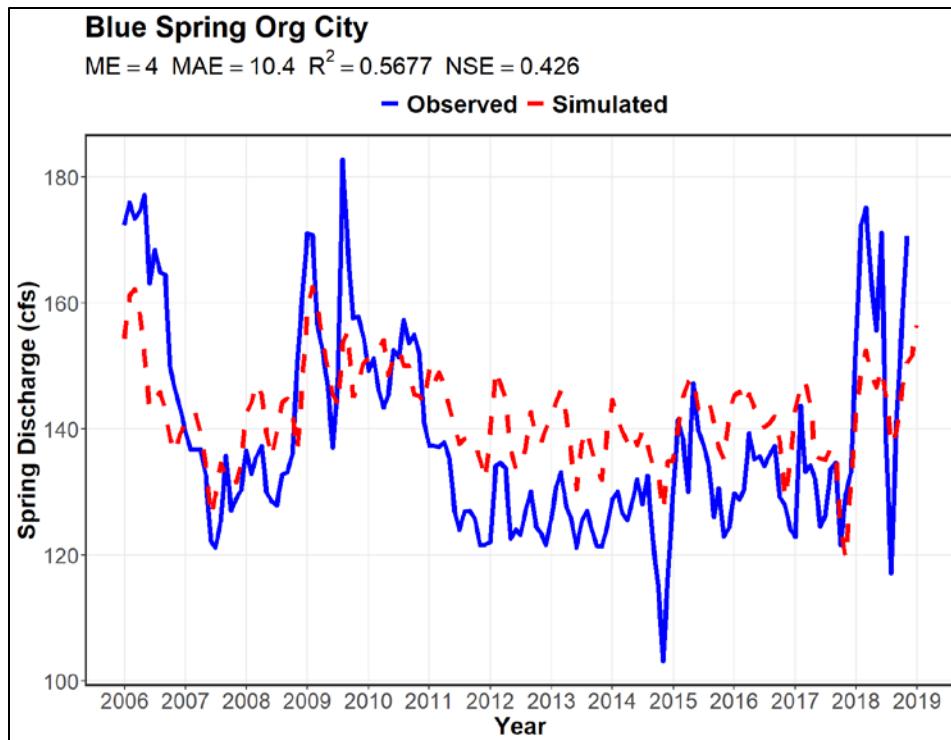


Figure 6-26. Simulated and observed hydrographs for Blue Spring in Orange City

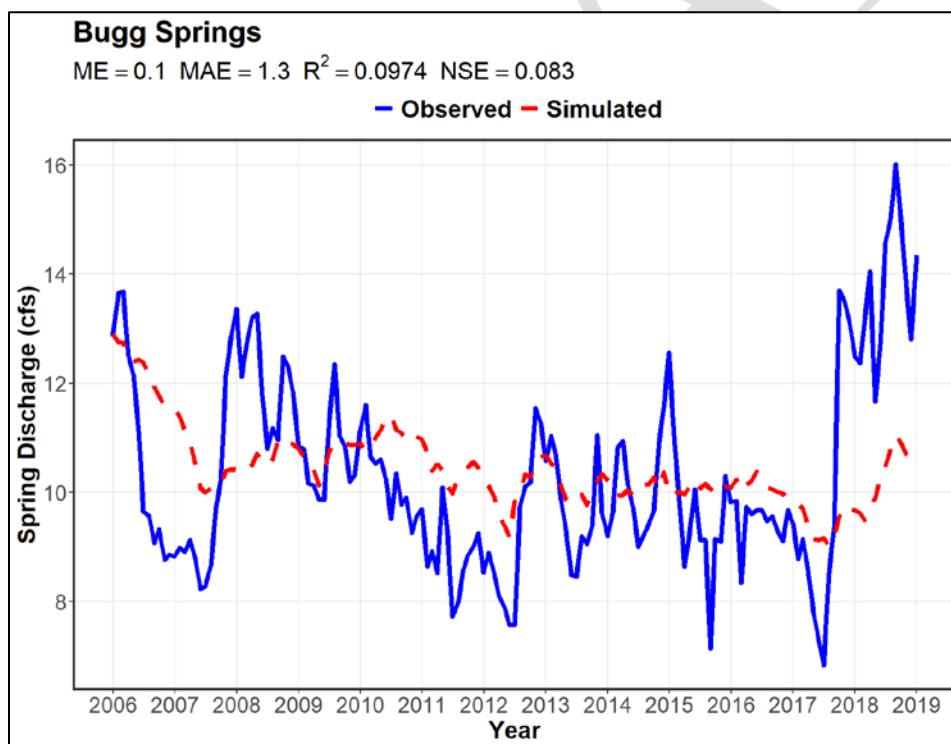


Figure 6-27. Simulated and observed hydrographs for Bugg Spring

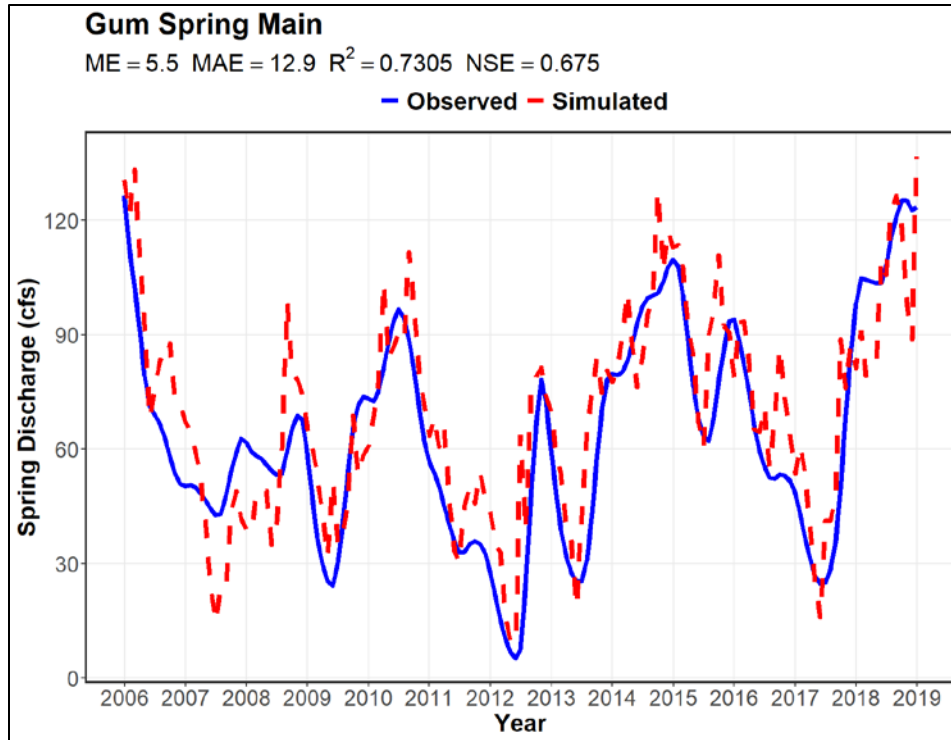


Figure 6-28. Simulated and observed hydrographs for Gum Spring Main

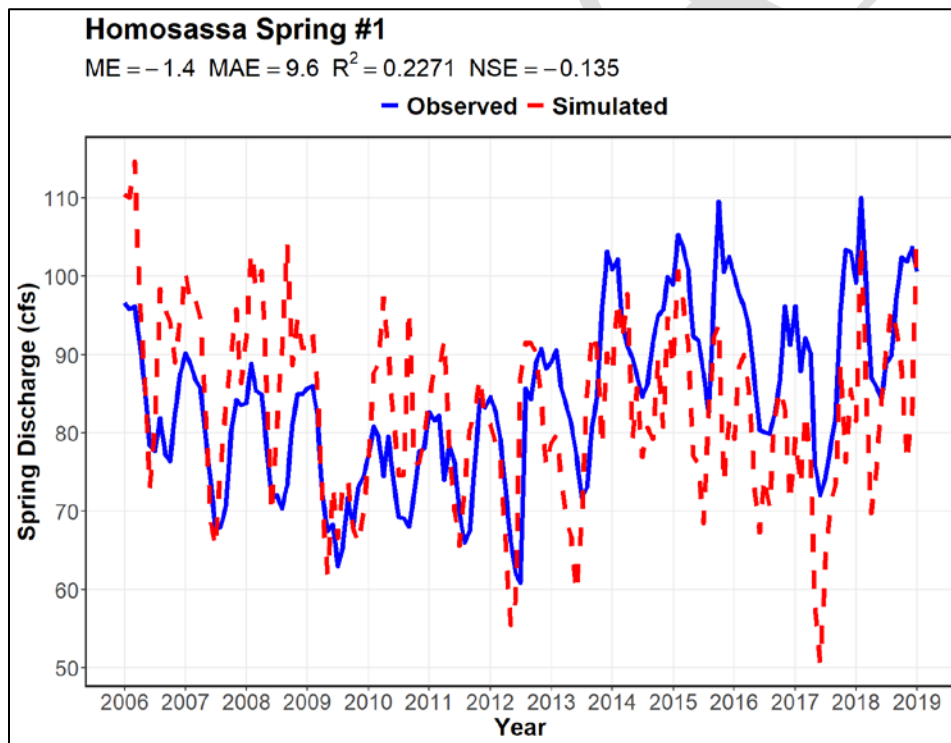


Figure 6-29. Simulated and observed hydrographs for Homosassa Spring #1

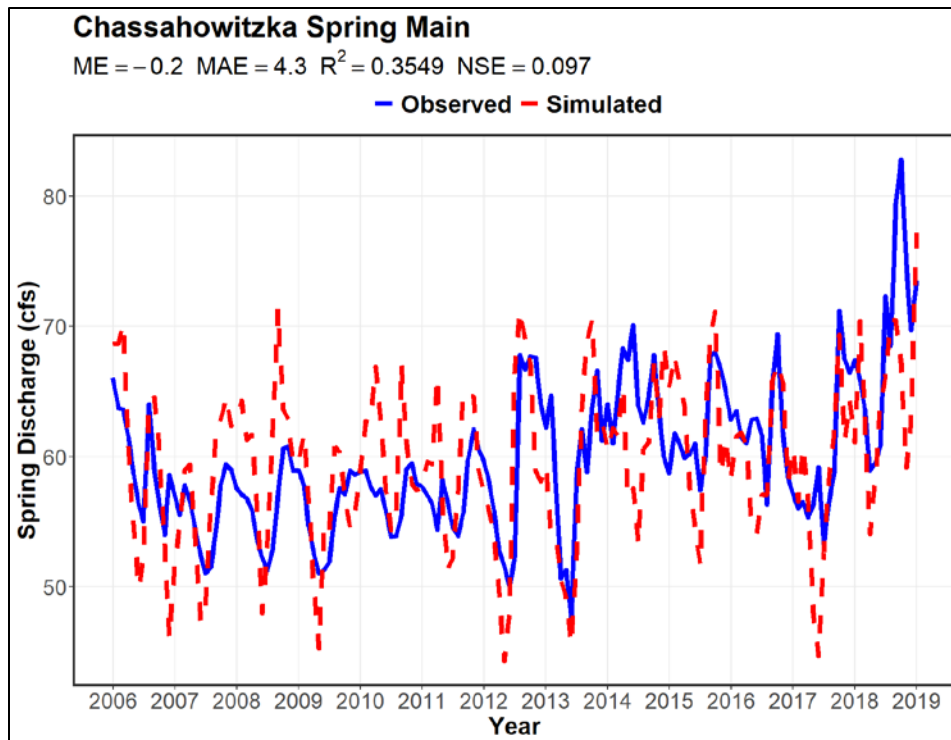


Figure 6-30. Simulated and observed hydrographs for Chassahowitzka Spring Main

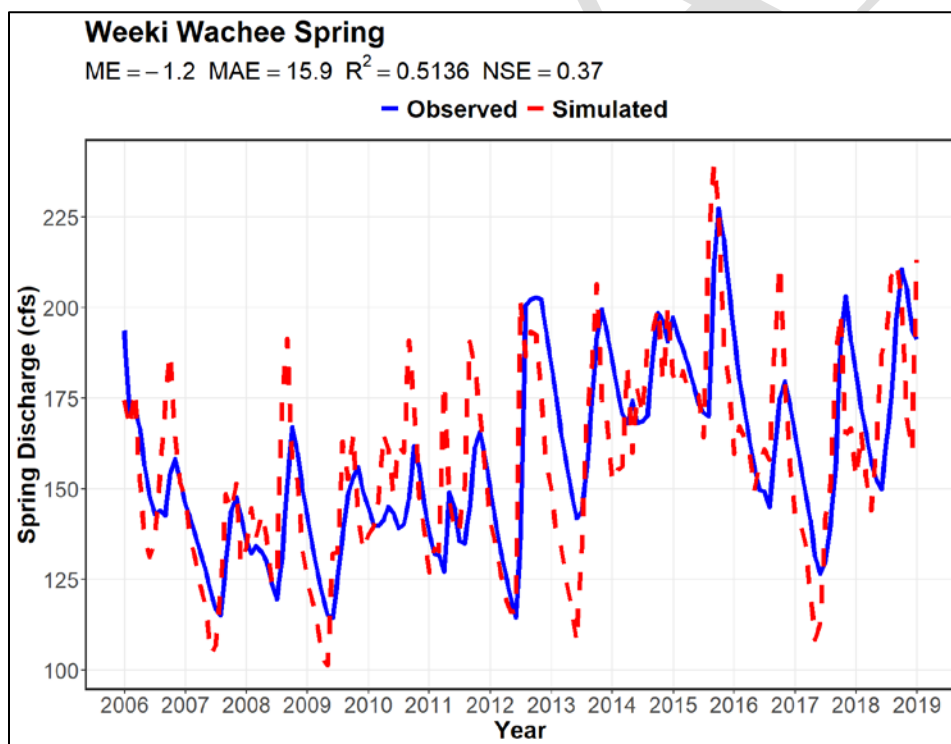


Figure 6-31. Simulated and observed hydrographs for Weeki Wachee Spring

River Baseflows

River baseflows were estimated using techniques from the USGS GW Toolbox (Barlow et al., 2014) and Perry method (Perry, 1995). There are eight hydrograph techniques implemented in the USGS GW Toolbox including six graphical hydrograph-separation techniques and two digital filtering techniques. The six graphical hydrograph-separation techniques include the Base-Flow Index (BFI Standard and Modified), HYSEP (Fixed Interval, Sliding Interval, and Local Minimum) and PART methods. The two digital filtering techniques include the SWAT Bflow and Eckhardt approaches. The ninth separation technique is Perry method, a low pass filter method that utilizes a moving window of 121 days. The baseflows derived from the USGS GW Toolbox methods generally tend to fall at the high end of the estimated range, while the estimates resulting from the Perry method tend to fall at the low end. Baseflow rates were not estimated for tidally-affected sites, local sites influenced by structures, or sites missing more than a few daily flows. Potential errors in baseflow estimates may be an important factor contributing to the discrepancies between simulated and estimated values. Thus, the calibration criteria specify that simulated baseflow fall within the range of baseflow estimated by the nine methods described above.

The model-simulated baseflow is compared to both estimated cumulative baseflow and baseflow pickup. Cumulative baseflows are defined as the total baseflows above a given USGS gage station. A baseflow pickup measures the contribution of the groundwater system to streamflow between a downstream gage and one or more upstream gages.

Model simulated hydrographs of the cumulative baseflow at 38 USGS gages were compared with the minimum and maximum estimated baseflows, as shown in Table 6-3 and included in Appendix G. Minimum baseflow was estimated using the Perry method and maximum baseflow was estimated using the methods in the USGS Groundwater Toolbox (Barlow et al., 2014). Selected hydrographs of baseflow discharge at four major rivers (St. Johns, Ocklawaha, Withlacoochee, and Hillsborough) are shown on Figure 6-32 through Figure 6-35, with additional data included as Appendix H.

Observed water levels obtained from the USGS river gages were used to interpolate the stages of the river cells. Bathymetry data from various sources was compiled to determine the *RBOT* parameters in the river package. The river conductance in the steady-state model was calculated by PEST on a subbasin level. In the transient model, the river conductance was adjusted based on the recharge ratio of the river cells.

Rivers can be gaining streams when the river stage is below the groundwater level or losing streams when the stage is above groundwater level. The result of the transient simulations showed spatial-temporal variation of the exchange between a river and the groundwater system. Most of the rivers received groundwater discharge through their course with few exceptions. Most simulated baseflows are more consistent with the minimum baseflows estimated with the Perry method than the maximum baseflow estimated with the USGS Groundwater Toolbox. The simulated baseflow hydrographs display seasonal patterns similar to that of the baseflow estimated from measured discharge at river gages. In general, the transient CSM performed well in simulating spatial and temporal variation of the groundwater-river interactions.

Table 6-3. Comparison of simulated average 2005 to 2018 baseflow with river baseflow estimated from observed discharge at USGS gages in the transient Central Springs Model (cubic feet per second)

USGS ID	Station Name	HUC8	Watershed	Simulated Baseflow	Estimated Baseflow	
					Min	Max
02232500	St. Johns River near Christmas, FL	03080101	Upper St. Johns	64.8	27.7	104
02233500	Econlockhatchee River near Chuluota, FL	03080101	Upper St. Johns	8.8	67.2	240
02234000	St. Johns River Above Lake Harney near Geneva, FL	03080101	Upper St. Johns	212	154	498
02234010	St. Johns River at Osceola, FL	03080101	Upper St. Johns	246	88.9	456
02234344	Howell Creek at State Hwy 434 near Oviedo, FL	03080101	Upper St. Johns	3.9	16.3	51.8
02234384	Soldier Creek near Longwood, FL	03080101	Upper St. Johns	2.5	1.7	9.7
02234400	Gee Creek near Longwood, FL	03080101	Upper St. Johns	2.4	1.9	12.6
02234440	St. Johns River at State Hwy 415 near Sanford, FL	03080101	Upper St. Johns	309	104	708
02234500	St. Johns River near Sanford, FL	03080101	Upper St. Johns	379	122	894
02234990	Little Wekiva River near Altamonte Springs, FL	03080101	Upper St. Johns	22.5	4.6	24.2
02235000	Wekiva River near Sanford, FL	03080101	Upper St. Johns	197	175	248
02235200	Blackwater Creek near Cassia, FL	03080101	Upper St. Johns	20.4	12.7	43.2
02236000	St. Johns River near De Land, FL	03080101	Upper St. Johns	832	232	1342
02236350	Green Swamp Run near Eva, FL	03080102	Ocklawaha	0.2	1.7	12.0
02236500	Big Creek near Clermont, FL	03080102	Ocklawaha	0.2	2.7	16.3
02239000	Ocklawaha River near Ocala, FL	03080102	Ocklawaha	-3.9	19	101
02240000	Ocklawaha River near Conner, FL	03080102	Ocklawaha	559	490	651
02240500	Ocklawaha River at Eureka, FL	03080102	Ocklawaha	604	538	724
02243000	Orange Creek at Orange Springs, FL	03080102	Ocklawaha	10.5	16.8	55.5
02244333	Haw Creek above Russells Landing near St Johns Park, FL	03080103	Lower St. Johns	43.0	4.2	77.6
02247510	Tomoka River near Holly Hill, FL	03080201	Daytona-St. Augustine	0.1	3.2	25.1
02301990	Hillsborough River above Crystal Spring near Zephyrhills, FL	03100205	Hillsborough	20.1	12.2	43.7
02303000	Hillsborough River at State Park near Zephyrhills, FL	03100205	Hillsborough	212	67.0	161
02303330	Hillsborough River at Morris Bridge near Thonotosassa, FL	03100205	Hillsborough	252	66.4	207
02303350	Trout Creek near Sulphur Springs, FL	03100205	Hillsborough	0.8	0.3	17.5
02303420	Cypress Creek at SR 54 at Worthington Gardens, FL	03100205	Hillsborough	21.3	1.8	41.2
02303800	Cypress Creek near Sulphur Springs, FL	03100205	Hillsborough	40.0	3.7	63.3
02310000	Anclote River at Little Rd near Elfers, FL	03100207	Crystal-Pithlachascotee	12.4	4.8	53.1
02310280	Pithlachascotee River near Fivay Junction, FL	03100207	Crystal-Pithlachascotee	0.04	0.25	4.3

USGS ID	Station Name	HUC8	Watershed	Simulated Baseflow	Estimated Baseflow	
					Min	Max
02310300	Pithlachascotee River near New Port Richey FL	03100207	Crystal-Pithlachascotee	4.6	1.1	18.9
02310947	Withlacoochee River near Cumpressco, FL	03100208	Withlacoochee	36.4	6.4	80.2
02311500	Withlacoochee River near Dade City, FL	03100208	Withlacoochee	47.6	10.7	116
02312000	Withlacoochee River at Us 301 at Trilby, FL	03100208	Withlacoochee	66.5	34.1	190
02312500	Withlacoochee River at Croom, FL	03100208	Withlacoochee	85.5	57.0	235
02312600	Withlacoochee River near Floral City, FL	03100208	Withlacoochee	90.9	64.6	217
02312667	Shady Brook near Sumterville, FL	03100208	Withlacoochee	23.3	12.4	25.6
02312762	Withlacoochee River near Inverness, FL	03100208	Withlacoochee	267	158	389
02313000	Withlacoochee River at SR 200 near Holder, FL	03100208	Withlacoochee	353	252	515

Note: The CSM domain only covers a portion of the St. Johns River watershed, therefore, the observed baseflows at the main stem of the St. Johns River were adjusted using the ratio of drainage area inside CSM domain over the total drainage area of the river station.

HUC = hydrologic unit code

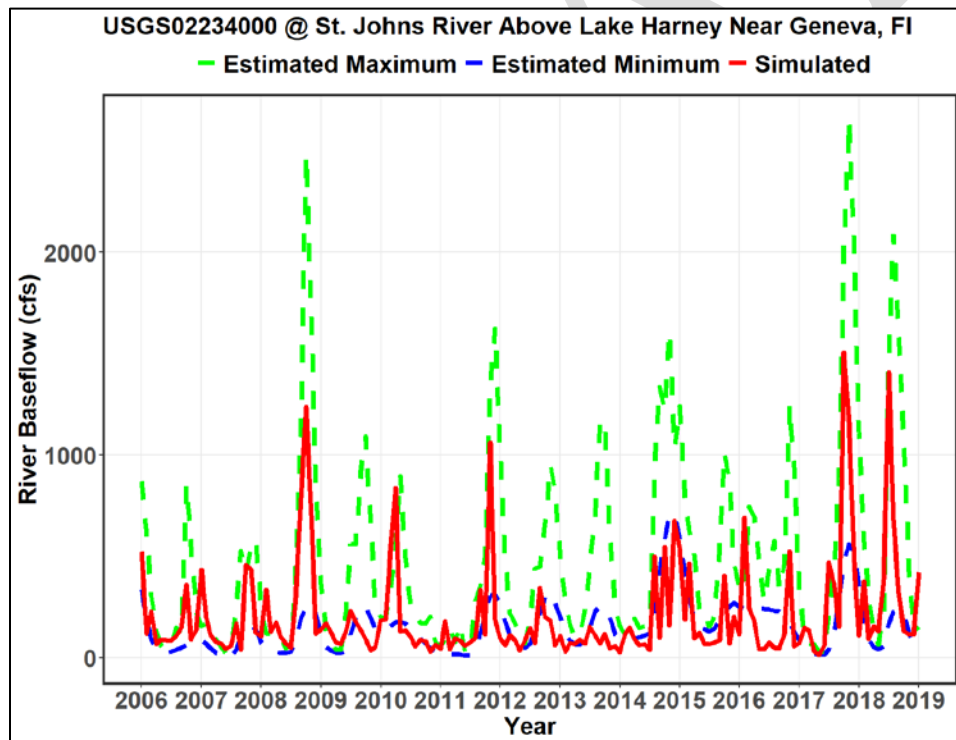
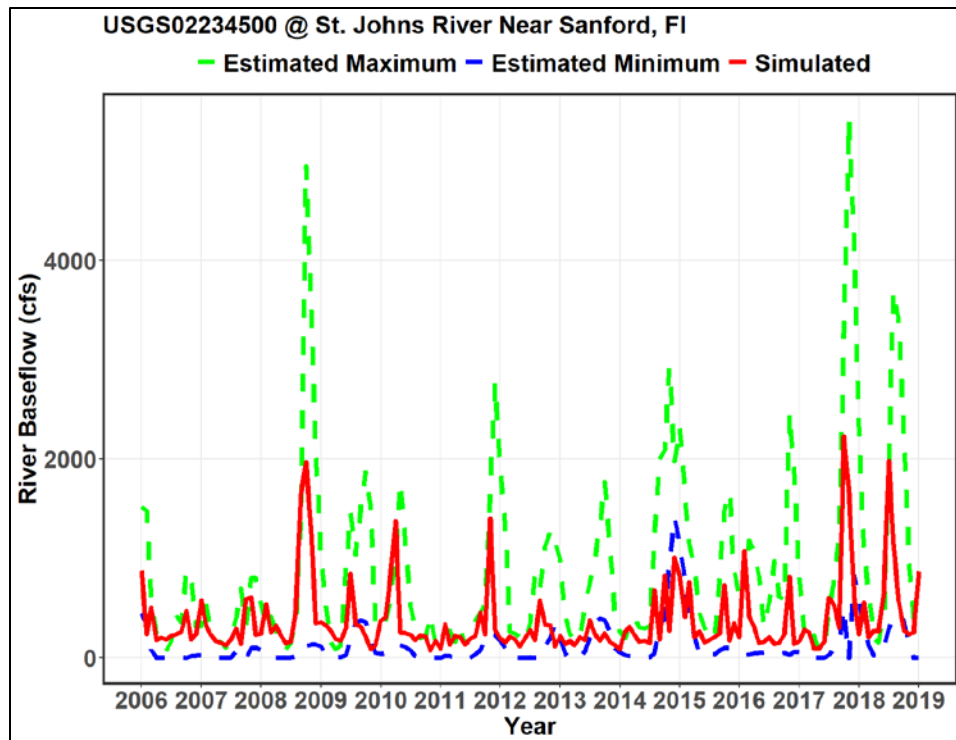


Figure 6-32. Simulated and estimated baseflow at selected St. Johns River gages

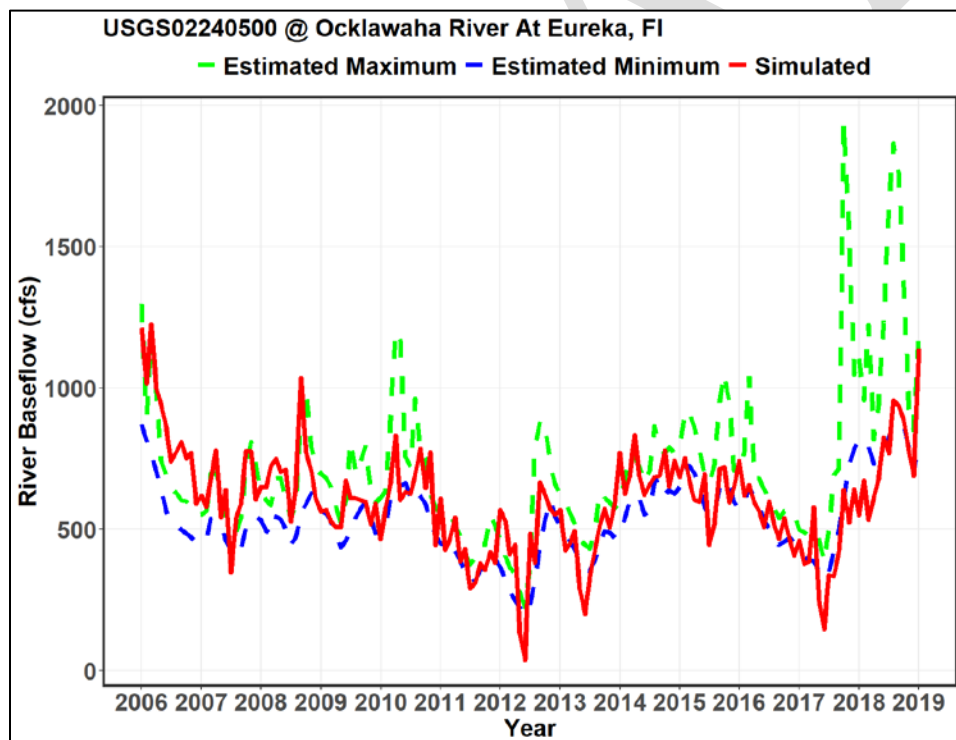
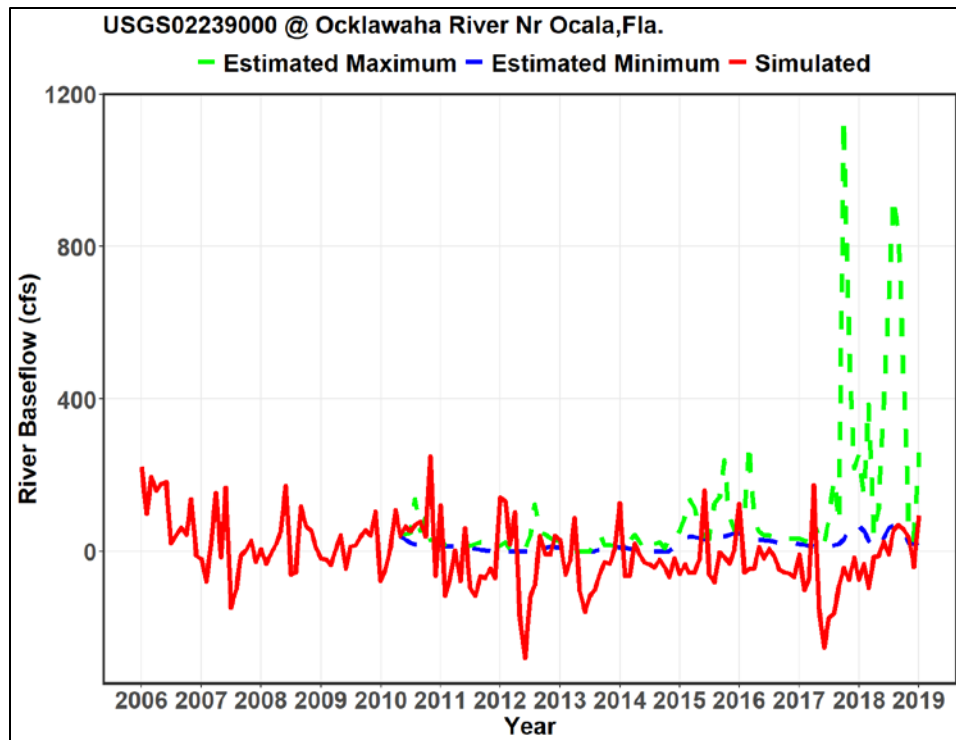


Figure 6-33. Simulated and estimated baseflow at selected Ocklawaha River gages

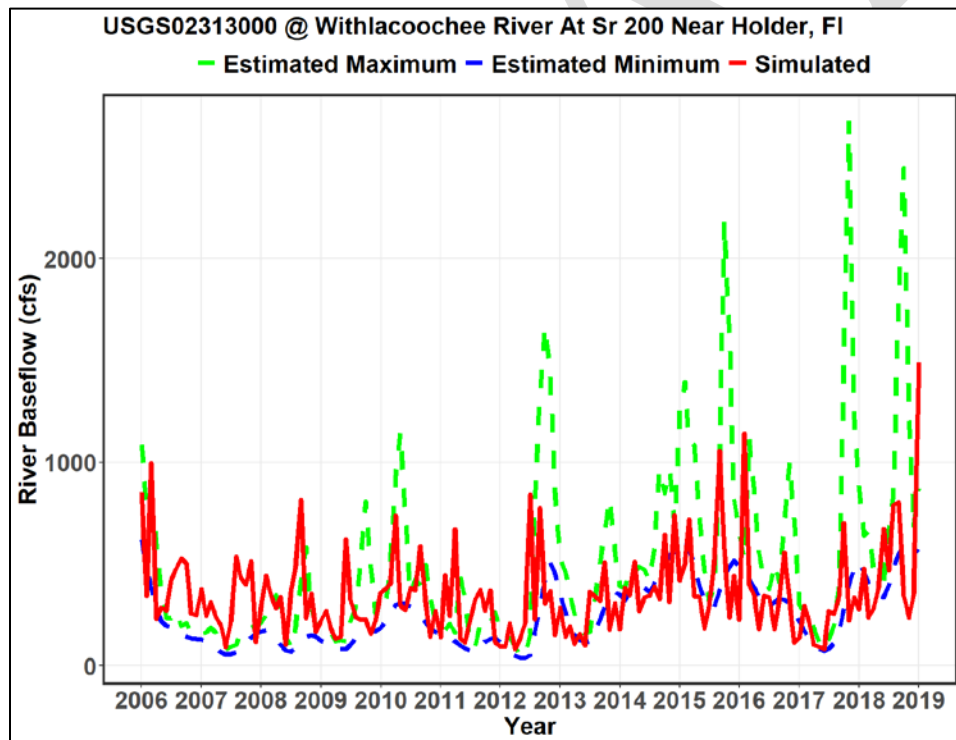
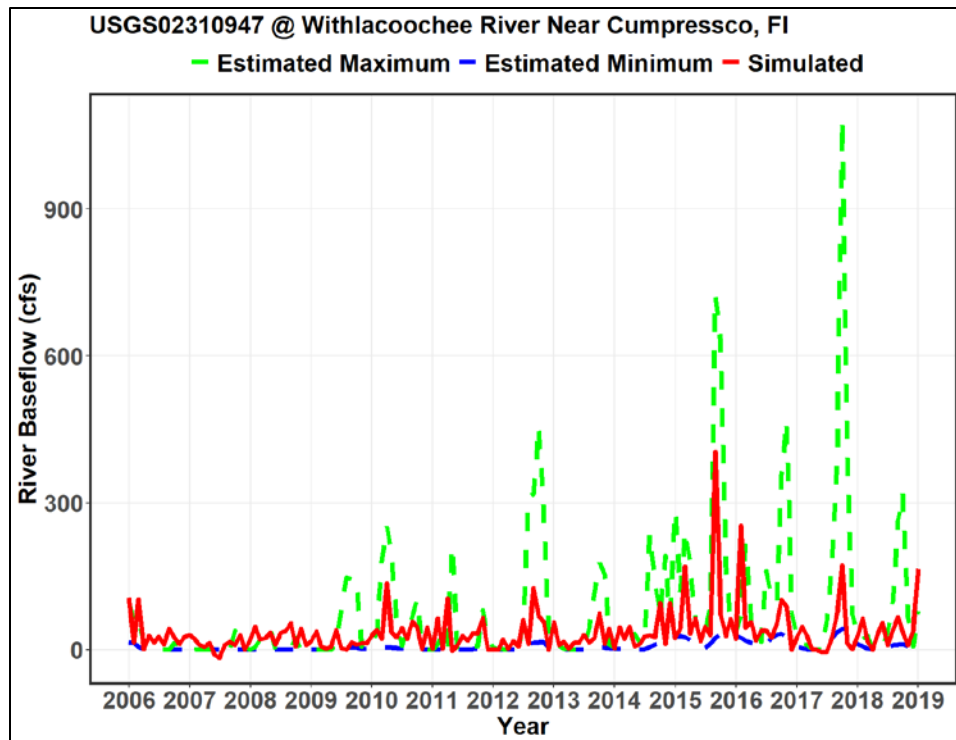


Figure 6-34. Simulated and estimated baseflow at selected Withlacoochee River gages

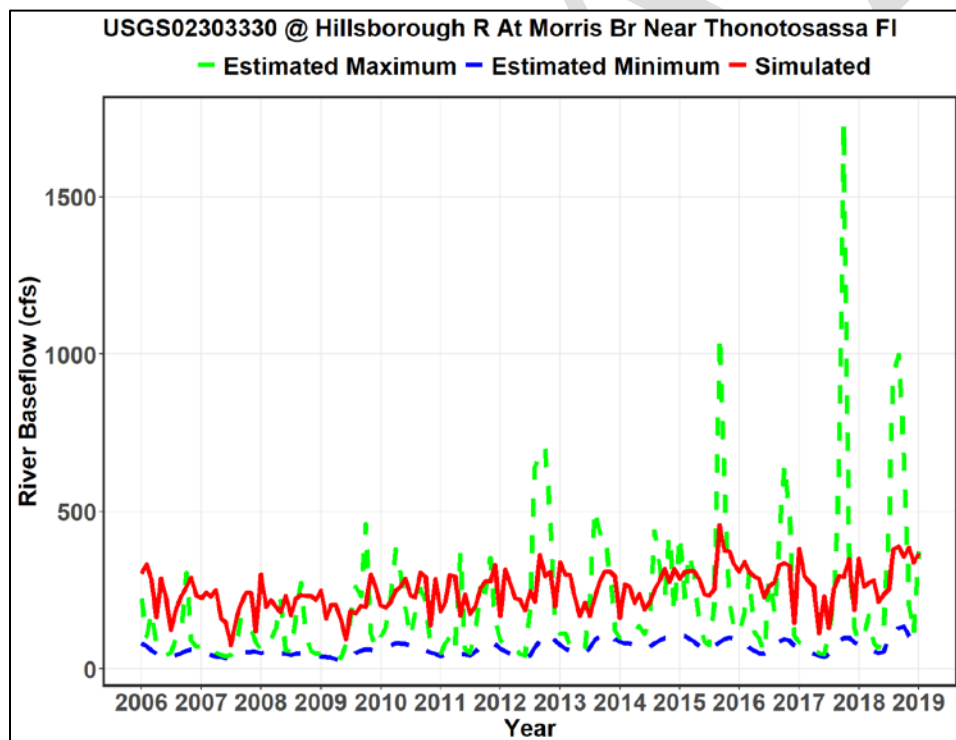
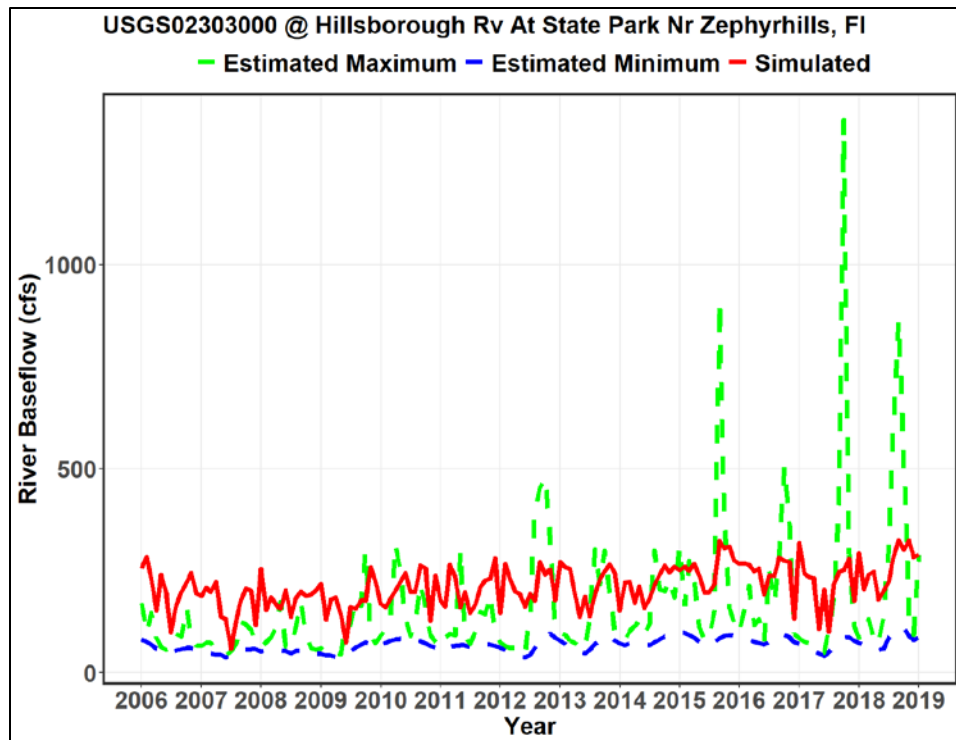


Figure 6-35. Simulated and estimated baseflow at selected Hillsborough River gages

Lake Vertical Leakages

The spatial distribution of average leakage values for the simulated lakes are shown on Figure 6-36. Hydrographs for selected MFL lakes are displayed on Figure 6-37. A complete set of simulated hydrographs of lake leakage is provided in Appendix I. Comparisons of transient simulated lake vertical leakage with the reported leakage values compiled from water budget analyses for MFL lakes are summarized in Table 6-4.

The transient lake stages in the CSM were set at the measured levels when observed data was available. For lakes without measured lake levels, the stages were calculated based on the stages at nearby lakes. Lake conductance in the steady-state model was adjusted at the subbasin level during PEST calibration. For the transient model, the steady-state conductance was further adjusted based on the recharge ratio at lake cells to reflect the seasonal variation in lake and aquifer interaction.

Among the 486 lakes simulated in the CSM, 426 (88 percent) lakes had average leakage values of ± 20 in/yr. A comparison with reported leakage values from water budget studies (Table 6-4) shows that the model generally simulated less lake leakage to the aquifer than reported values. It should be noted that the reported leakage values were calculated from different time periods while the simulated leakage values were averages over the transient simulation period. In addition, the lake leakage calculations included in the water budget analyses were based on various localized assumptions and are not comparable to the regional groundwater model. Therefore, the reported lake leakage values were not used as PEST calibration targets but instead as qualitative calibration targets. The comparison in Table 6-4 demonstrates that the simulated lake leakage values fell into ranges comparable to the water budget studies and were generally in the same flow direction.

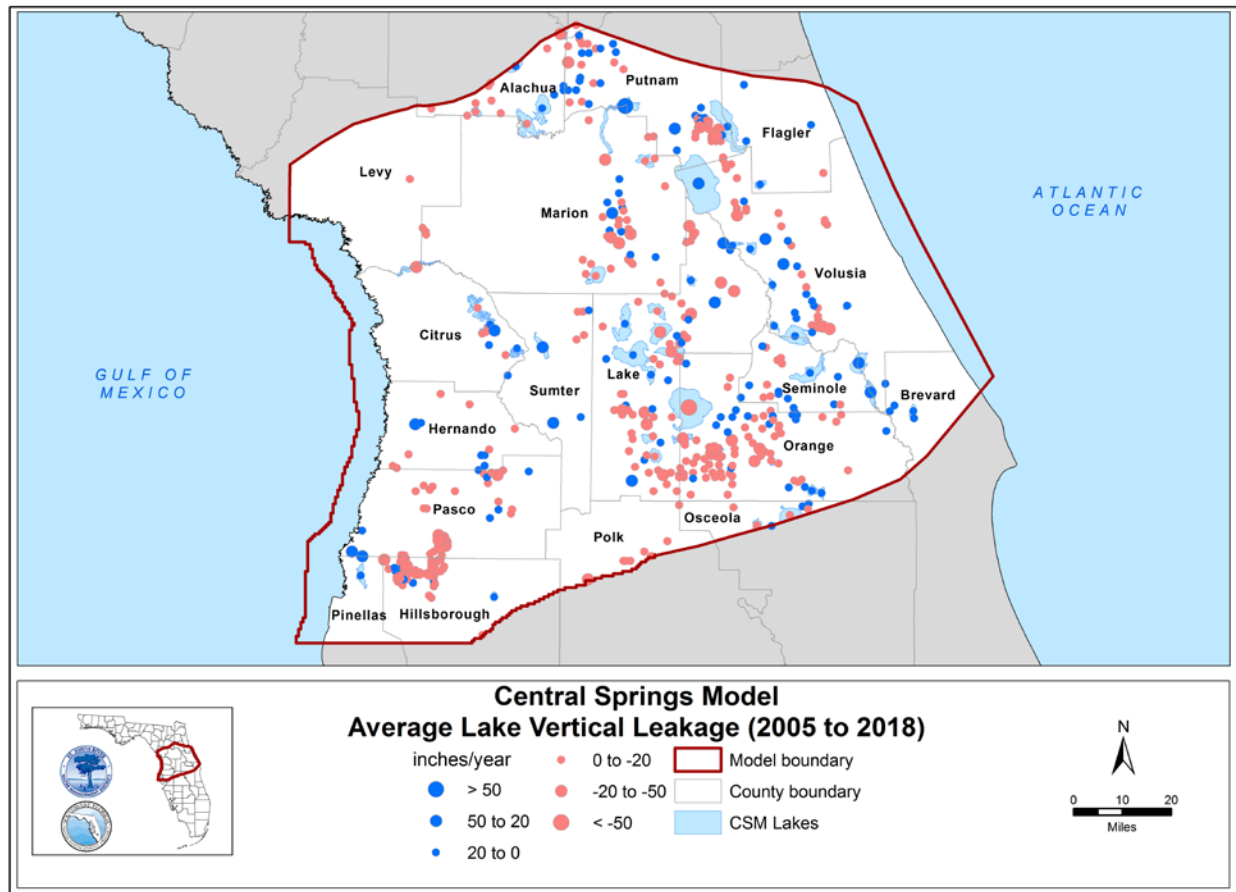


Figure 6-36. Transient simulated 2005 to 2018 average lake vertical leakage (inches/year)

Note: CSM = Central Springs Model

Table 6-4. Comparison of transient model simulated lake vertical leakages to reported values (positive = inflow from aquifer to lake; negative = outflow from lake to aquifer)(inches per year)

Lake Name	County	Water Management District	Leakage	
			Simulated	Reported
Orange	Alachua	SJRWMD	-6.1	-18.7
Dora	Lake	SJRWMD	-25	-16.8
Dorr	Lake	SJRWMD	1.6	-11.6
Louisa	Lake	SJRWMD	-6.5	-19.6
Kerr	Marion	SJRWMD	-9.8	-14.4
Weir	Marion	SJRWMD	-3.7	-13.5
Apopka	Orange	SJRWMD	-48	-8.1
Conway	Orange	SJRWMD	-17	-8
Sherwood	Orange	SJRWMD	8	-78.7
Grandin	Putnam	SJRWMD	1.4	-20
Orienta	Seminole	SJRWMD	-2.7	-14.4
Alice	Hillsborough	SWFWMD	0.36	-28.1
Allen	Hillsborough	SWFWMD	-7.8	-18.4
Bird	Hillsborough	SWFWMD	-11.4	-36.5
Brant	Hillsborough	SWFWMD	-8.8	-10.2
Calm	Hillsborough	SWFWMD	-5.6	-26.6
Charles	Hillsborough	SWFWMD	-3.1	-54.4
Church	Hillsborough	SWFWMD	-5.2	11.1
Dan	Hillsborough	SWFWMD	-26.7	-20
Deer	Hillsborough	SWFWMD	-13	-36.1
Dosson	Hillsborough	SWFWMD	-3.5	-26.6
Echo	Hillsborough	SWFWMD	-1.8	11.1
Harvey	Hillsborough	SWFWMD	22.6	-18.4
Hobbs	Hillsborough	SWFWMD	-2.1	-43.2
Horse	Hillsborough	SWFWMD	-9.9	-24.3
Jackson	Hillsborough	SWFWMD	-3.3	-32.5
Juanita	Hillsborough	SWFWMD	-1.5	-17.2
Little Moon	Hillsborough	SWFWMD	-5.8	-17.2
Merrywater	Hillsborough	SWFWMD	-11.8	-35.5
Rainbow	Hillsborough	SWFWMD	-1.2	-17.2
Saddleback	Hillsborough	SWFWMD	-8.6	-35
Starvation	Hillsborough	SWFWMD	-4.8	-21.2
Strawberry	Hillsborough	SWFWMD	-8.7	-44.1
Sunshine	Hillsborough	SWFWMD	-4.6	-26.6
Marion	Levy	SWFWMD	-17.1	-8.9
Big Fish	Pasco	SWFWMD	-11	-43.4
Moon	Pasco	SWFWMD	-3.1	-7.3
Pierce	Pasco	SWFWMD	-3.8	-11.8

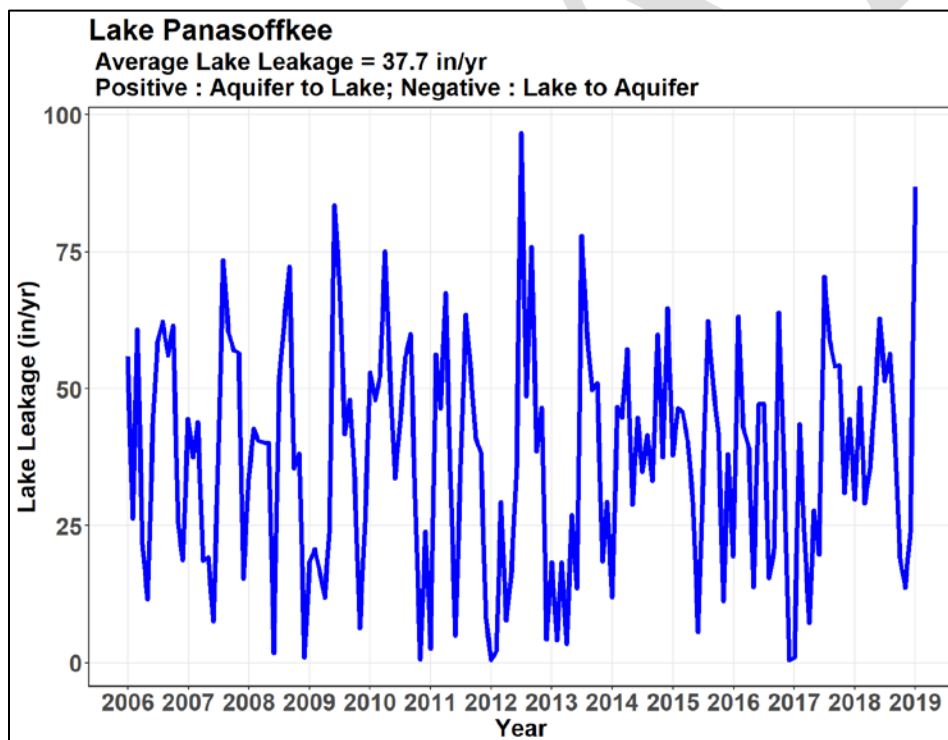
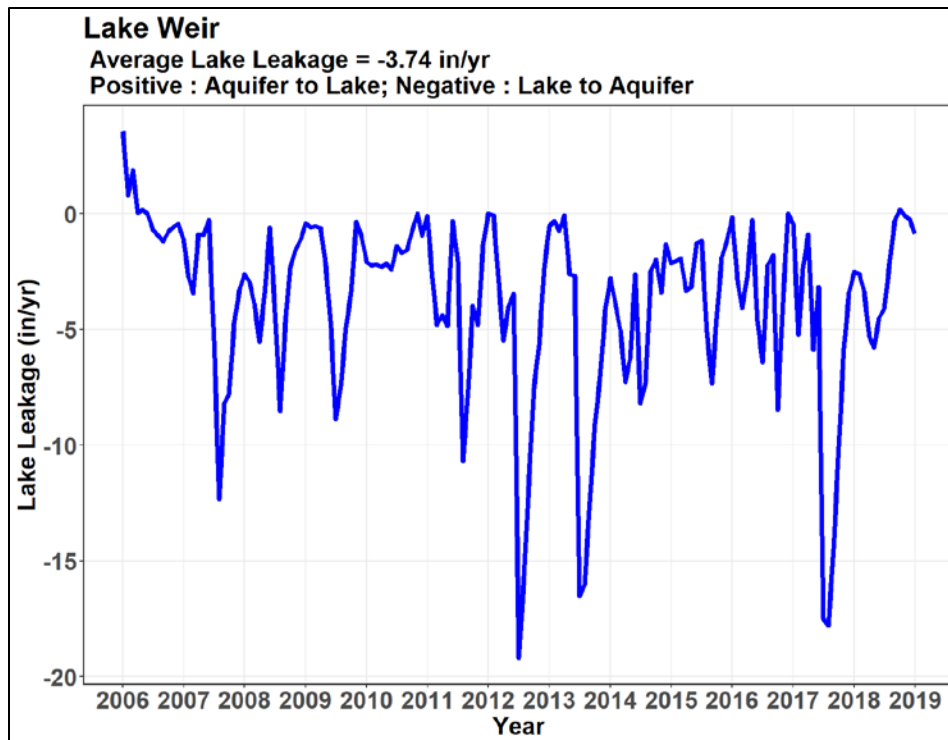


Figure 6-37. CSM simulated hydrographs of vertical leakage at lakes Weir and Panasoffkee

Water Budgets

Simulated water budgets of boundary condition inflow and outflow, inter-layer vertical flux, and storage calculated from the transient simulation are given in Table 6-5 through Table 6-7 for each model layer. The net flux, calculated as influx minus outflux, is well preserved throughout the transient simulation (Table 6-7). Net fluxes for each major component of the water budget during the calibration period included recharge of 14.2 in/yr, ET of -5.0 in/yr, net discharge to river, lake, and wetland of -2.3 in/yr (summation of -1.3 in/yr of River/Lake and -1.0 in/yr of Drain), and spring discharge of -4.1 in/yr. The overall groundwater withdrawal is -1.5 in/yr (outflux) and groundwater recharge through drainage wells and RIBs is 0.3 in/yr (influx), resulting in a net groundwater withdrawal of -1.3 in/yr. A total net storage change of 0.2 in/yr in the SAS and a total of 0.1 in/yr in the remaining aquifer units occurred over the simulation period based on the model results.

There is a net CHD flux of -2.0 in/yr along coastal boundaries in the SAS simulated in layer 1, whereas total net CHD flux of 0.8 in/yr in layer 2 through layer 7 was simulated in the model. The net GHB flux is -0.2, -0.3, and 0.0 in/yr, in layers 3, 4, and 6, respectively along the non-coastal boundaries. These boundary fluxes are consistent with the hydrogeologic understanding of the SAS and UFA in the area.

The transient model water budget is close to the steady-state model water budget given in Table 5-8 through Table 5-10. The main difference is the higher baseflow simulated with the transient drain package, which is balanced out by a reduced groundwater ET. The transient model simulates the discharge from groundwater to surface water during flooding events, which is not captured in the averaged hydrologic conditions in the steady-state model. This difference between the two models indicates the value of time-dependent simulations in evaluating groundwater flow, especially in the SAS.

The hydrological system is simulated using HSPF models for surface water and MODFLOW for groundwater. The two models are calibrated separately without direct feedback. The groundwater recharge calculated from HSPF includes river baseflow and groundwater ET, which is also simulated in MODFLOW. Due to the lack of direct coupling between HSPF and MODFLOW, there is a need to compare the overlapping water balance components to avoid major water budget discrepancies.

The time series of HSPF-calculated baseflow (AGWO) was compared to the cumulative baseflow calculated in the DRN and RIV packages of MODFLOW (Appendix J). The comparison at the 13 HSPF model basins show that the two models are in agreement for the major river basins (St. Johns, Ocklawaha, Withlacoochee, and Hillsborough). There are relatively large discrepancies between HSPF and MODFLOW in their baseflow calculations for peripheral basins due to the lack of applicable baseflow data.

Comparisons of HSPF-simulated saturated ET (AGWET+ BASET) and groundwater ET calculated using the EVT package of MODFLOW are provided in Appendix K. The groundwater ET is comparable in most of the basins except for the Ocklawaha River. Further investigation of the water balance in the Ocklawaha River watershed is needed to improve the model performance.

Table 6-5. Boundary condition influx in the CSM transient model (2005-2018) by layer (inches/year)

Layer	CHD	GHB	Well	River/Lake	Recharge	Vertical	Storage
1	0.0	-	0.1	1.0	14.2	4.7	3.3
2	0.1	-	-	-	-	5.9	0.5
3	0.1	0.1	0.2	-	-	5.8	0.2
4	0.2	0.1	-	-	-	2.6	0.2
5	0.1	-	-	-	-	2.5	0.0
6	0.3	0.2	-	-	-	0.2	0.0
7	0.1	-	-	-	-	-	0.0
Total	0.9	0.3	0.3	1.0	14.2	-	4.2

Note: CHD = constant head boundaries (coastal)

GHB = general head boundaries (non-coastal)

Rounding of fluxes accounts for nominal discrepancies.

Table 6-6. Boundary condition outflux in the CSM transient model (2005-2018) by layer (inches/year)

Layer	CHD	GHB	Well	River/Lake	Drain	Spring	ET	Vertical	Storage
1	-2.0	-	-0.0	-2.3	-1.0	-	-5.0	-9.9	-3.0
2	-0.0	-	-	-	-	-	-	-11.2	-0.5
3	-0.1	-0.3	-0.5	-	-	-	-	-10.5	-0.2
4	-0.0	-0.4	-0.7	-	-	-4.1	-	-2.5	-0.2
5	-0.0	-	-0.1	-	-	-	-	-2.4	-0.0
6	-	-0.2	-0.3	-	-	-	-	-0.1	-0.0
7	-	-	-	-	-	-	-	-	-0.0
Total	-2.1	-0.9	-1.5	-2.3	-1.0	-4.1	-5.0	-	-3.9

Note: CHD = constant head boundaries (coastal)

GHB = general head boundaries (non-coastal)

Rounding of fluxes accounts for nominal discrepancies.

Table 6-7. Boundary condition net flux in the CSM transient model (2005-2018) by layer (inches/year)

Layer	CHD	GHB	Well	River/Lake	Drain	Spring	Recharge	ET	Vertical	Storage
1	-2.0	-	0.1	-1.3	-1.0	-	14.2	-5.0	-5.2	0.2
2	0.1	-	-	-	-	-	-	-	-5.3	0.0
3	0.0	-0.2	-0.3	-	-	-	-	-	-4.8	0.0
4	0.2	-0.3	-0.7	-	-	-4.1	-	-	0.1	0.0
5	0.1	-	-0.1	-	-	-	-	-	0.1	-0.0
6	0.3	-0.0	-0.3	-	-	-	-	-	0.1	-0.0
7	0.1	-	-	-	-	-	-	-	-	-0.0
Total	-1.2	-0.5	-1.3	-1.3	-1.0	-4.1	14.2	-5.0	-	0.3

Note: CHD = constant head boundaries (coastal)

GHB = general head boundaries (non-coastal)

Rounding of fluxes accounts for nominal discrepancies.

Interlayer Vertical Flux

Mean vertical leakage from the ICU downward (into) or upward (out) of the UFA during the transient simulation period is shown on Figure 6-38. The largest values of 10 to 30 in/yr occur within the unconfined karst region in the western part of the model domain and in areas with a deep water table. Upward flux occurs in the coastal regions, the St. Johns River valley, and along the Withlacoochee and Hillsborough rivers.

Mean vertical leakage from MCU I downward or upward from the LFA during the transient simulation period is shown on Figure 6-39. Recharge of the LFA from the UFA mainly occurred in the southern extent of the LFA on the order of 5 to 20 in/yr.

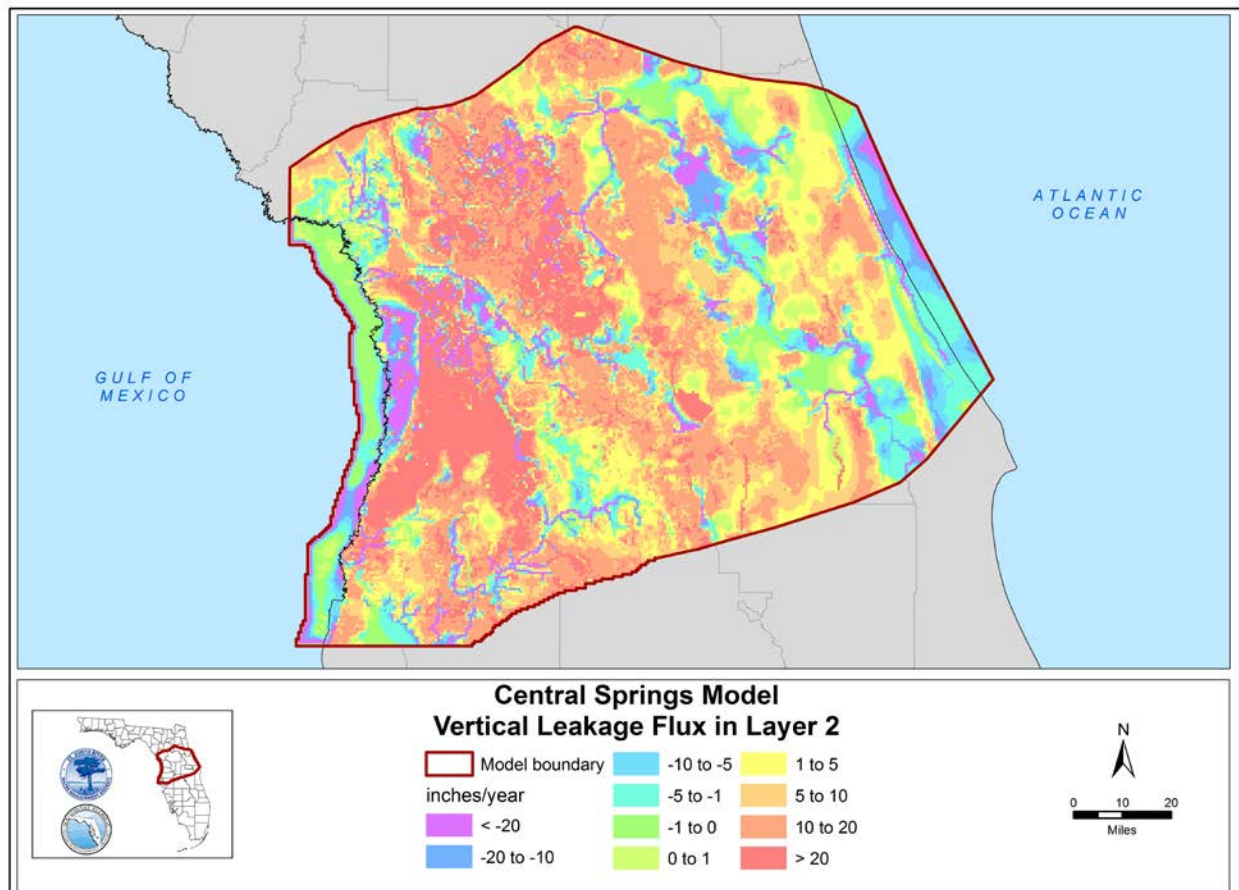


Figure 6-38. Spatial distribution of average 2005 to 2018 interlayer vertical leakage flux in the CSM transient model between the ICU and UFA

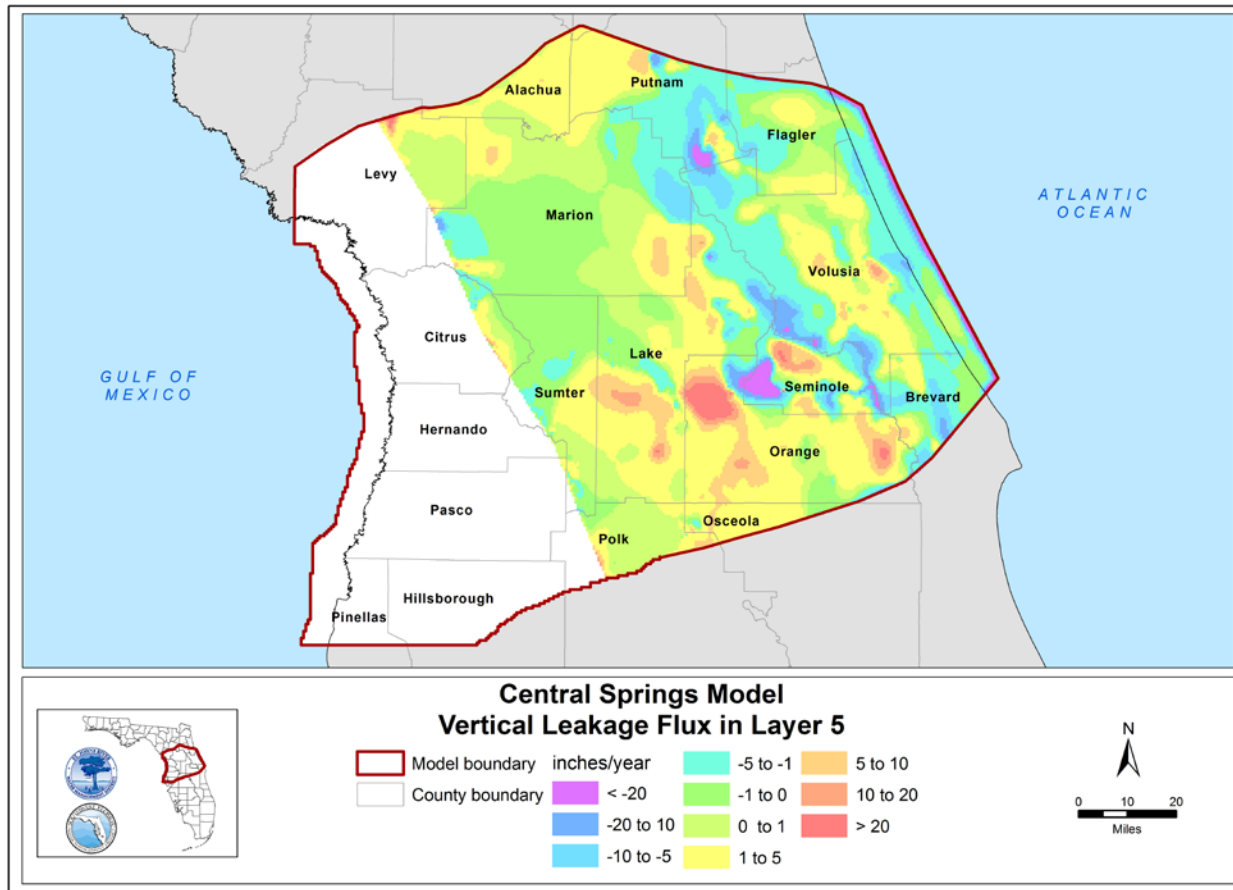


Figure 6-39. Spatial distribution of average 2005 to 2018 interlayer vertical leakage flux in the CSM transient model between MCU I and the LFA

Note: Vertical leakage flux values are not provided in the western portion of the model domain where the MCU I is not present.

7. SUMMARY, CONCLUSIONS, AND LIMITATIONS

SUMMARY AND CONCLUSIONS

The CSM was developed through a collaborative effort by a technical groundwater model development team of experts and professionals from SJRWMD, SWFWMD, and HGL. The technical team's objective was to apply sound science to model development, data analysis, and calibration, and to ensure that the work completed was defensible and collaboratively developed. The CSM was designed as a tool to be utilized to evaluate groundwater pumping effects within the individual districts, as well as inter-district effects. A primary function of the model is to simulate the regional effects of pumping on groundwater levels, springflows, and river baseflows. Intended applications of the model include evaluations of proposed consumptive use permits, support for MFL analyses, and regional water supply planning.

The CSM consists of two three-dimensional groundwater flow models; a steady-state model which represents average 2005 to 2018 hydrologic conditions and a transient model which represents 2005 annual average hydrologic conditions followed by 2006 to 2018 monthly hydrologic conditions. The CSM was calibrated using PEST, a state-of-the-art groundwater model calibration tool, to minimize the differences between various types of observations and their model-simulated equivalents through adjustment of model parameters within defined ranges.

Quantitative calibration targets included groundwater heads, vertical differences in groundwater heads across confining units, and springflows, in addition to qualitative targets including river baseflows, lake leakages, and comparisons to APT-derived UFA transmissivities and UFA potentiometric surface maps. In addition to the constraints dictated by groundwater head and springflow targets, a comprehensive set of penalty functions was implemented to utilize expert knowledge of the hydrogeological system that was not captured by the quantitative targets. The inclusion of flooding penalties and boundary-flux penalties substantially improved the model's representation of the overall water budget of the system. The calibrated steady-state model achieved the calibration criteria for groundwater heads, vertical head differences across confining units, and springflows. In addition, the calibrated UFA transmissivity values were comparable to values measured by APTs.

The PEST calibrated parameters were directly transferred to the transient model to evaluate the model's capability to simulate the temporal variation of the aquifer system. In the transient simulation, storage parameters including specific yield and specific storage were assigned values based on previous observations in the region. The transient model met the calibration criteria for simulated groundwater heads and springflows. Transient groundwater head residuals indicated a good match between observed and corresponding simulated values. Simulated potentiometric surfaces were in good agreement with regional UFA potentiometric surface maps. The strong correlation between simulated and observed hydrographs of groundwater heads and springflow demonstrates that the model successfully reproduced the seasonal dynamics of groundwater flow.

The transient model performance was also evaluated with regard to qualitative targets including river baseflow and lake leakage. Most simulated river baseflows were within range

of baseflows estimated using the Perry and USGS Groundwater Toolbox methods. The simulated baseflow hydrographs demonstrated similar seasonal patterns to those of measured river discharges. The simulated lake leakage values were generally in the same flow direction and were comparable to the range of values reported from water budget studies.

The steady-state and transient models exhibited almost identical water budget results throughout the simulation period in all layers except the SAS. The difference in ET and drain flux in the SAS indicates the importance of the transient model in examining temporal changes to hydrologic inputs on groundwater flow, especially for the SAS. The similarity between the two water budgets for other model layers suggests the ability of the steady-state model to reasonably evaluate long-term average effects of the groundwater system.

The CSM technical team achieved the objective to collaboratively develop a defensible groundwater model using sound science and generally accepted standards for groundwater model development. The CSM effectively represents regional hydrologic conditions within the model domain and is capable of simulating the spatial and temporal variations of aquifer levels, springflows, and river baseflows. The model will be used to evaluate the effects of current and future groundwater withdrawal scenarios and provide data for regional water supply planning, MFL evaluations, and regulatory decisions in the Central Springs Region.

MODEL LIMITATIONS

Limitations of the CSM are like those of other regional groundwater flow models and are typically related to uncertainties and simplifications that are necessary for development of large regional groundwater models. A description of limitations to be considered during the model's application is described below.

- The CSM is simulated using MODFLOW-NWT. MODFLOW-NWT is limited to that of the freshwater groundwater flow system and assumes the fixed locations of freshwater boundaries. Equivalent freshwater heads were used in the model to mimic the impact of density on flow; however, the user should consider the limitation of the model in simulating variable density flow or qualifying the saltwater-freshwater interface under coastal areas.
- The CSM is a groundwater only model. The recharge and maximum ET inputs to the model were calculated using independent HSPF models. The dynamic interaction between surface water and groundwater was not explicitly simulated.
- One limitation inherent to all regional groundwater models is grid-cell resolution. The 2,500 ft by 2,500 ft grid spacing of the CSM limits its ability to simulate conditions on smaller spatial scales. Because of the vertical discretization, conditions such as head changes due to pumping or other stresses are similarly averaged over vertical layers.
- The conceptual model is a simplified representation of the groundwater-flow system. The FAS is a complex, heterogeneous aquifer system. Most areas are carbonate rocks, and some areas have significant karstification that may have numerous zones of differential pathways associated with secondary porosity features. Solution features such as conduits that occur

near springs and discharge from the FAS are not explicitly represented in the CSM and limit the use of CSM in determining travel times to springs in karstic areas of the FAS.

- The no-flow, general-head, and constant-head lateral boundaries only approximate physical boundaries at fixed locations and might limit the accuracy of model results near lateral boundaries. The streambed and lakebed conductance are also simplified and adjusted at the subbasin level due to the lack of available data.
- The hydrogeologic parameter estimates obtained from the calibration are non-unique, and many possible combinations of alternate parameter values could achieve calibration, which is the norm for all regional groundwater models. This lack of uniqueness was well recognized, and uncertainty analyses will be performed to quantify the uncertainty of model parameters and predictions.

Because of the data and model limitations, the CSM is most appropriate at the sub-regional and regional scales. Accurately simulating hydrologic conditions at a very local or site-specific scale will require a refined local model.

8. REFERENCES

- American Society of Civil Engineers (ASCE), 1993. Criteria for Evaluation of Watershed Models. *Journal of Irrigation and Drainage Engineering* 119(3):429-442.
- Andersen, P. and M. Stewart. 2016. Peer Review of the Northern District Model Version 5 and Predictive Simulations, October 10, 2016. Final Report. In files of SJRWMD and SWFWMD, Palatka and Brooksville, FL.
- Anderson, M.P., and W.W. Woessner, 1992. *Applied Groundwater Modeling*. Academic Press, San Diego, California.
- Arthur, J.D., A.E. Baker, J.R. Cichon, A.R. Wood, and A. Rudin, 2005. *Florida Aquifer Vulnerability Assessment (FAVA): Contamination Potential of Florida Principal's Aquifer Systems*. Report submitted to the Division of Water Resource Management, Florida Department of Environmental Protection by the Division of Resource Assessment and Management, Florida Geological Survey.
- Barlow, P. M., W. L. Cunningham, T. Zhai, and M. Gray. 2014. *U.S. Geological Survey groundwater toolbox, a graphical and mapping interface for analysis of hydrologic data (version 1.0): user guide for estimation of base flow, runoff, and groundwater recharge from streamflow data*, p.40. Technical Report 3-B10. Reston, Va.: U. S. Geological Survey.
- Bicknell, B.R., J.C. Imhoff, J.L. Kittle, T.H. Jobes, and A.S. Donigian, 2001. *Hydrological Simulation Program - Fortran (HSPF). User's Manual for Release 12*. U.S. EPA National Exposure Research Laboratory, Athens, GA, in cooperation with U.S. Geological Survey, Water Resources Division, Reston, VA.
- Brooks, H. K. 1981. *Physiographic divisions of Florida: map and guide*. Cooperative Extension Service, Institute of Food and Agricultural Sciences, University of Florida, Gainesville, Florida.
- Cera, T., D. Clapp, and Y. Jia, 2018. Development and Calibration of Surface Water Models to support the North Florida/Southeast Georgia (NFSEG V 1.1) Groundwater Model (Draft). St. Johns River Water Management District.
- CFWI HAT, 2020. *Model Documentation Report East-Central Florida Transient Expanded (ECFTX) Model*. Prepared by Central Florida Water Initiative (CFWI) Hydrologic Analysis Team (HAT). https://cfwiwater.com/pdfs/ECFTX_Model_Final_Report_Feb_2020.pdf
- Copeland, R., S.B. Upchurch, T.M. Scott, C. Kromhout, R. Green, J. Arthur, F. Rupert, Frank, and P. Bond, 2010. *Hydrogeological Units of Florida*. Florida Geological Survey SP 28.
- Doherty, J., 2010. *PEST, Model-Independent Parameter Estimation*. User Manual: 5th Edition. Watermark Numerical Computing.
- Durden, D., F. Gordu, D. Hearn, T. Cera, T. Desmarais, L. Meridith, A. Angel, C. Leahy, J. Oseguera, and T. Grubbs, 2019. *North Florida/Southeast Georgia Groundwater Model (NFSEG V 1.1)*. Technical Publication SJ2019-01. St. Johns River Water Management District.
- Florida Department of Environmental Protection (FDEP), 2002 (updated 2022). Florida Lakes. Accessed on August 31, 2023, from <https://geodata.dep.state.fl.us/datasets/97b765ff2b70400d8bcab23fbe2a5e88/explore>.

- FDEP, 2014 (updated 2023). Upper Floridan Aquifer Potentiometric Surface; September 2012. Accessed on September 8, 2023, from <https://geodata.dep.state.fl.us/datasets/FDEP::upper-floridan-aquifer-potentiometric-surface/about>.
- FDEP, 2017. Florida Springs (2016). Accessed on August 28, 2023, from <https://geodata.dep.state.fl.us/datasets/florida-springs-2016/explore>.
- Florida Marine Research Institute (FMRI), 1989. Major River Lines in Florida. Accessed on August 31, 2023, from <https://hub.arcgis.com/datasets/3158502d6e094de8b5871a9a9666bb18/explore>.
- Freese, R., 2019. *North Florida Southeast Georgia Groundwater Model (NFSEG V1.1)*, Appendix D. Palatka, Fla.: St. Johns River Water Management District.
- Gordu, F., D. Durden, and T. Grubbs. 2016. *Development and Calibration of the North Florida Southeast Georgia Groundwater Model (NFSEG V1.0)*. Palatka, Fla.: St. Johns River Water Management District (Draft).
- Gordu, F., L. Sisco, R. Basso, H. Zhang, J. Patterson, P. Kwiatkowski, A. Obeysekera, 2022. [East-Central Florida Transient Expanded \(ECFTX\) V2.0 Model Report](#), March 2022.
- Faulkner, G.L., 1976. Flow Analysis of Karst Systems with Well Developed Underground Circulation. Proceedings from the Yugoslavian Symposium on Karst Hydrology. v1 June 1975:137-164.
- Florida Department of Environmental Protection (FDEP), 2020. *2019 Reuse Inventory*. Division of Water Resource Management, Florida Department of Environmental Protection, March 2020.
- Harbaugh, A.W., 2005. *MODFLOW-2005, The U.S. Geological Survey Modular Ground-Water Model-The Ground-Water Flow Process*. U.S. Geological Survey Techniques and Methods 6-A16.
- HydroGeoLogic, Inc. (HGL), 2008. *Northern District Groundwater Flow Model Version 1.0*. Report submitted to the St. Johns River Water Management District, and the Southwest Florida Water Management District.
- HydroGeoLogic, Inc. (HGL), 2010. *Northern District Groundwater Flow Model Version 2.0*. Report submitted to the St. Johns River Water Management District, and the Southwest Florida Water Management District.
- HydroGeoLogic, Inc. (HGL), 2011. *Northern District Groundwater Flow Model Version 3.0*. Report submitted to the St. Johns River Water Management District, and the Southwest Florida Water Management District.
- HydroGeoLogic, Inc. (HGL), 2013. *Northern District Groundwater Flow Model Version 4.0*. Report submitted to the St. Johns River Water Management District, and the Southwest Florida Water Management District.
- HydroGeoLogic, Inc. (HGL), 2014. *Central Springs Groundwater Flow Model; Conceptual Model Development*. Draft Report submitted to the St. Johns River Water Management District, the Southwest Florida Water Management District, Marion County, and the Withlacoochee River Water Supply Authority.

- HydroGeoLogic, Inc. (HGL), 2015. *Central Springs Groundwater Flow Model: Regional Groundwater Model Development*. Report submitted to the St. Johns River Water Management District, the Southwest Florida Water Management District, Marion County, and the Withlacoochee River Water Supply Authority.
- HydroGeoLogic, Inc. (HGL), 2016. *Northern District Groundwater Flow Model Version 5.0*. Report submitted to the St. Johns River Water Management District, and the Southwest Florida Water Management District.
- HydroGeoLogic, Inc. (HGL), January 2023. *Central Springs Model Update Project Final Draft Report*. Report submitted to the St. Johns River Water Management District and the Southwest Florida Water Management District.
- Hickey, J.J., 1990. *An Assessment of the Flow of Variable-Salinity Ground Water in the Middle Confining Unit of the Floridan Aquifer System, West-Central Florida*. U.S. Geological Survey Water-Resources Investigations Report 89-4142.
- Hickey, J.J. and W.E. Wilson, 1982. Results of deep-well injection testing at Mulberry, Florida: U.S. Geological Survey Water-Resources Investigations 81-75, 15 p.
- Holzwardt, K.R., Y. Ghile, R. Basso, D. Leeper, and S. King, 2017. *Recommended Minimum Flow for the Rainbow River System, Revised Final Draft*. Southwest Florida Water Management District, Brooksville, Florida.
- Hood, J., M. Kelly, R. Basso, and P.J. Morales, 2010. *Proposed Minimum Flows and Levels for the Upper and Middle Withlacoochee River*. Southwest Florida Water Management District. Brooksville, FL.
- Janosik, A.L., 2011. Hydrogeology, Water Quality and Well Construction-Blitch Plantation Well Site, Marion County, Florida, Southwest Florida Water Management District, 152p.
- Johnston, R.H., R.E. Krause, F.W. Meyer, P.D. Ryder, C.H. Tibbals, and J.D. Hunn. 1980. *Estimated potentiometric surface for the Tertiary limestone aquifer system, southeastern United States, prior to development*. Open-File Report 80-406. Tallahassee, Fla.: U.S. Geological Survey.
- Knochenmus, L.A. and D.K. Yobbi, 2001. *Hydrology of the coastal springs ground-water basin and adjacent parts of Pasco, Hernando, and Citrus Counties, Florida*. (Vol. 1, No. 4230). US Department of the Interior, US Geological Survey.
- Kuniansky, E.L., Bellino, J.C., and Dixon, J.F., 2012. *Transmissivity of the Upper Floridan aquifer in Florida and parts of Georgia, South Carolina, and Alabama*: U.S. Geological Survey Scientific Investigations Map 3204, 1 sheet, scale 1:100,000, (Also available at <http://pubs.usgs.gov/sim/3204/>.)
- Kuniansky, E.L., Dixon, J.F., and Kinnaman, S.L. 2017, Potentiometric surface contours, wells, and groundwater basin divides for the Upper Floridan aquifer in Florida and parts of Georgia, South Carolina, and Alabama, May-June 2010 – Updated: U.S. Geological Survey data release, <https://doi.org/10.5066/F75Q4TZD>.
- McGurk, B., and P.F. Presley, 2003. *Simulation of the Effects of Groundwater Withdrawals on the Floridan Aquifer System in East-Central Florida*. St. Johns River Water Management District, Palatka Florida, Technical Publication SJ2003-3.

- Miller, J.A., 1986. *Hydrogeologic Framework of the Floridan Aquifer System in Florida and in Parts of Georgia, Alabama, and South Carolina*. U.S. Geological Survey Professional Paper 1403-B.
- Moore, K. 2007. BASINS Technical Note 2: Two Automated Methods for Creating Hydraulic Function Tables (FTABLES). EPA BASINS Technical Note 2. United States Environmental Protection Agency, Office of Water.
- Moore, R.B., L.D. McKay, A.H. Rea, T.R. Bondelid, C.V. Price, T.G. Dewald, and C.M. Johnston, 2019. *User's guide for the national hydrography dataset plus (NHDPlus) high resolution*. U.S. Geological Survey Open-File Report 20191096, 66 p.,.
- Motz, L.H., 1998. Vertical leakage and vertically averaged vertical conductance for karst lakes in Florida. *Water Resources Research* 34(2):159-67.
- Motz, L.H., and A. Sedighi, 2009. *Representing the coastal boundary condition in regional groundwater flow modes*. Journal of Hydrologic Engineering, Vol. 14, No. 8, August 1, 2009.
- Niswonger, R.G., Panday, Sorab, and Ibaraki, Motomu, 2011. *MODFLOW-NWT, A Newton formulation for MODFLOW-2005: U.S. Geological Survey Techniques and Methods 6-A37*, 44 p., <https://doi.org/10.3133/tm6A37>.
- O'Reilly, A.M., R.M. Spechler, and B.E. McGurk, 2002. *Hydrogeology and Water Quality Characteristics of the Lower Floridan Aquifer in East-Central Florida*. U.S. Geological Survey Water Resources Investigation Report 02-4193, Tallahassee, FL.
- Perry, R.G., 1995. *Regional Assessment of Land Use Nitrogen Loading of Unconfined Aquifers*. Ph.D. Dissertation, University of South Florida, Tampa, Florida, and October 1995.
- Randazzo, A.F., and D.S. Jones (editors), 1997. *The Geology of Florida*. University Press of Florida.
- Rosenau, J.C., G.L. Faulkner, C.W. Hendry, Jr., and R.W. Hull, 1977. *Springs of Florida* (revised): Tallahassee, Florida Bureau of Geology Bulletin no. 31, 461p.
- Ryder, P.D., 1985. *Hydrology of the Floridan Aquifer System in West-Central Florida*. U.S. Geological Survey Professional Paper 1403-F.
- Sacks, L.A., 1996. *Geochemical and Isotopic Composition of Ground Water with Emphasis on Sources of Sulfate in the Upper Floridan Aquifer in Parts of Marion, Sumter, and Marion Counties, Florida*. U.S. Geological Survey Water-Resources Investigations Report 95-4251.
- Sepúlveda, N., 2002. *Simulation of Ground-Water Flow in the Intermediate and Floridan Aquifer Systems in Peninsular Florida*. U.S. Geological Survey Water-Resources Investigations Report 02-4009.
- Sepúlveda, N., 2021, *Data sets of actual evapotranspiration rates from 2000 to 2017 for basins in Florida and parts of Alabama and Georgia, calculated using the water-balance method, the bias-corrected Operational Simplified Surface Energy Balance (SSEBop) model, and the land-use crop coefficients model*: U.S. Geological Survey data release, <https://doi.org/10.5066/P99AB3X4>.
- Shah N., M. Nachabe, and M. Ross. 2007. Extinction Depth and Evapotranspiration from Ground Water under Selected Land Covers. *Ground Water* 45(3).

- Southwest Florida Water Management District (SWFWMD), 1997. *Water-quality and hydrology of the Homosassa, Chassahowitzka, Weeki Wachee, and Aripeka Spring complexes, Citrus and Hernando Counties, Florida—Origins of increasing nitrate concentrations*: Brooksville, Report on file, 166 p.
- SWFWMD, 2017. *Recommended Minimum Flow for the Crystal River/Kings Bay system*. Southwest Florida Water Management District, Brooksville, Fla.
- Sun Q., 2017. Volusia Groundwater Flow Model - 2015 Conditions, St. Johns Water Management District, October 2017 (Draft). St. Johns River Water Management District, Palatka, Fla.
- Sutherland, A.B., R. Freese, J.B. Slater, F. Gordu, J. Di, and G.B. Hall, 2017. *Minimum Flows Determination for Silver Springs; Marion County, Florida*. Technical Publication SJ2017-2, St. Johns River Water Management District, Palatka, Fla.
- Walsh, S. J., L. Knowles, B.G. Katz, and D.G. Strom, 2009. *Hydrology, water quality, and aquatic communities of selected springs in the St. Johns River Water Management District, Florida*. U. S. Geological Survey Scientific Investigations Report 2009-5046, 116p.
- Williams, S.A., 2006. *Simulation of the Effects of Groundwater Withdrawals from the Floridan Aquifer System in Volusia County and Vicinity*. Technical Publication SJ2006-4, St. Johns River Water Management District, Palatka, Fla.
- Williams, S.A., 2013. Verification and recalibration of the Volusia regional ground water flow Model, 09/13/2013 (Draft). St. Johns River Water Management District, Palatka, Fla.
- Williams, L.J. and J.F. Dixon, 2015. *Digital Surfaces and Thicknesses of Selected Hydrogeologic Units of the Floridan Aquifer System in Florida and Parts of Georgia, Alabama, and South Carolina*. U.S. Geological Survey Data Series 926.
- Williams, L.J., and Kuniansky, E.L., 2016, *Revised hydrogeologic framework of the Floridan aquifer system in Florida and parts of Georgia, Alabama, and South Carolina (ver 1.1, March 2016)*: U.S. Geological Survey Professional Paper 1807, 140 p., 23 pls, <https://pubs.usgs.gov/publication/pp1807>.
- Wolansky, R.M., G.L. Barr, and R.M. Spechler, 1980. *Configuration of the top of the highly permeable dolomite zone of the Floridan Aquifer*. Southwest Florida Water Management District (No. 80-433). Brooksville, Fla.

APPENDIX A – LIST OF SIMULATED SPRINGS

(This appendix is provided as a separate pdf file)

DRAFT

APPENDIX B - SIMULATED VERSUS OBSERVED HYDROGRAPHS OF SURFICIAL AQUIFER SYSTEM CALIBRATION TARGET WELLS

(This appendix is provided as a separate pdf file)

DRAFT

APPENDIX C - SIMULATED VERSUS OBSERVED HYDROGRAPHS OF UPPER FLORIDAN AQUIFER CALIBRATION TARGET WELLS

(This appendix is provided as a separate pdf file)

DRAFT

APPENDIX D - SIMULATED VERSUS OBSERVED HYDROGRAPHS OF LOWER FLORIDAN AQUIFER CALIBRATION TARGET WELLS

(This appendix is provided as a separate pdf file)

DRAFT

APPENDIX E - SIMULATED VERSUS OBSERVED MAY AND SEPTEMBER POTENTIOMETRIC SURFACE MAPS

(This appendix is provided as a separate pdf file)

DRAFT

APPENDIX F - SIMULATED VERSUS OBSERVED HYDROGRAPHS OF CALIBRATION TARGET SPRINGS

(This appendix is provided as a separate pdf file)

DRAFT

APPENDIX G – SIMULATED VERSUS ESTIMATED HYDROGRAPHS OF CUMULATIVE RIVER BASEFLOW AT GAGING STATIONS

(This appendix is provided as a separate pdf file)

DRAFT

APPENDIX H - SIMULATED VERSUS ESTIMATED HYDROGRAPHS OF RIVER PICKUP BASEFLOW BETWEEN GAGING STATIONS

(This appendix is provided as a separate pdf file)

DRAFT

APPENDIX I – SIMULATED HYDROGRAPHS OF LAKE LEAKAGE

(This appendix is provided as a separate pdf file)

DRAFT

APPENDIX J – COMPARISON OF HSPF AND MODFLOW-SIMULATED CUMULATIVE BASEFLOW OF MAJOR RIVER BASINS

(This appendix is provided as a separate pdf file)

DRAFT

APPENDIX K – COMPARISON OF HSPF AND MODFLOW-SIMULATED GROUNDWATER EVAPOTRANSPIRATION OF MAJOR RIVER BASINS

(This appendix is provided as a separate pdf file)

DRAFT